DEVELOPMENT OF A TWO-WAY MICROWAVE COMMUNICATION SYSTEM FOR TRAFFIC APPLICATIONS

TAK KWONG CHAN

A Thesis submitted in partial fulfilment of the requirements of
the University of Northumbria at Newcastle
for the degree of Doctor of Philosophy

June 1994

Dedicated to my father

ABSTRACT

This thesis presents the results of the research that has been carried out in order to realise a highly reliable two-way microwave based digital communication link between a radio beacon and a moving vehicle. Such a system can be used for traffic applications such as automatic road and corridor (lane) tolling.

The emphasis of the research has concentrated on the design of the system in order to meet the required system specifications in terms of range, data rate and communication zone, etc. In particular the research has also focused on the design and realisation of the in-vehicle-unit (called on-board-unit) which has to be small in size and inexpensive. To achieve the above objectives, novel designs have been produced for both a circularly polarised patch antenna and a single-diode approach for the on-board-unit. Circular polarisation is obtained using a microstrip square patch antenna and a 3dB two-branch coupler. In order to match the coupler to the antenna, the characteristic impedance of the matching line has to be very high and this results in a very narrow microstrip line that is difficult to realise. Thus the design of the coupler has been modified in order to have a lower characteristic impedance of this matching line, making it wider and easier to realise.

In respect of the design of the road-side beacon's antennae, a 4 by 4 planar antenna array has been developed, including the effect of mutual coupling between the patches. The mutual coupling between two patches has also been studied in detail using both the transmission line model and the cavity model. For the transmission line model, a new approach has been developed in deriving a simpler expression for the mutual conductance between the patches. The new derived formula for the mutual conductance can be readily evaluated.

Further, a unique method has been implemented for an ASK demodulation and a PSK modulation using a single diode at the on-board-unit. An analysis for a non-ideal PSK modulation was also presented. Finally a two-way microwave communication system has been successfully realised and evaluated. Good performance was achieved.

As a result of the above work, two reports have been published in the Commission of the European Communities documents (November 1992 and May 1994), one paper has been published in the IEE Colloquium Proceedings (11 June 1993), one paper is to be published in the 24th Microwave Conference Proceedings (5-8 September 1994) and one paper is to be published in the Microwaves 94 Conference and Exhibition Proceedings (25-27 October 1994) and these are listed in Appendix M.

ACKNOWLEDGEMENTS

I wish to thank my director of studies Professor E. Korolkiewicz for his constant support, guidance and encouragement. Thanks are also due to my second supervisor Dr. R. Armstrong for his helpful discussions.

I would like to thank my friends, especially Mr. Peter Elsdon, Dr. M.W. Mak, Mr. Krates Ng, Mr. Mike Pattison and Mr. Hugh Ross for their help and encouragement.

Appreciation is also especially expressed to all the members of the Communication Research Group (Department of Electrical, Electronic Engineering and Physics, University of Northumbria at Newcastle) for their invaluable contributions and assistance.

Special thanks are due to Mr. Stanley Scott for his help with the mathematics.

To the technical staff Mr. Peter Elsdon and Mr. Sid Greaves I would like to offer my thanks for their technical assistance.

Finally I wish to thank my family for their continued support and understanding during my studies abroad, and also Julie and her family for their encouragement.

ABBREVIATIONS

ADEPT	Automatic Debiting and Electronic Payment for Transport
AMTICS	Automatic Mobile Traffic Information and Control System
ASK	Amplitude Shift Keying
BER	Bit Error Rate
BPSK	Bipolar Phase Shift Keying
CACS	Comprehensive Automobile Communication System
CEPT	The Conference of European Posts and Telecommunications
CP	Circular Polarisation
CPU	Central Processing Unit
CRCS	Close Range Road/Vehicle Communication System
CW	Continuous Wave
DC	Direct Current
DSB	Double Side-Band
DPSK	Differential Phase Shift Keying
EIRP	Effective Isotropic Radiated Power
ERP	Electronic Road Pricing
FSK	Frequency Shift Keying
HELP	Heavy Vehicle Electronic Number Plate
IDT	Inter-digital Transducers
IF	Intermediate Frequency
IRM	Image Rejection Mixer
IVHS	Intelligent Vehicle-Highway System
MC	Mutual Coupling
NRZ	Not Return to Zero
OBU	On-Board Unit
PAMELA	Pricing And Monitoring ELectronically of Automobiles
PREMID	Programmable REMote IDentification
PSK	Phase Shift Keying
RACS	Road-Automobile Communication System
RF	Radio Frequency
RSU	Road-Side Unit
RTI	Road Transport Informatics
'S' parameter	Scattering parameter
SAW	Surface Acoustic Wave

ABBREVIATIONS

SSB	Single Side-Band
TLM	Transmission Line Model
TSS	Tangential Signal Sensitivity
TTL	Transistor-Transistor Logic
λo	Wavelength in free space

CONTENTS

CHAPTER 1

1.1 Introduction

Traffic growth depends mainly on income and to a lesser degree on the price of fuel. Between 1970 and 1990 traffic growth in UK has doubled. Based on forecasts of income growth and fuel price traffic growth could increase again by 140% by the year 2010. Consequently traffic congestion on roads will likely increase to unacceptable levels. Building of new road is increasingly opposed by strong and highly organised environmental groups supported generally by public opinion.

One option to ease congestion which is now being examined in this country and Europe is that of road-pricing which not only raises revenue for the construction of new roads but also makes more efficient use of the existing road space. In a road-pricing system a motorist will be charged for using a specific road or motor-way at a specific time of day. A system must be designed which will allow for an automatic payment of tolls on roads and multi-lane motor-ways.

In order to implement any form of road-pricing system, it is necessary to obtain a secure two-way communication between a tolling system and a moving vehicle. One way of achieving this is to use microwave frequency system to obtain a digital, two-way communication, between a road-side radio beacon and a moving vehicle.

This thesis presents the research that has been carried out in order to realise such a microwave system operating at 5.8GHz. The important area of the research has been the detailed design of the antennae for both the road-side radio beacon and for the device placed inside a moving vehicle (in-vehicle unit). Further, the research has concentrated particularly on the design of the in-vehicle unit (or called on-board unit, OBU) to ensure not only that is small in size but also inexpensive.

1.2 Overview of the Thesis

Chapter 2 reviews the main technologies that have recently been developed in Europe, USA and Japan. It was found that microwave technology offers the best options when the error-free data transmission is required. This is very important as there is a financial transaction involved.

The specifications of the system for the down and up-link operations are described in Chapter 3. The effect of the side-lobe levels of the road-side unit antenna on the communication zone is also examined.

Chapter 4 investigates the design of the microstrip antennae for both the OBU and the RSU. Two transmission line models have been compared in respect of the design of single patch antenna for the OBU. It is found that it is necessary to consider the mutual coupling between the two radiating slots of the patch in order to obtain a more accurate value of the resonant impedance and resonant frequency.

In the design of a 4 by 4 antenna array for the RSU, mutual coupling between the adjacent patches affects the array performance. Two approaches were employed to investigate it analytically namely using a transmission-line model (TLM) and a Cavity Model presented in Chapter 5. New formulae are proposed for calculating the mutual admittance. For the Cavity Model a mathematical analysis for the mutual impedance was included.

Chapter 6 is concerned with the design of a 4 by 4 antenna array. It is found that the mutual coupling has a negligible effect on the array performance when the spacing between elements is $0.75\lambda_o$.

Chapter 7 is concerned with the design and performance of an ASK detector/PSK modulator and an image rejection mixer (IRM). In the case of the combined ASK detector/PSK modulator, a matching network is realised to obtain a maximum performance for the PSK modulation and this device also functions as an ASK detector. Due to the unavoidable mismatch of the matching network the tangential signal sensitivity (TSS) is degraded by approximately 5dB.

The design of the OBU and the RSU and the performance of the system are presented in Chapter 8. In order to simplify the circuitry of the OBU, a single diode is employed for PSK modulation on the carrier for the up-link and also for ASK detection on the down-link operation. Finally the system has been evaluated in the field and the communication zone has also been measured. It was found that there is a good agreement between the theoretical and the practical results.

CHAPTER 2

Review of Current Systems

2.1 Introduction

The requirement, for a two-way digital communication system between a Road-Side Unit (RSU) and a moving vehicle, is that it can be used for a variety of traffic applications. Such a system normally consists of two fundamental sub-systems: a Road-Side Unit (RSU) and a vehicle mounted transponder (On-Board Unit, OBU). Important design requirements of the system are that the On-Board Unit (OBU) placed behind the windscreen of a moving vehicle should be small in size, low profile and inexpensive. The system should also satisfy the requirement of communication range, data rate and in addition, rain, snow, fog, ice, etc. should have minimum effect on the transmitted signal. It would show that the above requirements can best be achieved using microwave frequencies. Two frequencies have been allocated for use in traffic applications: in Europe the allocated frequency is 5.8GHz while in USA and Japan the frequency is 2.45GHz.

This chapter briefly reviews the main technologies that are currently under investigation in Europe, USA and Japan.

2.2 Review of Existing Technologies

The main technologies used in traffic systems and described in this section are

(i) Inductive Loops,

(ii) Surface Acoustic Wave,

(iii) Infrared and

(iv) RF and Microwave Frequency.

2.2.1 Inductive Loop System

Inductive systems utilise the inductive coupling properties of coils or ferrite rods in the frequency range of 30 to 300kHz. Communication can be established between two inductive loops, one buried under the surface of the road and the other fitted underneath a vehicle. The frequency of operation is 147kHz, data rate is 9.2kbps and the communication range is between 0.1m to 1m. The inductive loop fitted under the road cannot only detect the presence and the type of vehicles but it can also determine the length of the vehicle and its speed. Such systems have been widely used in traffic monitoring to provide relevant information of the actual traffic conditions on sections of roads.

Early systems used an active transponder which generated its own low-frequency signal but because of the cost and power consumption such systems are unattractive. More recently passive and semi-passive transponders have been developed. These are operated by receiving energy from the road-side loops which is then coded by the transponder and re-transmitted back to the road-side loops. When the transponder enters the fields of the inductive loop, a signal operates a transistor switch and the transponder transmits a reply signal of identification data message. This fix-coded message is repeated at least seven times before the transponder switches off to save power. The custom-built chip used for the London buses are based on the ones developed by Plessey for the Hong Kong Electronic Road Pricing project (ERP) (Plessey,1985). The main parameters of the system are shown in Tables 2.1.

Communication systems using inductive loop technology have also been utilised for route guidance applications in the 1970s. In Japan, the Comprehensive Automobile Communications System (CACS) has been operating in Tokyo since 1977 (MITI,1977). Similar equipment has also been demonstrated in Germany (Jeffery,1987a). These systems have not however been adopted because of the following problems:

(a) the expense of installing inductive loops beneath the road surface,
(b) low data transmission rate,
(c) relatively large size of the transponder and
(d) because inductive loops are affected by steel-reinforced pavement.

The advantages of the inductive loops include

(a) indifference to environmental conditions,
(b) a choice of different sizes and shape detection areas,
(c) accurate determination of the position of vehicles and also their speeds and
(d) they cannot be seen or tampered with.

2.2.2 Surface Acoustic Wave (SAW)

SAW devices rely on the propagation of acoustic waves which allows the wavelength of signals in the frequency range 100MHz to 1GHz to be realistic, as the velocity of propagation is that of sound. Below this frequency range the devices become too large and above the propagation losses along the substrate become excessive and the interdigital transducers become to small to fabricate.

SAW devices are made by laying interlocking comb shaped electrodes, called interdigital transducers (IDT's), onto a piezoelectric substrate (Datta,S.). The interlocking fingers of the IDT are spaced at intervals equal to half a wavelength of the intended resonant frequency of the device. When the RSU sends a low power radio frequency to the SAW device at the OBU, the surface of the piezoelectric substrate is distorted in such a way that acoustic waves are produced. The waves will propagate along the surface where a series of etched metal poles may reflect part of the original acoustic signal in a time related manner which represents the code of a particular OBU. This information is then re-transmitted back to the RSU for identification of the particular vehicle owner for subsequent billing.

The KOFRI system, which was developed by Micro Design (Bogen,1989) is maintenance-free as there is no battery. It has a life-time of more than 20 years. The specifications of the system is given in Table 2.2.

The main problem with this system is that again limited amount of information can only be transmitted back to the RSU because the code is fixed for each transponder by the pre-determined pattern of the etched metal poles on the transponder.

2.2.3 Infrared System

The receiver consists of an array of photo-diodes while the transmitter uses a simple light emitting diode which is pulsed ON and OFF to represent the binary signal. An early example for AVI tolling application is the KILO transponder (Foote,1980) which was evaluated on the Lincoln Tunnel by the Port Authority of New York and New Jersey in the late 1970's. A current example of an active infrared system is the Siemens ALI-SCOUT electronic route guidance system which was demonstrated in the LISB experiment in Berlin and the AUTOGUIDE experiment in London (Jeffery,1987b and TCC,1988). The parameters of the system are shown in Table 2.3.

It was found that the infrared system operates well in good weather and light conditions. However, the performance was severely degraded by snow, ice and dirt on the windscreen. It was reported that a layer of snow 1/8" thick on the windscreen can completely block the infrared signal. However, it may be suitable for route guidance applications, where the reliability of data is not crucial and it can support two-way communications. As the reliability

of the system is low, it is not suitable for the tolling applications which require financial transactions and a low bit error rate (BER < 10^{-9} after error correction).

2.2.4 RF and Microwave Frequency

In USA, the Heavy Vehicle Electronic Number Plate (HELP) programme is to integrate heavy vehicle monitoring, identification, weighing and classification systems. Optical, infrared, inductive-loop, radio frequency (RF), surface acoustic wave (SAW) and microwave based technology have all been used and evaluated (Davies,1989a). It was found that either a RF or a microwave system would best meet the requirements of a two-way communication between the RSU and the OBU. A system evaluated in the HELP experiment has been installed on the Dallas Toll Road in Virginia (Davies, 1989b) developed by the AMTECH Corporation. Currently, the HELP program has entered a major operational evaluation phase known as the Crescent Demonstration (Sabounghi,1991). The Close-Range Road/Vehicle Communication System (CRCS) is able to support a number of IVHS (Intelligent Vehicle-Highway Systems). The Department of Transportation is expected to spend over $350B (more than the Apollo project) on developing a nation-wide IVHS infrastructure incorporating microwave and other technology over the next 30 years (Rose,1993).

Another system to emerge was AMTICS (Automatic Mobile Traffic Information and Control System) which operated in the RF band around 800MHz (JTMTA,1986 and Tsuzawa,1989a). Its aim was to develop advanced technology for every aspect of traffic management which included traffic signal control, traffic information collection, traffic database and traffic routing and diversion. Since 1986, a joint research and development project between Japanese Ministry of Construction and 25 private corporations has been developing a Road-Automobile Communication System (RACS) (Tsuzawa,1989b; Okamoto,1989 and Shibano,1991). The AMTICS project was successfully used in the first pilot experiment in metropolitan Tokyo in 1988 and the second experiment was demonstrated in Osaka in 1990 (Okamoto,1990&1991).

Specific microwave and RF systems developed for use in a variety of traffic applications are discussed in the following sections.

The PREMID System

The PREMID system (Programmable REMote IDentification) (Philips,1987a, b & c and Skadsheim,1988) has been developed by Philips, operating at the frequency of 2.45GHz. The first applications was in the car and production industries. In 1985/86, the PREMID system was evaluated for automatic identification of cars in a road-toll system in Bergen, and in October 1987 the complete system was commissioned for the toll system in Alesund, Norway. In the UK, the PREMID system is being used at the Dartford River Crossing (Holmes,1992) and Jaguar's programme (Bhandal,1992).

The fundamental principle of operation of the PREMID system is shown in figure 2.1. When the identification-tag is not exposed to microwave signals, it remains in a 'sleeping' condition with a very low power consumption. When it enters the area in front of an antenna, it 'wakes up', and the communication is established between the tag and the antenna. The communication between RSU and OBU is a half-duplex system. In down-link transmission, the carrier is ASK modulated at the data rate of 167kbps. In up-link transmission, a continuous wave at 2.45GHz is transmitted from the RSU to the OBU, which is frequency shifted where a '0' is represented by 28kHz and a '1' by 25kHz at the data rate of 267kbps. Single sideband modulation is used for the uplink transmission.

The FSK (Frequency Shift Keying) modulator is in the form of a phase shift modulator which is driven by a constant ramp voltage whose slope is varied for different data logic, i.e. '1' or '0'. A constant varying phase shift produces frequency shift. The link parameters of this system are summarised in Table 2.4.

The AMTECH System

The AMTECH system (AMTECH,1989) is a vehicle identification system in which an ID-tag is mounted on a freight container. The system operates in the frequency ranges 850-950MHz or 2.4-2.5GHz. The tag uses a modified FSK code of two frequencies. A '0' bit is represented by one 20kHz square followed by two 40kHz square wave cycles while a '1' consists of two 40kHz square wave cycles followed by a 20kHz square wave cycle.

The reflected signal modulated by the modified FSK signal is received by the beacon where the data is decoded and sent to the automatic data processing systems. The link parameters of the AMTECH system are given in Table 2.5.

The BOSCH System

The BOSCH system (Blume,1992) is used for automatic fee collection. The system operates at 5.8GHz and consists of four sub-systems. They are the Charging System, the On-Board Unit (OBU), the Smart-card, and the Central Station.

The charging station comprises all necessary road-side installation such as transceiver units, video equipment and station processor. The transceiver units are mounted on two gantries which span on the carriageway at a spacing about 13 metres. When the car passes the first gantry, the OBU receives the microwave signals. It switches itself from standby mode to operating mode and sends an authentication request to the gantry. As the vehicle leaves the communication area of the first gantry, the OBU debits the fee from the smart-card and prepares an acknowledgement signal. When the vehicle has reached the communication zone of the second gantry, the OBU sends the acknowledgement. At the second gantry, the vehicle is detected by an inductive loop.

The TELEPASS System (5.8GHz)

The system is an Automatic Debiting System installed along the Autostrade Milan-Naples in Italy operated by Autostrade S.p.A. (Autostrade S.p.A.,1991). The link parameters are given in Table 2.6.

PAMELA/ADEPT Microwave System

In Europe under the DRIVE I project PAMELA (1989-91) a two-way digital communication system to be used for traffic application has been developed. The objectives of the project were to specify, design, develop and demonstrate equipment to facilitate two-way communications between a moving vehicle and a fixed roadside station for non-stop automatic debiting applications such as road-tolling, road-use pricing and car-parking. At the centre of the system is a reliable high-capacity, short-range microwave communication link. Initially, a system operated at 2.45GHz had been developed and tested (Dadds,1991 and Korolkiewicz,1991). Since then, the allocated frequency for traffic application has been changed from 2.45GHz to 5.8GHz by the CEPT recommendation. The new system operating at 5.8GHz system has been developed at the Northumbria University jointly with SAAB, Sweden and tested in three separate field trials,

(a) Non-stop automatic toll-collection (SAPN highway in France),
(b) On-street car-parking management and debiting (Lisbon, Portugal) and
(c) High-speed multi-lane communications for road-pricing and advance toll collection (Enjöping, Sweden).

The PAMELA field tests demonstrated the ability of the communications link to operate under a number of different conditions, both in a built-up urban area and a motorway environment, at low and very high vehicle passage speeds and in mono-lane and multi-lane road configurations (Blythe,1992).

In the DRIVE II project ADEPT (1992-93)(Automatic Debiting and Electronic Payment for Transport), the objectives are to use the results of the DRIVE I programme and to integrate the developed transponder and smart-card for various automatic debiting (ADS), electronic payment and other complementary RTI (Road Traffic Informatics) applications. A number of test sites were to be used. They were

(a) Göteborg (Sweden): Experiments on automatic debiting (November 1992),
(b) Thessaloniki (Greece): The multi-lane and mono-lane automatic tolling will be evaluated on a highway (November 1993),
(c) Lisbon (Portugal): A dynamic car-parking management and debiting system will be installed (March 1994) and
(d) Cambridge (UK): A prototype Congestion Metering System (CMS) will be developed and demonstrated (October 1993).

2.3 Summary

This chapter has reviewed the existing technologies applied to traffic systems. Microwave technology offers the best options if secure data transmission is required. The microwave system supports high data rate and line-of-sight secure two-way digital communication between the Road-Side Unit and the On-Board Unit. The system developed at the Northumbria University is being tested in four European countries and the research which results in the design and the realisation of the system forms the basis of this thesis.

Hong Kong ERP System (Plessey,1985)	
Frequency:	147kHz
System characteristics:	passive transponder, one-way communications, fixed code
Data rate:	9.2kbps, transfer of about 20bytes of data
Modulation:	PSK (Phase Shift Keying)
Range:	0.1-1m
Position of loops:	buried in road
Position of transponder:	underside of vehicle

Table 2.1 Hong Kong ERP System

KOFRI System	
Frequency:	440MHz and 915MHz
System characteristics:	Passive transponder, One-way communications, Fixed code
Data rate:	N/A
Modulation:	N/A
Range:	< 15m
Passing speed:	0-200km/h
Max. system response time for information to driver:	0.1 sec.
Position of RSU:	Gantry, above the road surface
Position of transponder:	Behind driving mirror

Table 2.2 KOFRI System

AUTOGUIDE System	
Infrared wavelength:	950nm
System characteristics:	Active transponder, Two-way communications, Variable code
Data rate:	Present: 125kbps Future: 515kbps
Modulation:	ASK (Amplitude Shift Keying)
Range:	50m each way
Position of RSU:	2.5-3.5m high on lamp post of traffic light
Position of transponder:	Behind driving mirror, 0.5-2.0m high

Table 2.3 AUTOGUIDE System

PREMID System:	
Frequency:	2450MHz
EIRP:	25mW
System characteristics:	Semi-passive, one or two-way communications, fixed or various code
Data rate:	present 166kbps, 20bytes (future 266kbps, >1kbytes)
Modulation:	ASK Downlink FSK Uplink
Range:	up to 15m
Max. speed of tag:	100km/h
Position of beacon:	1-2m at side of road or 5-6m on gantry above road
Position of transponder:	1-2m high in side window or mounted behind the windscreen

Table 2.4 PREMID System

AMTECH System	
Frequency:	880, 915, 2450MHz
System characteristics:	passive or semi-passive transponder, one-way communications, fixed code
Data rate:	20 alphanumeric characters (120bits)
Modulation:	FSK (Frequency Shift Keying)
Range:	5-10m for tolling purposes
Position of beacon:	1-2m high at side of road
Position of transponder:	mounted behind the windscreen

Table 2.5 AMTECH System

TELEPASS System	
Frequency:	was 5.72GHz is 5.8GHz
Output power:	100mW
Antenna gain:	18/15dBi
Modulation:	FSK
Maximum vehicle speed:	50km/h
Data rate (Downlink):	960kpbs
Data rate (Uplink):	144kbps

Table 2.6 TELEPASS System

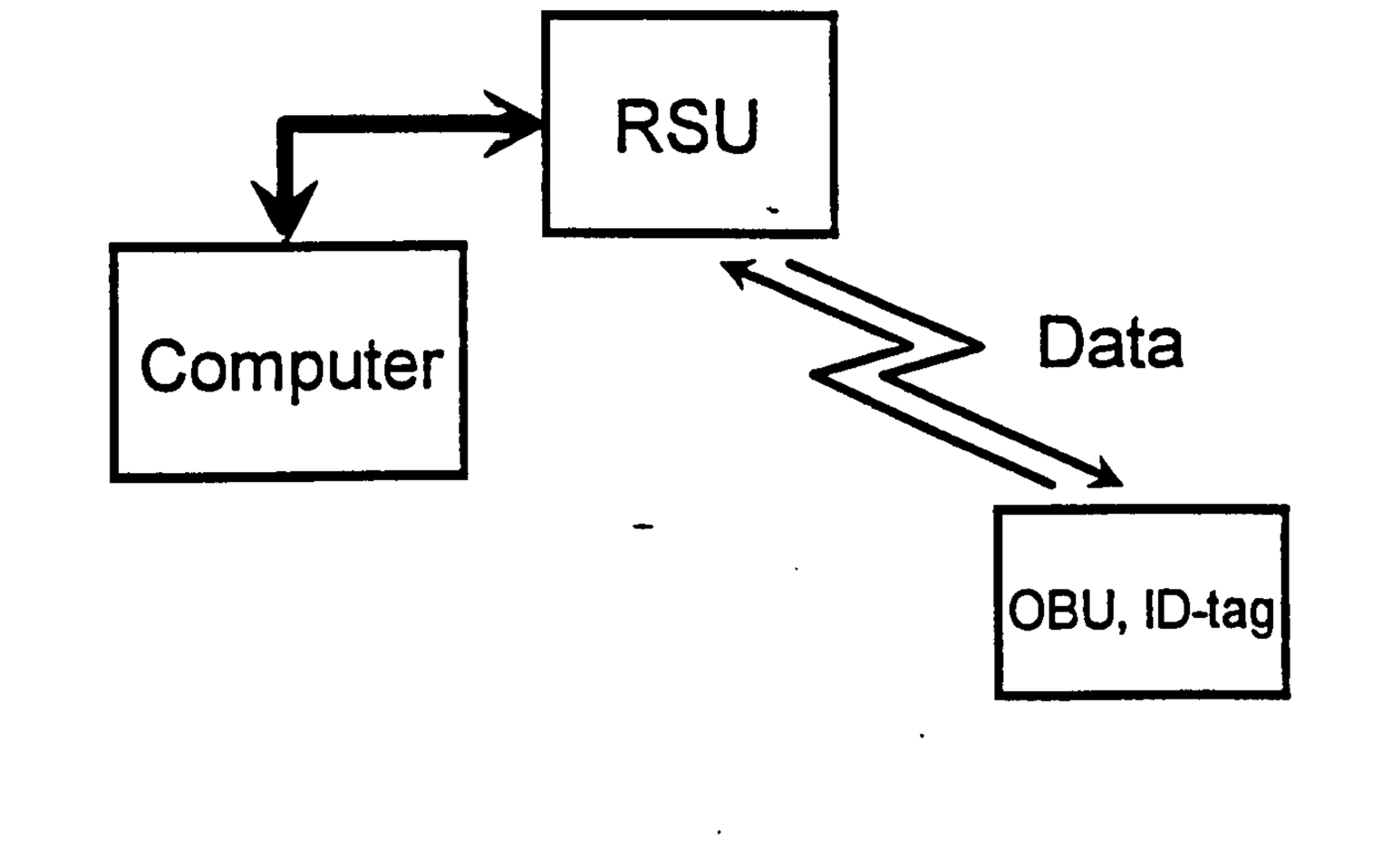

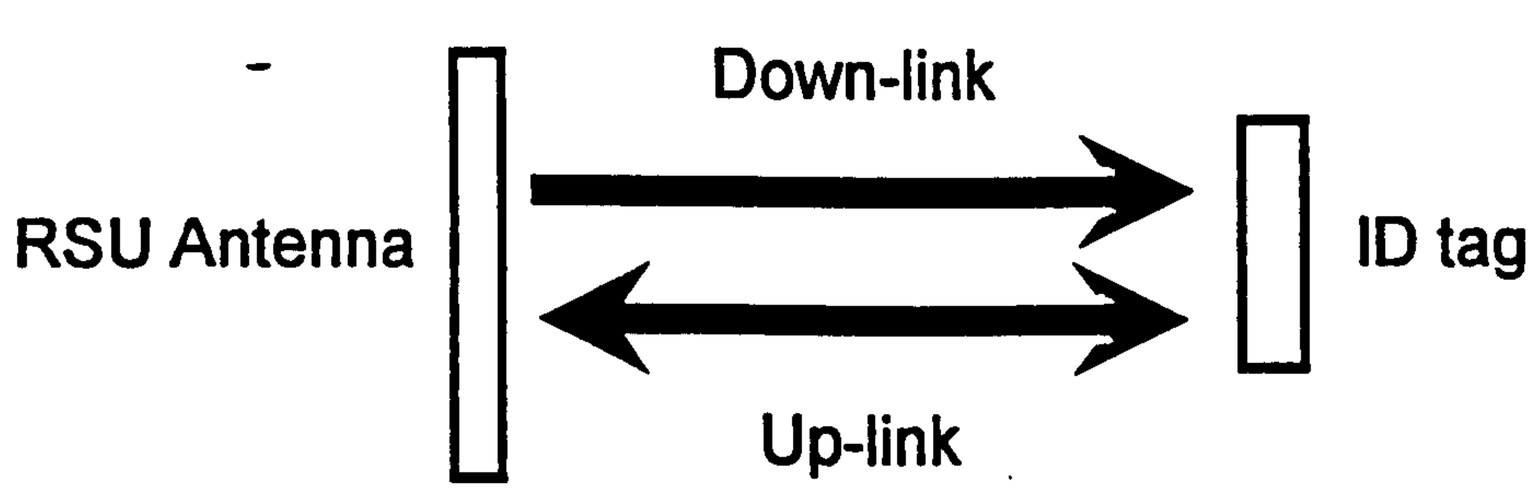

Figure 2.1 Basic elements of the PREMID system

CHAPTER 3

Specification of Communication Link

3.1 Introduction

This chapter presents the specification of a two-way communication system between a RSU and an OBU and includes the operating frequency, transmitted power, communication zone and the specification for down and up-link operations. The effect of the side-lobe levels of a RSU antenna on the communication zone is also discussed. Finally a comparison of the losses produced by direct modulation of the carrier and modulating the carrier by a 1MHz sub-carrier is presented.

3.2 System Parameters

CEPT Recommendations

The standard body 'The Conference of European Posts and Telecommunications' (CEPT) recommended in February 1991 (T/R22-04) that

1. "the frequency band 5.795 - 5.805 GHz is used for the initial road to vehicle system especially for the road toll system and the maximum 'Effective Isotropic Radiated Power' (EIRP) is 2W average",
2. an additional sub-band (5.805 - 5.815 GHz) may be used for multi-lane applications,
3. all vehicle-to-vehicle communication links should be developed in the band 63 - 64 GHz,
4. vehicular radar systems should be developed in the band 76 - 77 GHz,
5. in the development of RTI equipment special attention should be given to compatibility with the equipment of other services.

Consequently the 5.8 GHz frequency has been used in Europe. The frequency 2.45 GHz is however being used for traffic applications in Japan and the USA and therefore two systems in this project have been designed for the above two operating frequencies.

The system was designed to produce a two-way microwave digital data communication between a RSU and an OBU. To reduce the cost of the OBU a talk and listen technique as shown in figure 3.2.1 has been implemented. Link definition is made by the information to sends. In the system, information is initially transmitted from the RSU to the OBU (Down-Link). The OBU then transmits information and the RSU listens (Up-Link). For the up-link

operation the RSU transmits an unmodulated carrier (CW) which is then modulated at the OBU before being re-radiated back to the RSU.

It is important to ensure that the design of the OBU is simple and inexpensive when deciding on the type of modulation to be used. Consequently ASK modulation is used for the down-link as the information can be recovered using a simple diode detector. For the up-link the CW is PSK modulated by a DPSK 1MHz sub-carrier signal. A simple diode can be used to produce PSK modulation of the 5.8 GHz signal at the OBU (see chapter 9). In order to reduce the effects of multi-path reflections circular polarisation is implemented at the OBU and RSU.

For the down-link, a 5.8GHz signal oscillator is ASK modulated by a single-pole-single throw (SPST) switch and transmitted on left-hand circular polarisation as shown in figure 3.2.2a. At the OBU (see figure 3.2.2b), the received signal is demodulated using a diode detector and then the signal conditioning unit produces TTL signal.

For the up-link, single-pole-double-throw (SPDT) as shown in figure 3.2.2a switches the CW signal so that it is transmitted on right-hand circular polarisation. At the OBU (see figure 3.2.2b) the received CW is PSK modulated by a 1MHz DPSK signal and re-radiated back at the RSU. At the RSU the signal is synchronously demodulated using an image rejection mixer (IRM).

Power

According to the CEPT recommendation the maximum 'Effective Isotropic Radiated Power' (EIRP) for the 5.8 GHz frequency is 2W average.

Communication Mode

For a two-way communication there are two ways of exchanging information between the RSU and the OBU, namely

1. Half Duplex: Data is transmitted in both directions but not at the same time and
2. Duplex: Data is transmitted in both directions simultaneously.

The duplex mode requires an oscillator to be used for the OBU which increases the size

and cost of the OBU significantly. Consequently half-duplex or talk-and-listen mode has been employed.

Bit Error Rate

To obtain a secure communication for financial transaction it is necessary to have a raw bit error rate of 10^{-6}. With an error detection and correction coding a bit error rate of 10^{-9} can be achieved.

Circular Polarisation

Circular Polarisation can offer the following advantages:

1. the orientation of the OBU on the windscreen and the RSU mounting is not critical and
2. the problem associated with multipath reflections between the metallic vehicle bonnet and the OBU is reduced as the hand of CP is reversed on reflection.

The principle of realisation of circular polarisation antennae is discussed in detail in chapter 4.

Communication Zone and Range

The required length of the communication zone does depend on the speed of vehicle and the amount of data rate required to be transmitted between the RSU and the OBU. A 6m x 4.5m communication zone is recommended which allows a time of 135ms for the transmission of required data when the speed of the vehicles is 160km/hr. The height of the antenna on a typical mounting is normally in the range 4m to 7m and to achieve a communication zone of 6m the required range for the communication should be of the order 7-15m.

Bandwidth

For down-link the data is Manchester encoded at a data rate of 250kbps and therefore the required bandwidth is 1MHz, centred at the 5.8GHz carrier frequency. For up-link the data rate is 250kbps which PSK modulates the 1MHz sub-carrier. The required bandwidth is 1MHz centred at the frequencies of 5.8GHz±1MHz.

Frequency Spacing

In a multi-lane situation it is necessary to ensure that the antenna patterns of the two RSU's do not overlap in order to avoid destructive interference at the OBU. Three channels can be accommodated within a 10 MHz bandwidth. Consequently it is possible to have a channel spacing of 3 MHz with the following centre frequencies:

channel 1: 5.797 GHz
channel 2: 5.800 GHz
channel 3: 5.803 GHz

The frequency spectrum of each channel for down and up-links with respect to the three frequencies is shown in figure 3.2.3. In addition the 5.805 - 5.815 GHz frequency band is available for the multi-lane applications and the corresponding centre channel frequencies are:

channel 4: 5.806 GHz
channel 5: 5.809 GHz
channel 6: 5.812 GHz

The above centre frequencies have been chosen to ensure that inter-modulation products of the three lower channels do not fall into the RSU receive bandwidth of the upper channel.

3.2.1 Specification of Down-Link Operation

Modulation

ASK modulated signal is transmitted by the RSU and this signal is demodulated by means of a diode detector thus making the OBU design simple and inexpensive.

Data Encoding

For synchronous transmission clock information must be contained within the transmitted data regardless of its actual content and hence a 'self-clocking' data encoding is used as it contains good clock information, for example, Manchester encoding.

Down-link Budget

The fixed losses for the down-link are given below:

Loss due to windscreen and weather:	2dB
OBU acceptance angle:	3dB
RSU acceptance angle:	3dB
Losses due to switches, two-branch coupler, cable and connectors:	2dB
Total fixed loss:	L_D = 10dB

The power received at the OBU is given by (Schwartz,1981):

$$P_R = \frac{P_T G_T G_R}{L_D}\left(\frac{\lambda_o}{4\pi R}\right)^2 \quad \text{(W)} \qquad (3.2.1)$$

where P_T is the power transmitted from the RSU. G_T, G_R are the gain of the transmit and receive antennae respectively. R is the communication range between the RSU and the OBU. λ_o is the wavelength in air and L_D is the total fixed losses. Equation (3.2.1) can be modified into the form of

$$P_R = P_T + G_T + G_R - L_D + 20\log_{10}\left(\frac{\lambda_o}{4\pi}\right) - 20\log_{10} R \quad \text{(dBm)} \qquad (3.2.2)$$

where G_T, G_R and L_D are in dB and P_T is in dBm. The maximum transmitted EIRP for the 5.8GHz systems is 2W while the EIRP for the 2.45GHz system is 100mW. The link parameters are given as

Frequency	P_T	G_T	G_R	L_D	λ_o
2.45GHz	4dBm	16dBi	5dBi	10dB	122.4mm
5.8GHz	17dBm	16dBi	5dBi	10dB	51.7mm

where the gain of the antenna (in dBi) is with respect to an isotropic point source. Hence the power received at the OBU becomes

$$P_R = -(25.23+20\log_{10}R)\text{dBm} \quad \text{for 2.45GHz and} \tag{3.2.3}$$

$$P_R = -(19.71+20\log_{10}R)\text{dBm} \quad \text{for 5.8GHz} \tag{3.2.4}$$

Equation (3.2.3) and (3.2.4) have been plotted as shown in figure 3.2.4 to determine the range (R) for both 2.45GHz and 5.8GHz systems.

For the down-link using ASK modulation to obtain a bit error rate BER = 10^{-6} it can be shown that (see chapter 7) the minimum required input power P_r is given by:

$$P_r = (P_{TSS} + 5.3) \text{ dBm} \tag{3.2.5}$$

The typical value of Tangential Signal Sensitivity (P_{TSS}) of the diode detector is -50dBm and hence the required received power at the OBU should be at least -44.7dBm. From figure 3.2.4 it can be seen for P_R = -44.7dBm, the obtained range is 10m for the 2.45GHz system and 18m for the 5.8GHz system.

Effect of the RSU Antenna's Side-lobe Level

The side-lobe level of the RSU antenna should be as low as possible otherwise, depending on the height of the RSU mounting, the projection angle of the antenna and the sensitivity of the RSU receiver (for down-link), or the OBU receiver (for up-link), communication nulls can be produced. Based on the polar pattern of the 4×4 planar antenna array (see chapter 6), the received power levels at the OBU as a function of the horizontal distance on the road from the RSU have been determined (see Appendix A). For the geometry of the RSU mounting as shown in figure 3.2.5, figure 3.2.6 shows that a good communication zone of about 6.9m long for the projection angle of 60° can be achieved. It is also shown that the communication nulls are produced by the RSU antenna side-lobes in the range of 0 to 3.5m.

3.2.2 Requirement of Up-Link Operation

Modulation

In order to reduce the contribution of flicker noise (i.e. low frequency noise) of the mixer diodes a sub-carrier is used at the frequency of 1MHz. This frequency is high enough to suppress the noise to a negligible level and readily available from CPU clock. The modulation of the microwave carrier by the 1MHz sub-carrier can either be amplitude or phase

modulation. The modulation of the 1MHz sub-carrier can either be DPSK, FSK or ASK. The DPSK (NRZI) modulation is used for the 1MHz sub-carrier as it does not contain a DC signal and it is easier to decode.

Coherent detection requires a reference carrier which is synchronised in both frequency and phase to the received signal. This means that carrier recovery needs to be carried out before signal detection. The reference carrier can be made available by splitting the local oscillator and coupling the output to the mixer at the RSU. For coherent detection of a SSB signal it is necessary for a reference carrier to have the same frequency but not necessarily in phase. For coherent detection of a DSB signal however it is necessary that the reference carrier has the same frequency and be in phase with the received signal and is a problem for this application, as the phase of the reflected signal is continuously changing due to the motion of a vehicle.

The received DSB-SC modulated signal (x_r) at the RSU can be expressed as

$$x_r = e^{\pm j[\omega_c t - \omega_L t + \Phi(R)]} + e^{\pm j[\omega_c t + \omega_u t + \Phi(R)]} \tag{3.2.6}$$

where
$$\Phi(R) = 2\pi R/\lambda_o + \theta \tag{3.2.7}$$

The reference carrier voltage of the local oscillator (u_{LO}) is

$$u_{LO} = e^{\pm j\omega_c t} \tag{3.2.8}$$

where ω_c = the angular frequency of the carrier,
$\omega_c - \omega_L$ = the angular frequency of the lower side-band of carrier,
$\omega_c + \omega_u$ = the angular frequency of the upper side-band of carrier,
R = the range between the RSU and the OBU,
$\Phi(R)$ = the phase shift between the reference r.f. signal and the returned r.f. signal from a moving vehicle,
θ = the fixed phase difference between the reference r.f. signal and the returned r.f. signal at the OBU, and
λ_o = the wavelength in air.

After synchronous demodulation using a double balanced mixer followed by low pass filtering, the output (Y) becomes:

$$Y = 2\cos(\omega_u t + \Phi(R)) + 2\cos(\omega_L t - \Phi(R)) = 4\cos\omega_m t \cos(\frac{2\pi R}{\lambda_o} + \theta) \qquad (3.2.9)$$

where $\omega_m = \omega_L = \omega_u = 2\pi \times 10^6$ (sub-carrier frequency).

As can be seen communication nulls (or a standing wave pattern) are produced since the magnitude of sub-carrier varies due to the cosine term when OBU is travelling to RSU. It is therefore not possible to use a double balanced mixer to demodulate the DSB signal.

One way of overcoming this problem is to use an Image Rejection Mixer (IRM) (Murphy,1990) which is shown in figure 3.2.7. The received signal is split into I and Q-channels. The I-channel signal is mixed directly with the reference signal from the LO and the Q-channel signal is mixed with the reference signal after it has been phase-shifted by 90°. Each of the I and Q-channel outputs is band-pass filtered (BPF) and amplified separately. Then the Q-channel output is phase shifted by 90° before being combined with the I-channel signal. The I-channel output is

$$Y_I = u_{LO} x_r = e^{\pm j[\omega_u t + \Phi(R)]} + e^{\pm j[\omega_L t - \Phi(R)]} \qquad (3.2.10)$$

and the Q-channel output is

$$Y_Q = \left(u_{LO} e^{-j\frac{\pi}{2}}\right) * x_r = e^{\pm j\left[\omega_u t + \Phi(R) - \frac{\pi}{2}\right]} + e^{\pm j\left[\omega_L t - \Phi(R) + \frac{\pi}{2}\right]} \qquad (3.2.11)$$

Hence the output of the IRM is

$$Y = Y_I + \left(Y_Q e^{-j\frac{\pi}{2}}\right) = 4\cos[\omega_L t - \Phi(R)] \qquad (3.2.12)$$

Equation 3.2.12 shows that now magnitude of lower side-band of the sub-carrier which contains information is independent of the distance (R) between the OBU and the RSU.

Consequently it is possible to demodulate a DSB signal using an IRM to recover the data transmitted for the up-link transmission. Full design of the IRM is given in chapter 8.

Up-link Budget

The fixed losses are given below:

Loss due to windscreen and weather:	4dB
OBU acceptance angle:	6dB
RSU acceptance angle:	6dB
Conversion Loss (maximum) of PSK modulator:	8dB
Losses due to switches, two-branch coupler, cable and connectors:	2dB
Total loss:	$L_U = 26$dB

The power received at the OBU is given by

$$P_R = \frac{P_T (G_T G_R)^2}{L_u} \left(\frac{\lambda_o}{4\pi R} \right)^4 \quad \text{(W)} \qquad (3.2.13)$$

or expressed in decibel form

$$P_R = P_T(dBm) + 2G_T(dB) + 2G_R(dB) - L_u(dB) + 40\log_{10}\left(\frac{\lambda_o}{4\pi}\right) - 40\log_{10} R \quad \text{(dBm)} \quad (3.2.14)$$

Similarly, the power received at the RSU becomes:

$P_R = -(60.46+40\log_{10}R)$dBm for 2.45GHz and (3.2.15)

$P_R = -(62.43+40\log_{10}R)$dBm for 5.8GHz (3.2.16)

For the PSK coherent detection, in order to obtain BER = 10^{-6}, the S/N at the output of the IRM should be better than 10.6dB (Shanmugam,1979). The block diagram of the PSK coherent detection using an IRM is shown in figure 3.2.8 where

F_1 ($1/G_1$=Cable Loss):	0.5dB
F_2 (LNA Noise Figure):	1dB
F_3 (Conversion Loss of IRM):	8dB (approx.)
G_2 (LNA Gain):	30dB
Bandwidth:	500kHz

The input signal power to the receiver can be expressed as

$$S_i = F\left(\frac{S}{N}\right)_{o/p} N_i \qquad (3.2.17)$$

where

$$F = F_1 + \frac{F_2 - 1}{G_1} + \frac{F_3 - 1}{G_1 G_2} \qquad (3.2.18)$$

$N_i = kTB = 1.38*10^{-23} * 290 * 500kHz = -117dBm$. Therefore, $S_i = 1.5dB + 10.6dB + (-117dBm) = \underline{-104.9dBm}$. From the graph in figure 3.2.9 it can be seen that the maximum range of the system is 12.9m for the 2.45GHz and 11.5m for the 5.8GHz.

Effect of the RSU Antenna's Side-lobe Level

For the down-link, the received power levels at the RSU as a function of the horizontal distance on the road from the OBU have been calculated. In figure 3.2.10 it is shown that a good communication zone of about 4.5m long for the projection angle of 60° of the RSU antennae can be obtained. It is also shown that the communication nulls are produced by the side-lobes of the RSU's antenna in the range of 0 to 3.5m.

Comparison of Losses for Direct and Sub-Carrier Modulation Schemes

To reduce the flicker noise of the mixer diodes a sub-carrier is employed to modulate the microwave carrier. It is therefore necessary to compare the losses produced by direct modulation with that produced by sub-carrier modulation. The analysis assumes that the up-link modulation scheme uses BPSK on the 5.8GHz carrier and DPSK on the 1MHz sub-carrier and the data rate is 250kbps. Data modulated onto the sub-carrier is DPSK and the NRZ-I encoding scheme is used. Data which directly modulates the carrier uses FM0 encoded. It is shown that the extra signal loss is only 0.6dB when using a sub-carrier as compared with loss produced by direct modulation.

Data Modulated on a Sub-Carrier

The Fourier coefficient, C_n , obtained from the Fourier analysis of the 1MHz sub-carrier wave (see figure 3.2.11) is given by

$$C_n = B\left(\frac{\sin\frac{n\pi}{2}}{\frac{n\pi}{2}}\right) \tag{3.2.19}$$

where B is the peak amplitude of the 1MHz sub-carrier square wave signal

A 1MHz sub-carrier will contain the fundamental, the third, the fifth etc. harmonics. When using BPSK onto the carrier, the power in the carrier is suppressed and all the energy is in the sidebands. Some power will be lost in the higher harmonics. The relation between the power content of the fundamental and the total power is given by

$$\frac{P_f}{P_{total}} = \frac{\frac{B^2}{2}\left(\frac{\sin\frac{\pi}{2}}{\frac{\pi}{2}}\right)^2}{\sum_{n=1,3,5...}^{\infty}\frac{B^2}{2}\left(\frac{\sin\frac{n\pi}{2}}{\frac{n\pi}{2}}\right)^2} = \frac{8}{\pi^2} = 0.81 \tag{3.2.20}$$

where P_f is the power in the fundamental frequency and P_{total} is the total power in the sidebands.

This shows that 81% of the power is contained within the fundamental frequency. The sub-carrier is then modulated using DPSK & NRZ-I encoding. The spectrum of the DPSK & NRZI signal (see figure 3.2.12) can be expressed as:

$$V(f) = AT_b\left(\frac{\sin\pi fT_b}{\pi fT_b}\right) \tag{3.2.21}$$

where A is the peak amplitude of data signal (±A) and T_b is the bit time (4us). The energy contained in the main lobe (E) (in the frequency between $-1/T_b$ and $1/T_b$):

$$E = \frac{(AT_b)^2}{2} \int_{-1/T_b}^{1/T_b} \left(\frac{\sin \pi f T_b}{\pi f T_b} \right)^2 df = \frac{A^2 T_b}{2\pi} \int_{-\pi}^{\pi} \left(\frac{\sin x}{x} \right)^2 dx \qquad (3.2.22)$$

The total energy of the data pulse is

$$E_{total} = \frac{(AT_b)^2}{2} \int_{-\infty}^{\infty} \left(\frac{\sin \pi f T_b}{\pi f T_b} \right)^2 df = \frac{A^2 T_b}{2\pi} \int_{-\infty}^{\infty} \left(\frac{\sin x}{x} \right)^2 dx \qquad (3.2.23)$$

and

$$\frac{E}{E_{total}} = \frac{\int_{-\pi}^{\pi} \left(\frac{\sin x}{x} \right)^2 dx}{\int_{-\infty}^{\infty} \left(\frac{\sin x}{x} \right)^2 dx} = \frac{2.835}{\pi} = 0.90 \qquad (3.2.24)$$

where the above equation has been evaluated using numerical methods.

The result of using the sub-carrier is that the useful power will be 0.81*0.90=0.729 which is -1.3dB of the total power. If SSB demodulation is used (using an IRM to demodulate the DSB signal) another 3dB will be lost, giving -4.3dB total conversion loss.

Data Modulated Directly on the Carrier

If data is modulated directly onto the carrier, it will not be favourable to use NRZ-I encoding because the spectrum will then be centred on the carrier. If FM0 is used, its spectrum (see figure 3.2.13) which is the same as Manchester encoding is symmetric around the microwave carrier. The main lobe will be between 0 and 500kHz (and an image between 0 and -500kHz). The spectrum can be expressed as:

$$V(f) = jAT_b \left(\frac{\sin \frac{\pi f T_b}{2}}{\frac{\pi f T_b}{2}} \right) \sin \frac{\pi f T_b}{2} \qquad (3.2.25)$$

The energy contained in the main lobe (E) above the carrier:

$$E = \frac{1}{2}\int_0^{2/T_b} |V(f)|^2 df = \frac{A^2 T_b}{\pi}\int_0^{\pi} \frac{\sin^4 x}{x^2} dx = \frac{A^2 T_b}{\pi} 0.672 \qquad (3.2.26)$$

The total energy:

$$E_{total} = \frac{1}{2}\int_0^{\infty} |V(f)|^2 df = \frac{A^2 T_b}{\pi}\int_0^{\infty} \frac{\sin^4 x}{x^2} dx = \frac{A^2 T_b}{\pi}\left(\frac{\pi}{4}\right) \qquad (3.2.27)$$

The ratio of E to the total energy E_{total} can be calculated as:

$$\frac{E}{E_{total}} = 0.672 * \frac{4}{\pi} = 0.856 \quad (-0.68dB) \qquad (3.2.28)$$

The result of modulating data directly onto the carrier is that the useful power (within a 500kHz band) will be -0.68dB of the total power. If SSB demodulation is used, another 3dB will be lost, giving -3.7dB total loss.

Two modulation schemes have been considered. The first is BPSK modulation on the carrier and DPSK on the 1MHz sub-carrier. The second one is to modulate FM0 encoded data directly onto the carrier using BPSK modulation. It is found that if SSB demodulation is used the sub-carrier scheme will lose 4.3dB of the total power while if data is modulated onto the carrier 3.7dB is lost, producing only a difference in loss of 0.6dB.

3.3 Summary

The specification of communication link between the RSU and the OBU has been discussed. For down-link operation, ASK with Manchester encoding was employed. For up-link operation, SSB and DSB can be employed. Using DSB modulation it is possible to have a simple circuit at the OBU but then an IRM is required at the RSU. This can prevent the signal loss due to the motion of vehicle.

The link budget for the down and up-link operations has also been shown. Having defined the requirements of bit error rate and the type of modulation, the required signal-to-noise ratio and the received power level can be determined. The communication range can then be determined by using the budget link equations. The effect of the RSU's antenna on the

communication zone has also been discussed. It is important for the antenna to have a low side-lobe in order to ensure a good communication zone.

Finally a comparison of losses using direct and sub-carrier modulation schemes has been presented. If an IRM is used the sub-carrier scheme will lose 4.3dB while if data is modulated onto the carrier 3.7dB is lost. Since the flicker noise of the mixer diodes can be reduced when using a sub-carrier scheme, such a scheme should be employed in this communication system. Consequently the improvement in sensitivity by reducing the flicker noise is obtained by using a sub-carrier.

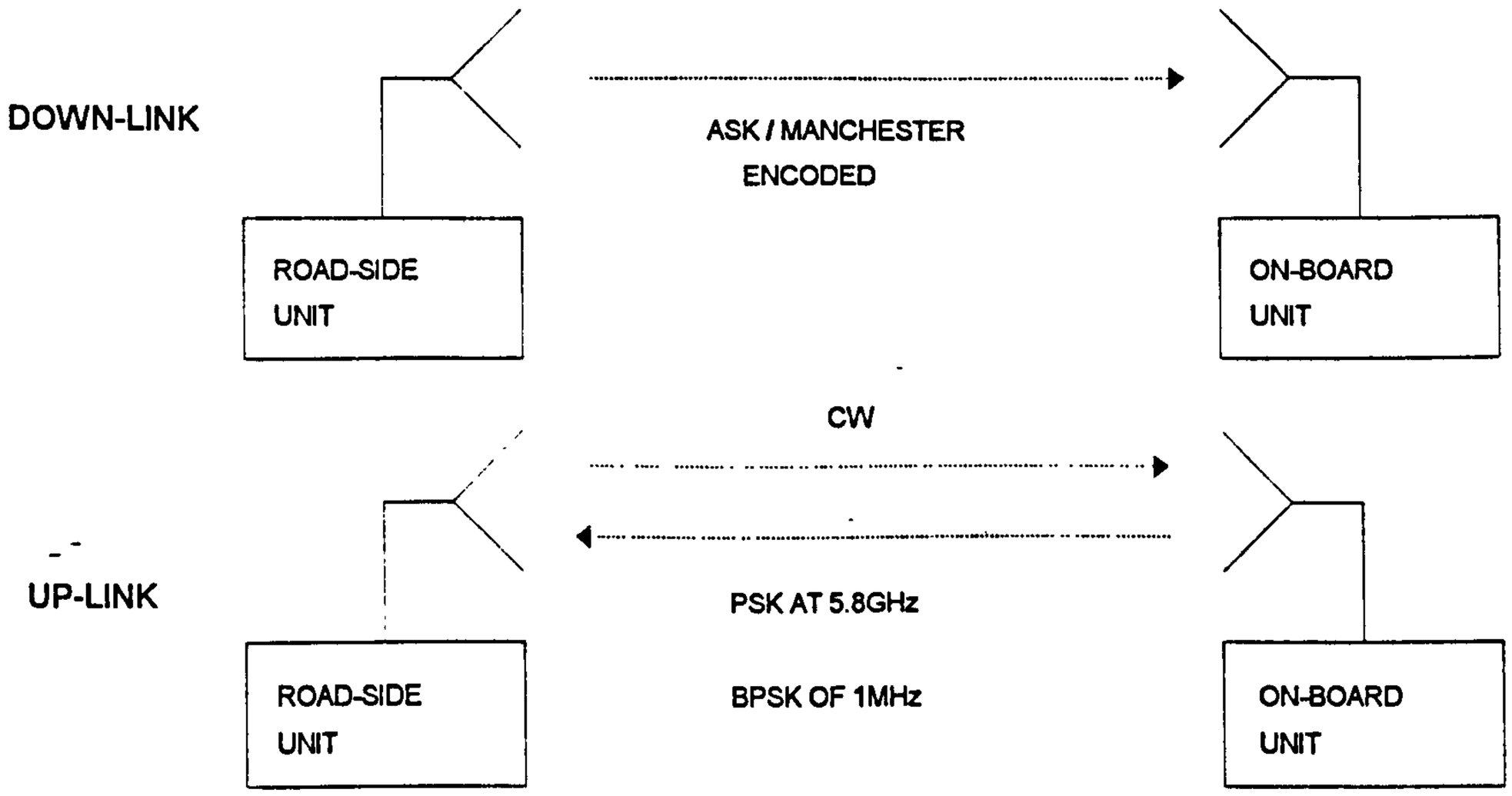

CIRCULAR POLARIZATION AT ROAD-SIDE AND ON-BOARD UNITS

Figure 3.2.1 Talk and Listen Two-Way Communication System

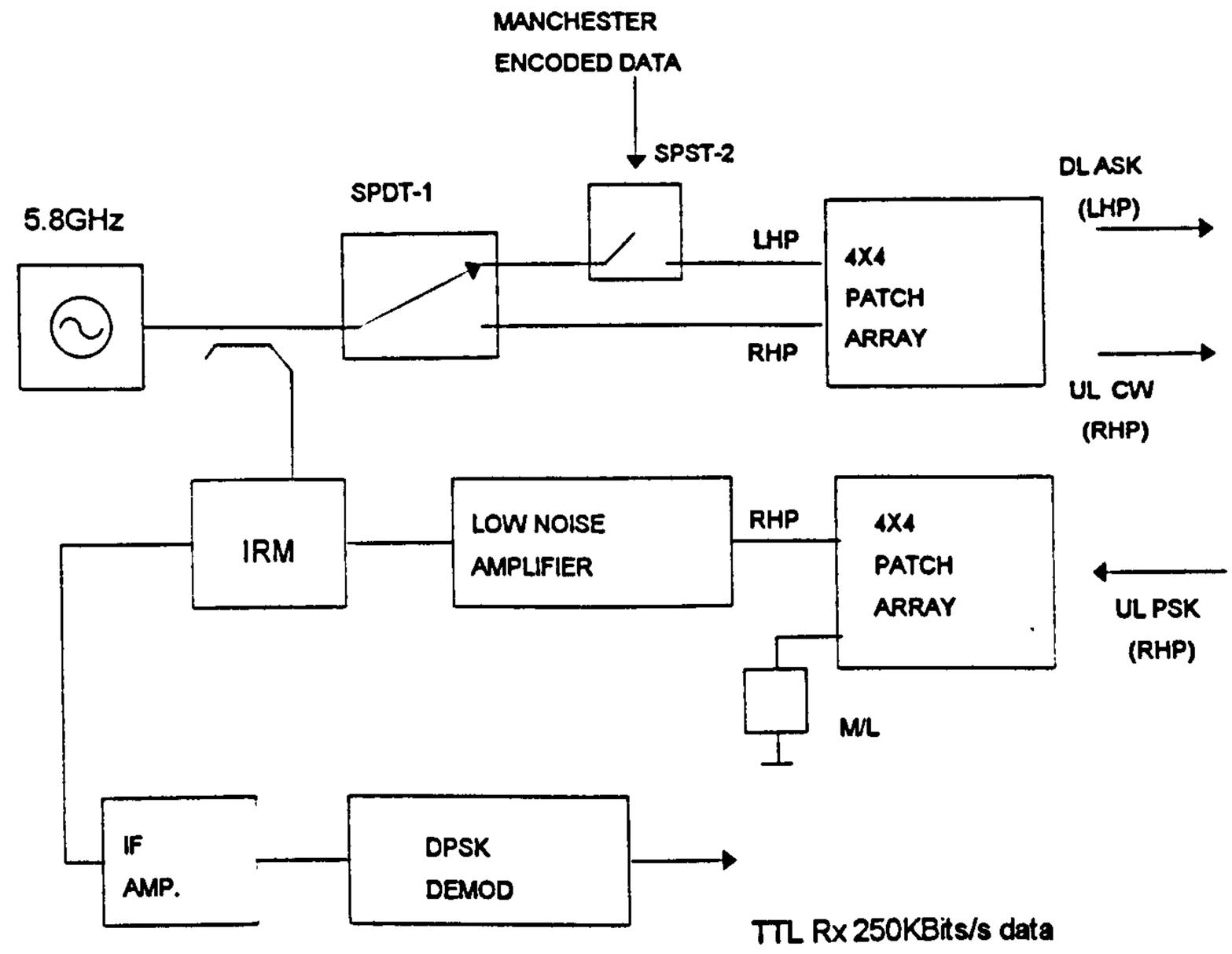

Figure 3.2.2a Block Diagram of the Road-Side Unit (RSU)

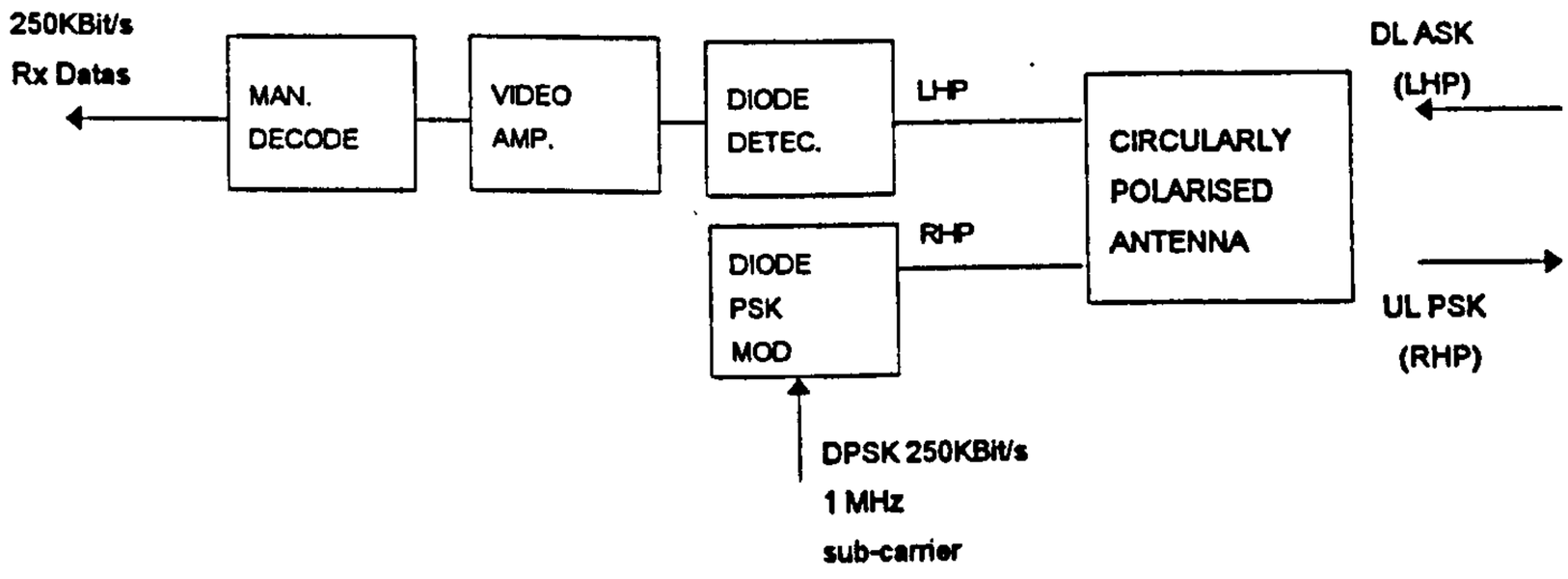

Figure 3.2.2b Block Diagram of the On-Board Unit (OBU)

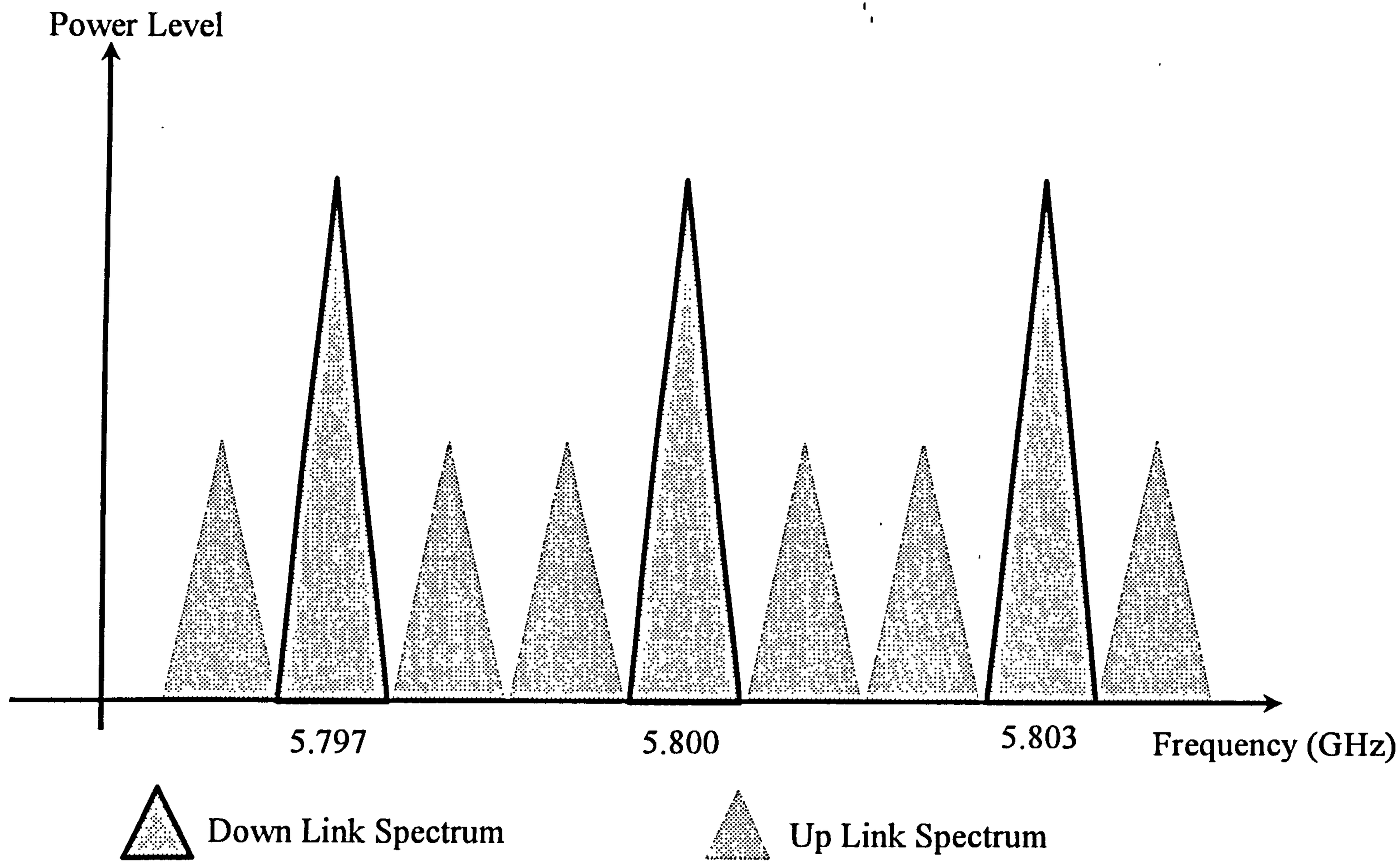

Figure 3.2.3 Frequency Spectrum of Each Channel for Down and Up-Links

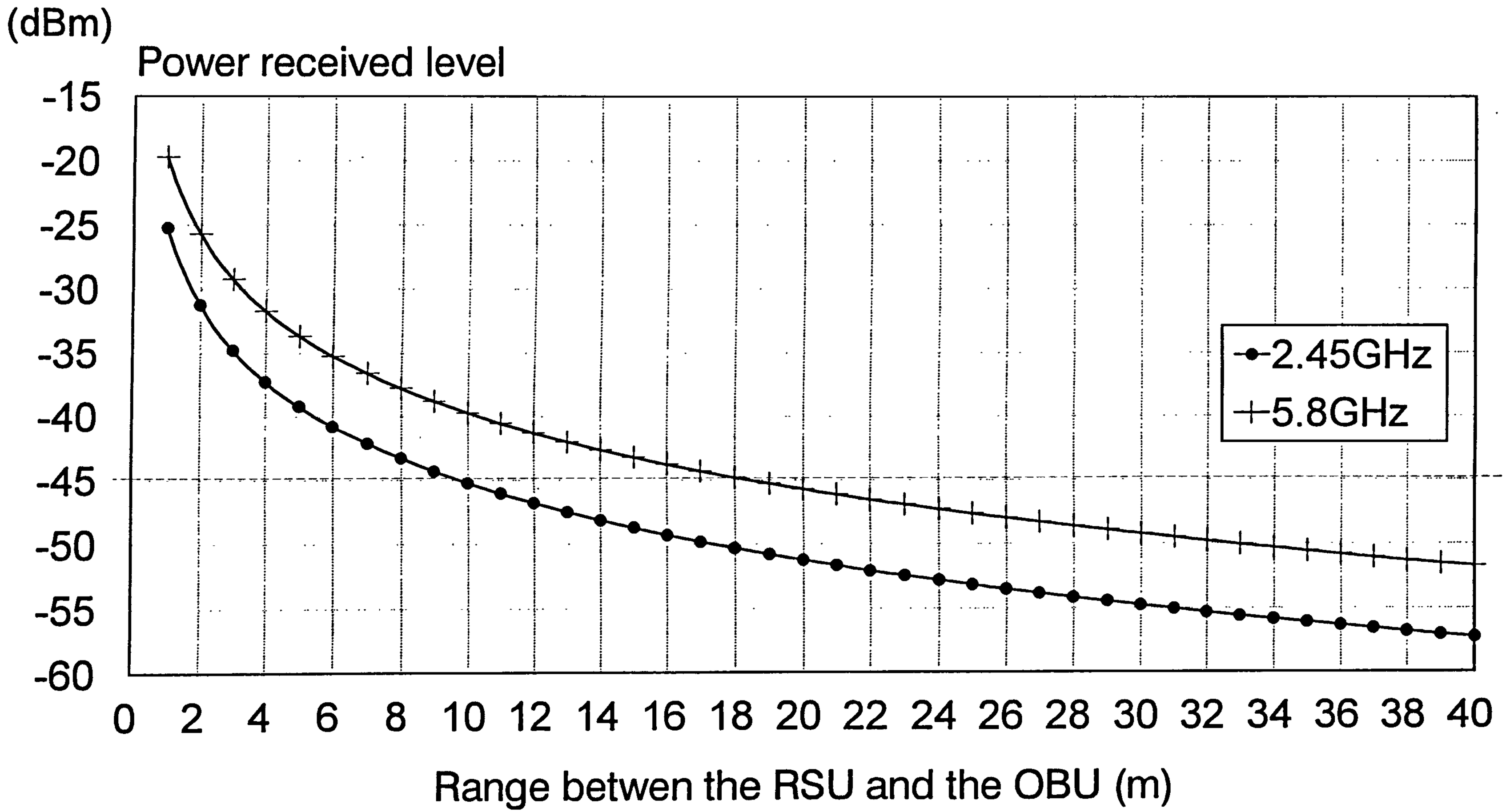

Figure 3.2.4 Down link Budget

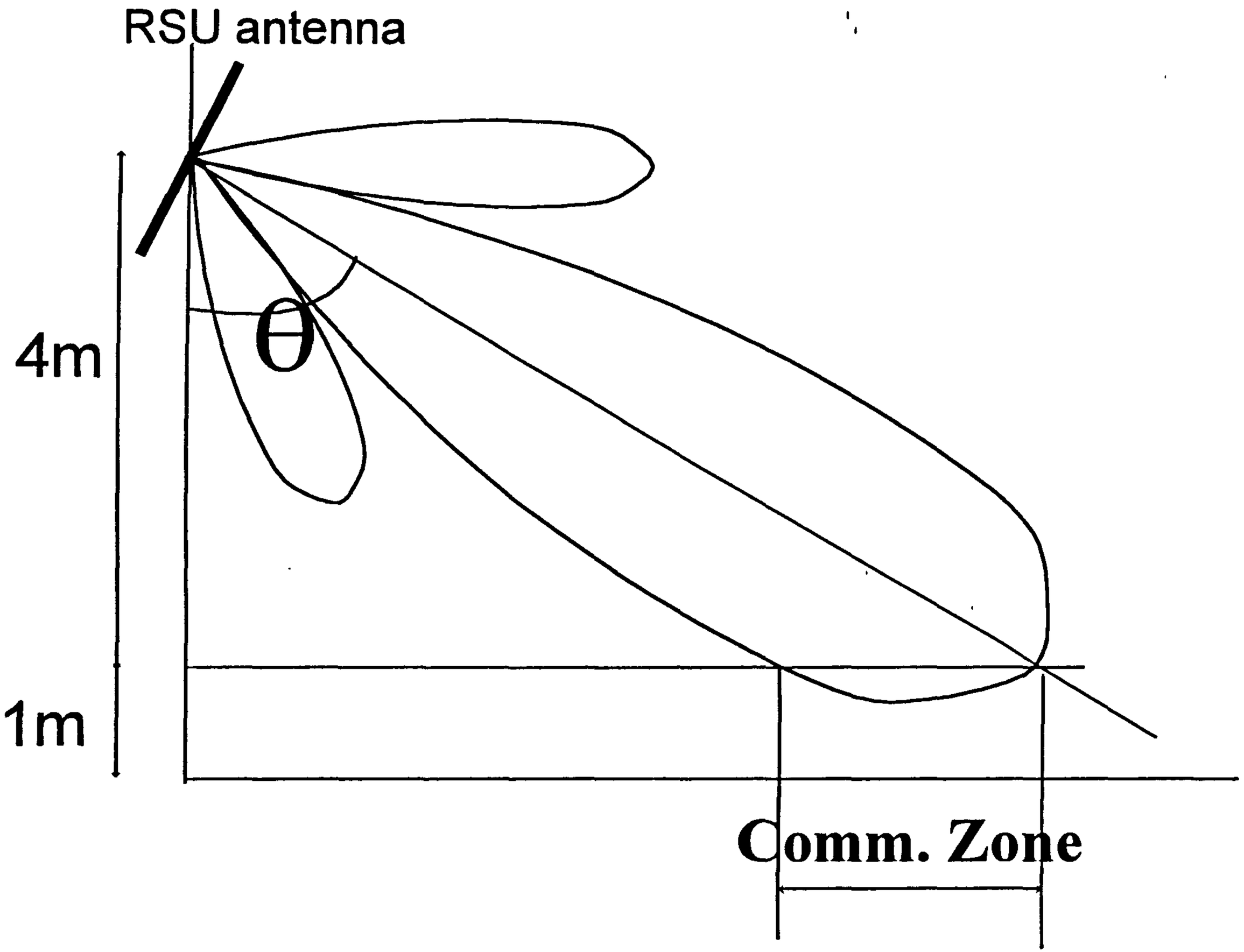

Figure 3.2.5 Geometry of the RSU antenna mounting

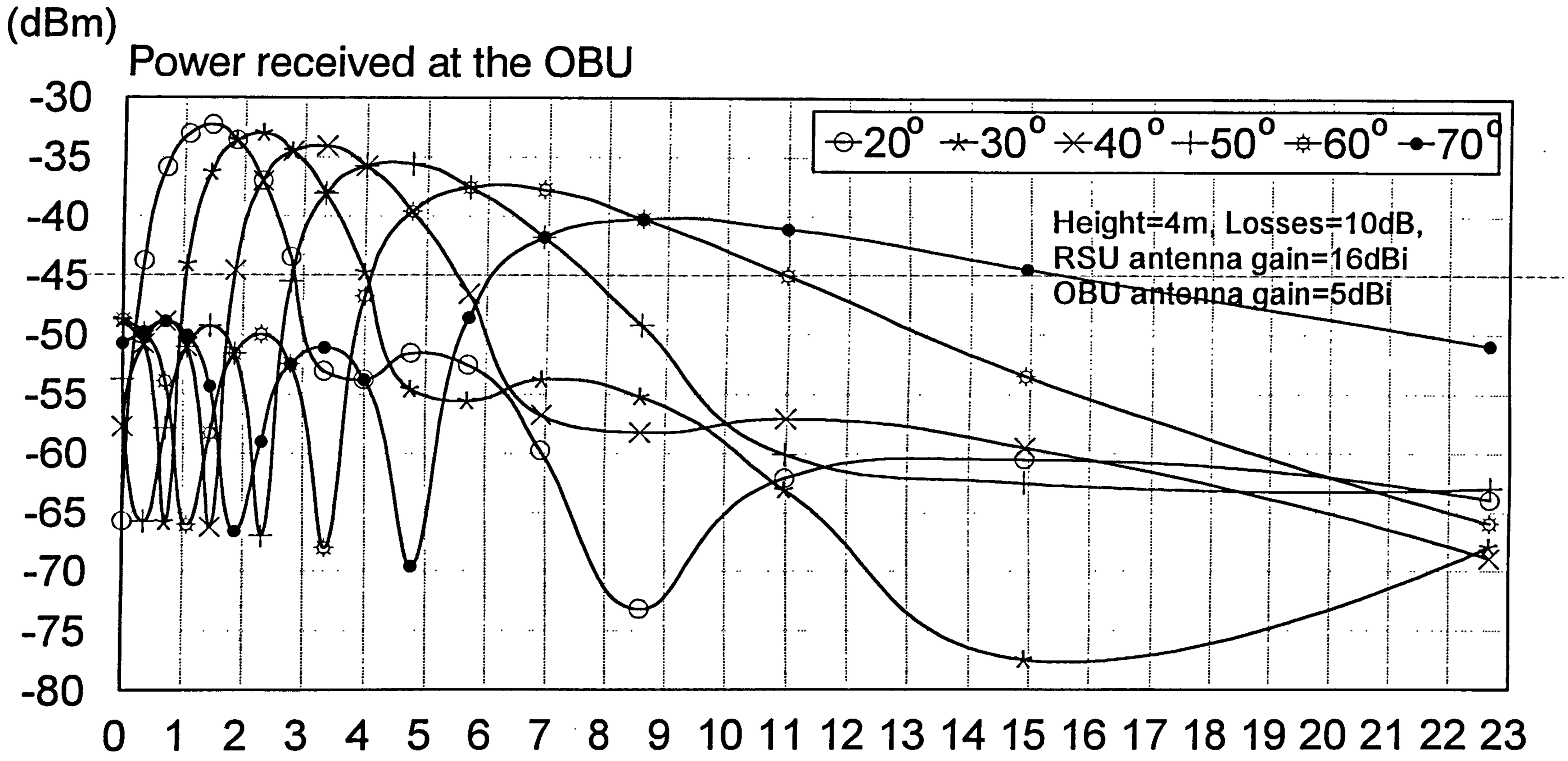

FIgure 3.2.6 Power received at the OBU (Downlink)

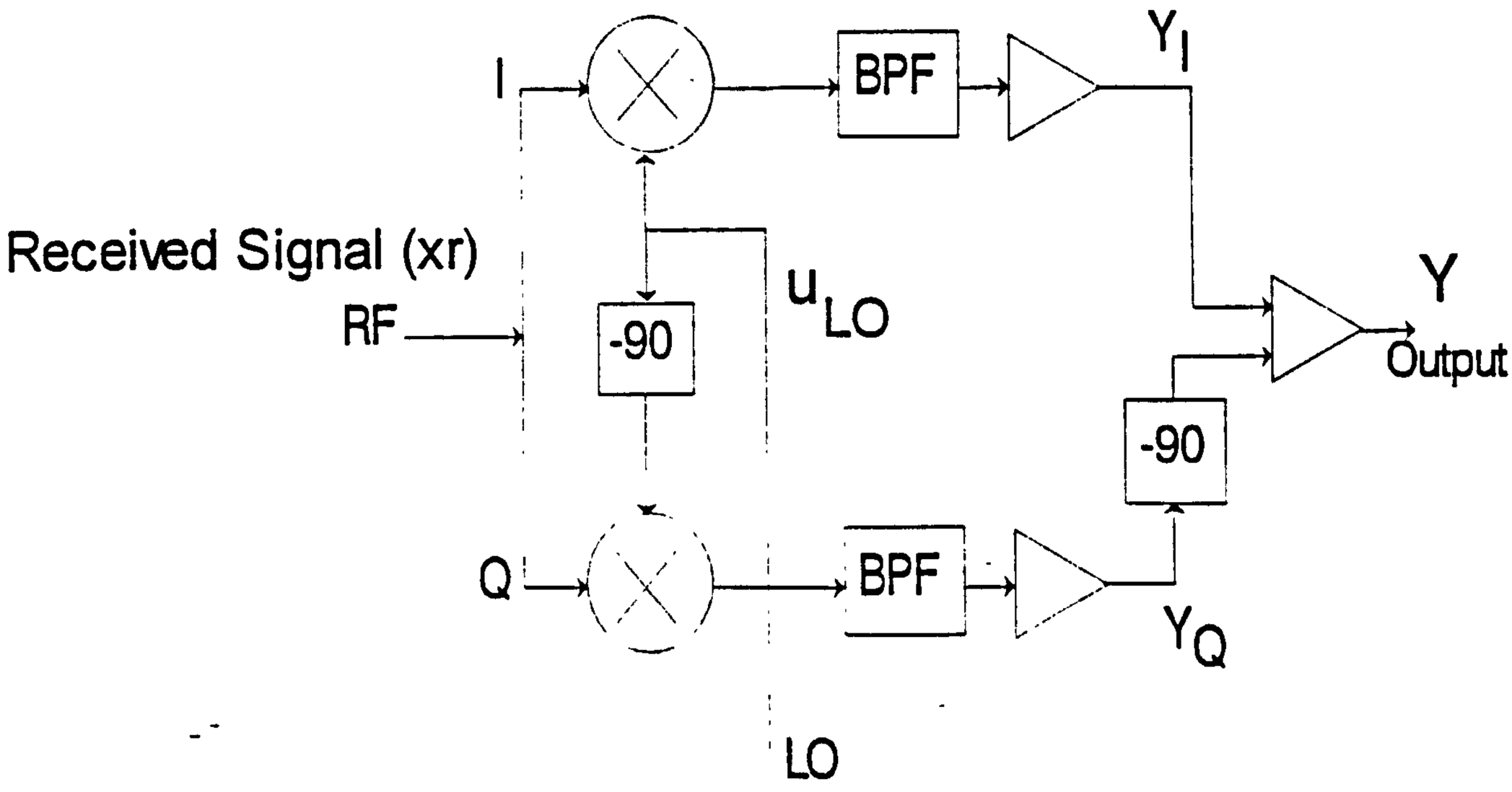

Figure 3.2.7 Image Rejection Mixer

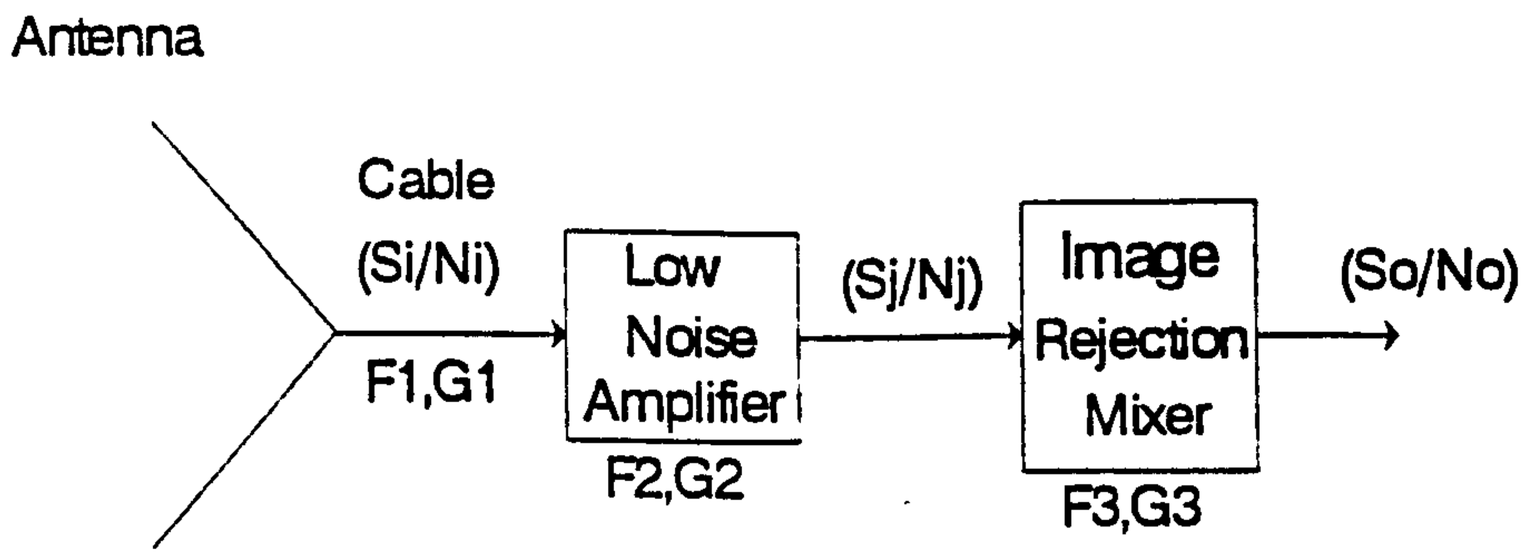

Figure 3.2.8 RSU Receiver

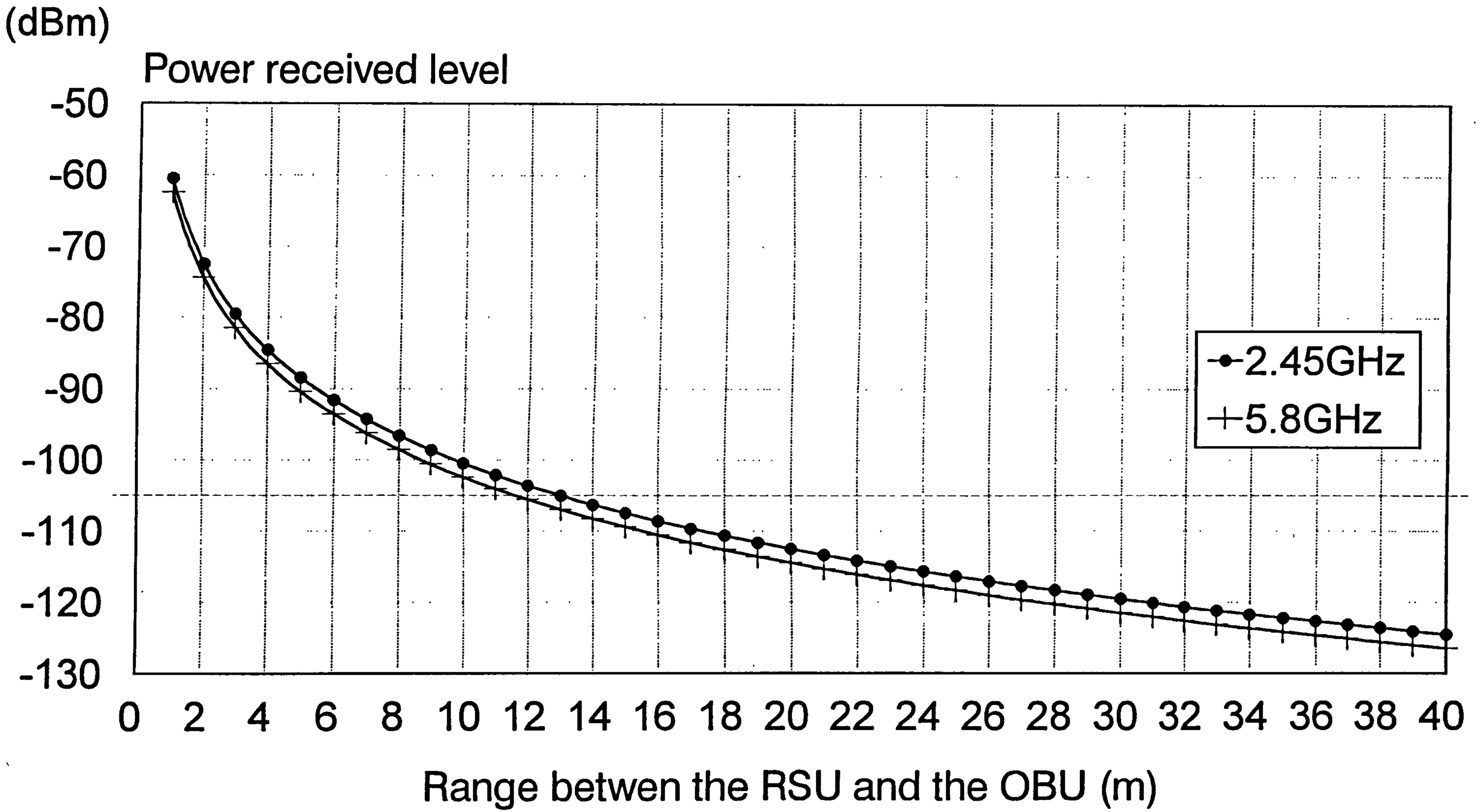

Figure 3.2.9 Up link Budget

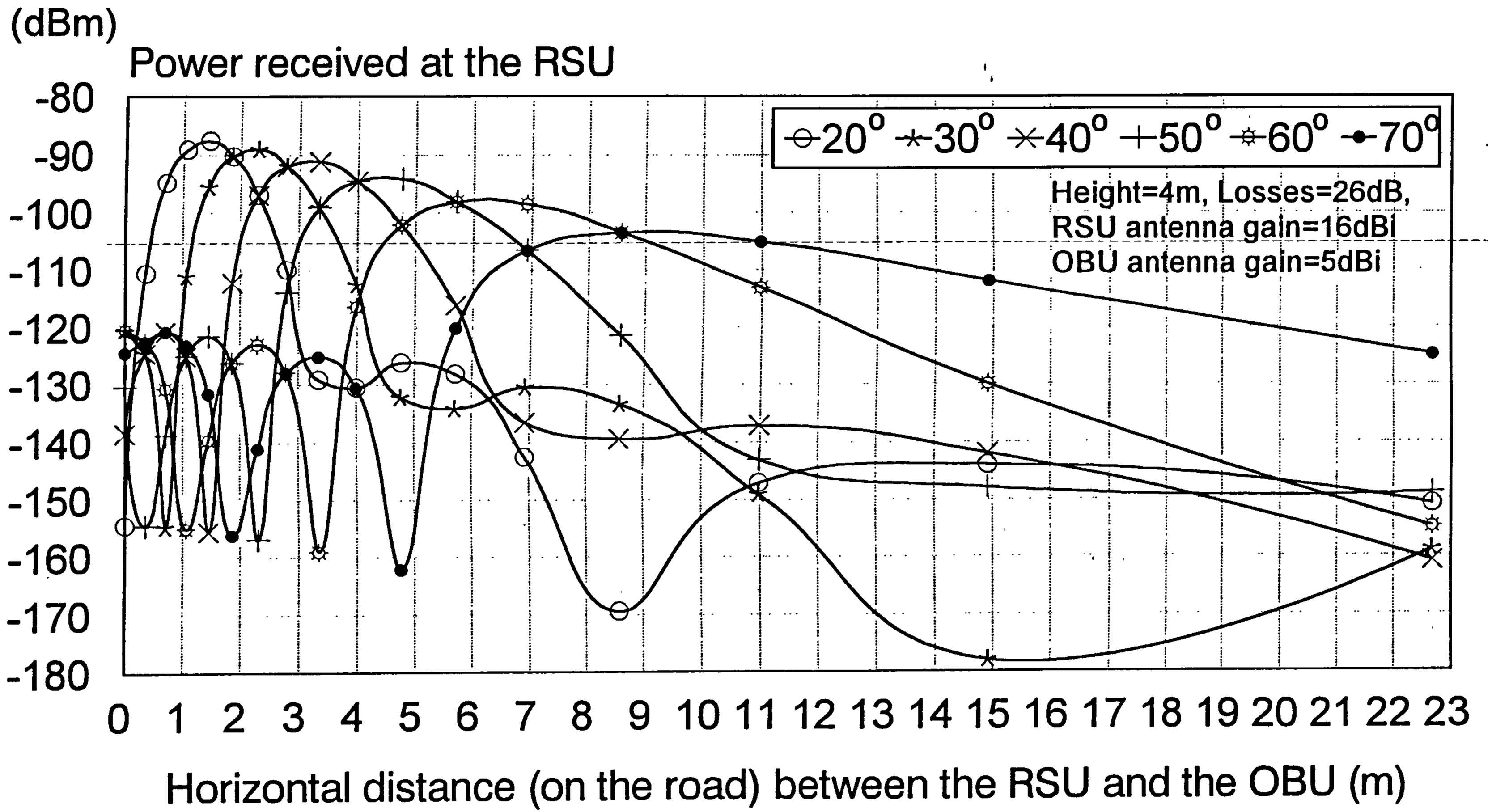

FIgure 3.2.10 Power received at the RSU (Uplink)

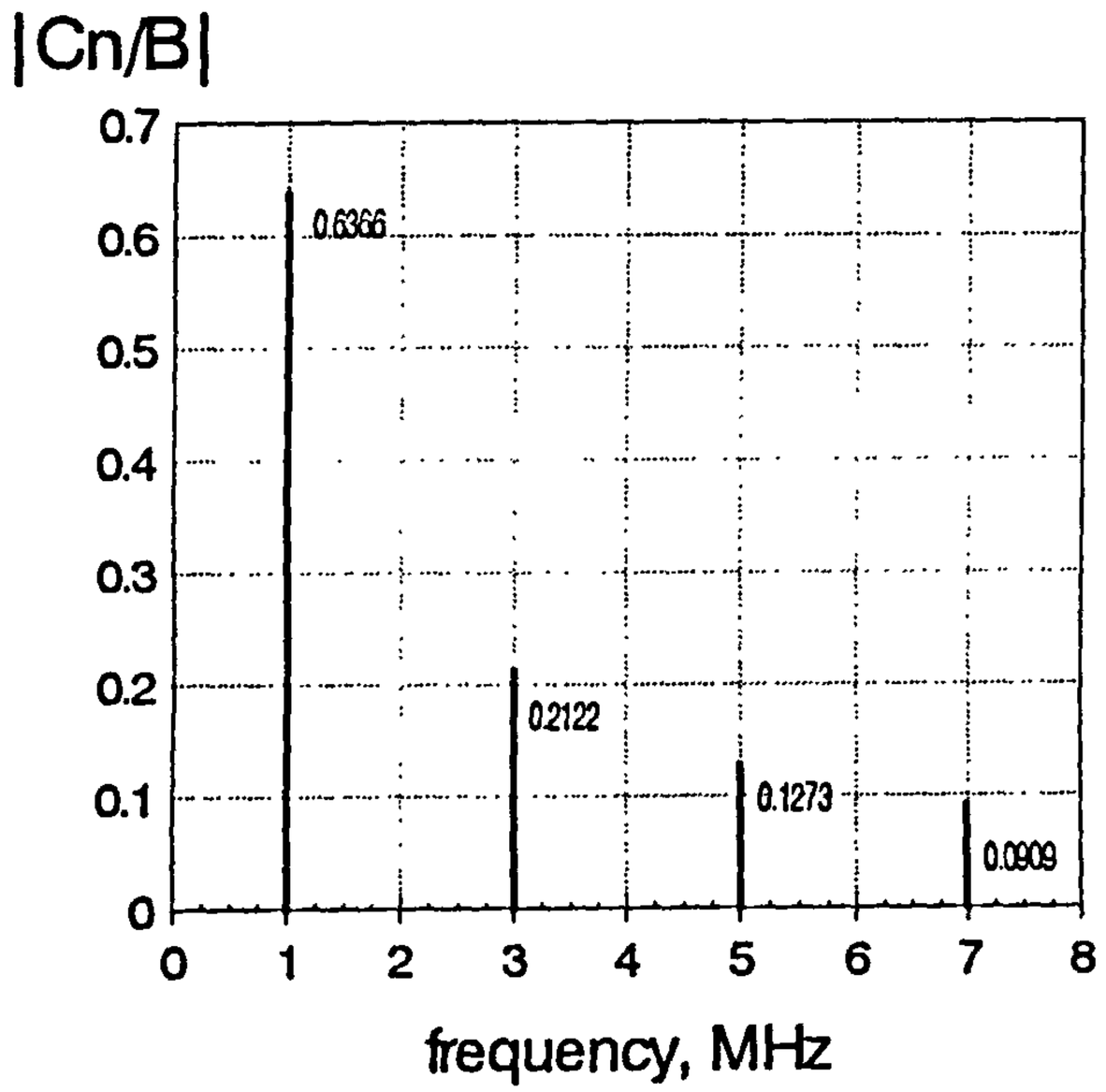

Figure 3.2.11 Plain subcarrier harmonics

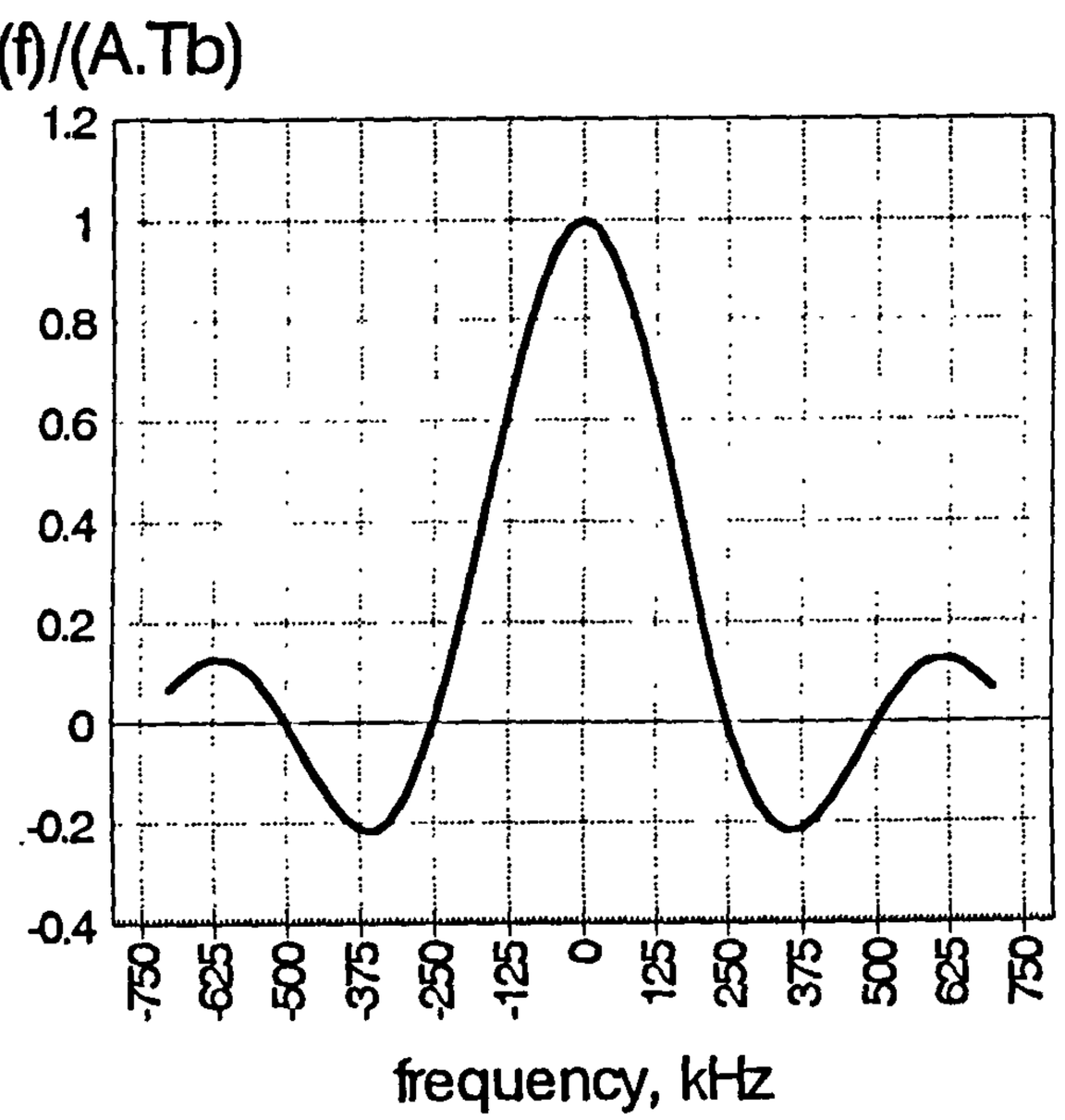

Figure 3.2.12 Spectrum of DPSK modulated with NRZ-I encoded random data

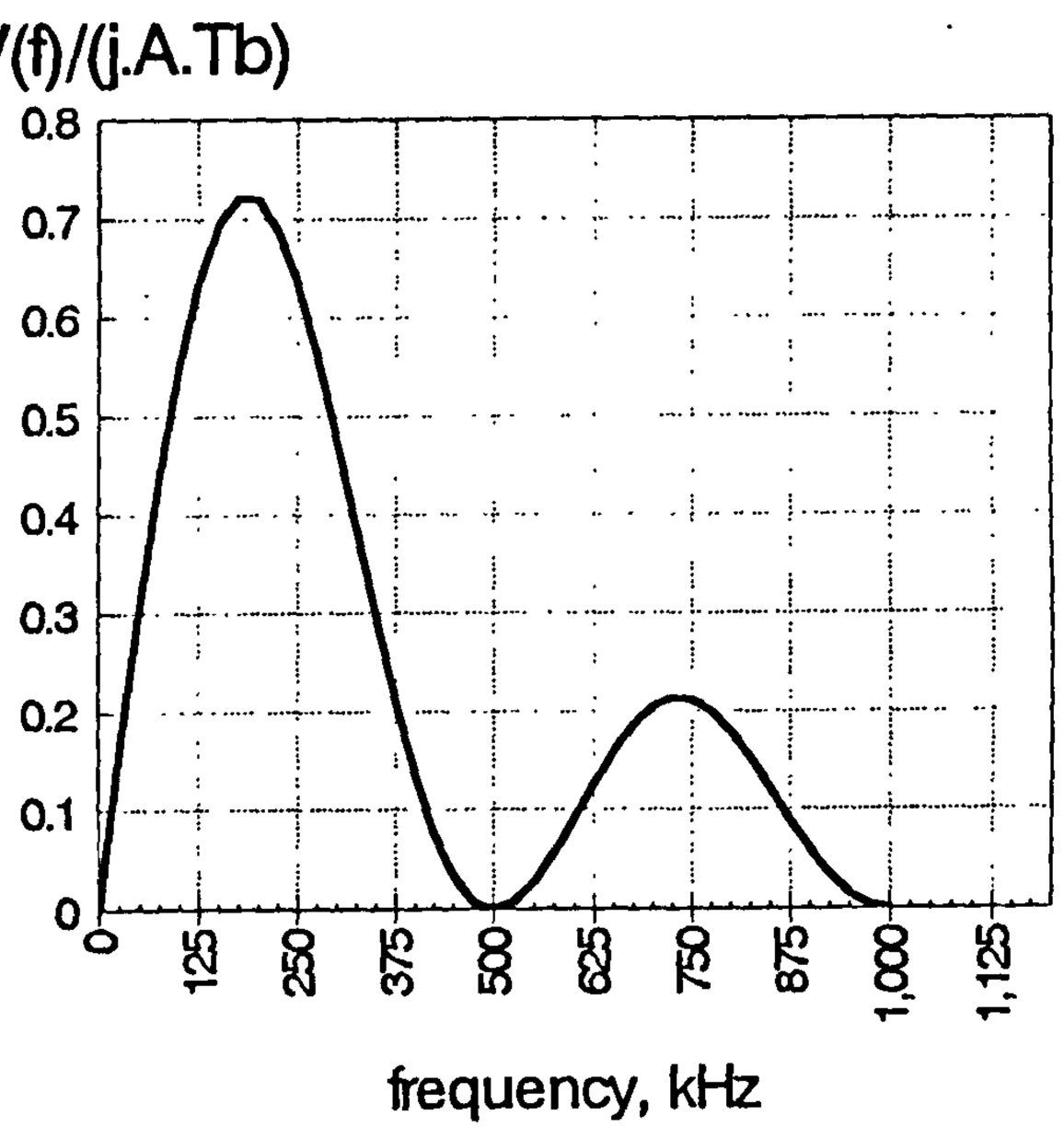

Figure 3.2.13 Manchester encoded spectrum

CHAPTER 4

Review of Patch Antenna's Parameters and Design

4.1 Introduction

This chapter initially reviews the theory of a linearly polarised single patch microstrip antenna using first a simple transmission line model and secondly an improved transmission line model (TLM). The improved model includes the effect of mutual coupling between two main radiating slots and the radiation from side wall. There is a good agreement between the predicted and practical results. Finally, the theory, analysis and design of a circularly polarised antenna is also presented.

4.2 Review of Design Methods and Models

Radiation from a microstrip antenna occurs through the fringing fields connecting the edges of microstrip antenna conductor and the ground plane. Radiation from discontinuities in a microstrip was first examined by Lewin (1960). In his analysis the effect of radiation on the overall Q-factor is described as a function of resonator dimensions, operating frequency, relative dielectric constant and thickness of the substrate. His results showed that at high frequencies the radiation loss is much larger than conductor and dielectric losses. It was also confirmed that open-circuited microstrip lines radiate more power for thick and low dielectric constant substrates.

In figure 4.2.1 it is assumed that there is no variation of the electric field along the width and the thickness of the microstrip structure. With only the fundamental (0,1) mode being excited the electric field configuration of the rectangular (or square) patch antenna can be represented as shown in figure 4.2.2. The fields vary along the patch length which is approximately half a wavelength. Radiation may be ascribed chiefly to the fringing fields at the open-circuited edges of the patch. The fringing fields can be resolved into normal and tangential components with respect to the ground plane where the normal components are out of phase because the electrical length of the patch line is one half a wavelength. The tangential components (those parallel to the ground plane) are in phase, and the resulting fields combine to give a maximum radiated field normal to the surface of the structure i.e. the broadside direction.

4.2.1 Comparison of the Transmission-Line Models (TLM)

Simple TLM

The patch may be represented by two slots half a wavelength apart excited in phase and radiating in the space above the ground plane and the transmission line model is shown in figure 4.2.3. This model neglects the mutual coupling between the two main radiating slots. The rectangular patch is represented by a transmission line with a characteristic admittance Y_C, a propagation constant γ and a physical length L. The self admittance ($Y_S = G_S + jB_S$) are terminated at both open-ends of the patch. The real part G_S of the self admittance Y_S represents the radiation effect and the imaginary part B_S models the stored energy in the extra line length. The accuracy of the model depends on the choice of the expressions for G_S and B_S. In the original model proposed by Munson (1974) approximate expressions for G_S and B_S are given below based on the work presented by Harrington (1961):

$$\text{Self-Conductance } G_s \approx \frac{\pi}{\lambda_o \eta_o}\left[1-\frac{(\beta_o \delta L)^2}{24}\right]W \tag{4.2.1}$$

$$\text{Self-Susceptance } B_s \approx \left[\frac{3.135-2\ln(\beta_o \delta L)}{\lambda_o \eta_o}\right]W \tag{4.2.2}$$

where W is the width of the patch, and δL is the line extension of the open-end of the patch given by Hammerstad (1975)

$$\delta L = \frac{0.412h(\varepsilon_{re}+0.3)\left(\frac{W_{eff}}{h}+0.264\right)}{(\varepsilon_{re}-0.258)\left(\frac{W_{eff}}{h}+0.8\right)} \tag{4.2.3}$$

Van de Capelle (1989) also derived simple expressions for G_S and B_S as shown below:

$$\text{Self-Conductance } \quad G_s \approx \frac{\beta_o \varepsilon_{re} W}{2\eta_o}\left(1-\frac{s^2}{24}\right) \tag{4.2.4}$$

$$\text{Self-Susceptance} \quad B_s \approx -\frac{\beta_o \varepsilon_{re} W}{\pi \eta_o}\left[\left(\ln\frac{s}{2}+C_e-\frac{3}{2}\right)\left(1-\frac{s^2}{24}\right)+\frac{s^2}{288}\right] \qquad (4.2.5)$$

where $s=\beta_0\delta L$ (normalised slot width) and $C_e=0.577216$ (Euler's constant) and ε_{re} is the effective permitivity given by

$$\varepsilon_{re} = \frac{\varepsilon_r+1}{2}+\frac{\varepsilon_r-1}{2}\left[1+\frac{12h}{W_{eff}}\right]^{-\frac{1}{2}} \quad \text{for} \quad \frac{W_{eff}}{h}>1 \qquad (4.2.6)$$

James(1981) derived the expression for radiation conductance in the form

$$G_s = \frac{1}{120\pi^2}F_2\left(\frac{2\pi}{\lambda_o}W_{eff}\right) \qquad (4.2.7)$$

where

$$F_2(x) = xSi(x)-2\sin^2\left(\frac{x}{2}\right)-1+\frac{\sin x}{x} \qquad (4.2.8)$$

and the effective width is given by

$$W_{eff} = W+\frac{t}{\pi}\left(1+\ln\frac{2h}{t}\right) \quad \text{for} \quad \frac{W}{h}>0.159 \qquad (4.2.9)$$

These equations can be replaced by one of three approximate equations, depending on the antenna width:

$$G_s = \frac{W_{eff}^2}{90\lambda_o^2} \quad \text{for} \quad W_{eff}<0.35\lambda_o \qquad (4.2.10a)$$

$$G_s = \frac{W_{eff}}{120\lambda_o}-\frac{1}{60\pi^2} \quad \text{for} \quad 0.35\lambda_o \le W_{eff} \le 2\lambda_o \qquad (4.2.10b)$$

$$G_s = \frac{W_{eff}}{120\pi^2} \quad \text{for} \quad W_{eff}>2\lambda_o \qquad (4.2.10c)$$

The self-susceptance is given by

$$B_s = Y_c \tan\left(\frac{2\pi}{\lambda_g}\delta L\right) \tag{4.2.11}$$

where

$$Y_c = \frac{\sqrt{\varepsilon_{re}} W_{eff}}{120\pi h} \tag{4.2.12}$$

The input admittance can be expressed as

$$Y_i = \frac{Y_s^2 + Y_c^2 + 2Y_s Y_c \coth \gamma L}{Y_s + Y_c \coth \gamma L} \tag{4.2.13}$$

where Y_C is the characteristic impedance of the patch and $\gamma = \alpha + j\beta$, the propagation constant; $\alpha = 0.5\beta_o \sqrt{\varepsilon_{re}} \tan\delta$ and $\beta = \beta_o \sqrt{\varepsilon_{re}}$.

Improved TLM

Figure 4.2.4 and 4.2.5 show the four-slot aperture model and its equivalent circuit proposed by Pues (1984). In the circuit Y_s is the self admittance of the open-end terminations of the patch and Y_m is the mutual admittance between two radiating slots. Mutual coupling is represented by voltage-dependent current sources. The input admittance is given by:

$$Y_i = \frac{Y_s^2 + Y_c^2 - Y_m^2 + 2Y_s Y_c \coth \gamma L - 2Y_m Y_c \operatorname{csc} h \gamma L}{Y_s + Y_c \coth \gamma L} \tag{4.2.14}$$

The mutual admittance discussed in this chapter is a special case where the two radiating slots are placed in E-plane orientation in line. For the arbitrary horizontal and vertical displacements for the two radiating slots, new expressions for the mutual admittance have been derived and are fully discussed in chapter 5.

To model the parasitic effects of the feed line the self-admittance of the open-end termination facing the feed line is reduced by a factor

$$r = 1 - \frac{W_m}{W_{eff}} \tag{4.2.15}$$

where W_m is the width of the microstrip feed line and W_{eff} is the effective width of the patch. The antenna input admittance is thus given by

$$Y_i' = Y_i - \frac{W_m}{W_{eff}} Y_s = Y_i + (r-1)Y_s$$

$$= rY_s + \frac{Y_c^2 - Y_m^2 + Y_s Y_c \coth \gamma L - 2Y_m Y_c \operatorname{csc} h \gamma L}{Y_s + Y_c \coth \gamma L} \qquad (4.2.16)$$

The self susceptance B_S is given by

$$B_s = Y_c \tan\left(\beta_o \sqrt{\varepsilon_{re}}\, \delta L\right) \qquad (4.2.17)$$

where δL is the open-end extension of the patch and given by (Kirschning,1981):

$$\delta L = \frac{h \xi_1 \xi_3 \xi_5}{\xi_4} \qquad (4.2.18)$$

where

$$\xi_1 = 0.434907 \left(\frac{\varepsilon_{re}^{0.81} + 0.260}{\varepsilon_{re}^{0.81} - 0.189} \right) \left(\frac{\left(\frac{W}{h}\right)^{0.8544} + 0.236}{\left(\frac{W}{h}\right)^{0.8544} + 0.870} \right) \qquad (4.2.18a)$$

$$\xi_2 = 1 + \frac{\left(\frac{W}{h}\right)^{0.371}}{2.358\varepsilon_r + 1} \qquad (4.2.18b)$$

$$\xi_3 = 1 + \frac{0.5274 \arctan\left[0.084 \left(\frac{W}{h}\right)^{1.9413/\xi_2} \right]}{\varepsilon_{re}^{0.9236}} \qquad (4.2.18c)$$

$$\xi_4 = 1 + 0.0377 \arctan\left[0.067 \left(\frac{W}{h}\right)^{1.456} \right] \left(6 - 5e^{0.036(1-\varepsilon_r)} \right) \qquad (4.2.18d)$$

$$\xi_s = 1 - 0.218e^{-7.5W/h} \tag{4.2.18e}$$

The self conductance G_S is given by

$$G_s = \frac{1}{\pi\eta_o}\left[\left(wSi(w) + \frac{\sin w}{w} + \cos w - 2\right)\left(1 - \frac{s^2}{24}\right) + \frac{s^2}{12}\left(\frac{1}{3} + \frac{\cos w}{w^2} - \frac{\sin w}{w^3}\right)\right] \tag{4.2.19}$$

where $w=\beta_o W_{eff}$ and $s=\beta_o \delta L$ are the normalised slot length and slot width. The equation does not include the effect of surface waves and is acceptable (James,1989) for $\beta_o h\sqrt{\varepsilon_r} \le 0.3$. The mutual admittance $Y_m=G_m+jB_m$ (Pues,1983) can be written as

$$G_m = G_s F_g K_g \tag{4.2.20}$$

$$B_m = B_s F_b K_b \tag{4.2.21}$$

where G_S and B_S are self admittance. F_g and F_b are coupling functions expressing the ratio between the per-unit-length mutual admittance and the per-unit-length self admittance of two infinite-length TE-excited slot radiators. K_g and K_b are correction functions which are introduced to take into account the finite length of the main slots and the influence of the side slots. Their expressions are given by

$$F_g = J_o(l) + \frac{s^2}{24 - s^2} J_2(l) \tag{4.2.22a}$$

$$F_b = \frac{\pi}{2} \frac{Y_o(l) + \frac{s^2}{24 - s^2} Y_2(l)}{\ln\frac{s}{2} + C_e - \frac{3}{2} + \frac{s^2/12}{24 - s^2}} \tag{4.2.22b}$$

$$K_g = 1 \tag{4.2.22c}$$

$$K_b = 1 - e^{-0.21w} \tag{4.2.22d}$$

where $l = \beta_o L_e$ = normalised centre distance between the slots. $J_i(x)$ and $Y_i(x)$ are the ith-order Bessel functions of the first and second kind respectively; C_e = 0.577216... is the

Euler's constant. In section 4.2.4 a comparison of different models will be made to determine the input impedance of a patch antenna.

4.2.2 Antenna Parameters

Radiation Pattern

The radiation pattern can be found by treating the antenna as an aperture (see figure 4.2.6). Since the feed lines are chosen to excite only a TEM-mode the y-component of the electric field at the aperture can be assumed constant. The far-field radiation pattern for one of the radiation slots is given with (Balanis,1982):

$$E_r \approx 0$$
$$E_\theta \approx 0$$

$$E_\phi \approx -j\frac{\beta_o h E_o W}{2\pi r} e^{-j\beta_o r}\left[\sin\theta \frac{\sin\left(\frac{h\beta_o \sin\theta\cos\phi}{2}\right)}{\frac{h\beta_o \sin\theta\cos\phi}{2}} \frac{\sin\left(\frac{W\beta_o\cos\theta}{2}\right)}{\frac{W\beta_o\cos\theta}{2}}\right] \qquad (4.2.23)$$

For a thin substrate, $\beta_o h \ll 1$, so to a good approximation the above expression can be written as

$$E_\phi \approx -j\frac{V_o\, e^{-j\beta_o r}}{\pi r}\sin\left(\frac{\beta_o W\cos\theta}{2}\right)\tan\theta \qquad (4.2.24)$$

The radiation pattern for a patch antenna (i.e. two slots) is obtained on multiplying E_ϕ by the array factor. The 2-element array factor along y-axis is

$$AF_y = 1+e^{j\beta_o l\sin\theta\sin\phi} = 2e^{j\frac{\beta_o l}{2}\sin\theta\sin\phi}\cos\left[\frac{\beta_o l}{2}\sin\theta\sin\phi\right], \qquad (4.2.25)$$

and therefore the polar pattern for a single patch is given by

$$E_\phi \approx -j\frac{2V_o}{\pi r}\, e^{-j\beta_o r} e^{-j\frac{\beta_o l}{2}\sin\theta\sin\phi}\sin\left(\frac{\beta_o W\cos\theta}{2}\right)\tan\theta\cos\left[\frac{\beta_o l}{2}\sin\theta\sin\phi\right] \qquad (4.2.26)$$

where $V_0=hE_0$ is the voltage across the slot.

Directivity and Antenna Gain (James,1981)

The directivity (D) is defined as the maximum power density at a range r, divided by the average power density at the same distance r. The maximum power density (P_{max}) is given by

$$P_{\max} = \frac{\left(E_{\phi,\max}\right)^2/2}{120\pi} = \frac{16V_o^2W^2}{8\lambda_o^2 120\pi} \tag{4.2.27}$$

where $E_{\phi,\max} = E_\phi$ ($\phi = 180°$ and $r = 1m$) and the average power density (P_{av}) is given by

$$P_{av} = \frac{\frac{V_o^2}{2}\cdot 2G_s}{4\pi r^2} = \frac{V_o^2 G_s}{4\pi} \tag{4.2.28}$$

where G_s is the self conductance (or radiation conductance) of the slot and therefore the directivity (D) is given by

$$D = \frac{P_{\max}}{P_{av}} = \frac{W^2}{15\lambda_o^2 G_s} \tag{4.2.29}$$

The antenna gain (G) is given by

$$G = \eta D \tag{4.2.30}$$

where η is the efficiency of the antenna.

Efficiency

The efficiency is defined as the radiated power divided by the total input power and is given by the ratio of radiation conductance to total conductance as

$$\text{efficiency} \quad \eta = \frac{G_s}{G_s + G_{diel} + G_{Cu}} \tag{4.2.31}$$

Dielectric and Copper Losses

The dielectric and copper loss conductances are given by

$$G_{diel} = \frac{\omega_o C}{Q_{diel}} \tag{4.2.32}$$

$$G_{Cu} = \frac{\omega_o C}{Q_{Cu}} \tag{4.2.33}$$

Q-factor and Bandwidth (James,1981,p.67-109)

The total Q-factor of the antenna is equal to the sum of the Q-factors of radiation, copper loss and dielectric loss. The Q-factor of radiation is given by

$$Q_{rad} = \frac{\pi}{4 Z_c G_s} \tag{4.2.34}$$

where Z_C is the characteristic impedance of the line. The formulas for Q-factors of dielectric loss and copper loss are independent of the antenna geometry and are given by

$$Q_{diel} = \frac{1}{\tan \delta} \tag{4.2.35}$$

$$Q_{Cu} = h\sqrt{\mu_o \pi f_r \sigma_c} \tag{4.2.36}$$

where tanδ is the loss tangent of dielectric substrate, σ_C is the bulk conductivity of the conductor and f is the resonant frequency of the antenna. The total Q-factor is therefore equal to

$$Q_{total} = \left(\frac{1}{Q_{rad}} + \frac{1}{Q_{diel}} + \frac{1}{Q_{Cu}} \right)^{-1} \tag{4.2.37}$$

If the antenna is assumed to be a simple tuned RLC circuit, the usable bandwidth of the antenna is given by

$$BW = 100 \frac{2|\rho|}{Q_{total}\sqrt{1-|\rho|^2}} \% \tag{4.2.38}$$

where ρ is the required input reflection coefficient of the patch antenna.

Capacitance of the Patch Antenna

The total capacitance (C) of a rectangular microstrip antenna can be found by summing the static capacitance with the dynamic capacitance of the two main radiating slots and the two side slots (Abbound,1988):

$$C = C_{o,dyn}(\varepsilon) + 2C_{e1,dyn}(\varepsilon) + 2C_{e2,dyn}(\varepsilon) \tag{4.2.39}$$

where $C_{o,dyn}(\varepsilon)$ is the dynamic capacitance of the patch without the fringing fields.

$$C_{o,dyn}(\varepsilon) = \frac{\varepsilon_o \varepsilon_r WL}{h\gamma_n \gamma_m} \tag{4.2.40}$$

For an antenna operating in the TM_{01} (m=0 & n=1) mode, γ_0=1 and γ_1=2.

$$C_{e1,dyn}(\varepsilon) = \frac{1}{2\gamma_n}\left[\frac{Z(W,h,\varepsilon_r = 1)}{cZ^2(W,h,\varepsilon_r)} - \frac{\varepsilon_o \varepsilon_r W}{h}\right]L \tag{4.2.41}$$

$$C_{e2,dyn}(\varepsilon) = \frac{1}{2\gamma_m}\left[\frac{Z(L,h,\varepsilon_r = 1)}{cZ^2(L,h,\varepsilon_r)} - \frac{\varepsilon_o \varepsilon_r L}{h}\right]W \tag{4.2.42}$$

and

$$Z(W,h,\varepsilon_r) = \frac{377}{\sqrt{\varepsilon_{re}(W)}}\left[\frac{W}{h} + 1.393 + 0.667\ln\left(\frac{W}{h} + 1.444\right)\right]^{-1} \tag{4.2.43}$$

$$\varepsilon_{re}(W) = \frac{\varepsilon_r + 1}{2} + \frac{\varepsilon_r - 1}{2}\left[1 + \frac{12}{W/h}\right]^{-1/2} \tag{4.2.44}$$

where $Z(W,h,\varepsilon_r)$ is the characteristic line impedance of the microstrip line with dimensions of W and h and $Z(W,h,\varepsilon_r=1)$ is the impedance on a substrate of relative dielectric constant equal to 1.

4.2.3 Measurement of Input Impedance and Resonant Frequency

Method (I)

The patch antenna is probe-fed. At resonance the input impedance at an arbitrary feed point a distance X from one end of the line resonator is strictly real and is given by (Derneryd,1978)

$$Z_{input}(x) = \frac{1}{2G_s}\left(\cos^2\beta x + \frac{G_s^2 + B_s^2}{Y_c^2}\sin^2\beta x - \frac{B}{Y_c}\sin 2\beta x\right) \tag{4.2.45}$$

where Y_C is the characteristic admittance and β is the propagation constant of a microstrip line of width W. Usually $G/Y_C \ll 1$ and $B/Y_C \ll 1$ and equation (4.2.45) simplifies to

$$\mathrm{Re}\left[Z_{input}(x)\right] = R_{input} = \frac{1}{2G_s}\cos^2\beta x \tag{4.2.46}$$

Z_{input} was measured by putting x=0. The SMA connector was then soldered directly to the edge of the patch on the other side of the substrate as shown in figure 4.2.7.

Method (II)

The antenna is now microstrip-fed instead of being probe-fed. The network analyser is first calibrated using the standard loads. Then the reference plane is moved from the end of the test cable of the network analyser to the edge of the patch. This can be done by using the same length as the antenna feed line and terminating in open or short circuit as shown in figure 4.2.8. However it is not recommended for use at higher frequency and for a lossy substrate since the reference plane cannot be established accurately due to the losses.

Method (III)

In order to match the high input impedance of a square, microstrip-fed patch antenna to 50Ω, the impedance of the quarter wavelength matching feed line is very high and hence the feed line is usually very narrow. To maintain this high impedance feed line and measure the corresponding input impedance of the patch antenna, a novel method of measurement is presented. The circuit board shown in figure 4.2.9 was fabricated. The equivalent circuit

consisting of two quarter-wave transformers is shown in figure 4.2.10. The input impedance Z_{ant} of the patch is given by

$$Z_{ant} = \left(\frac{Z_1}{Z_2}\right)^2 Z_{input} \qquad (4.2.47)$$

where Z_{ant} = Input impedance of the patch at resonance;
Z_{input} = Measured impedance at resonance;
Z_1 = the high impedance of the $\lambda/4$ feed line;
Z_2 = the 50Ω $\lambda/4$ line.

The test procedures are as follows:

1. Calibrate the network analyser;
2. Connect the SMA connector (see figure 4.2.11(b)) whose centre conductor was shortened and short-circuited in order to produce a more accurate reference plane (see figure 4.2.12);
3. Adjust the network analyser to establish the reference plane as shown in figure 4.2.12 for a short circuit condition;
4. Using the established reference plane the input impedance of the patch can then be determined.

4.2.4 Comparison Between Measured and Predicted Results

In order to test the accuracy of the design equations and the theory antennae have been constructed and tested on the low-loss microwave substrates. The dimensions of the patch antennae were checked with a travelling microscope. The substrate specifications are as follows:

1. RT/Duroid 5788,ε_r=2.20,h=0.785mm,t=0.018mm, tanδ=0.0012 max@10GHz,
2. RT/Duroid 5880,ε_r=2.20,h=1.570mm,t=0.018mm, tanδ=0.0012 max@10GHz,
3. RT/Duroid 5780, ε_r=2.33, h=0.79mm,t=0.0355mm, tanδ=0.0012 max@10GHz and
4. RT/Duroid 6010, ε_r=10.5, h=1.27mm,t=0.018mm, tanδ=0.0028 max@10GHz.

Input Impedance and Resonant Frequency

Patch antennae have been constructed and the input impedance and the resonant frequency have been measured. The measured results are then compared with the results

predicted for the Simple and the Improved TLMs as shown in Tables 4.2.1a-d. Because of the manufacturing accuracy, the results of the ±1.5% worst case tolerance analysis for the patch dimensions were obtained as shown in Table 4.2.1e.

Antenna	Substrate	L(mm)	W(mm)	W_m(mm)	L_m(mm)	W_f(mm)	L_f(mm)
#A	#1	33.15	33.17	0.47	18.71	2.40	18.50
#B	#2	39.90	39.90	1.06	22.04	4.85	21.97
#C	#2	70.02	70.02	1.08	37.86	4.85	38.68
#D	#3	16.18	16.18	0.19	9.12	2.34	9.04
#E	#4	18.37	48.98	0.20	11.77	1.15	11.78

Table 4.2.1(a) Antenna Dimensions

where L and W are the length and the width of the patch. L_m and W_m are the length and the width of the matching λ/4 line (for method (III), L_f and W_f are the length and the width of the 50Ω λ/4 feed line).

Simple Transmission-Line Model:

Antenna	Munson (1974)		Van de Capelle (1989)		James (1989)	
	Rin(Ω)	fr(GHz)	Rin(Ω)	fr(GHz)	Rin (Ω)	fr(GHz)
#A	172.1	2.990	86.5	2.872	382.1	3.025
#B	177.8	2.459	91.4	2.320	406.8	2.494
#C	171.5	1.417	86.1	1.363	379.9	1.433
#D	184.1	5.883	91.4	5.478	433.5	5.960
#E	120.6	2.538	17.2	2.110	218.9	2.450

Table 4.2.1(b) Simple TLM

Improved Transmission-Line Model:

Antenna	Pues (1984) For Ym=0 & Wm=0		Pues (1984) For Ym=0		Pues (1984)			
	Rin(Ω)	fr(GHz)	Wm(mm)	Rin(Ω) fr(GHz)	Wm(mm)	Ym(mS)	Rin(Ω)	fr(GHz)
#A	270.9	2.989	0.47	271.8 2.990	0.47	0.203-j0.339	244.2	2.994
#B	288.5	2.447	1.06	290.8 2.448	1.06	0.216-j0.356	257.4	2.453
#C	296.7	1.417	1.08	270.8 1.417	1.08	0.202-j0.337	243.2	1.419
#D	309.4	5.824	0.19	310.4 5.825	0.19	0.245-j0.353	267.9	5.841
#E	169.1	2.385	0.20	169.1 2.385	0.20	1.227-j0.071	119.2	2.386

Table 4.2.1(c) Improved TLM

Measured Results:

Antenna	Method (I)		Method (II)		Method (III)				
	Rant(Ω)	fr(GHz)	Rant(Ω)	fr(GHz)	Rinput(Ω)	Z1(Ω)	Z2(Ω)	Rant(Ω)	fr(GHz)
#A	282.2	2.995	249.8	3.013	53.0	118	50	295.2	2.998
#B	313.9	2.446	234.1	2.480	61.6	113	50	314.6	2.462
#C	281.8	1.411	261.7	1.416	58.0	112	50	291.0	1.416
#D	299.9	5.772	------	------	32.9	158	50	328.5	5.820
#E	147.1	2.370	------	------	42.3	93	50	146.3	2.383

Table 4.2.1(d) Measured results

±1.5% Worst Case Analysis (Improved TLM):

Antenna	Pues (1984) (0%)			Pues (1984) -1.5% for L and W		Pues (1984) +1.5% for L and W	
	Wm(mm)	Rin(Ω)	fr(GHz)	Rin(Ω)	fr(GHz)	Rin(Ω)	fr(GHz)
#A	0.47	244.2	2.994	244.2	3.045	243.5	2.957
#B	1.06	257.4	2.453	256.4	2.500	255.7	2.428
#C	1.08	243.2	1.419	243.4	1.443	242.6	1.401
#D	0.19	267.9	5.841	266.5	5.957	265.8	5.790
#E	0.20	119.2	2.386	119.2	2.420	118.6	2.353

Table 4.2.1(e) Worst Case Analysis (Improved TLM)

Method (I) gives a consistent set of results for the resonant frequency but that of the measured resonant input impedance does not agree with that predicted by the improved model. This is because the probe-feed causes losses at the input of the patch.

Method (II) gives a good agreement both for resonant frequency and input impedance at resonance. However the method cannot be used for a lossy substrate and/or at high frequencies.

Method (III) shows a close agreement for the resonant frequency between the practical measurement and those predicted by the improved model as the narrow quarter-wavelength transformer is taken into account.

Radiation Pattern

The co-polar radiation pattern for E- and H- plane has been measured for an antenna on RT/Duroid 5780 (ε_r=2.33 h=0.79mm) at 5.8GHz. The measurement was carried out in a laboratory in which microwave absorbers were placed around the antenna under test in order to reduce the reflection due to the walls. The measured radiation pattern is compared with the theory (equation 4.2.26) as shown in figure 4.2.13. The 3dB beamwidth was measured as 85°. The results show that the radiation pattern is displaced to one side due to the reflections due from the walls and the specific location of the antenna above the ground plane.

Antenna Gain

Antenna gain was measured using a three-antenna gain method described by Balanis (p.718-720). The efficiency and directivity of antennae were calculated and the results obtained are compared with the theory as shown in Table 4.2.2. Again good agreement is obtained between the practical and those predicted results.

Substrate used	L mm	W mm	Theory Gr mS	Gcu mS	Gdiel mS	η %	Directivity dBi	Gain dBi	Measured Gain dBi
#1	33.15	33.17	1.140	0.511	0.393	55.8	8.08	5.55	6.02
#2	39.90	39.90	1.103	0.185	0.258	71.3	8.07	6.61	6.06
#2	70.02	70.02	1.140	0.386	0.410	58.9	8.09	5.79	6.17
#3	16.18	16.18	1.026	0.209	0.224	70.3	8.03	6.50	5.40
#4	18.37	48.98	1.532	0.824	2.133	34.1	8.20	3.52	4.10

Gs here was calculated using equations from Pues (where Gr≡Gs).

Table 4.2.2 Antenna Gain

4.2.5 Circular Polarisation

Circular Polarisation can be generated by using two feeding systems: one is a dual-feed circularly polarised antenna with an external 3dB hybrid, and the other is a singly-fed one as shown in figure 4.2.14 (James, 1989). A 3dB hybrid offers a better tolerance for the 180° phase shift and equal magnitude of the signal due to the fabrication process and gives two hands of polarisation (Left and right hand C.P.) at two separate ports. Consequently the dual-feed C.P. antenna with an external 3dB two-branch coupler is discussed in this section.

Figure 4.2.15 shows the dual-feed C.P. antenna. The [S] parameters of the 3dB coupler are given by

$$\begin{bmatrix} b_1 \\ b_2 \\ b_3 \\ b_4 \end{bmatrix} = -\frac{1}{\sqrt{2}} \begin{bmatrix} 0 & 0 & 1 & j \\ 0 & 0 & j & 1 \\ 1 & j & 0 & 0 \\ j & 1 & 0 & 0 \end{bmatrix} \begin{bmatrix} \Gamma_1 b_1 \\ \Gamma_2 b_2 \\ a_3 \\ a_4 \end{bmatrix} \tag{4.2.48}$$

Since the coupler is matched to 50Ω, giving $\Gamma_1 = \Gamma_2 = 0$ and the received signals (b_1 and b_2) obtained at ports 1 and 2 are given respectively by

$$b_1 = -\frac{1}{\sqrt{2}}(a_3 + ja_4) \tag{4.2.49}$$

$$b_2 = -\frac{1}{\sqrt{2}}(ja_3 + a_4) \tag{4.2.50}$$

If a left-hand C.P. wave is transmitted into the antenna, the signals picked up at ports 3 and 4 are given by

$$\text{At port 3:} \qquad a_3 = E_y = E_o \cos(\omega_c t - 90°) \tag{4.2.51}$$

$$\text{At port 4:} \qquad a_4 = E_x = E_o \cos\omega_c t \tag{4.2.52}$$

where E_o is the peak electric field of the C.P. wave and E_x and E_y are the electric fields at x and y-direction and ω_c is the angular frequency of the carrier.

Substituting expressions 4.2.51 and 4.2.52 into 4.2.49 and 4.2.50 the received signals at ports 1 and 2 are

$$b_1 = 0 \text{ and } b_2 = -\sqrt{2}E_o \tag{4.2.53}$$

Hence only port 2 picks up the left hand C.P. wave. Similarly port 1 only picks up the right hand C.P. wave.

Analysis of Imperfect Circular Polarisation

A combination of two orthogonal linearly polarised radiating elements can be used to obtain a circularly-polarised (C.P.) wave which has a 0dB axial ratio. In practice an imperfect C.P. wave is generated due to excitation with unequal amplitudes (amplitude error) and a departure from quadrature-phase difference (phase error). The formula for axial ratio (in dB) for arbitrary fields is given by (Balanis, 1982)

$$AR = 10\log_{10} \frac{E_x^2 + E_y^2 + \sqrt{E_x^4 + E_y^4 + 2E_x^2 E_y^2 \cos 2\theta}}{E_x^2 + E_y^2 - \sqrt{E_x^4 + E_y^4 + 2E_x^2 E_y^2 \cos 2\theta}} \tag{4.2.54}$$

where E_X and E_Y are the magnitudes of the orthogonal radiated field components, and θ is the phase difference between them. For a perfect C.P. wave (0dB axial ratio), $|E_X| = |E_Y|$ and $\theta = 90°$. The effect of amplitude and phase errors can be quantified in terms of the axial ratio. Pozar and Targonski (1990) presented a graph based on equation 4.2.54 showing the contours of constant axial ratio versus amplitude and phase errors as shown in figure 4.2.16.

With the aid of the graph the designer can predict the axial ratio for the given values of amplitude and phase errors.

4.2.6 Design and Testing of a C.P. Antenna

One of the essential elements of the microwave module of the On-Board-unit is the square patch antenna driven by a 3dB two-branch coupler in order to produce a circular polarisation as shown in figure 4.2.17. The usual method of matching the high input impedance of a patch antenna to the two-branch coupler is to use a $\lambda/4$ line transformer. However the required characteristic impedance of this $\lambda/4$ transformer is unacceptably high, making it difficult to realise as the copper track becomes too narrow. A novel design has been implemented to overcome this problem and this design is fully discussed below.

Novel Design of a Modified 3dB Two-Branch Coupler

Normally the two-branch coupler is designed to operate between a 50Ω source and load impedances. For this application however, the operating impedance at the source has been reduced to 31.25Ω so that the characteristic impedance of the $\lambda/4$ transformer is also reduced making it easier to realise. The output of the two-branch coupler is still maintained at 50Ω. This unbalanced two-branch coupler is shown in figure 4.2.18. A novel method has been used in the design of the coupler where the impedance of the two ports of the coupler connected to the patch antenna (Z=328.5Ω, see Table 4.2.1d) have been reduced to 31.25Ω. This allows the $\lambda/4$ matching line to have an impedance of 101.3Ω. The full design of the modified coupler is presented below.

Consider the case 1 where port (1) is an input port, port (2) is isolated and half of the power is absorbed at ports (3) and (4) respectively. The equivalent circuit is shown in figure 4.2.19a. The characteristic impedances are calculated as Z4=31.25Ω and Z1=27.9Ω.

Similarly for case 2: Power fed at port (2), half of the power absorbed at port (3) and (4) with no power going out from port (1). The equivalent circuit is shown in figure 4.2.19b. Therefore, Z4=31.25Ω and Z2=27.9Ω.

Case 3: Power fed at port (3), half of the power absorbed at port (1) and (2) with no power going out from port (4). The equivalent circuit is shown in figure 4.2.19c. Therefore, Z4=50Ω and Z1=27.9Ω.

Case 4: Power fed at port (4), half of the power absorbed at port (1) and (2) with an isolated port (3). The equivalent circuit is shown in figure 4.2.19d. Therefore, Z4=50Ω and Z1=27.9Ω.

Since it is not possible to model this coupler with two ports terminated each with a 50Ω resistor and the other two ports each with a 31.25Ω resistor using 'Touchstone', the dummy matching network was instead connected to the ports (3) and (4). The dummy network is shown in figure 4.2.20. The complete 'Touchstone' program and the simulated results are shown in the appendix B.

If 0dBm of power is fed at port (1) there should be -3dBm of power dissipated across the 31.25Ω resistors at port (3) and (4), respectively. If the dummy network is connected there should be -9.20dBm of power dissipated at the 50Ω terminations.

Practical Results of the Coupler

The 5.8GHz coupler was fabricated on the RT/Duroid 5870 ε_r=2.33 tand=0.0012 @ 10GHz, h=0.79mm as shown in figure 4.2.21. Since 31.25Ω standard loads were not available it was decided to use the 50Ω standard loads of the network analyser. The power out of the 31.25Ω outputs ports should be the same, namely S_{21} and S_{31}.

The S-parameters at 5.8GHz were measured as shown in figure 4.2.22a-c:

S_{11} = -18.40dB	(Return Loss)
S_{21} = -3.805dB, 144.29°	(Coupling)
S_{31} = -3.983dB, 54.64°	(Coupling)
S_{41} = -16.49dB	(Isolation)

The results show only 0.2dB difference in the magnitude and a close to 90° phase difference. This is sufficient to produce a good circular polarisation.

Circularly Polarised Antenna Patch

The dimension of the square patch was 16.18mm by 16.18mm (see Table 4.2.1). The antenna together with the coupler was then fabricated on the same substrate as shown in figure 4.2.17. The 'S'-parameters were measured and are shown in figure 4.2.23. At 5.8GHz, S_{11}=-18.37dB, S_{21}=-17.05dB and S_{22}=-12.50dB. The antenna gain and the axial ratio were measured as 5.5dBi and 3dB. Figure 4.2.24 shows the polar pattern which was good enough for the present application.

4.3 Summary and Conclusions

This chapter has reviewed the theory of a single patch antenna. A comparison of a number of published methods to determine the resonant frequency, input impedance and antenna gain is given in section 4.2. The improved TLM which includes the mutual coupling between the two main radiating slots gives a better agreement to the practical results compared with the simple model. Finally a circularly polarised antenna using a novel designed unbalanced two-branch coupler has been fabricated for the On-Board Unit. With such a design it is possible to reduce the characteristic impedance of the $\lambda/4$ matching transformer so that it can readily be realised.

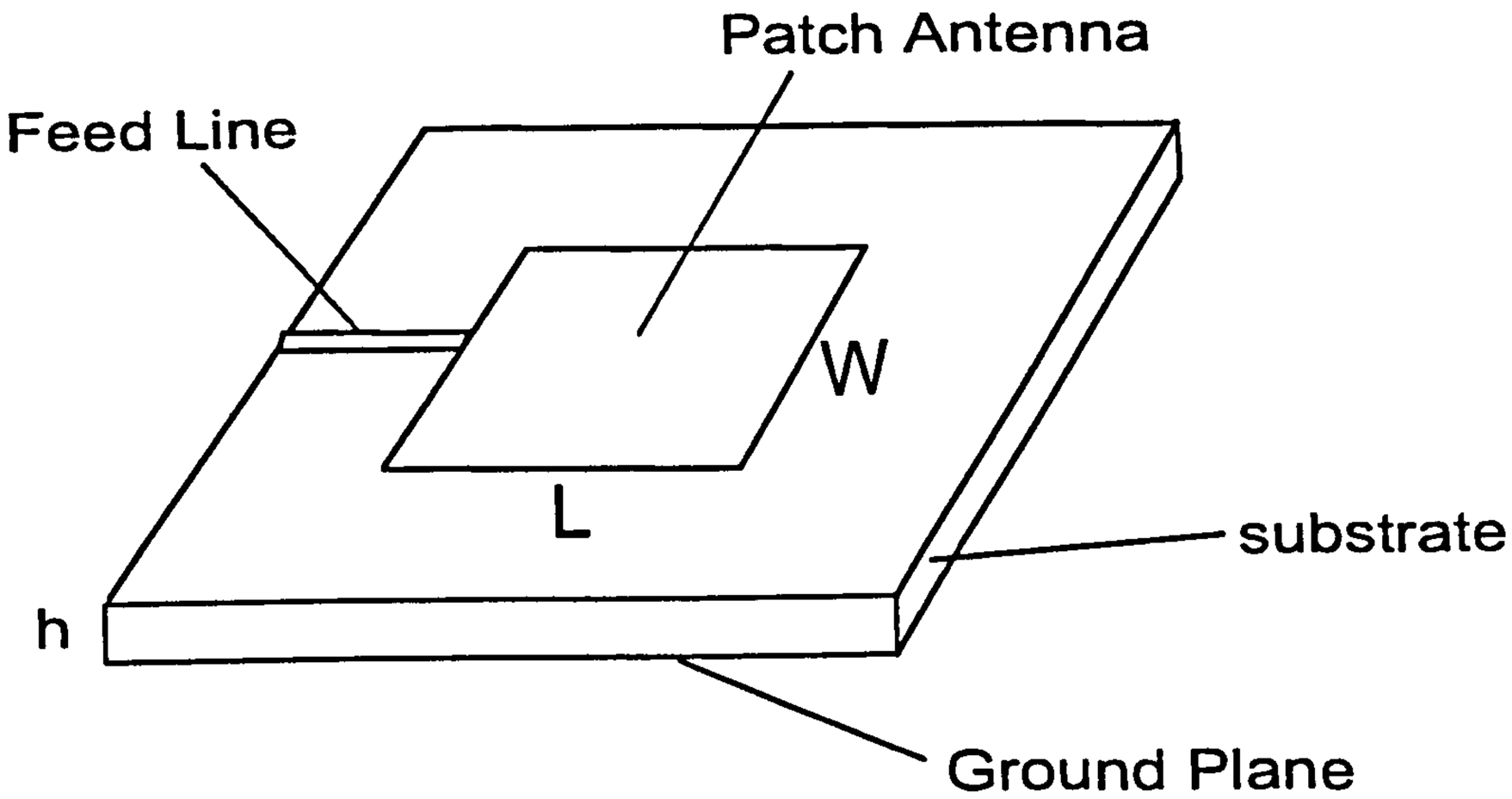

Figure 4.2.1 Microstrip Antenna

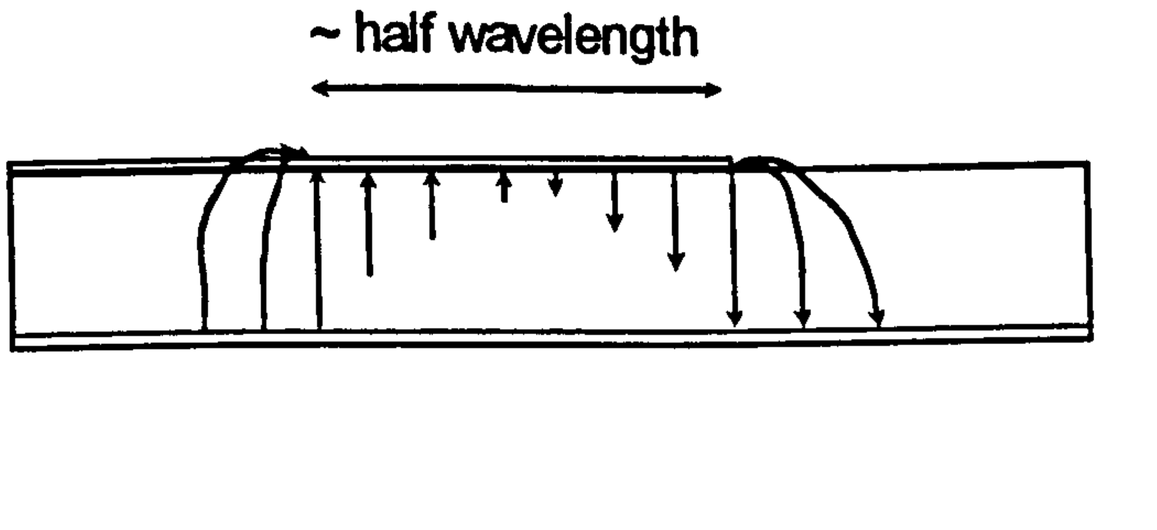

Figure 4.2.2 Side and Top View of Patch Antenna

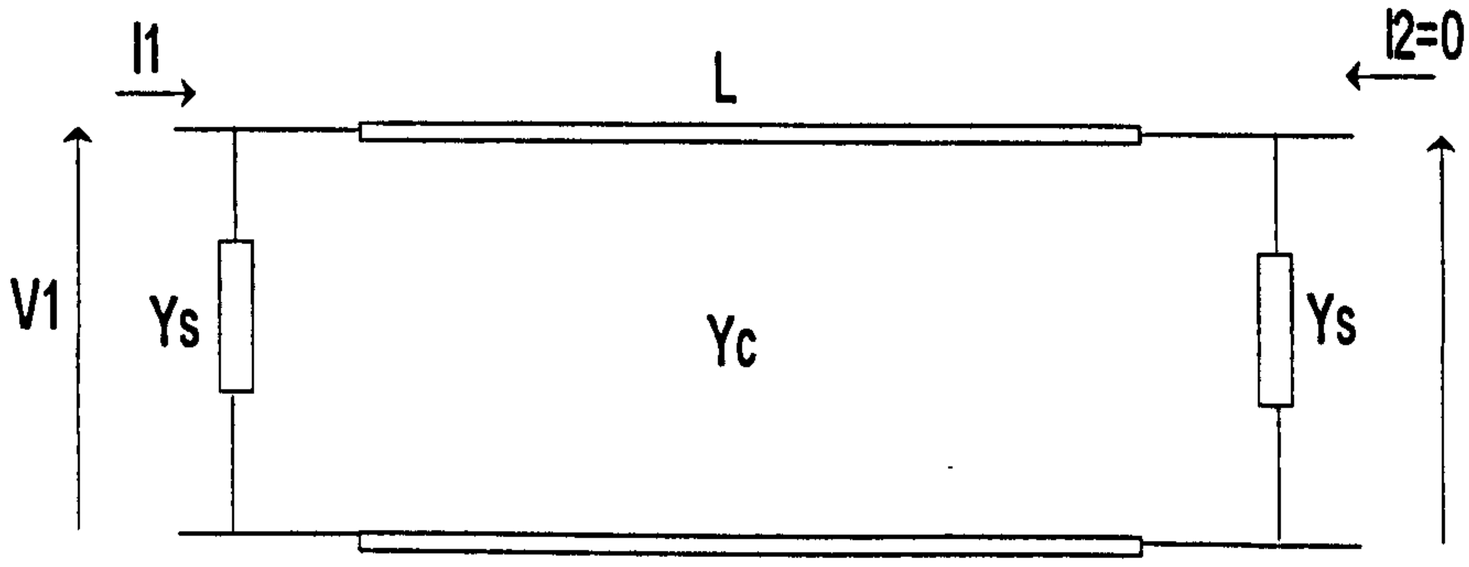

Figure 4.2.3 Simple Transmission Line Model

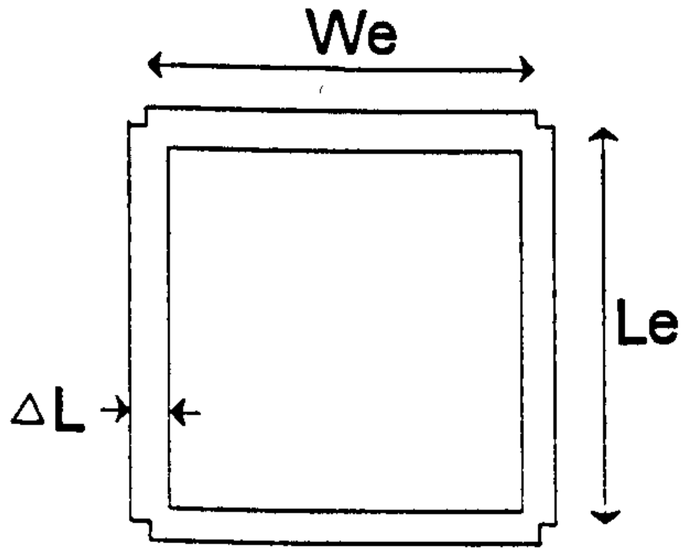

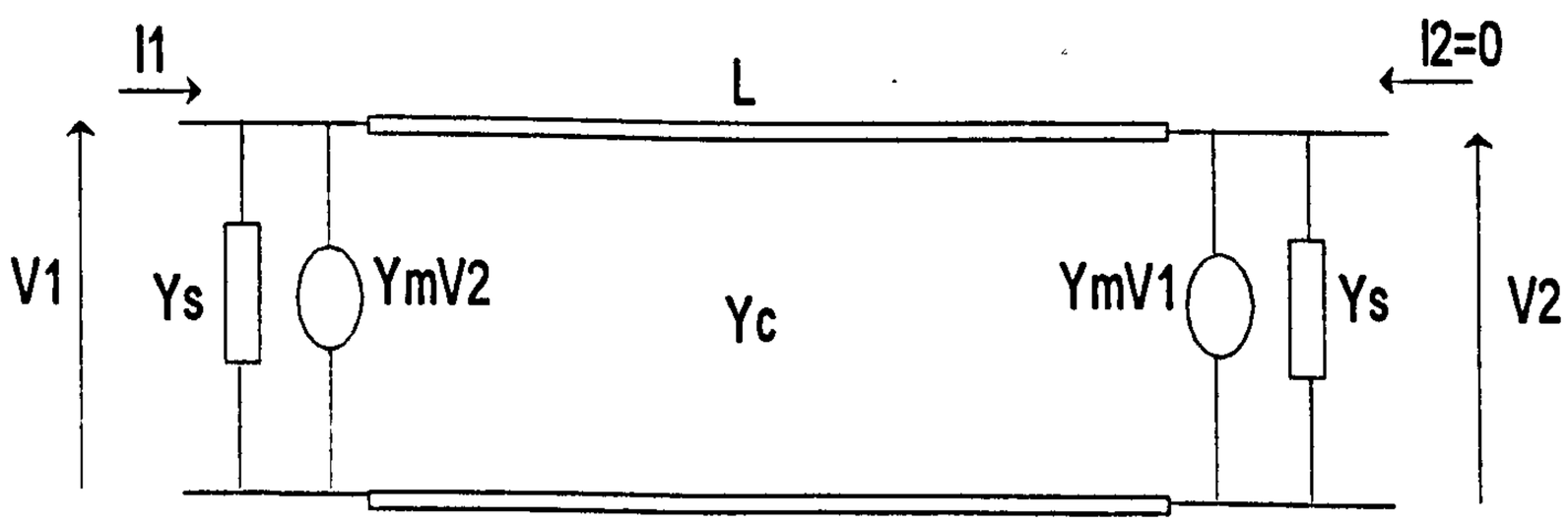

Figure 4.2.4 Improved Transmission Line Model

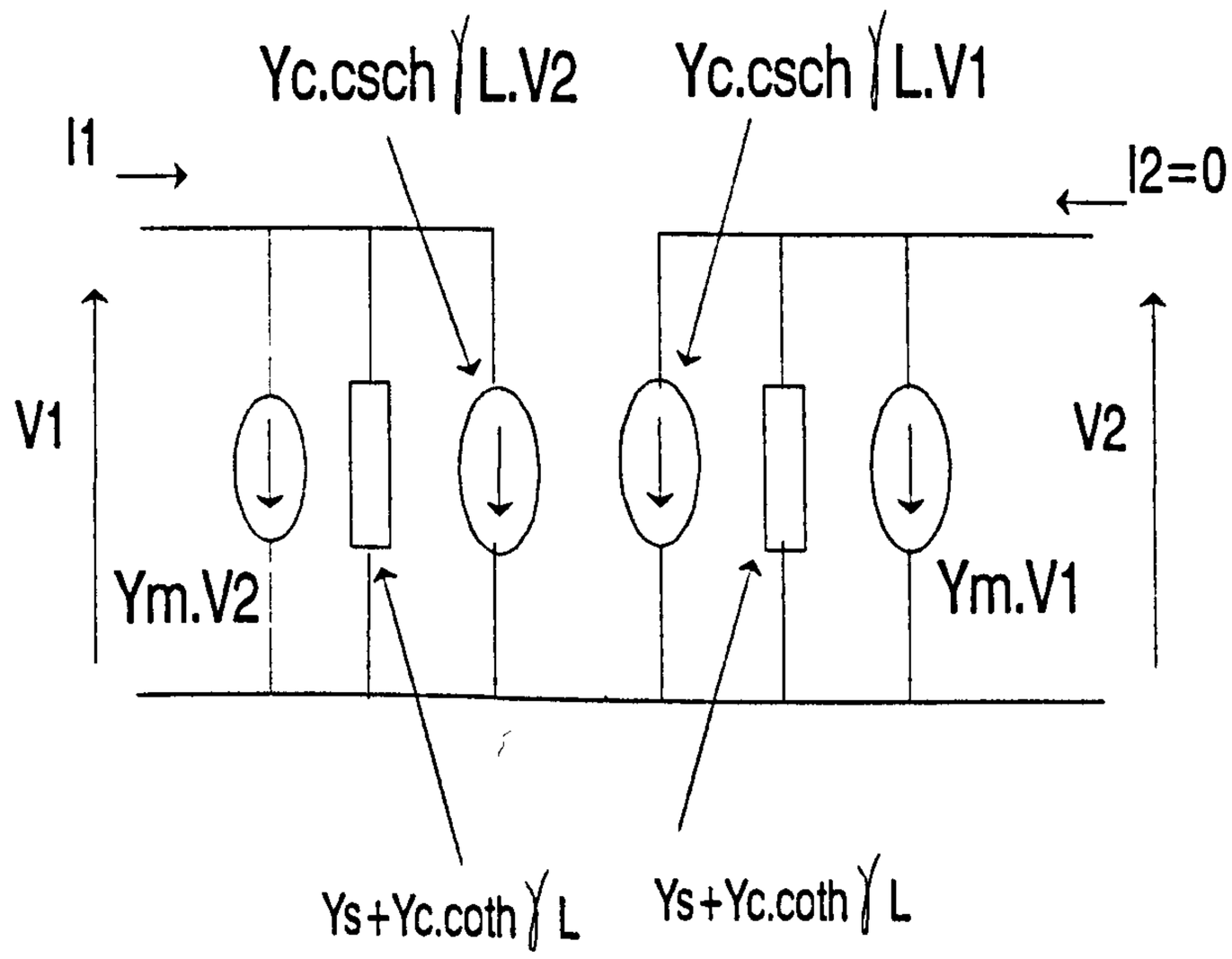

Figure 4.2.5 Equivalent Circuit of Improved TLM

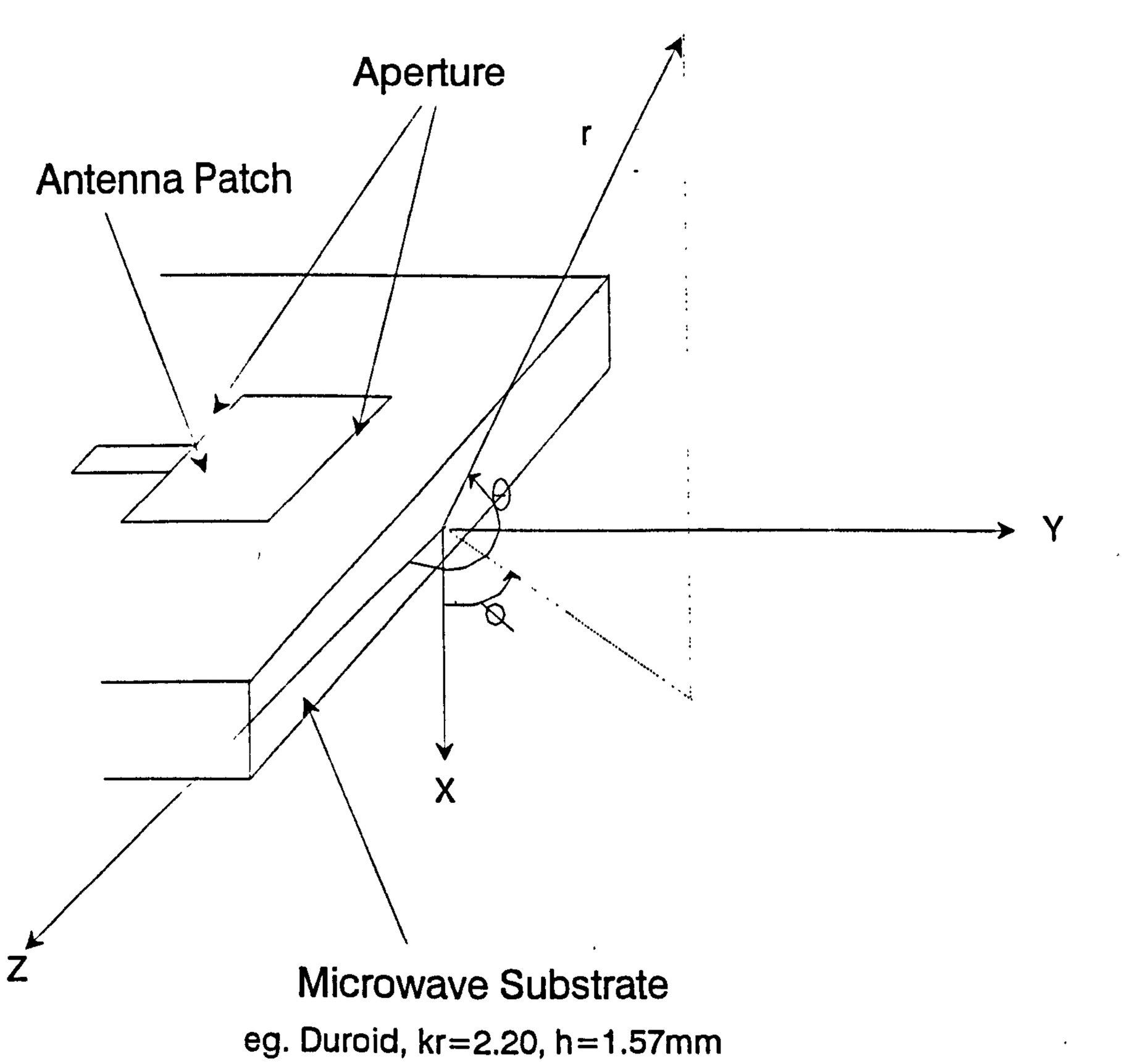

Figure 4.2.6 Co-ordinate for Single Patch Antenna

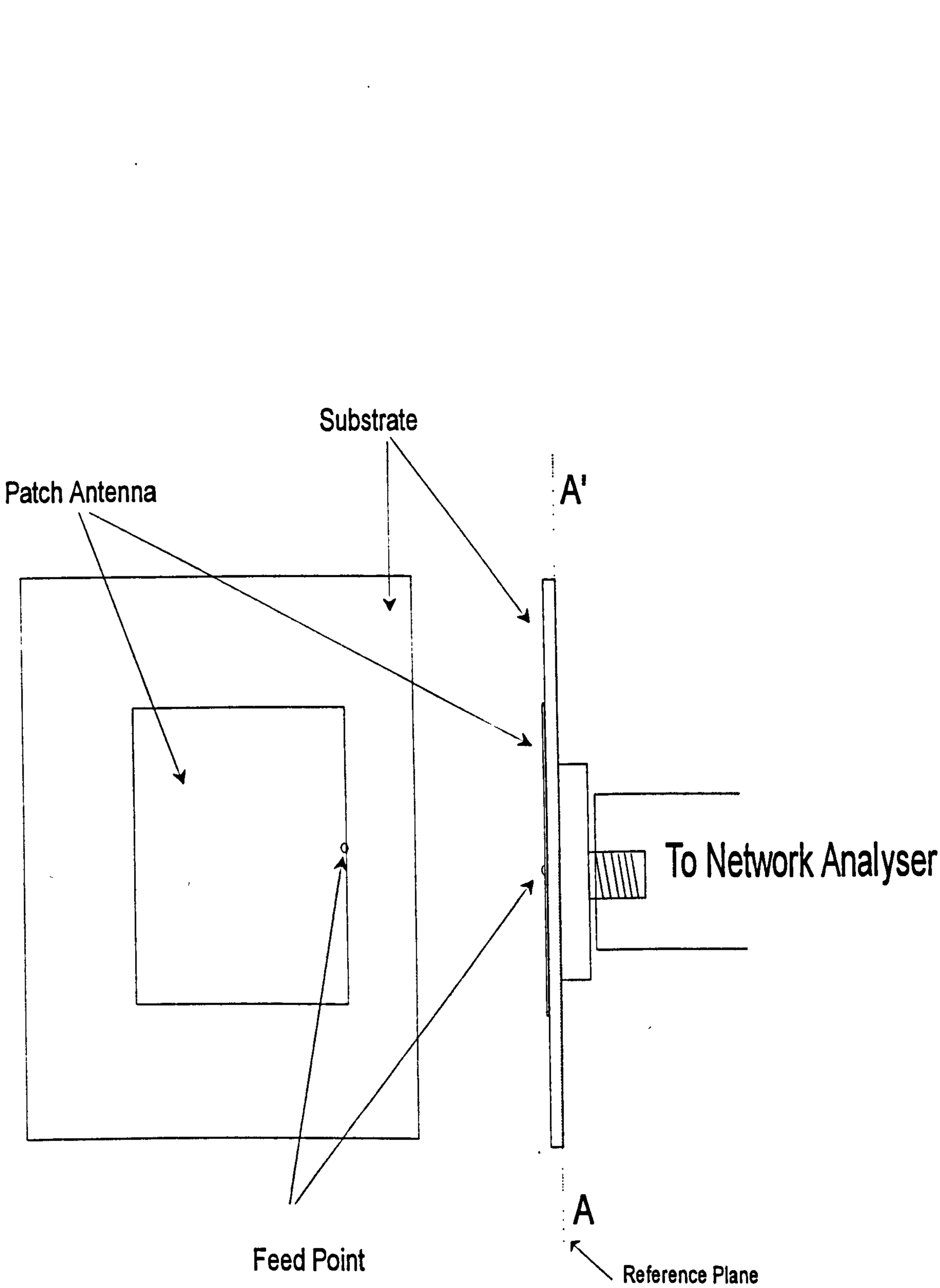

Figure 4.2.7 Circuit Layout for Method (I)

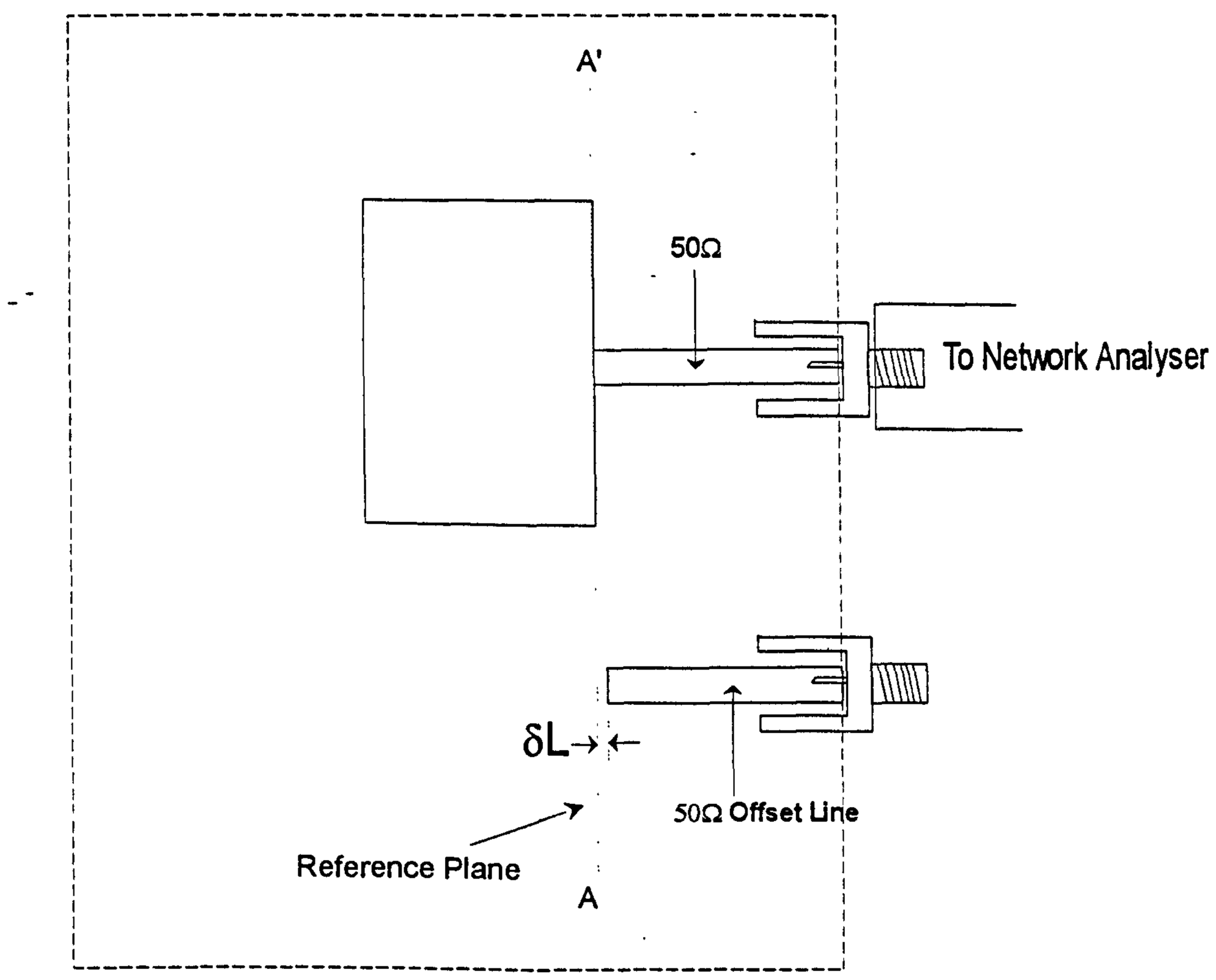

Figure 4.2.8 Circuit Layout for Method (II)

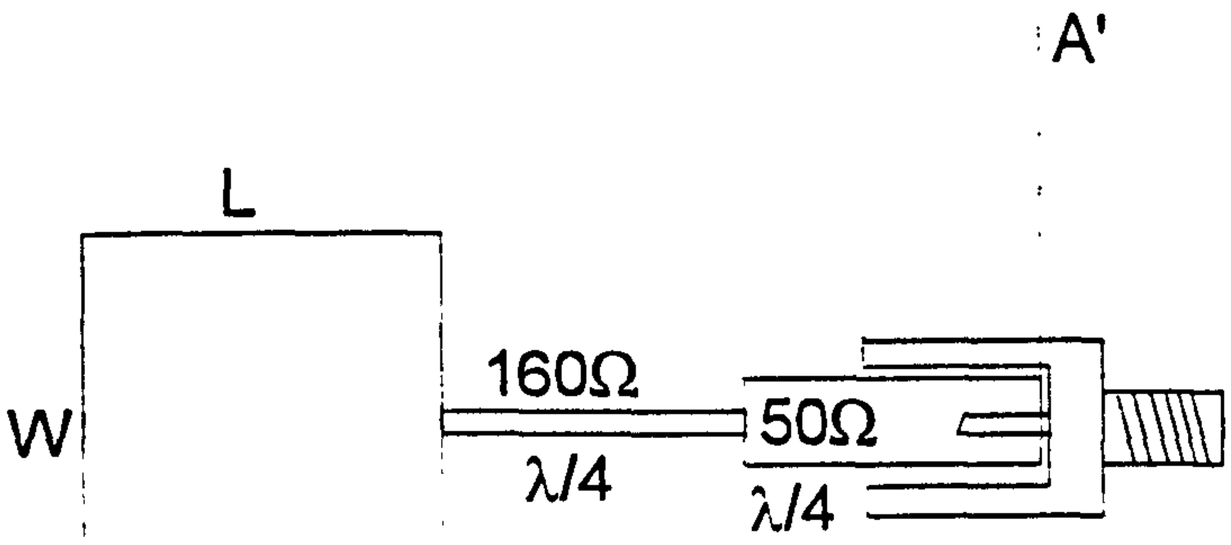

Figure 4.2.9 Circuit Board Layout for Measuring Input Impedance and Resonant Frequency using Method (III)

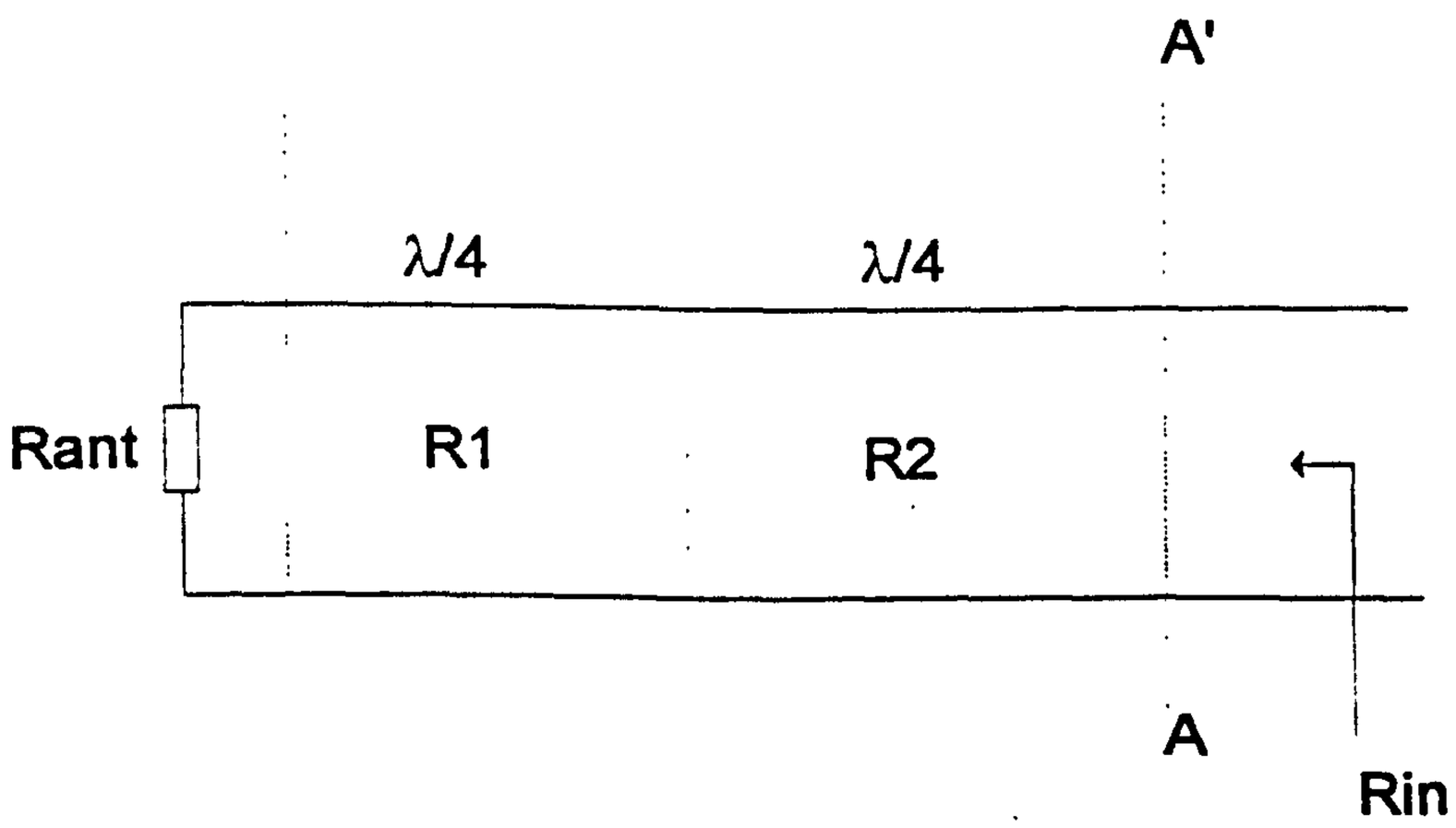

Figure 4.2.10 Equivalent Circuit for the circuit layout shown in Figure 4.2.9

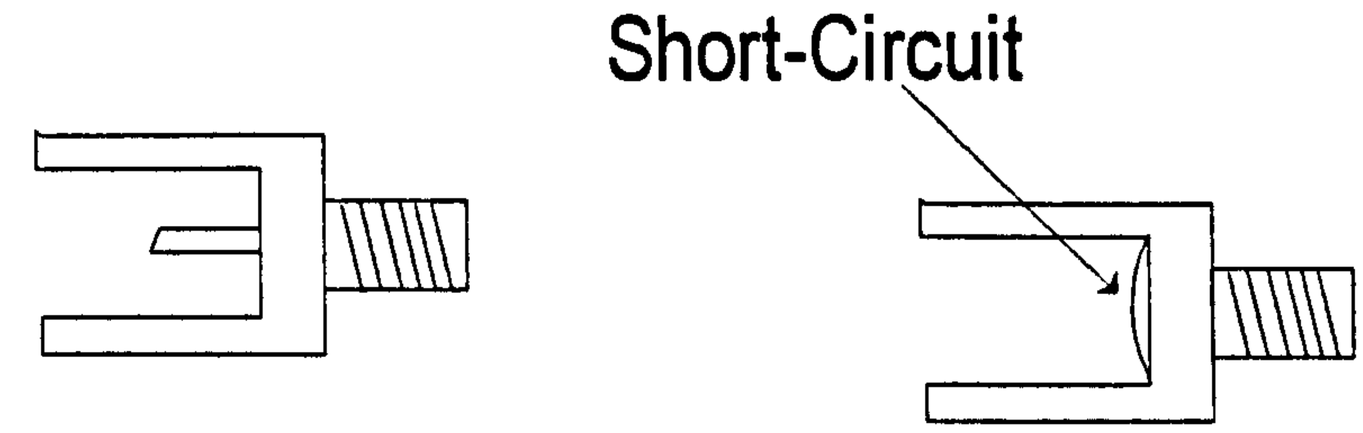

(a) (b)

Figure 4.2.11 SMA Connector

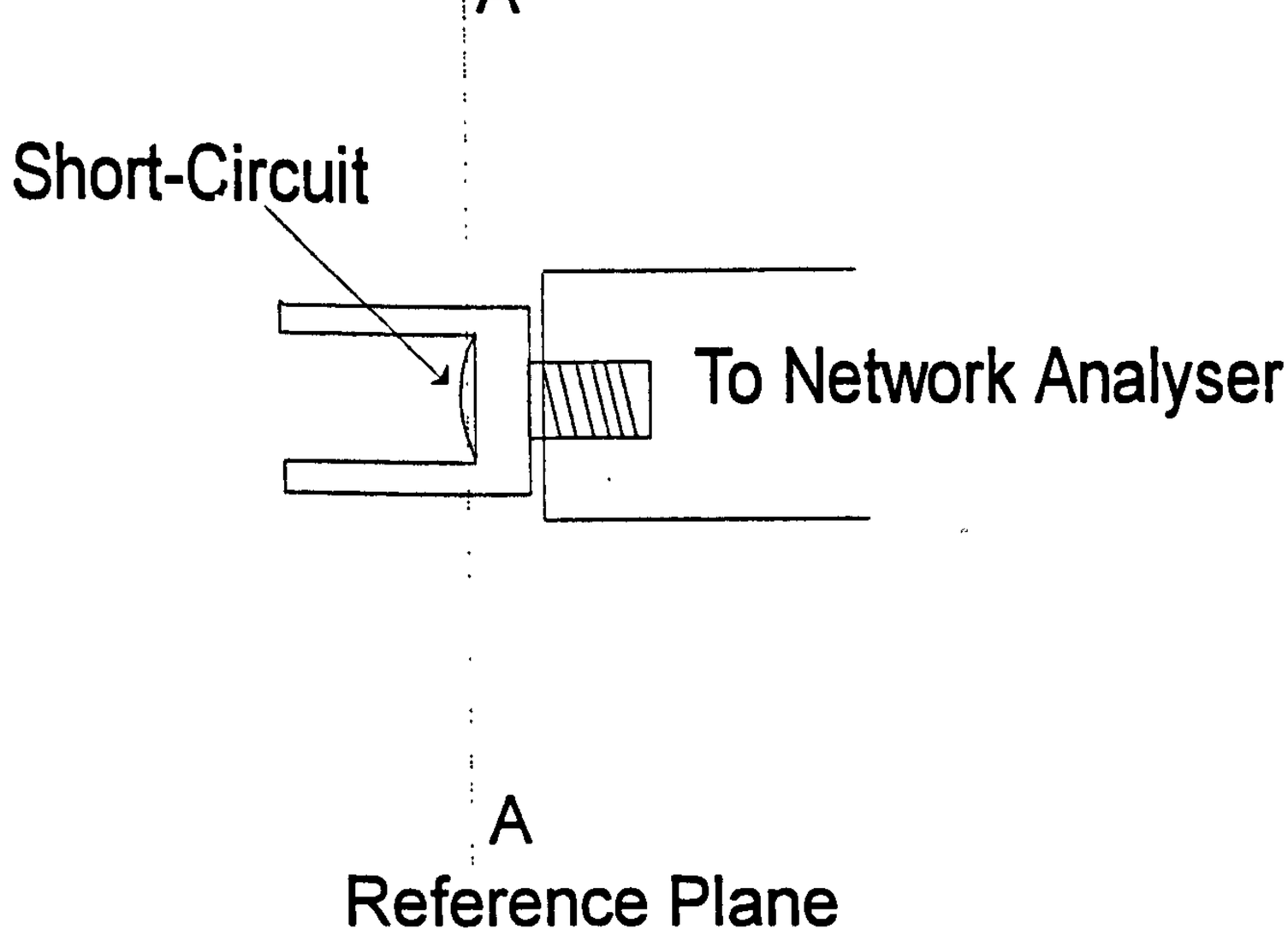

Figure 4.2.12 Reference Plane for Measurement

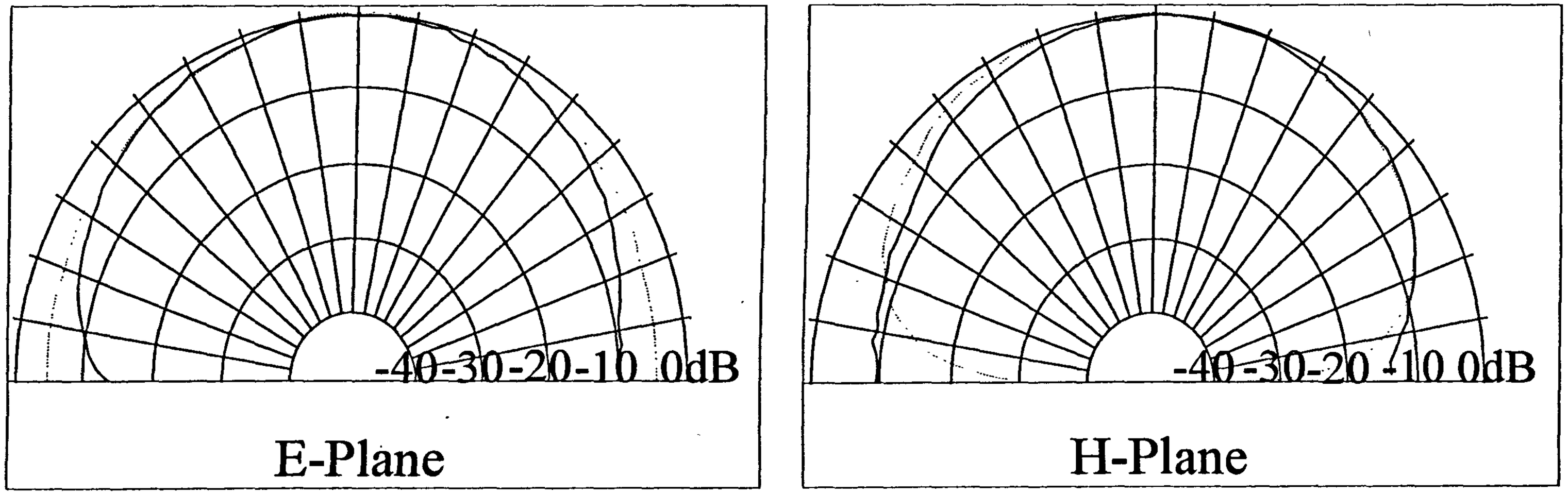

Figure 4.2.13 Polar Pattern for a Single Patch Antenna

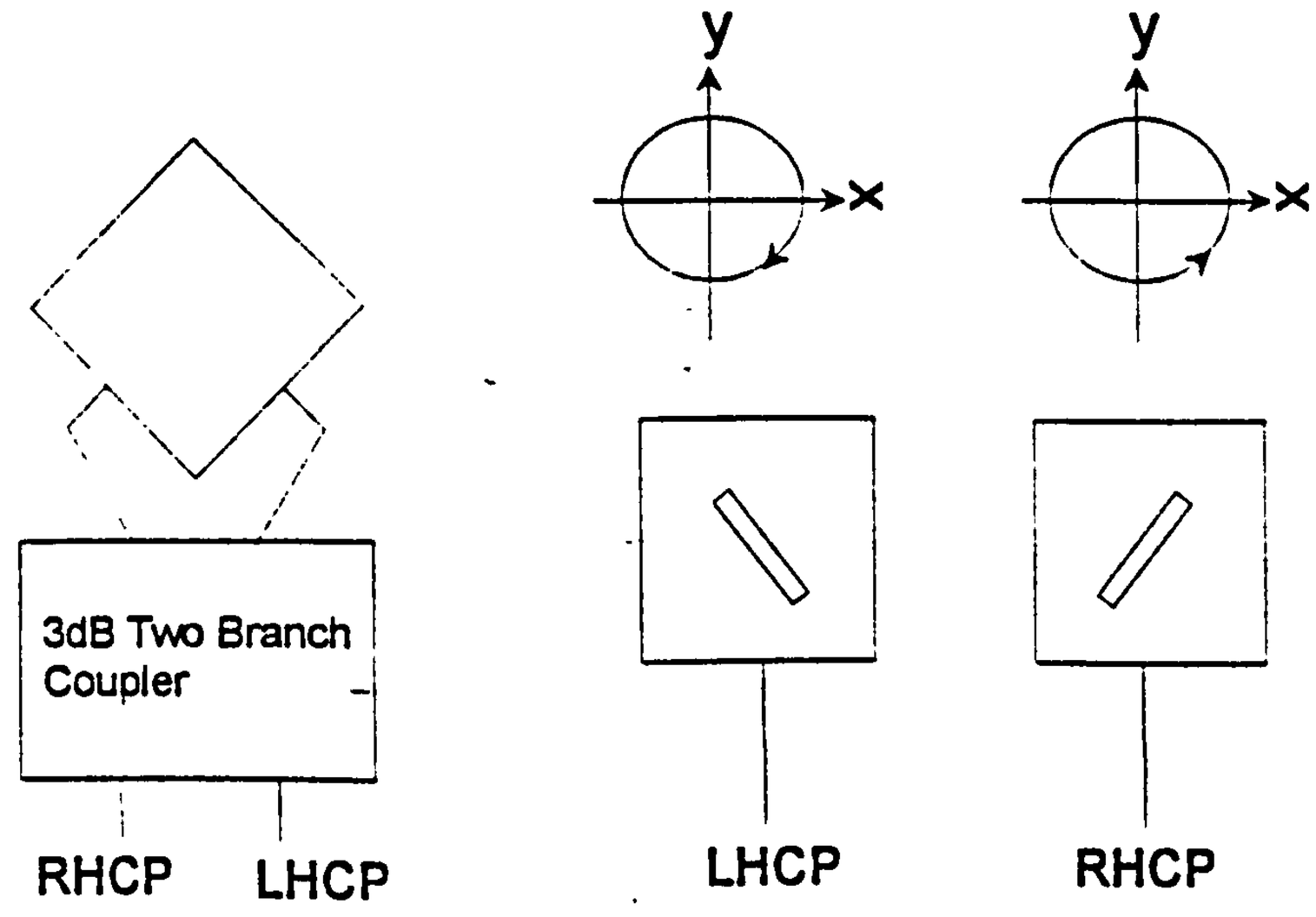

Figure 4.2.14 Dual and Singly fed C.P. Patch Antennae

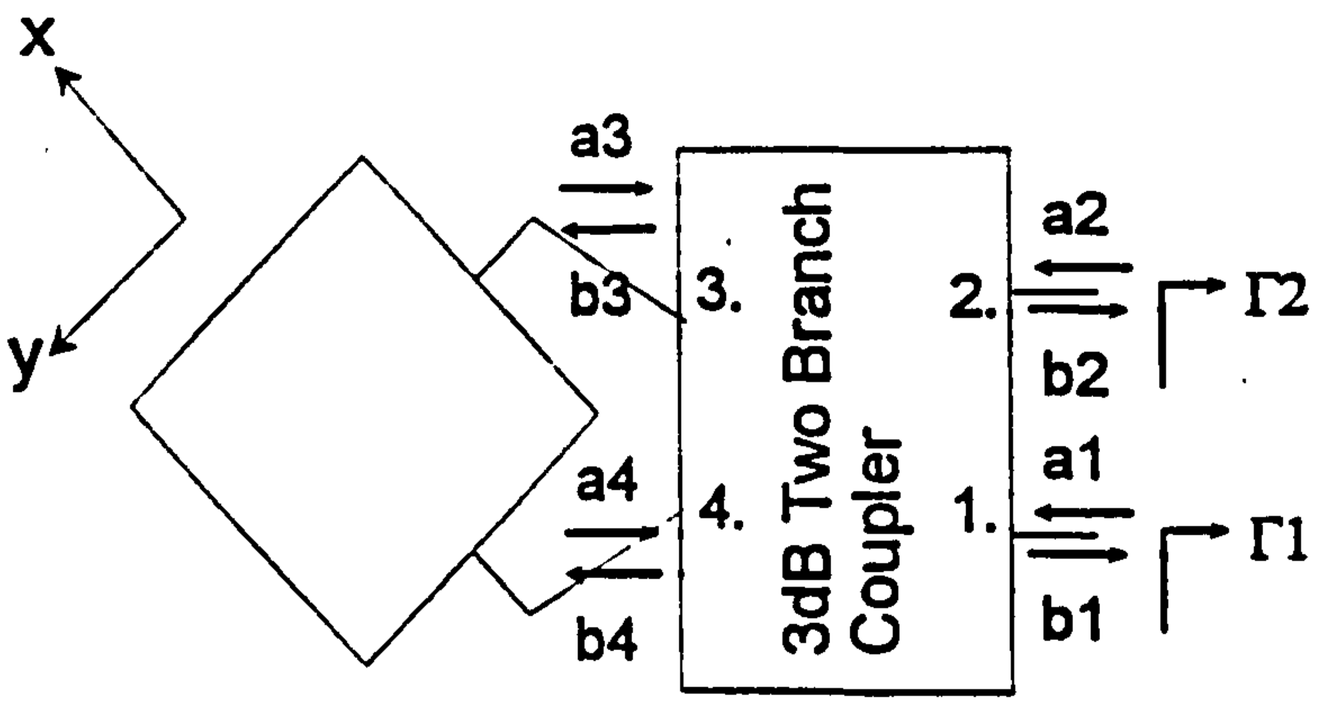

Figure 4.2.15 [S] Parameters for a Dual-fed C.P.Antennae

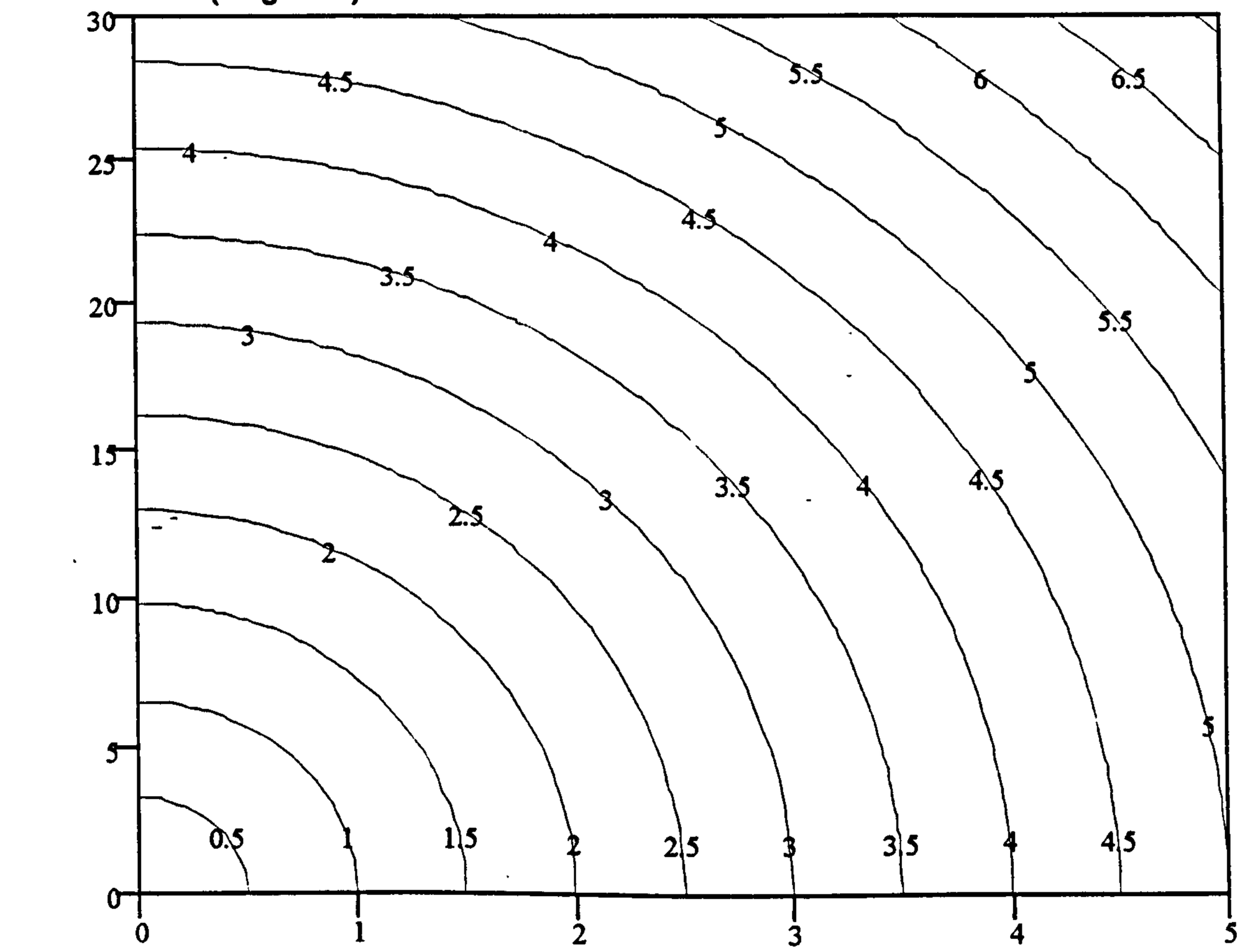

where amplitude error = $20\log\left(\frac{E_x}{E_y}\right)$, and phase error = $\theta - 90^o$.

Figure 4.2.16 Contours of Constant Axial Ratio versus Amplitude and Phase Error

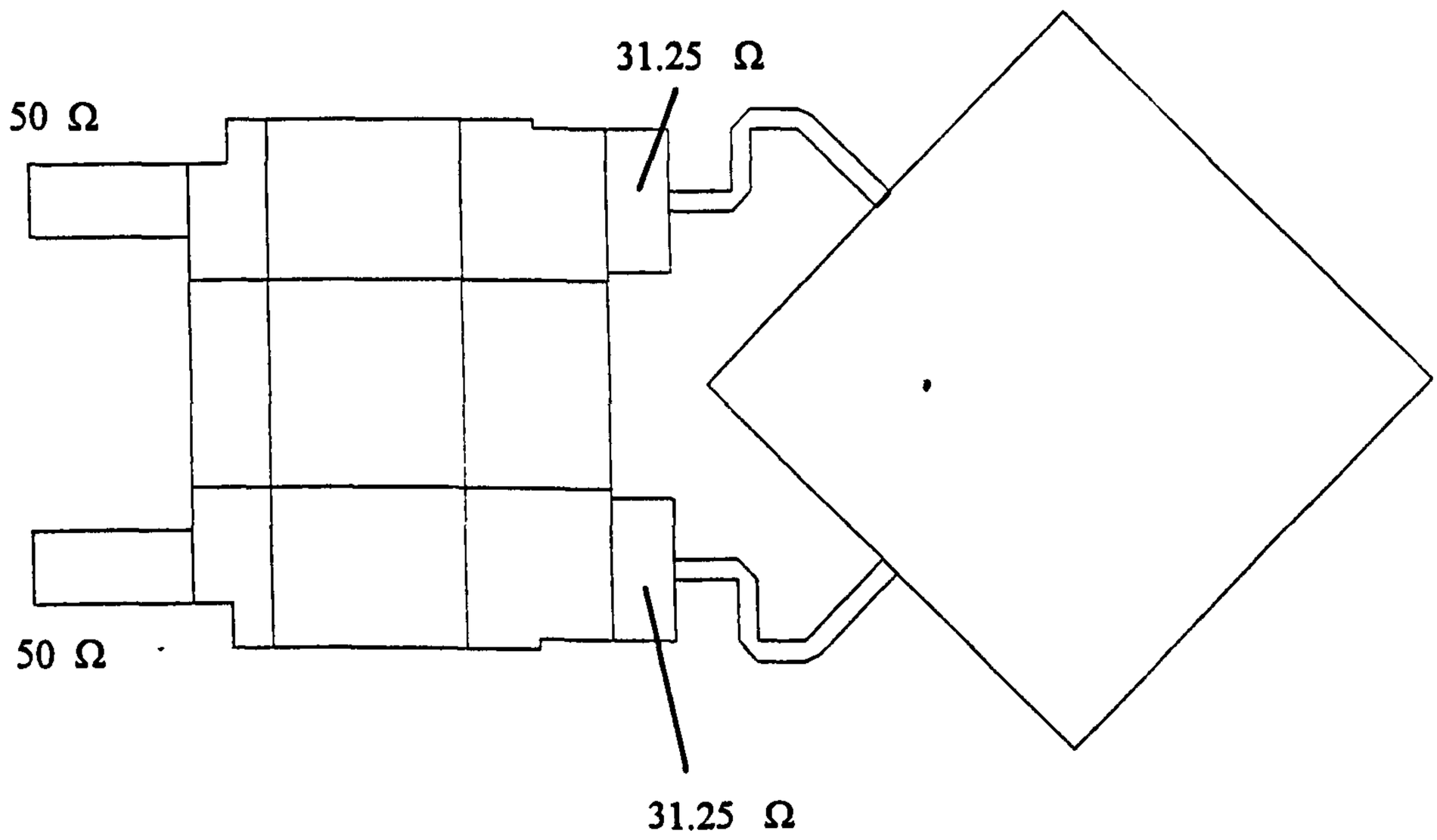

Figure 4.2.17 On-Board Unit Antenna

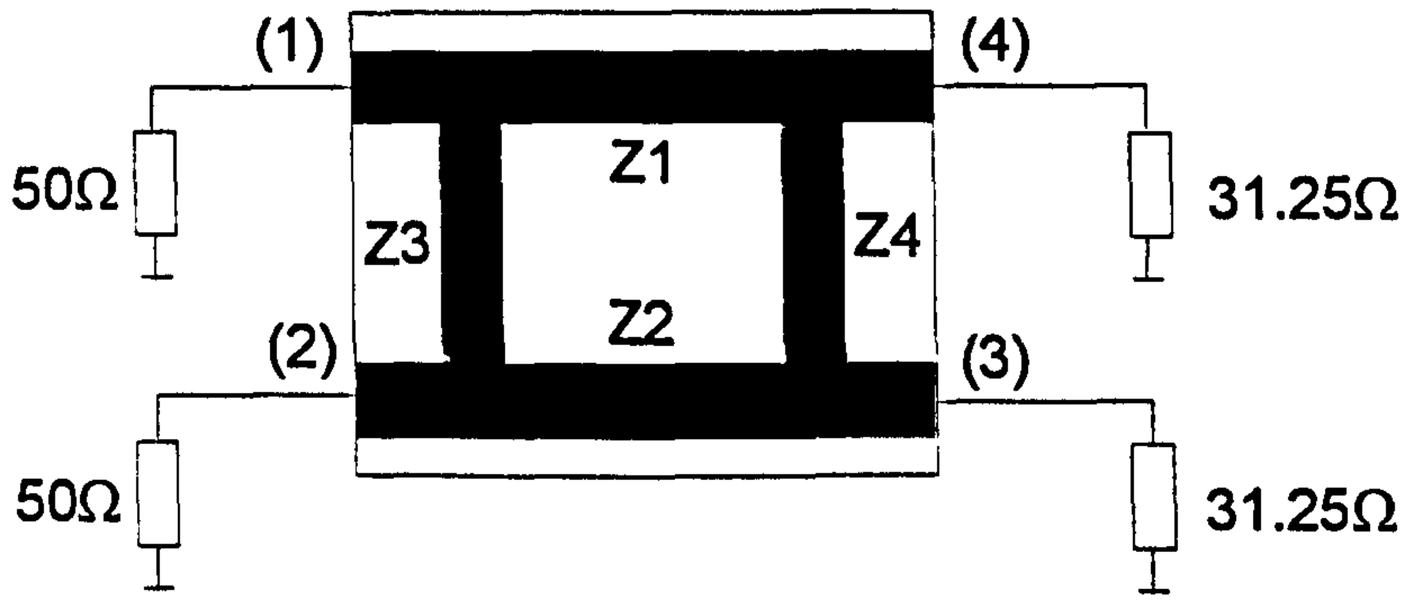

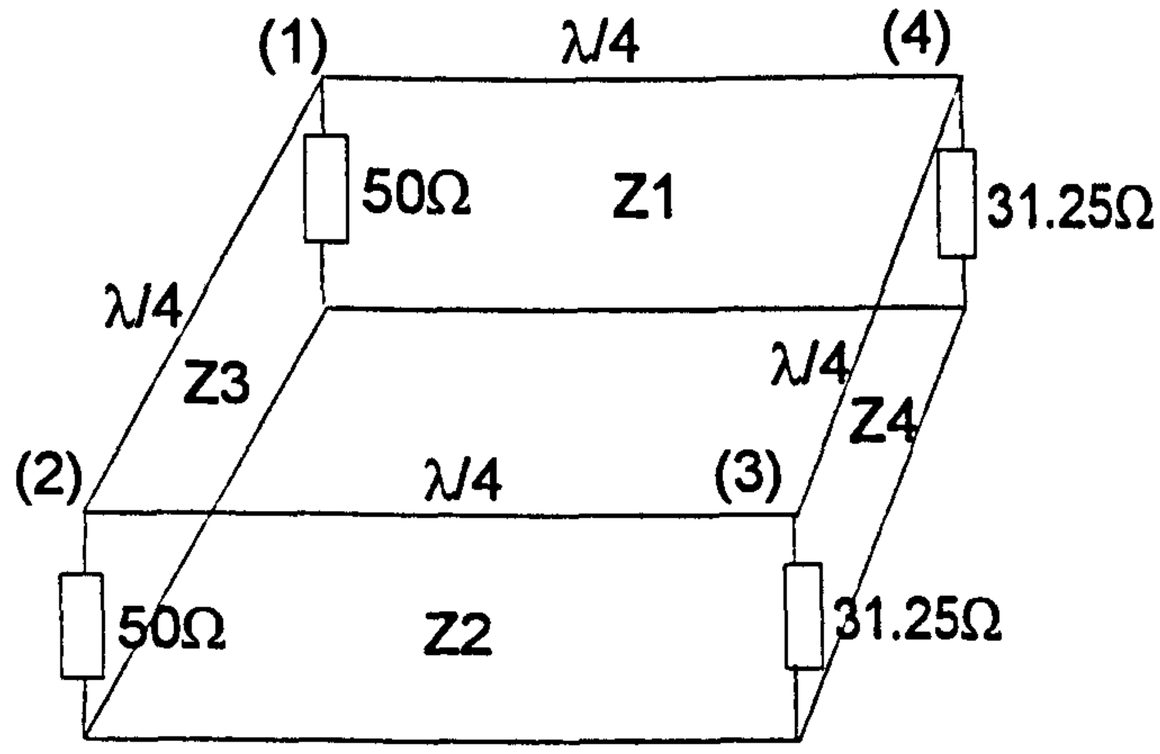

where ports (1) & (2) and ports (3) & (4) are isolated ports

Figure 4.2.18 Coupler Design for the OBU C.P. Antenna

(a):

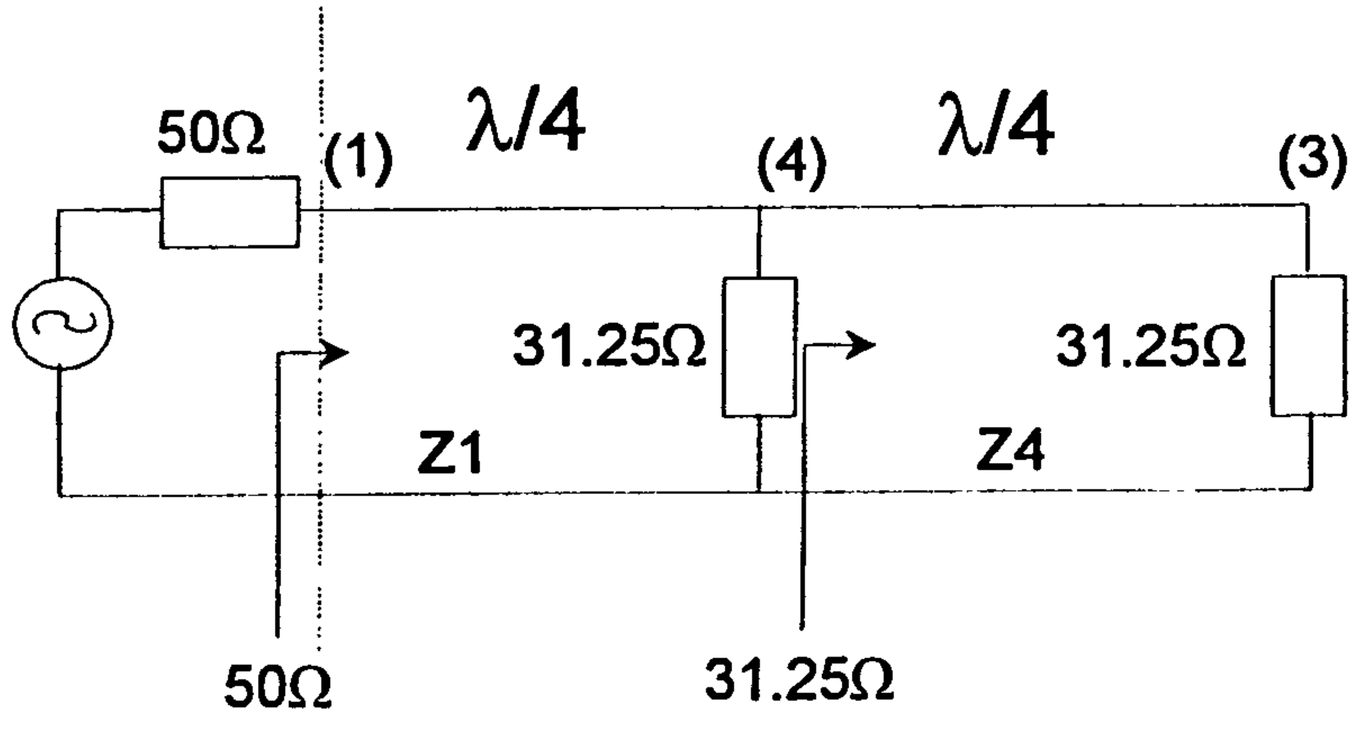

(b):

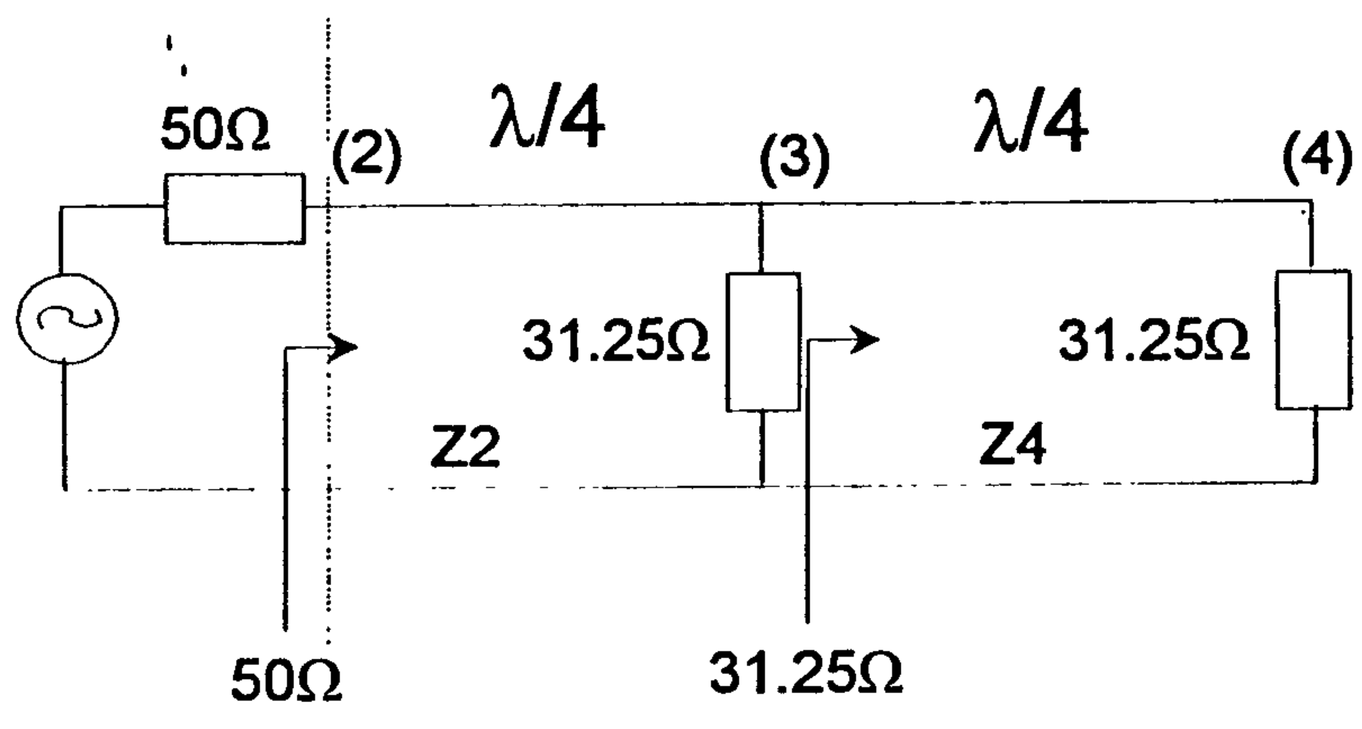

(c):

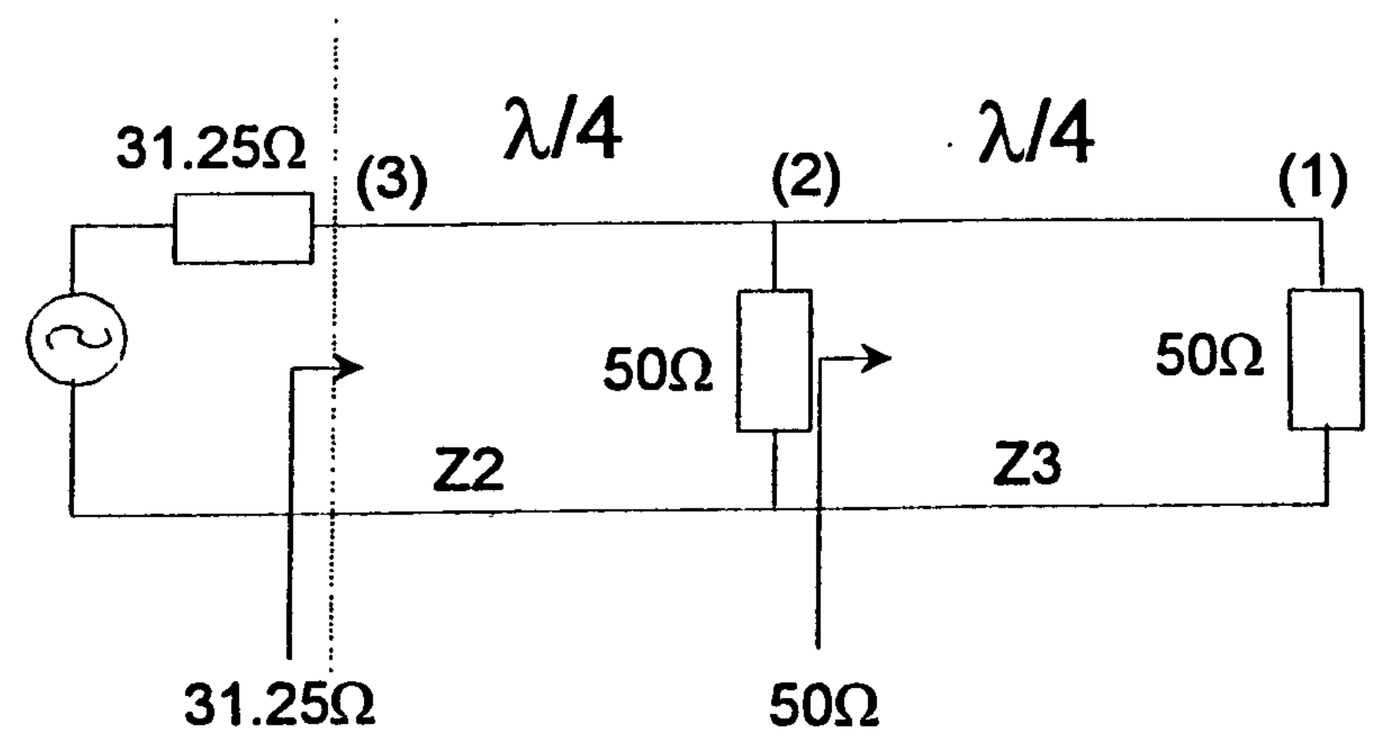

(d):

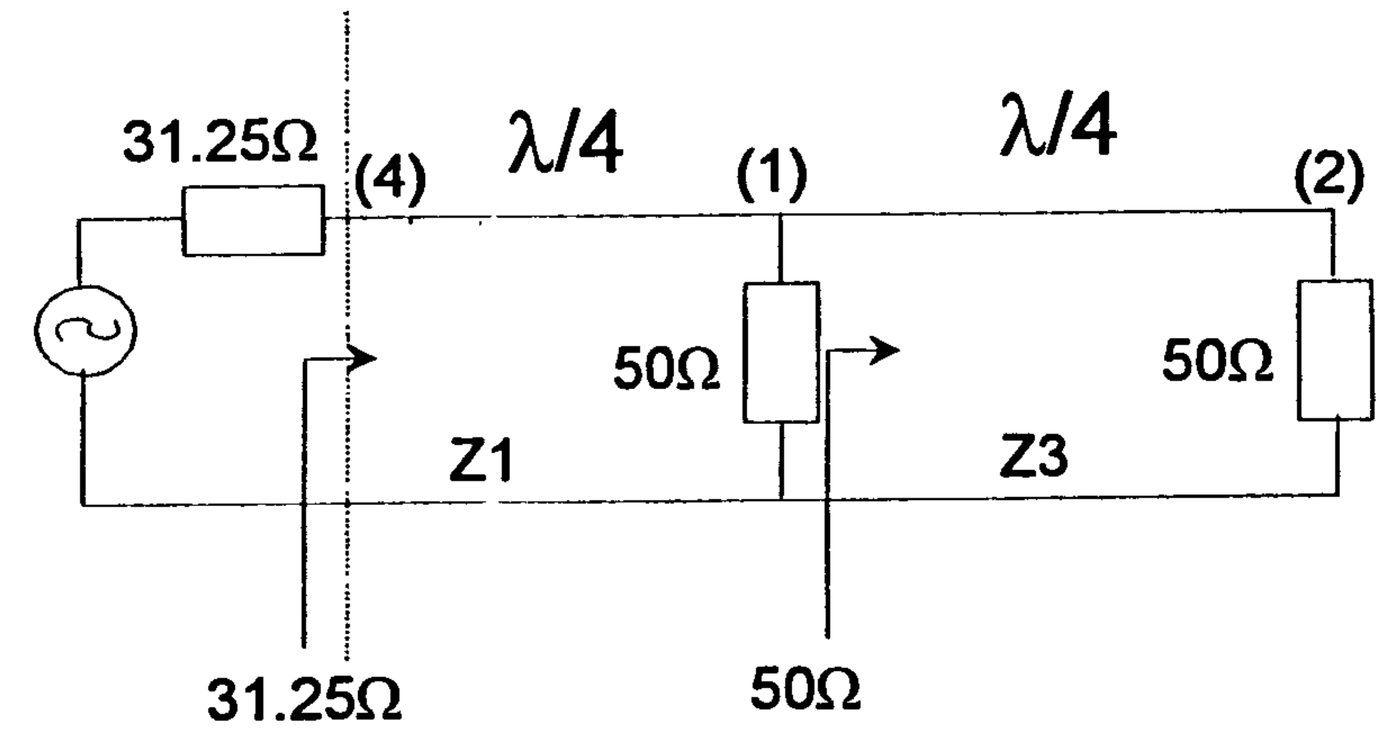

Figure 4.2.19(a)-(d) Equivalent Circuits for Coupler Design

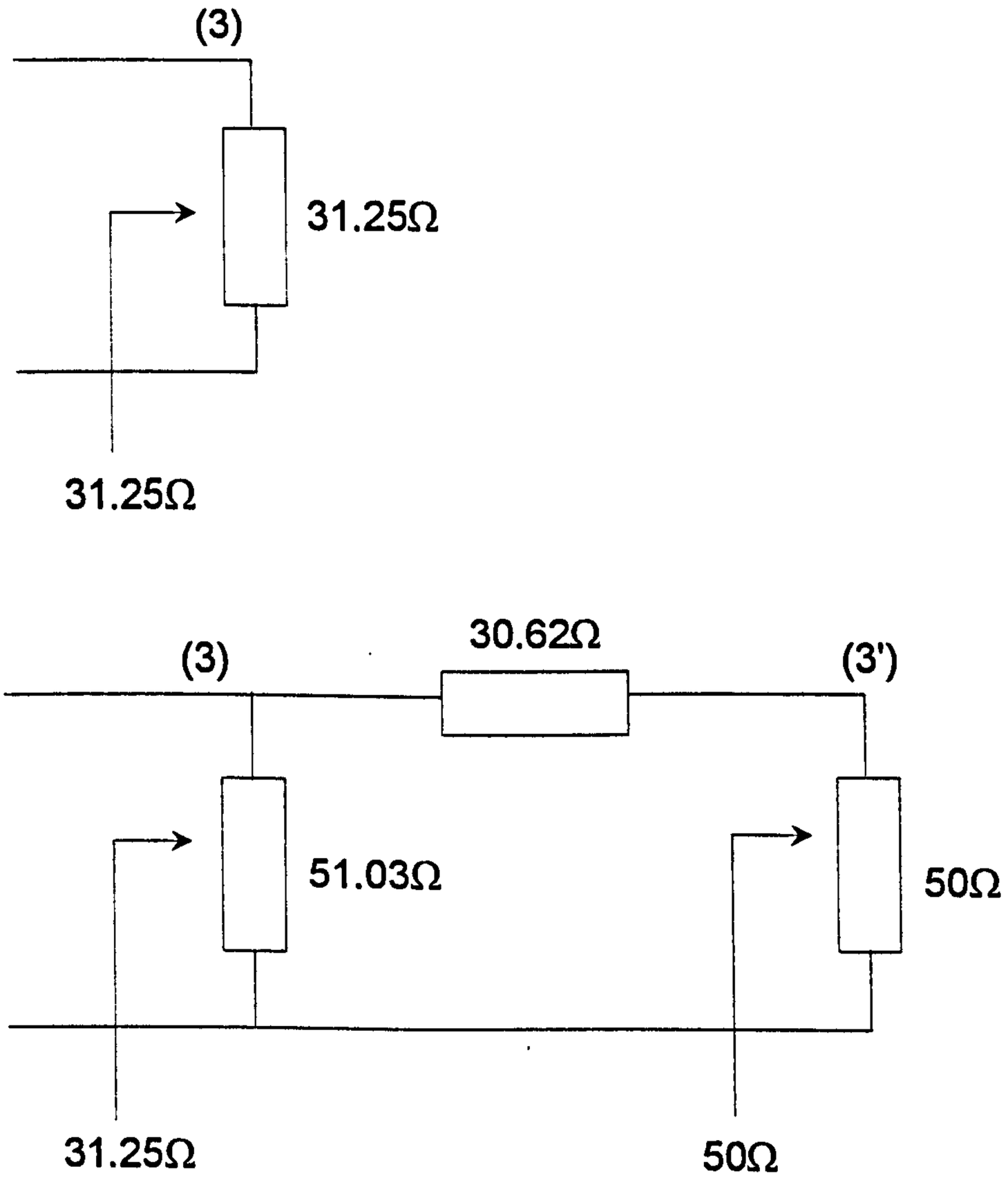

Figure 4.2.20 Dummy Circuit for Transforming 31.25Ω into 50Ω

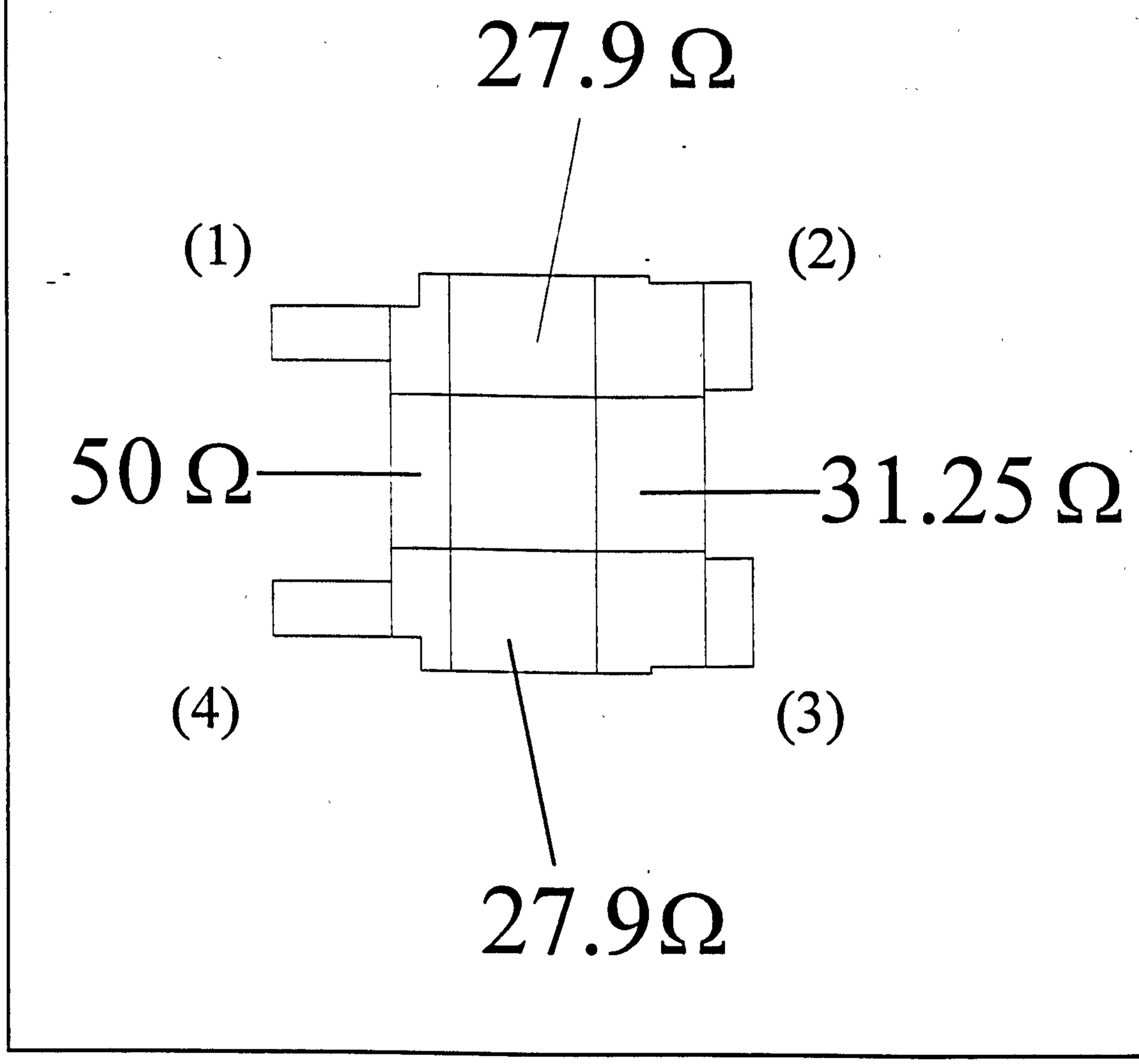

Figure 4.2.21 Coupler for OBU C.P. Antenna

(a)

S11

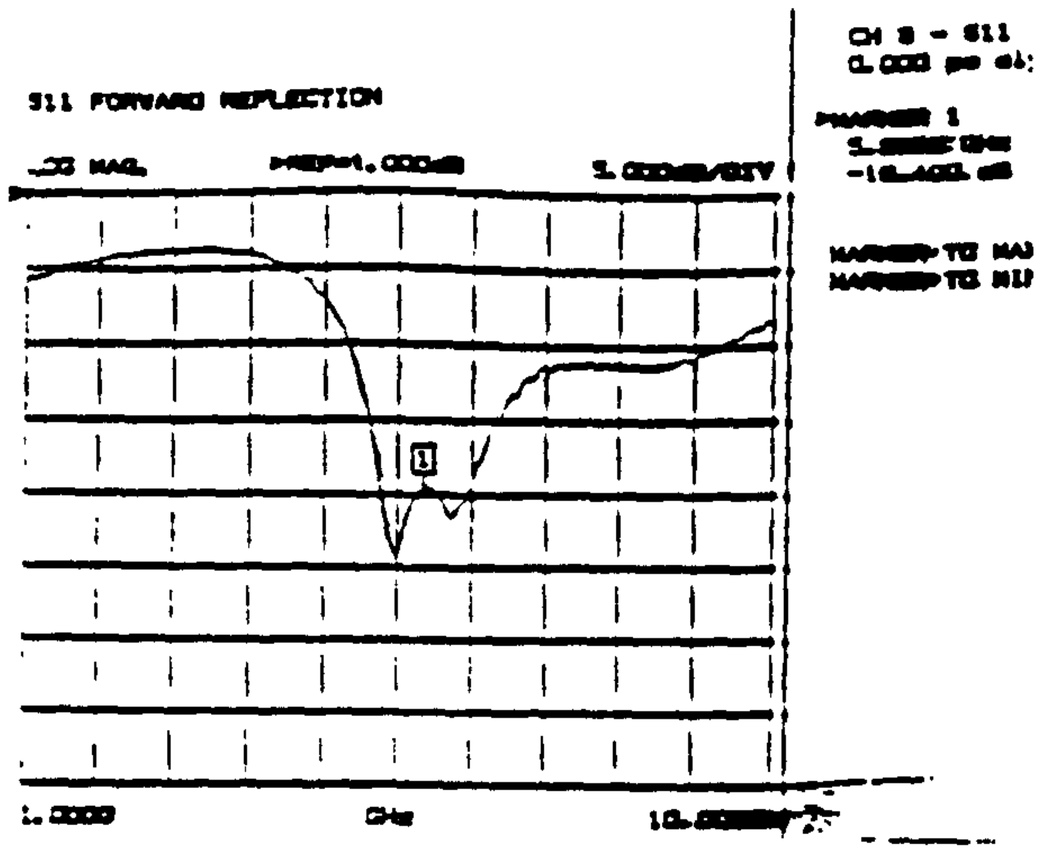

(b)

S21

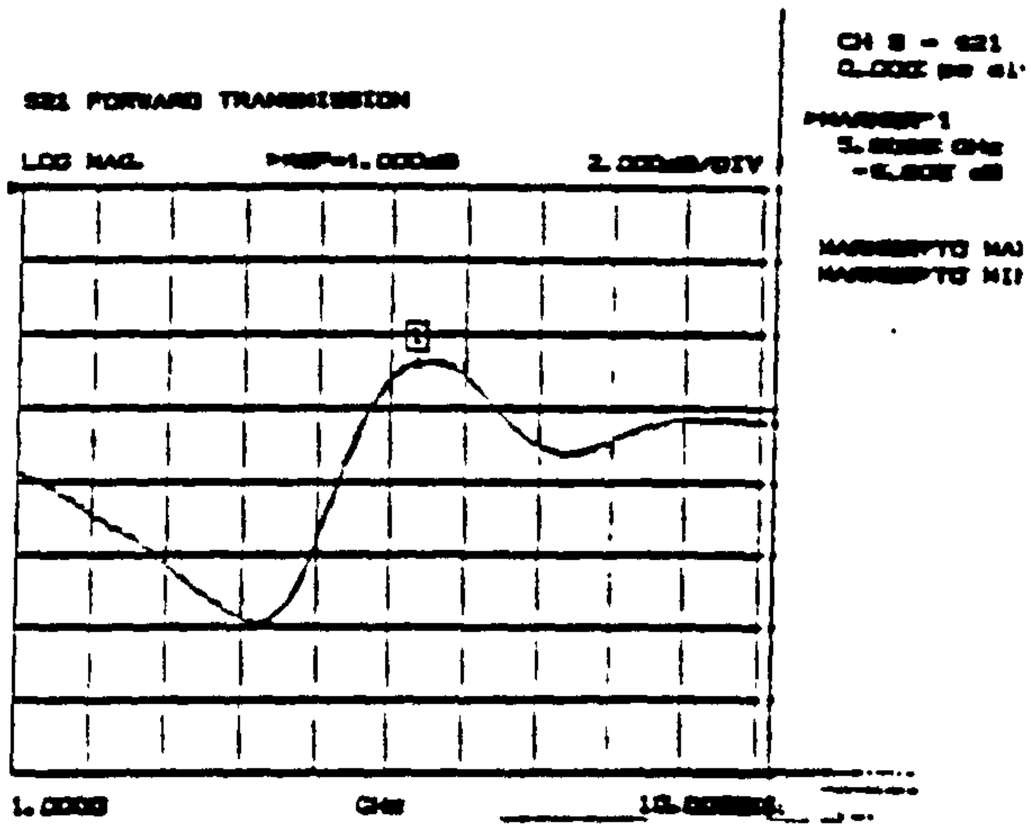

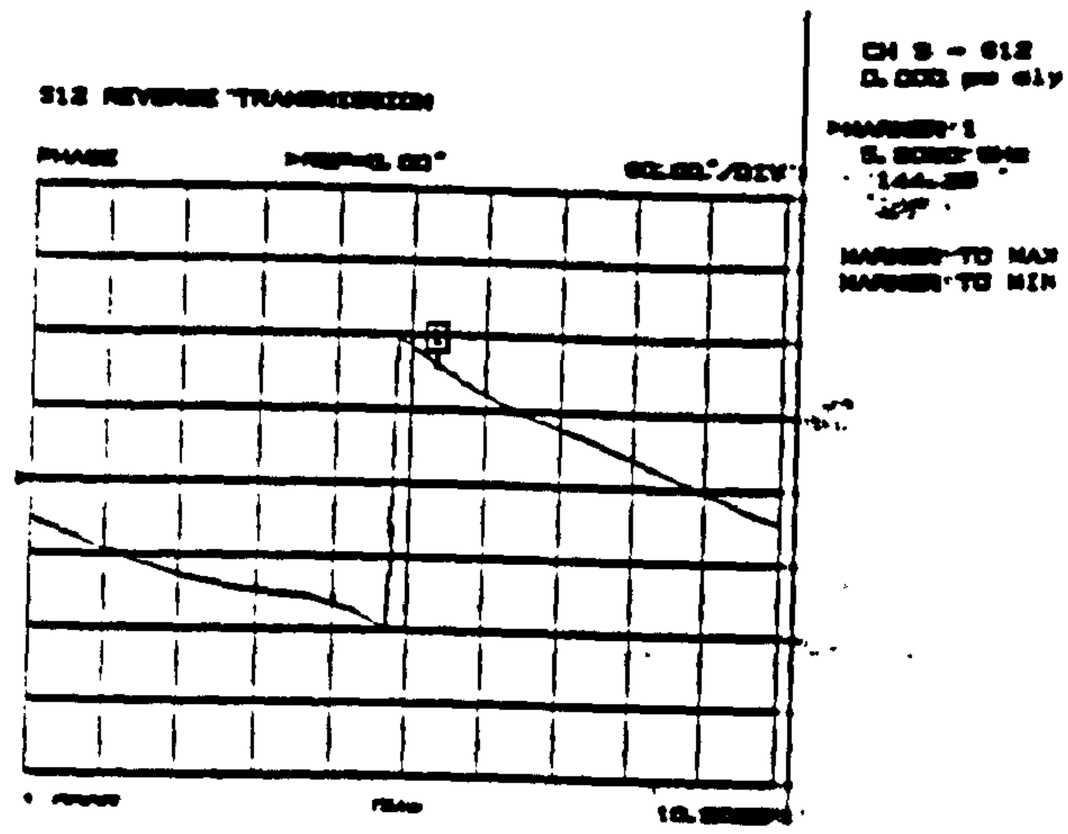

(c)

S31

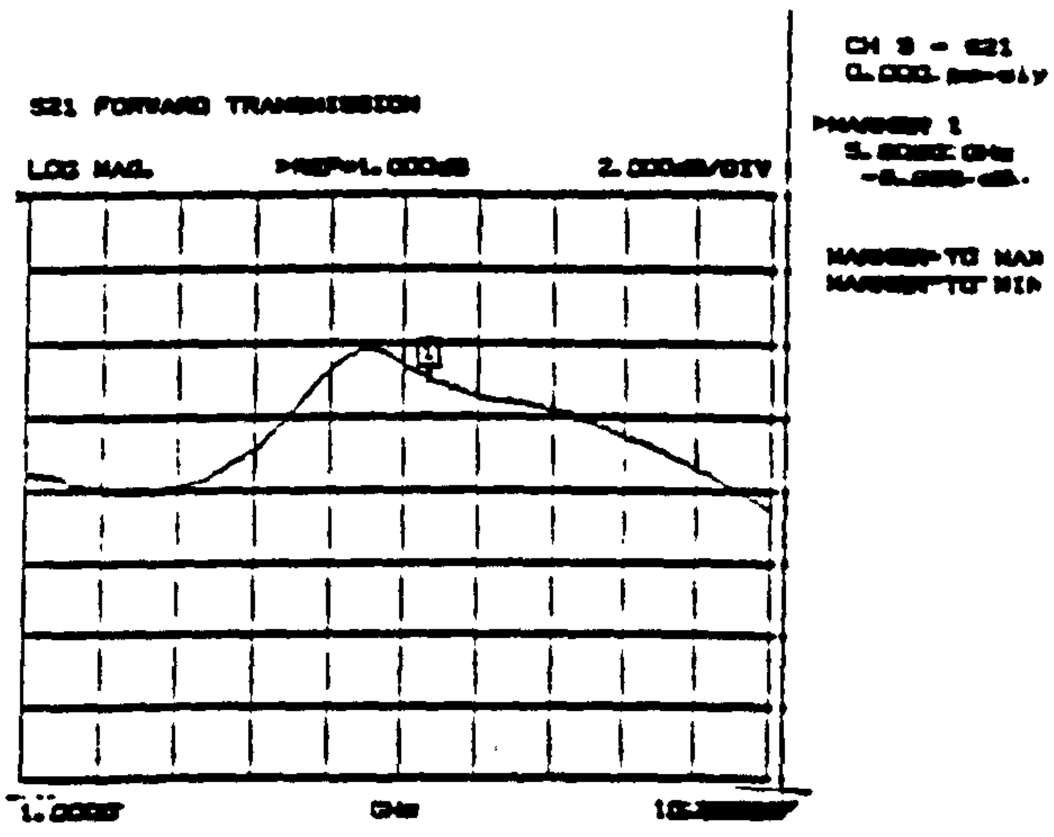

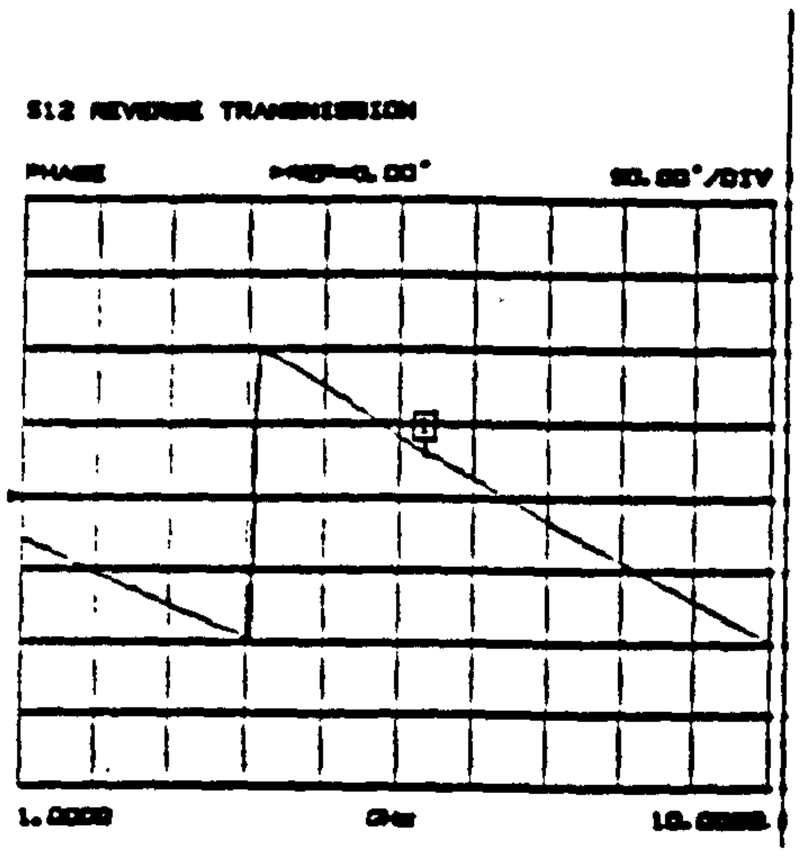

(d)

S41

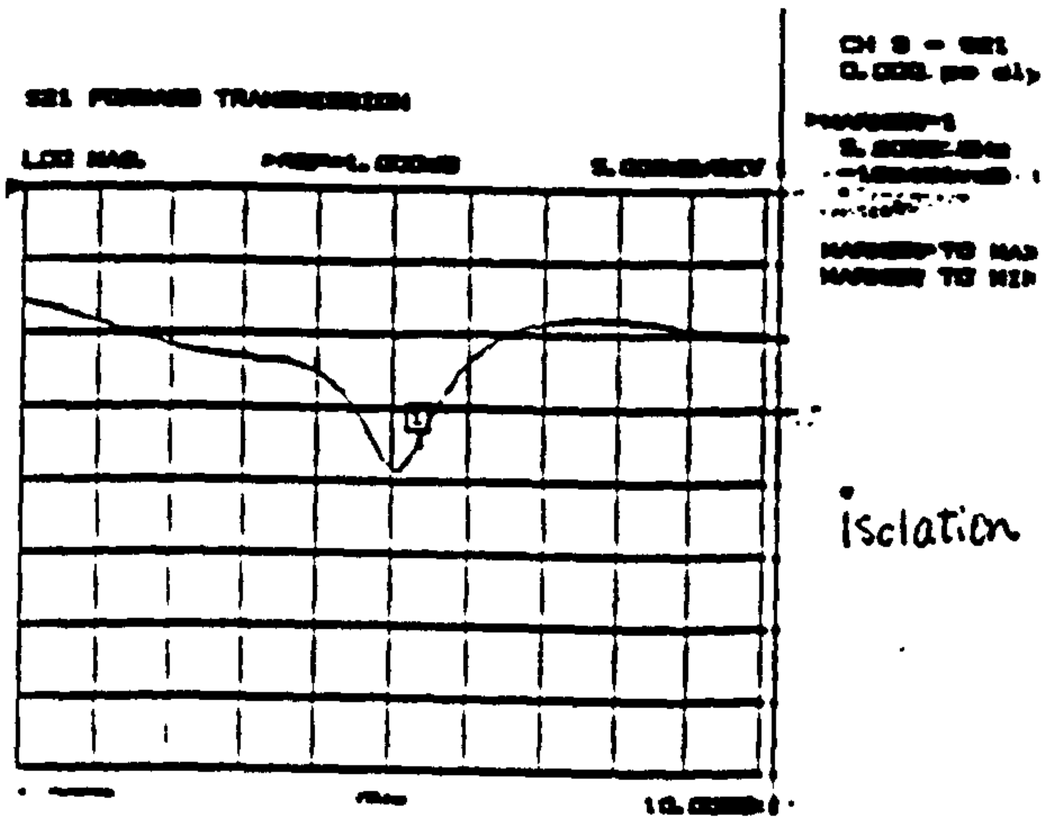

Isolation

Figure 4.2.22 'S'-Parameters for OBU Coupler

S11

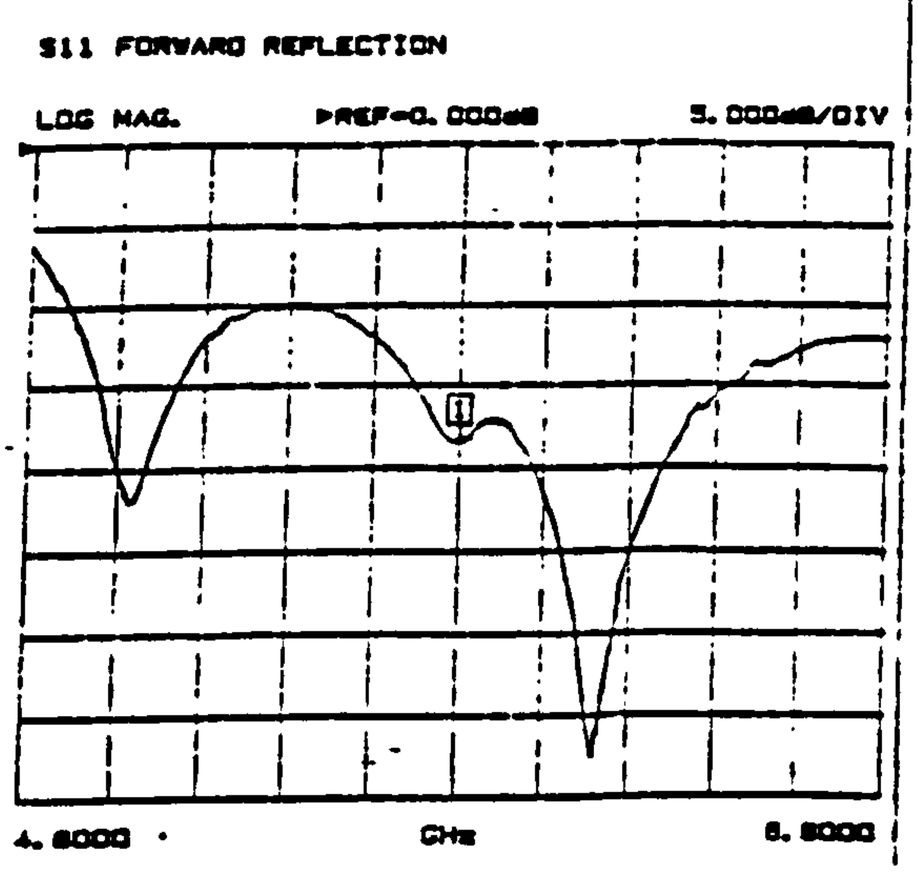

S12

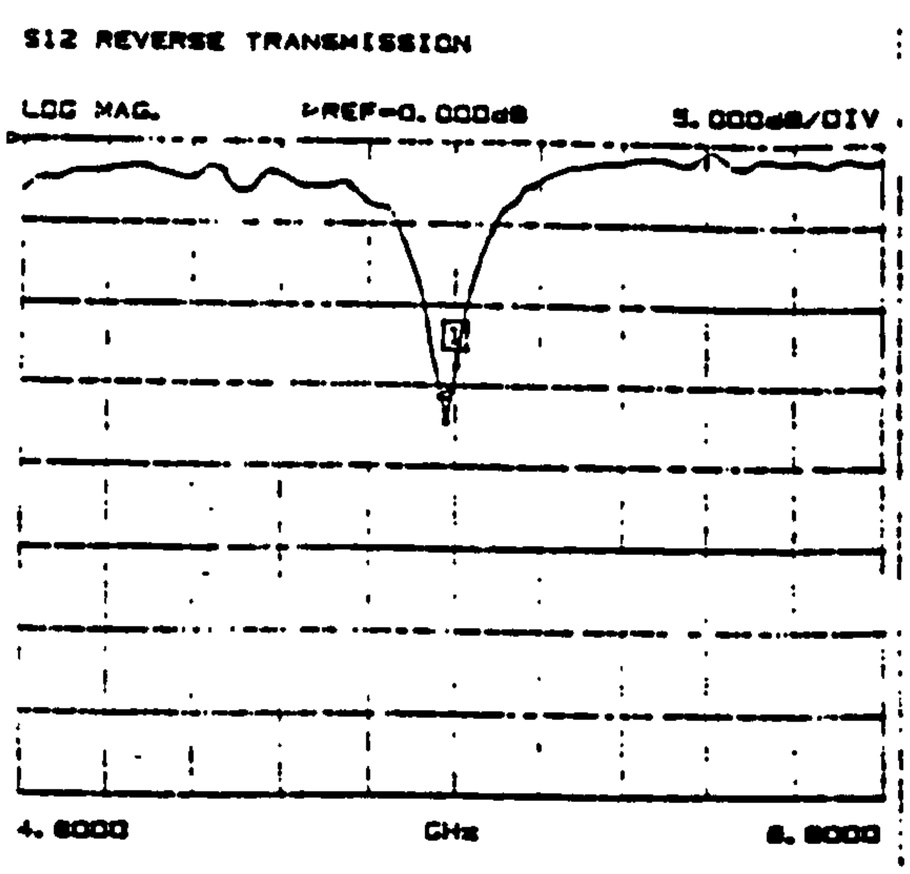

S21

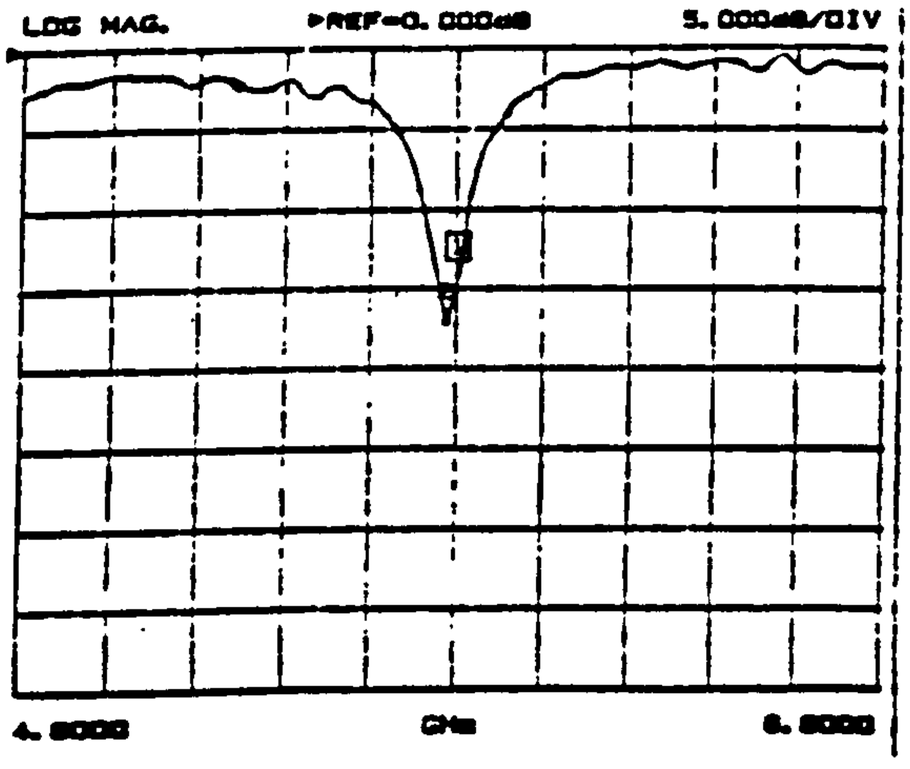

S22

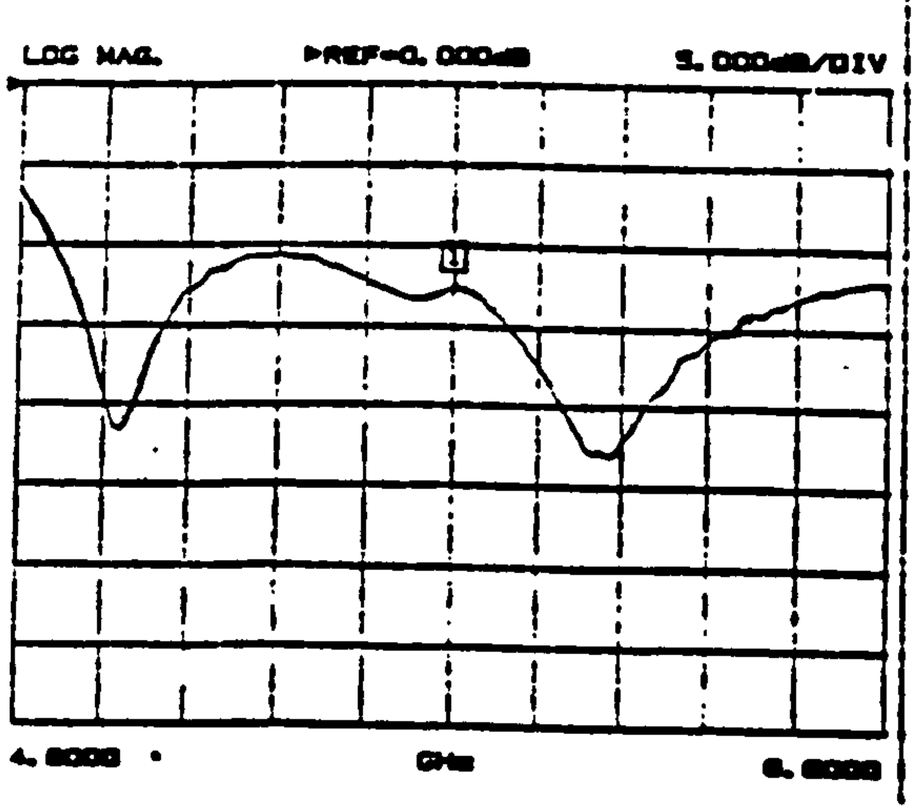

Figure 4.2.23 'S' Parameters for OBU C.P. Patch Antenna

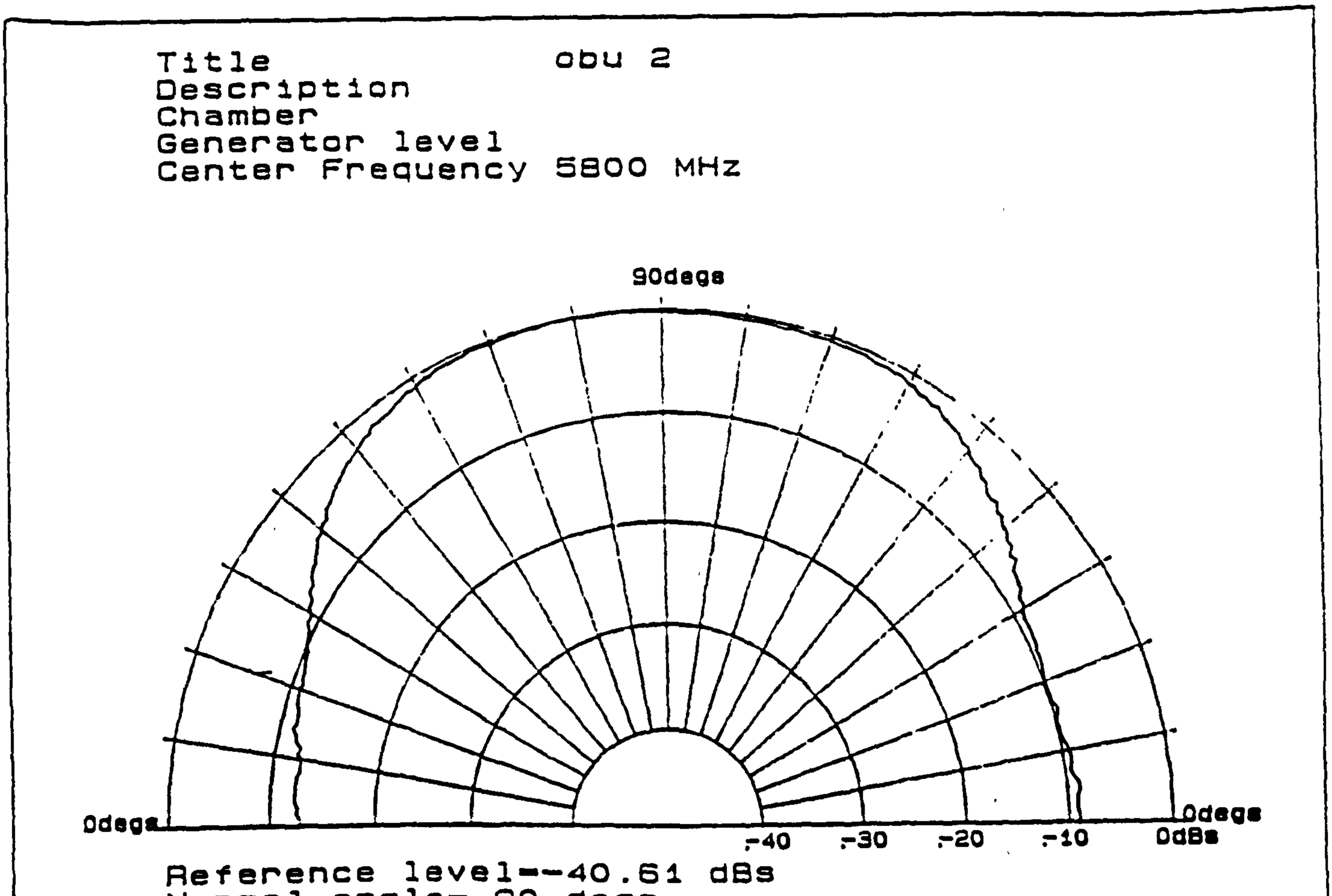

Gain = 5.5dBi

Half-Power Beamwidth = 84°

Figure 4.2.24 Polar Pattern for OBU C.P. Patch Antenna

CHAPTER 5

Mutual Coupling Between Two Patch Antennae

5.1 Introduction

The analysis of mutual coupling between two patch antennae is developed in this chapter based on two approaches, namely the transmission line model (TLM) and the cavity model. For the TLM, the mutual admittance integrals of the two radiating slots have been derived. Nauwelaers and Capelle (1985 and 1993) proposed a set of formulae for mutual admittance however, their analysis breaks down if the two radiating slots are placed very close to each other. In the design of antenna array the spacing between radiating slots varies. Consequently a set of new formulae for the mutual admittance have been derived which are valid for all spacing between the radiating slots.

This chapter also presents the analysis of the mutual coupling between two antennae using cavity model. The results obtained for the TLM and the cavity model show a good agreement with published results.

5.2 TLM Approach

The mutual coupling between radiation slots is caused by the simultaneous effect of free space radiation and surface waves but for a substrate of small electrical thickness and low permittivity the surface wave can be neglected (Jedlicka,1981).

E.H. Van Lil (1980 and 1984) developed a model for calculating the mutual coupling however, the mutual admittance expressed by the coupling integrals has to be evaluated numerically.

Initially this section presents the derivation of the expression for the mutual admittance between two arbitrarily placed radiating slots, and then a set of formulae is obtained which can be used to calculate the mutual coupling (S_{21}) between two rectangular microstrip antennae. Finally the predicted results of the mutual coupling for E and H- plane are compared to the published results where good agreement is obtained.

5.2.1 Derivation of Mutual Admittance Expression Between Two Radiating Slots

A microstrip antenna can be modelled by a transmission line terminated at both ends by a radiation admittance (Y_S). The mutual coupling between two main radiation slots can be

represented by the mutual admittance (Y_m) (Pues,1984). Such mutual admittances can be determined by evaluating the coupling integrals numerically (Pues,1982; Lier,1983; and Van Lil,1980). However, Nauwelaers and Van de Capelle (1985) presented a simple method for calculating the mutual admittance. Their paper derived a series of approximations for the source integrals (ref.10) in order to obtain the values of both mutual conductance (G_{12}) and susceptance (B_{12}).

The work presented in this section is based on the paper by Nauwelaers, however two main problems have been identified. The first one is that the numerical results obtained based on the formulae derived did not agree. This was due to errors in the derived formulae which is shown in the Appendix E. The second problem with the paper is that the formulae could not be used if the two radiating slots are very close to each other. This is shown in the next section and the latter problem has been overcome by deriving a new set of equations valid for all spacings between radiating slots.

Formulation of Mutual Admittance

The coupling integrals for mutual admittance are first derived. It is assumed that the electric field in the apertures (i.e. radiating slots) is evenly distributed and the slots are far enough apart so that the field in the apertures would not be affected. Considering a radiating slot as shown in figure 5.2.1, the radiated power is given by

$$P_r = \int_{-\infty}^{\infty}\int_{-\infty}^{\infty} \frac{E \times H^*}{2} \bar{i}_z ds \qquad (5.2.1)$$

Using the integral form of Parseval's theorem (Harrington, p.182) equation (5.2.1) becomes

$$P_r = \frac{1}{8\pi^2} \int_{-\infty}^{\infty}\int_{-\infty}^{\infty} \left[\xi_y \mathcal{H}_x^*\right]_{z=0} dk_x dk_y \qquad (5.2.2)$$

where ξ , $\mathcal{H}$ are the Fourier transform of E and H, respectively and

$$\xi_y\big|_{z=0} = \int_{-\infty}^{\infty} E_y(y)\big|_{z=0}\, e^{-jk_y y} dy \qquad (5.2.3)$$

If the wave function ψ is chosen as (Harrington,p.180)

$$\Psi = \frac{1}{4\pi^2}\int_{-\infty}^{\infty}\int_{-\infty}^{\infty} f(k_x,k_y)e^{jk_x x}e^{jk_y y}e^{jk_z z}dk_x dk_y \qquad (5.2.4)$$

where the transform of ψ is

$$\overline{\Psi} = f(k_x,k_y)e^{jk_z z} \qquad (5.2.5)$$

then the Maxwell equations (Harrington,p.181) become

$$\begin{aligned} \xi_x &= 0 & \mathcal{H}_x &= \frac{k^2-k_x^2}{j\omega\mu}\overline{\Psi} \\ \xi_y &= -jk_z\overline{\Psi} & \mathcal{H}_y &= -\frac{k_x k_y}{j\omega\mu}\overline{\Psi} \\ \xi_z &= jk_y\overline{\Psi} & \mathcal{H}_z &= -\frac{k_x k_z}{j\omega\mu}\overline{\Psi} \end{aligned} \qquad (5.2.6)$$

If the wave is in the transmission-line mode (TEM to z), ξ_y will be the only component of ξ while $\mathcal{H}_x$ will be the only component of $\mathcal{H}$. From equation (5.2.6):

$$\mathcal{H}_x = \frac{1}{\omega\mu}\frac{k^2-k_x^2}{k_z}\xi_y \qquad (5.2.7)$$

The radiated power P_r (Van Lil, 1980) is given by

$$P_r = \frac{1}{8\pi^2\omega\mu}\int_{-\infty}^{\infty}\int_{-\infty}^{\infty}\frac{(\xi_y k_y^*)(\xi_y^* k_y^*)+(k_z^*)^2\xi_y\xi_y^*}{\xi_z^*}dk_x dk_y \qquad (5.2.8)$$

where $k = 2\pi/\lambda_0$ and $k^2 = k_x^2 + k_y^2 + k_z^2$.

For two radiating slots as shown in figure 5.2.2, by substituting $\xi_y = \xi_{y1} + \xi_{y2}$ and identifying each part of the power expression term by term we have

$$P_r = \frac{1}{8\pi^2\omega\mu}\int_{-\infty}^{\infty}\int_{-\infty}^{\infty}\frac{\left(\xi_{y1}k_y^*\right)\left(\xi_{y1}^*k_y^*\right)+\left(k_z^*\right)^2\xi_{y1}\xi_{y1}^*}{\xi_z^*}dk_xdk_y$$

$$+\frac{1}{8\pi^2\omega\mu}\int_{-\infty}^{\infty}\int_{-\infty}^{\infty}\frac{\left(\xi_{y2}k_y^*\right)\left(\xi_{y2}^*k_y^*\right)+\left(k_z^*\right)^2\xi_{y2}\xi_{y2}^*}{\xi_z^*}dk_xdk_y$$

$$+\frac{2}{8\pi^2\omega\mu}\int_{-\infty}^{\infty}\int_{-\infty}^{\infty}\frac{\mathrm{Re}\left[\left(\xi_{y1}k_y^*\right)\left(\xi_{y2}k_y\right)^*\right]+\left(k_z^*\right)^2\mathrm{Re}\left[\xi_{y1}\xi_{y2}^*\right]}{\xi_z^*}dk_xdk_y$$

$$\equiv \frac{1}{2}|V_1|^2Y_{11}^* + \frac{1}{2}|V_2|^2Y_{22}^* + Y_{12}^*\,\mathrm{Re}\left[V_1V_2^*\right] \qquad (5.2.9)$$

The mutual admittance can be expressed as:

$$Y_{12}^* = \frac{1}{4\pi^2\omega\mu\mathrm{Re}\left[V_1V_2^*\right]}\int_{-\infty}^{\infty}\int_{-\infty}^{\infty}\frac{\mathrm{Re}\left[\left(\xi_{y1}k_y^*\right)\left(\xi_{y2}k_y\right)^*\right]+\left(k_z^*\right)^2\mathrm{Re}\left[\xi_{y1}\xi_{y2}^*\right]}{\xi_z^*}dk_xdk_y \qquad (5.2.10)$$

For the translated slot, the integrand should be multiplied by $\cos\left(k_x\Delta x + k_y\Delta y\right)$ and the expression (5.2.10) becomes

$$Y_{12}^* = \frac{1}{4\pi^2\omega\mu\mathrm{Re}\left[V_1V_2^*\right]}\int_{-\infty}^{\infty}\int_{-\infty}^{\infty}\frac{\mathrm{Re}\left[\left(\xi_yk_y^*\right)\left(\xi_yk_y\right)^*\right]\left(k_z^*\right)^2\mathrm{Re}\left[\xi_y\xi_y^*\right]}{\xi_z^*}\cos\left(k_x\Delta x + k_y\Delta y\right)dk_xdk_y \qquad (5.2.11)$$

The electric field is assumed to be constant over the width of the aperture so that

$$E_y\big|_{z=0} = E_a \text{ for } -\frac{W}{2} < x < \frac{W}{2}\ ;\ -\frac{\delta L}{2} < y < \frac{\delta L}{2} \qquad (5.2.12)$$

where E_a is given by (Hammer,1979):

$$E_a = \frac{hE_o}{2\delta L} \qquad (5.2.13)$$

where E_o is constant over the height of the substrate.

The present discussion departs from the line taken by Van Lil (1980) in that b=kδL is no longer assumed to be zero. Thus taking the Fourier transform of expression (5.2.12) gives

$$\xi_y = \int_{-\frac{\delta L}{2}}^{+\frac{\delta L}{2}} \int_{-\frac{W}{2}}^{+\frac{W}{2}} E_y\big|_{z=0} e^{-ik_x x} e^{-jk_y y} dxdy$$

$$= \frac{V_o W}{2} \sin c\left(\frac{k_x W}{2}\right) \sin c\left(\frac{k_y \delta L}{2}\right) \tag{5.2.14}$$

where sinc(x)=sin(x)/x. Substituting equations (5.2.14) into (5.2.11), Y_{12}^* becomes:

$$Y_{12}^* = \frac{W^2}{16\pi^2 \omega\mu} \int_{-\infty}^{\infty}\int_{-\infty}^{\infty} \frac{\left(k^2 - k_x^2\right) \sin c^2\left(\frac{k_x W}{2}\right) \sin c^2\left(\frac{k_y \delta L}{2}\right)}{k_z^*} \cos\left(k_x \Delta x + k_y \Delta y\right) dk_x dk_y \tag{5.2.15}$$

where k_z is chosen as

$$\begin{aligned} k &= \sqrt{k^2 - \left(k_x^2 + k_y^2\right)} \quad \text{for} \quad k > \left|\sqrt{k_x^2 + k_y^2}\right| \\ &= j\sqrt{\left(k_x^2 + k_y^2\right) - k^2} \quad \text{for} \quad k < \left|\sqrt{k_x^2 + k_y^2}\right| \end{aligned} \tag{5.2.16}$$

Note that the above integrand is real for $k > \left|\sqrt{k_x^2 + k_y^2}\right|$; and imaginary for $k < \left|\sqrt{k_x^2 + k_y^2}\right|$.

Since $Y_{12} = G_{12} + jB_{12}$, the mutual conductance can be expressed as:

$$G_{12} = \frac{W^2}{16\pi^2 \omega\mu} \int_{-k}^{+k} \int_{-\sqrt{k^2 - k_y^2}}^{+\sqrt{k^2 - k_y^2}} \frac{\left(k^2 - k_x^2\right) \sin c^2\left(\frac{k_x W}{2}\right) \sin c^2\left(\frac{k_y \delta L}{2}\right)}{\sqrt{k^2 - \left(k_x^2 + k_y^2\right)}} \cos\left(k_x \Delta x + k_y \Delta y\right) dk_x dk_y \tag{5.2.17}$$

The equation (5.2.17) can be transformed into a polar form by the substitution

$$k_x = k\sqrt{1-\Psi^2}\sin\theta$$
$$k_y = k\sqrt{1-\Psi^2}\cos\theta \qquad (5.2.18)$$

where $0<\psi<1$, $0<\theta<2\pi$ and the Jacobian is given by

$$J = \begin{vmatrix} \frac{\partial k_x}{\partial \Psi} & \frac{\partial k_x}{\partial \theta} \\ \frac{\partial k_y}{\partial \Psi} & \frac{\partial k_y}{\partial \theta} \end{vmatrix} = \Psi k^2 \qquad (5.2.19)$$

Finally G_{12} is then given by

$$G_{12} = \frac{a^2}{4\pi^2\eta_o}\int_0^{2\pi}\int_0^1 \sin c^2\left(\frac{a}{2}\sqrt{1-\Psi^2}\sin\theta\right)\sin c^2\left(\frac{b}{2}\sqrt{1-\Psi^2}\cos\theta\right)$$

$$\left(\cos^2\theta+\Psi^2\sin^2\theta\right)\cos\left[\left(c.\cos\theta+f.\sin\theta\right)\sqrt{1-\Psi^2}\right]d\Psi d\theta \qquad (5.2.20)$$

where $a=kW$; $b=k\delta L$; $c=k\Delta y$; $f=k\Delta x$ and $k=2\pi/\lambda_o$.

From equation (5.2.15) the mutual susceptance is given by

$$B_{12} = \frac{W^2}{4\pi^2\omega\mu}\int_k^{+\infty}\int_{\sqrt{k^2-k_y^2}}^{+\infty}\frac{\left(k^2-k_x^2\right)\sin c^2\left(\frac{k_xW}{2}\right)\sin c^2\left(\frac{k_y\delta L}{2}\right)}{\sqrt{\left(k_x^2+k_y^2\right)-k^2}}\cos\left(k_x\Delta x+k_y\Delta y\right)dk_xdk_y \qquad (5.2.21)$$

A polar form of the above expression is obtained by means of the substitution

$$k_x = k\sqrt{1+\Psi^2}\sin\theta$$
$$k_y = k\sqrt{1+\Psi^2}\cos\theta \qquad (5.2.22)$$

where $0<\psi<\infty$, $0<\theta<2\pi$ and the Jacobian $J = \psi k^2$. The result for the mutual susceptance B_{12} is then

$$B_{12} = \frac{a^2}{4\pi^2 \eta_o} \int_0^{2\pi} \int_0^{\infty} \sin c^2 \left(\frac{a}{2}\sqrt{1+\Psi^2}\,\sin\theta\right) \sin c^2 \left(\frac{b}{2}\sqrt{1+\Psi^2}\,\cos\theta\right)$$

$$\left(\cos^2\theta - \Psi^2 \sin^2\theta\right) \cos\left[\left(c.\cos\theta + f.\sin\theta\right)\sqrt{1+\Psi^2}\right] d\Psi d\theta \qquad (5.2.23)$$

These integrals printed incorrectly can be found in the paper of Nauwelaers (1985) and it was assumed that the width of the radiating slot (b) is equal to zero.

5.2.2 Derivation of New Formulae for Mutual Admittance and Results

Mutual Conductance

A fast converging infinite series representation for the integral in G_{12} was developed (Appendix F) on the assumption that the width of the radiating slot (b=kδL) is much smaller than the wavelength in free space i.e. b→0. The resulting formula for G_{12} is then given by

$$G_{12} = \frac{2}{\pi^2 \eta_o}\left(I_1 - I_2\right) \qquad (5.2.24)$$

where

$$I_1 = \frac{\pi}{4}\left(\frac{a^2 \sin c}{c} - a^2 - 2\cos f + \cos A + \cos B - 2f\,Si(f) + A\;Si(A) + B\;Si(B)\right)$$

$$+\frac{\pi}{8}\sum_{m=3}^{\infty}\frac{(-1)^m (m-1)!}{(2m-1)!}\sum_{i=2}^{m-1}\frac{c^{2m-2i}\left(2f^{2i} - A^{2i} - B^{2i}\right)}{(2i-1)(m-i)!\,i!} \qquad (5.2.25)$$

and

$$I_2 = \frac{\pi}{4}\left[\frac{2\sin\sqrt{c^2+f^2}}{\sqrt{c^2+f^2}} - \frac{\sin\sqrt{c^2+A^2}}{\sqrt{c^2+A^2}} - \frac{\sin\sqrt{c^2+B^2}}{\sqrt{c^2+B^2}}\right] \qquad (5.2.26)$$

where A=f+a, B=f-a and $Si(x) = \int_0^x \frac{\sin t}{t} dt$.

The infinite series above converges rapidly with no more than 30 terms required in the worst case situation for the parameters c=4π, f=0 and a=3.121. Considerably fewer terms are required for small value of 'c' and 'f'.

The self-conductance (G_s) is determined by taking c=f=0.

Mutual Susceptance

The departure from the Capelle treatment was necessitated by the fact that the coupling integral for the mutual susceptance B_{12} given by equation (5.2.23) is divergent if the width of the slot (b=kδL) is taken to be zero. In contrast the present formulation of B_{12} of the coupling integral results in a convergent integral.

Therefore the width of the slot has to be considered when evaluating the integral even if the width is very small compared to the wavelength in free space. However the integral is very difficult to evaluate numerically.

In order to evaluate the mutual susceptance the equation (5.2.23) has been re-arranged as

$$B_{12} = \frac{2}{\pi^2 \eta_o} \int_0^{\pi/2} \int_0^{\infty} \left[\frac{\sin\left(\frac{a}{2}\sqrt{1+\Psi^2}\sin\theta\right)}{\sin\theta} \frac{\sin\left(\frac{b}{2}\sqrt{1+\Psi^2}\cos\theta\right)}{\frac{b}{2}\sqrt{1+\Psi^2}\cos\theta} \right]^2 \left(\frac{1}{1+\Psi^2} - \sin^2\theta\right)$$

$$2\cos\left[c.\cos\theta\sqrt{1+\Psi^2}\right]\cos\left[f.\sin\theta\sqrt{1+\Psi^2}\right] d\Psi d\theta \qquad (5.2.27)$$

A profile of the integrand in the Ψ-plane showed that the difficulty in numerical evaluation was caused by very high frequency oscillations. This oscillation together with the amplitude decay factor of only $1/(1+\Psi^2)$ accounted for the long run-times which of necessity involved considerable round-off errors in the numerical integration.

The following Table 5.2.1 shows quite clearly that, as successive intervals of integration over the range of Ψ are taken, there is no definite evidence of numerical convergence. Individual contributions from the intervals of integration show sudden increases at Ψ=30 and Ψ=40 in the above cases. However in consideration of the long computation run times it may

be that the above increases are mainly due to round off errors. In that event the best available estimates of B_{12} are underlined in Table 5.2.1.

$$B_{12} = B_{12}(a,b,c,f)$$
$$= B_{12}(3.121,b,1.9573,5.00632)$$

Intervals of Integration for Ψ	b = 0.0238	b = 0.2
0 - 10	-1.1279262669E-4	-1.1602002379E-4
10 - 20	-2.8479527377E-5	-2.2563273750E-5
20 - 30	-5.2612688276E-6	4.2327857020E-6
30 - 40	1.6121568440E-5 *	2.9172081639E-7
40 - 50	5.2924585762E-7 *	3.7123504185E-6 *

Note: * Round-off errors appear at these values of Ψ.

Default tolerance for evaluating integral in 'MathCad' is 0.001.

Table 5.2.1 An Example of Evaluating the Mutual Susceptance

From Table 5.2.1, the value of B_{12} is calculated by adding the values between interval of 0-10, 10-20,... together. Therefore,

for a=3.121,b=0.0238,c=1.9573,f=5.00632, B_{12} = -1.465334228E-4; and
for a=3.121, b=0.2, c=1.9573, f=5.00632, B_{12} = -1.34058791E-4.

Comparison with Published Results

The Nauwelaers formulae (Appendix C) for the mutual conductance G_{12} do not give accurate results if the spacing is too small (i.e. $c^2 + f^2 < 1$). However in the new formula for G_{12} the parameter 'c' representing the spacing between the slots is in the numerator and hence convergence is excellent especially for small value of 'c'.

The mutual admittance is calculated using the equations (5.2.24) and (5.2.27) and compared with the results from Nauwelaers equations numerically. Table 5.2.2 shows the numerical results for the mutual conductance while Table 5.2.3 shows the results for the mutual susceptance.

G_{12} c:	f:	Equation (6.2.24) (N=30)	Nauwelaers' (N=10)
1.9573	5.0063	-1.28716E-4	-1.28716E-4
1.9573	10.6612	7.23246E-6	7.23316E-6
0	5	7.85551E-5	7.85551E-5
1	0	1.88795E-3	N=9 1.88895E-3 N=10 1.87872E-3 N=11 1.97400E-3 (Divergent)
5	0	-6.04669E-4	-6.04669E-4

Table 5.2.2 Comparison for Mutual Conductance (a=3.121,b=0)

B_{12} c:	f:	Equation (6.2.27) b=0.2*	Equation (6.2.27) b=0.0238**	Nauwelaers' (b=0) (N=10)
1.9573	5.0063	-1.34059E-4	-1.46533E-4	-1.36950E-4
1.9573	10.6612	-2.98878E-5	-2.95326E-5	-3.13596E-5
0	5	-1.92145E-4	-1.93123E-4	-1.84121E-4
1	0	-1.64608E-4	-1.88208E-4	Not Applied (∵c<1.2)
5	0	4.15296E-4	4.19429E-4	4.17109E-4

Note: *b=0.2 for comparison purpose;**b=0.0238 is the calculated normalised values of line extension.

Table 5.2.3 Comparison for Mutual Susceptance (a=3.121)

The equations from Nauwelaers (1993, private communication), Pues (1982) and Lier (1983) (Appendices C, D, G and H) were compared with the new formulae 5.2.24 and 5.2.27 (Appendix F). Figure 5.2.3 shows the comparisons for the mutual conductance and figure 5.2.4 for the susceptance, normalised to the self-conductance as a function of normalised distance for E-plane. It was found that the new formulae for both mutual conductance and susceptance are in good agreement with the published results.

Formulae for evaluating mutual admittance between rectangular microstrip antennae have been presented. These can be used for any distance between radiation slots but are especially efficient if the spacing between the slots is small when evaluating the mutual conductance.

Due to the fact that the integrand for mutual susceptance has a high degree of oscillations and diminishes only as $1/(1+\Psi^2)$, the computation of the integral is time-inefficient. However, for all values of 'c' the new integral for B_{12} can be computed as the infinite upper limit is replaced progressively through Ψ=10, 20,30,... using 'MathCad'. The formulae have also been compared with other published results and good agreement has been obtained.

In the following section the new formulae are used to examine the mutual coupling between patch antennae using theTLM.

5.2.3 Transmission Line Model for Mutual Coupling

It is assumed that the mutual coupling between two rectangular microstrip antennae can be evaluated as a function of the coupling between several narrow rectangular slots (Van Lil, 1984) as shown in figure 5.2.5. and the mutual coupling can be represented by the voltage-dependent current sources. The equivalent circuit of two antennae is shown in figure 5.2.6. The [Y] matrix related to the currents and voltages can be written as:

$$\begin{pmatrix} I_1 - Y_{m1}V_3 - Y_{mf}V_4 - Y_{me}V_2 \\ I_3 - Y_{m1}V_1 - Y_{mr}V_4 - Y_{ms}V_2 \end{pmatrix} = \begin{pmatrix} Y_{st1} & Y_{c1}\operatorname{csc}h\gamma L_1 \\ Y_{c1}\operatorname{csc}h\gamma L_1 & Y_{st1} \end{pmatrix} \begin{pmatrix} V_1 \\ V_3 \end{pmatrix} \tag{5.2.28}$$

and

$$\begin{pmatrix} I_2 - Y_{m2}V_4 - Y_{ms}V_3 - Y_{me}V_1 \\ I_4 - Y_{m2}V_2 - Y_{mr}V_3 - Y_{mf}V_1 \end{pmatrix} = \begin{pmatrix} Y_{st2} & Y_{c2}\operatorname{csc}h\gamma L_2 \\ Y_{c2}\operatorname{csc}h\gamma L_2 & Y_{st2} \end{pmatrix} \begin{pmatrix} V_2 \\ V_4 \end{pmatrix} \tag{5.2.29}$$

where $Y_{st1} = Y_{s1} + Y_{c1}\coth\gamma L_1$ and $Y_{st2} = Y_{s2} + Y_{c2}\coth\gamma L_2$. Since $I_3 = I_4 = 0$, the [Y] matrix of the two-port network (port 1 and port 2) can be derived as,

$$\begin{pmatrix} Y_{11} & Y_{12} \\ Y_{21} & Y_{22} \end{pmatrix} \begin{pmatrix} V_1 \\ V_2 \end{pmatrix} = \begin{pmatrix} I_1 \\ I_2 \end{pmatrix} \tag{5.2.30}$$

and

$$Y_{11} = \frac{Y_{st1}^2 Y_{st2} - Y_{st1}Y_{mr}^2 + 2Y_{mt1}Y_{mf}Y_{mr} - Y_{st2}Y_{mt1}^2 - Y_{mf}^2 Y_{st1}}{N} \tag{5.2.31}$$

$$Y_{12} = Y_{21} = \frac{Y_{st1}Y_{st2}Y_{me} - Y_{me}Y_{mr}^2 + Y_{mt1}Y_{mt2}Y_{mr} - Y_{mt1}Y_{ms}Y_{st2} + Y_{mf}Y_{ms}Y_{mr} - Y_{mt2}Y_{st1}Y_{mf}}{N} \tag{5.2.32}$$

$$Y_{22} = \frac{Y_{st1}Y_{st2}^2 - Y_{st2}Y_{mr}^2 + 2Y_{mt2}Y_{ms}Y_{mr} - Y_{st1}Y_{mt2}^2 - Y_{ms}^2 Y_{st2}}{N} \tag{5.2.33}$$

where

$$Y_{st1} = Y_{s1} + Y_{c1}\coth\gamma L_1$$
$$Y_{st2} = Y_{s2} + Y_{c2}\coth\gamma L_2$$
$$Y_{mt1} = Y_{c1}\operatorname{csc}h\gamma L_1 + Y_{m1}$$
$$Y_{mt2} = Y_{c2}\operatorname{csc}h\gamma L_2 + Y_{m2}$$
$$N = Y_{st1}Y_{st2} - Y_{mr}^2 \tag{5.2.34}$$

In the case of two identical patch antennae, we have

$$Y_{s1} = Y_{s2}\ ,\ Y_{c1} = Y_{c2}\ ,\ L_1 = L_2\ ,\ Y_{m1} = Y_{m2}\ ,\ Y_{st1} = Y_{st2} \text{ and } Y_{mt1} = Y_{mt2} \tag{5.2.35}$$

The [S] parameters can then be calculated by

$$S_{21} = \frac{-2\overline{Y_{12}}}{\left(1+\overline{Y_{11}}\right)^2 - \overline{Y_{12}}^2} \tag{5.2.36}$$

and

$$S_{11} = \frac{\left(1-\overline{Y_{11}}\right)\left(1+\overline{Y_{11}}\right) - \overline{Y_{12}}^2}{\left(1+\overline{Y_{11}}\right)^2 - \overline{Y_{12}}^2} \tag{5.2.37}$$

where $\overline{Y_{11}} = 50.Y_{11}$ and $\overline{Y_{12}} = 50.Y_{12}$. The mutual coupling (in dB) is given by

$$C_p = 20\log_{10}|S_{21}| \tag{5.2.38}$$

5.2.4 Comparison with Published Results

In order to check this TLM comparisons have been done with a number of published theoretical and experimental results for E and H-plane coupling. The coupling between two identical patch antennae has been examined and the specification of the patch antenna is shown in Table 5.2.4.

Length: L=66.28mm Width: W=105.7mm

Thickness: h=1.575mm ε_r=2.50

Propagation Constant: $\gamma=\alpha+j\beta$

where $\alpha = 0.5\beta_o\sqrt{\varepsilon_{re}}\tan\delta$ and $\beta = 2\pi\sqrt{\varepsilon_{re}}/\lambda_o$

The resonant frequency of the patch is determined by

$$f_r = \frac{c}{2(L+2\delta L)\sqrt{\varepsilon_{re}}}$$

Table 5.2.4 Antenna's Specifications

The experimental results published by Jedlicka and Carver (1981) and the theoretical model published by Van Lil (1984) were compared with the present model. The method of Van Lil is a transmission line model but uses a different method for evaluating the integral of mutual admittance. Figures 5.2.7 and 5.2.8 show the mutual coupling, for E and H-Plane, between two antennae as a function of the normalised distance (normalised to the wavelength in free space) between two nearest adjacent edges, respectively. Good agreement was obtained.

5.3 Cavity Model Approach

Compared with the TLM, the cavity model is generally recognised as superior in several aspects. The analysis can be employed to include any mode of excitation and applies equally to antenna of any geometric shape (Bahl,1980).

The electromagnetic advantages of the cavity model approach are as it will be seen added to by the ease of computer implementation and the fast computer run-times obtained using 'MathCad'.

For the above reasons and because of the difficulty in evaluated B_{12} by the TLM approach it was decided to give attention to the cavity model. A recent paper by Huynh and Lee (1992) outlined the relevant field analysis though in a somewhat cryptic form. However it was therefore interesting to work out the general case analytic formulae and in particular to

unfold the computational/mathematical detail required in the evaluation of a line integral contained within another line integral - quite a novel procedure.

Using the 'Reaction' theorem and the cavity model the double-line integral for mutual impedance are derived. The predicted results of the mutual impedance and the mutual coupling for E and H-plane coupling are then compared to the published results and good agreement is obtained.

5.3.1 Formulation of Mutual Impedance

Consider two rectangular microstrip antennae oriented in the x-y plane as shown in figure 5.3.1. The antenna O'A'B'C' is referred to as antenna #1 and the antenna OABC is referred to as antenna #2. Antennae #1 and #2 are geometrically identical. The length and the width of the patch are 'a' and 'b', respectively and are fabricated on a substrate of thickness 'h', relatively permitivity 'ε_r' and loss tangent 'tanδ'. The coaxial feeds are located at (x_1', y_1') and (x_2', y_2') respectively. The formulation is based on the cavity model in which the coupling is mainly due to the space wave and it is assumed that the substrate thickness is much less than the wavelength in free space so that the surface wave can be ignored.

The mutual impedance, Z_{21}, between the two antennae is given by Rumsey's Reaction theorem (1954):

$$Z_{21} = -\frac{1}{I_1 I_2} \oiint_{S_2} \left(\underline{E}^{(1)} \cdot \underline{J}^{(2)} - \underline{H}^{(1)} \cdot \underline{M}^{(2)} \right) dS_2 \qquad (5.3.1)$$

where I_1 and I_2 are the currents at the coaxial feeds of the patches and equal to 1 Ampere. $\underline{E}^{(1)}$, $\underline{H}^{(1)}$ refer to the electric and magnetic fields on antenna #2 due to antenna #1. $\underline{J}^{(2)}$, $\underline{M}^{(2)}$ are the equivalent electric and magnetic surface current density on antenna #2 when it is self-excited.

The integration is carried out over the surface of antenna #2. Since $\underline{E}^{(1)} \cdot \underline{J}^{(2)}$ is zero over the perfect conductive surface of the patch, we have

$$Z_{21} = \frac{1}{I_1 I_2} \oiint_{S_2} \underline{H}^{(1)} \cdot \underline{M}^{(2)} dS_2 \qquad (5.3.2)$$

The surface S_2 comprises of the four sides of the rectangle OABC and extends from 0 to h in the z-direction. Since $\underline{H}$ is uniform across $0 \le z \le h$ the above integral for Z_{21} can be expressed as the line integral

$$Z_{21} = \frac{1}{I_1 I_2} \oint_{l_2'} \underline{H}^{(1)} \cdot \underline{M}^{(2)} dl_2' \tag{5.3.3}$$

where $\underline{M}^{(2)}$ and $\underline{H}^{(1)}$ are given by (Richards,1981 and Huynh,1992)

$$\underline{M}^{(2)} = jh\omega\mu \sum_{m=0}^{\infty}\sum_{n=0}^{\infty} \frac{\Psi_{mn}(x,y)\Psi_{mn}(x_2',y_2')}{k_{eff}^2 - k_{mn}^2} \cdot \hat{z} \times \hat{n} \tag{5.3.4}$$

where $\hat{n}$ is a unit vector in the direction of the outward normal to the path of integration and

$$\underline{H}^{(1)} = \frac{1}{j\omega\mu\varepsilon_o}\left[k_o^2 \underline{F}^{(1)}(x,y) + \nabla\left(\nabla \cdot \underline{F}^{(1)}(x,y)\right)\right] \tag{5.3.5}$$

where

$$\underline{F}^{(1)} = \frac{\varepsilon_o}{4\pi} \oint \underline{M}^{(1)}(r') \frac{e^{-jk_o|\underline{r}-\underline{r}'|}}{|\underline{r}-\underline{r}'|} dl_1' \tag{5.3.6}$$

$$\underline{M}^{(1)} = 2\underline{M}^{(2)}\Big|_{(x_2',y_2')\to(x_1',y_1')} \tag{5.3.7}$$

$$\Psi_{mn} = \sqrt{\frac{\varepsilon_{om}\varepsilon_{on}}{ab}} \cos\frac{m\pi x}{a} \cos\frac{n\pi y}{b} \tag{5.3.8}$$

$$\varepsilon_{op} = \begin{cases} 1, & p = 0 \\ 2, & p \neq 0 \end{cases} \tag{5.3.9}$$

$$k_{eff}^2 = k_o^2 \varepsilon_r \left(1 - j\delta_{eff}\right) \tag{5.3.10}$$

$$k_{mn}^2 = \left(\frac{m\pi}{a}\right)^2 + \left(\frac{n\pi}{b}\right)^2 \tag{5.3.11}$$

The transmission coefficient S_{21} is given by

$$S_{21} = \frac{2Z_{21} \cdot 50}{(Z_{11} + 50)^2 - Z_{21}^2} \tag{5.3.12}$$

where Z_{11} is the input impedance of isolated antenna. The mutual coupling C_p is defined as

$$C_p = 20\log_{10}|S_{21}| \tag{5.3.13}$$

For the fundamental mode (mn=01), Ψ_{01} is given by

$$\Psi_{01}(x,y) = \sqrt{\frac{2}{ab}}\cos\left(\frac{\pi(y - L_y)}{b}\right) \tag{5.3.14}$$

On substituting the expression from 5.3.4 through 5.3.11 into 5.3.3, the following expression for Z_{21} is eventually obtained (Appendix I)

$$Z_{21} = jK\oint_{l_2}\oint_{l_1}\cos\left(\frac{\pi(y - Ly)}{b}\right)\cos\left(\frac{\pi y'}{b}\right)\left\{k_o^2 g\cdot(\hat{z}\times\hat{n}_1)\cdot(\hat{z}\times\hat{n}_2) + \frac{\partial^2 g}{\partial x^2}(\hat{y}\cdot\hat{n}_1)(\hat{y}\cdot\hat{n}_2)\right.$$

$$\left. + \frac{\partial^2 g}{\partial y^2}(\hat{x}\cdot\hat{n}_1)(\hat{x}\cdot\hat{n}_2) - \frac{\partial^2 g}{\partial x\partial y}\left[(\hat{y}\cdot\hat{n}_2)(\hat{x}\cdot\hat{n}_1) + (\hat{y}\cdot\hat{n}_1)(\hat{x}\cdot\hat{n}_2)\right]\right\}dl'_1\,dl'_2 \tag{5.3.15}$$

where

$$K = \frac{2h^2\omega\mu}{\left(k_{eff}^2 - k_{01}^2\right)^2 a^2 b^2 \pi}\cos\left(\frac{\pi}{b}y'_1\right)\cos\left(\frac{\pi}{b}y'_2\right) \tag{5.3.16}$$

$$g = \frac{e^{-jk_o d}}{d} \quad \text{and} \quad g = g(x,y,x',y') = \frac{e^{-jk_o\sqrt{(x-x')^2+(y-y')^2}}}{\sqrt{(x-x')^2+(y-y')^2}} \tag{5.3.17}$$

$$\frac{\partial^2 g}{\partial x^2} = -\frac{e^{-jk_o d}}{d^3}(1 + jk_o d)\left[1 + \frac{k_o^2(x-x')^2}{1+jk_o d} - \frac{3(x-x')^2}{d^2}\right] \tag{5.3.18}$$

$$\frac{\partial^2 g}{\partial y^2} = -\frac{e^{-jk_o d}}{d^3}(1+jk_o d)\left[1+\frac{k_o^2(y-y')^2}{1+jk_o d}-\frac{3(y-y')^2}{d^2}\right] \tag{5.3.19}$$

$$\frac{\partial^2 g}{\partial x \partial y} = -\frac{(x-x')(y-y')e^{-jk_o d}}{d^5}\left(k_o^2 d^2 - 3 - j3k_o d\right) \tag{5.3.20}$$

$$d = \sqrt{(x-x')^2+(y-y')^2} \tag{5.3.21}$$

The computation for Z_{21} takes into account all the interactions of the line integrations between the two antennae. This involves the integration of each segment of line ℓ_1 with in turn each segment of line ℓ_2. There are totally sixteen interactions involved giving rise to sixteen double integrations. Some of which can be combined to give the final set of integrations for Z_{21} as follows:

$$Z_{21} = Z_1 + Z_2 + Z_3 + Z_4 \tag{5.3.22}$$

where

$$Z_1 = jK\int_{Lx}^{Lx+a}\int_{0}^{a}\left\{\begin{array}{l} k_o^2 g(x,L_y,x',0)+\dfrac{\partial^2 g(x,L_y,x',0)}{\partial x^2} \\ +k_o^2 g(x,L_y+b,x',0)+\dfrac{\partial^2 g(x,L_y+b,x',0)}{\partial x^2} \\ +k_o^2 g(x,L_y,x',b)+\dfrac{\partial^2 g(x,L_y,x',b)}{\partial x^2} \\ +k_o^2 g(x,L_y+b,x',b)+\dfrac{\partial^2 g(x,L_y+b,x',b)}{\partial x^2} \end{array}\right\} dx'dx \tag{5.3.23}$$

$$Z_2 = jK \int_{Lx}^{Lx+a} \int_{0}^{b} \cos\left(\frac{\pi y'}{b}\right) \left\{ \begin{array}{l} \dfrac{\partial^2 g(x, L_y, a, y')}{\partial x \partial y} + \dfrac{\partial^2 g(x, L_y + b, a, y')}{\partial x \partial y} \\ - \dfrac{\partial^2 g(x, L_y, 0, y')}{\partial x \partial y} - \dfrac{\partial^2 g(x, L_y + b, 0, y')}{\partial x \partial y} \end{array} \right\} dy' dx \quad (5.3.24)$$

$$Z_3 = jK \int_{Ly}^{Ly+b} \int_{0}^{b} \cos\left(\frac{\pi(y - L_y)}{b}\right) \cos\left(\frac{\pi y'}{b}\right) \left\{ \begin{array}{l} k_o^2 g(L_x, y, 0, y') + \dfrac{\partial^2 g(L_x, y, 0, y')}{\partial y^2} \\ -k_o^2 g(L_x + a, y, 0, y') - \dfrac{\partial^2 g(L_x + a, y, 0, y')}{\partial y^2} \\ -k_o^2 g(L_x, y, a, y') - \dfrac{\partial^2 g(L_x, y, a, y')}{\partial y^2} \\ +k_o^2 g(L_x + a, y, a, y') + \dfrac{\partial^2 g(L_x + a, y, a, y')}{\partial y^2} \end{array} \right\} dy' dy \quad (5.3.25)$$

$$Z_4 = jK \int_{Ly}^{Ly+b} \int_{0}^{a} \cos\left(\frac{\pi(y - L_y)}{b}\right) \left\{ \begin{array}{l} -\dfrac{\partial^2 g(L_x, y, x', 0)}{\partial x \partial y} + \dfrac{\partial^2 g(L_x + a, y, x', 0)}{\partial x \partial y} \\ -\dfrac{\partial^2 g(L_x, y, x', b)}{\partial x \partial y} + \dfrac{\partial^2 g(L_x + a, y, x', b)}{\partial x \partial y} \end{array} \right\} dx' dy \quad (5.3.26)$$

5.3.2 Comparison of Mutual Impedance with Published Results

In order to verify the validity of the above derivations, comparisons were made with a number of published theoretical and experimental values as shown graphically. The equations (5.3.22) have been used to compute the mutual impedance Z_{21} and the mutual coupling C_p for two rectangular patches with the following parameters:

Case (1). a=45mm, b=30mm, ε_r=2.32, tanδ=0.001, h=0.5mm, the calculated resonant frequency = 3.262GHz. The feed points are located at $x'_1 = x'_2 = 27.5mm$ and $y'_1 = y'_2 = 8.7mm$. For this feed position the isolated input impedance for the TM01 mode is approximately 50Ω (i.e. Z_{11}=50Ω).

Case (2). a=105.7mm, b=66.28mm, ε_r=2.5, tanδ=0.001, h=1.575mm, the calculated resonant frequency = 1.418GHz. The feed points are located at $y'_1 = y'_2 = 19mm$. For this feed position, the isolated input impedance for the TM01 mode is approximately 50Ω (i.e. Z_{11}=50Ω).

Case (3). a=16.18mm, b=16.18mm, ε_r=2.33, tanδ=0.001, h=0.79mm. the calculated resonant frequency = 5.995GHz. The feed points are located at $y'_1 = y'_2 = 0$ (i.e. microstrip feed). For this feed position the isolated input impedance for the TM01 mode is approximately 270Ω (see chapter 4).

For the case (1) figure 5.3.2 shows the mutual impedance as a function of spacing between the two nearest edges of the antennae, normalised with respect to the free space wavelength λ_o for E and H-plane while Figure 5.3.3 shows the mutual coupling for E and H-plane. They were then compared with the results from Huynh (1992).

For the case (2) figure 5.3.4 shows the mutual coupling compared with the experimental results by Jedlicka and Carver (1979) and the theoretical results by Van Lil (1984) for E and H-Plane.

For the case (3) figure 5.3.5 shows the computed results for the mutual impedance while figure 5.3.6 shows the mutual coupling for E and H-plane for the microstrip-fed antennae.

It can be seen that the formulae for evaluating the mutual coupling (i.e. $20\log_{10}|S_{21}|$) give good agreement with the published results as shown in figures 5.3.3 and 5.3.4. However, it was found that the mutual coupling is very sensitive to the resonant frequency chosen. In order to compute the mutual coupling accurately using the present method the equation for calculating the resonant frequency f_r needed to be modified in the form

$$f_r = \frac{c}{2(b+1.75\delta L)\sqrt{\varepsilon_{re}}} \qquad (5.3.27)$$

whereas in the transmission line model the effective length of the patch is taken as (b+2δL) It is found that for the cavity model the results are highly sensitive to the effective length taken

and it was determined by numerical experiment that the effective length should be taken as (b+1.75δL).

5.4 Comparison Between Measured and Predicted Mutual Coupling Results

The arrangement for measuring the mutual coupling (S_{21}) is shown in figure 5.4.1. Antennae were mounted on a rigid aluminium ground plane in order to obtain a good ground plane condition.

Jedlicka (1981) showed that the mutual coupling takes place mainly due to the space wave and the surface wave can be neglected especially for the electrically thin substrate. This implied that it is not necessary to insert dielectric spacers between the two patches when the spacing is increased.

In order to ensure that the mutual coupling is measured at the correct frequency and to ensure that the two antennae have the same resonant frequencies, the return loss of the individual patch was measured with the network analyser as shown in figure 5.4.2. The mutual coupling (S_{21}) was then measured for E and H-plane as a function of normalised spacing between the edges of antennae.

The specification of the antenna is as follows:

Substrate: RT/Duroid 5780, ε_r=2.33, h=0.79mm, t=0.0355mm, tand=0.001
Length = 16.18mm, Width = 16.18mm
Resonant frequency = 5.8GHz
Return loss < -14dB
Feed: Microstrip feed

Measured Results

The return loss of the two antennae was measured as shown in figure 5.4.3. The impedance of the antennae (with the λ/4 matching line) was measured as:

Antenna #1 : 64.70-j15.72 Ω at 5.82GHz, S_{11}=-14.47dB
and Antenna #2 : 60.87-j18.50 Ω at 5.82GHz, S_{11}= -14.54dB

Note that ideally the impedance after the $\lambda/4$ matching line should be equal to 50Ω.

Figure 5.4.4 shows the measured mutual coupling for E and H-plane compared to the theoretical results predicted from section 5.3. It should be pointed out that the predicted mutual coupling is based on the assumption that the two antennae are identical and perfectly matched to 50Ω.

It can be seen that there is about a $\pm$ 2-5dB difference from the theory. One of the main reasons is due to the mismatch effect of the patch antennae (Huynh,1992). Moreover the discrepancy is also due to the reflections in the test chamber and the effect of an imperfect ground plane.

It was also found that the E-plane coupling is stronger than the H-plane coupling as expected. For the H-plane the coupling becomes very weak as the spacing between the edges of the antennae increased beyond one wavelength.

5.5 Summary and Conclusions

Mutual coupling has been studied in detail. Two approaches to evaluate the mutual coupling between two patch antennae have been attempted, namely the TLM and the cavity model. In the case of the TLM new formulae for evaluating the mutual admittance was presented. The new formulae work for any adjacent spacing between the two radiating slots of antennae and are especially good for small spacing this being very important when examining the mutual coupling effect in the design of antenna array. Expressions for evaluating the mutual impedance between two antennae using the cavity model were also presented. For both approaches good agreements with the published and measured results were obtained.

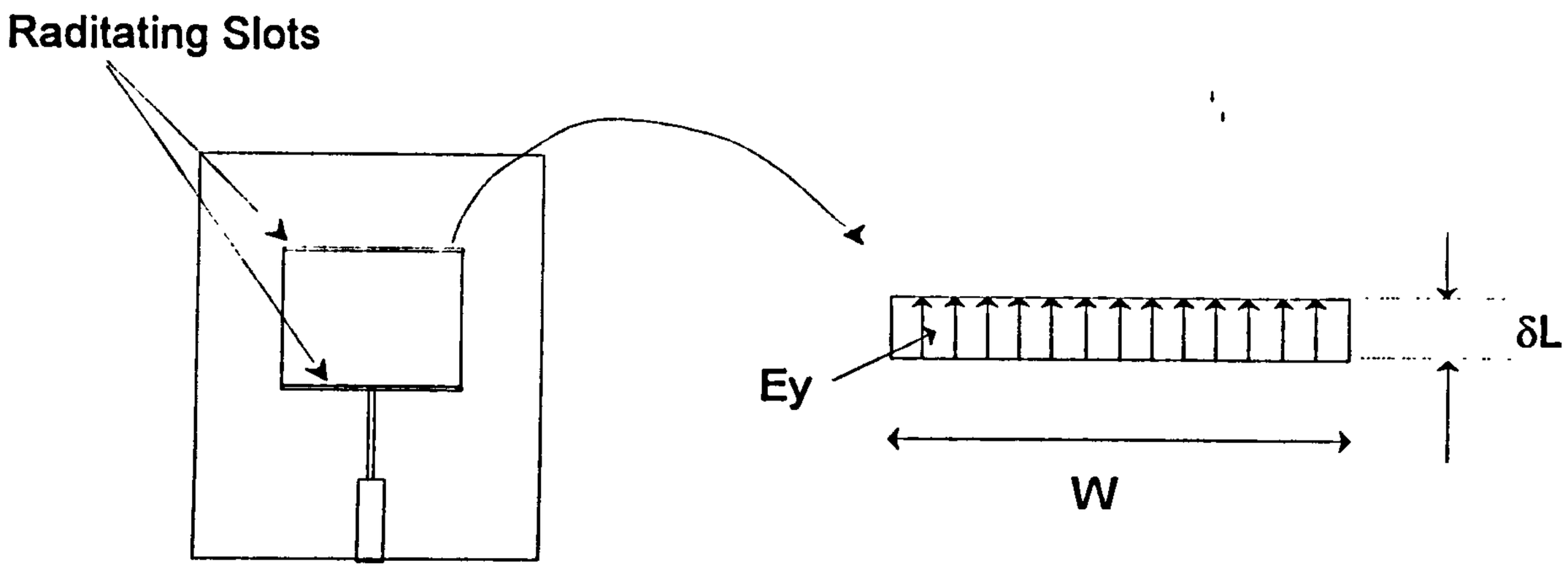

Figure 5.2.1 A Radiating Slot

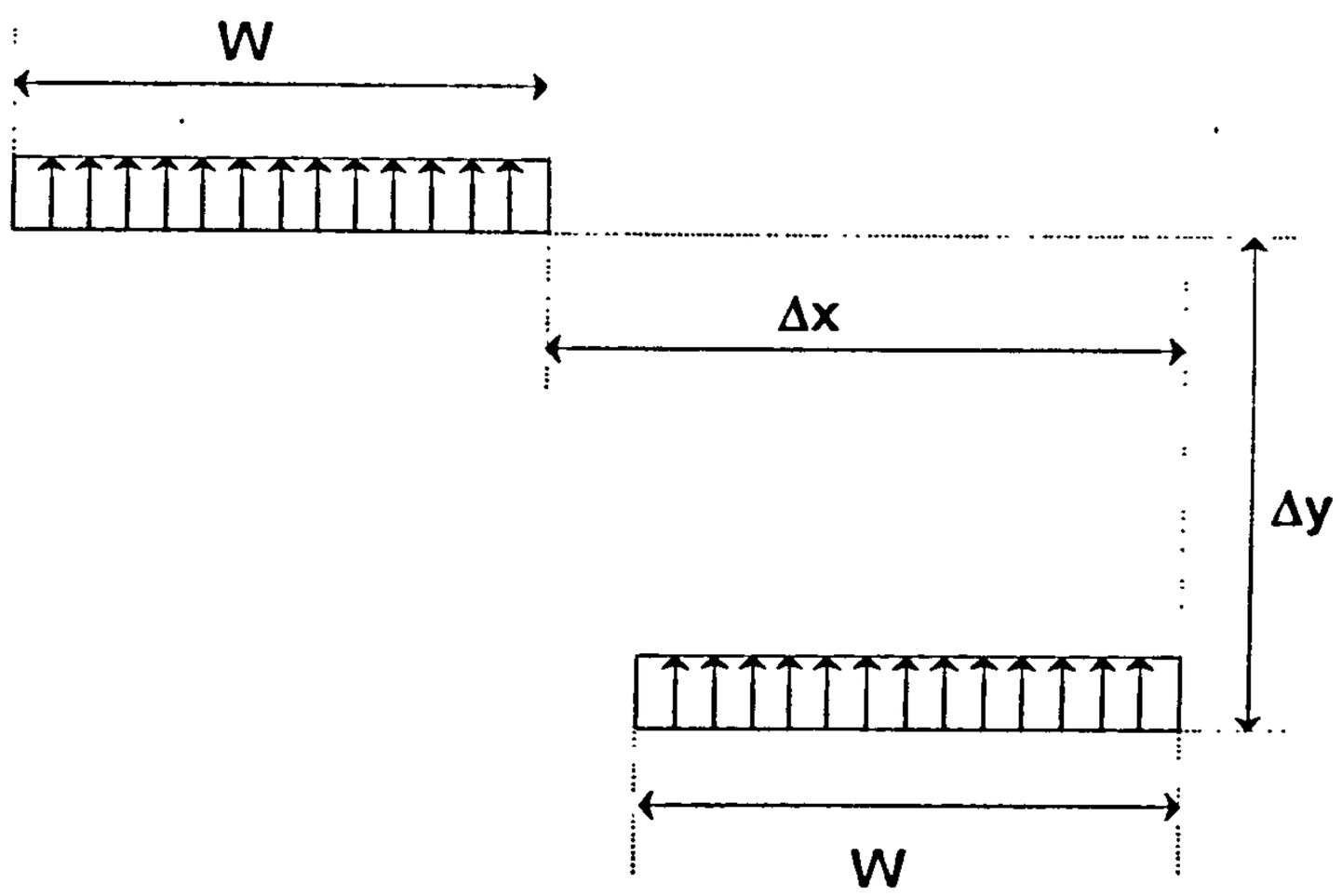

Figure 5.2.2 Two Radiating Slots

Gms

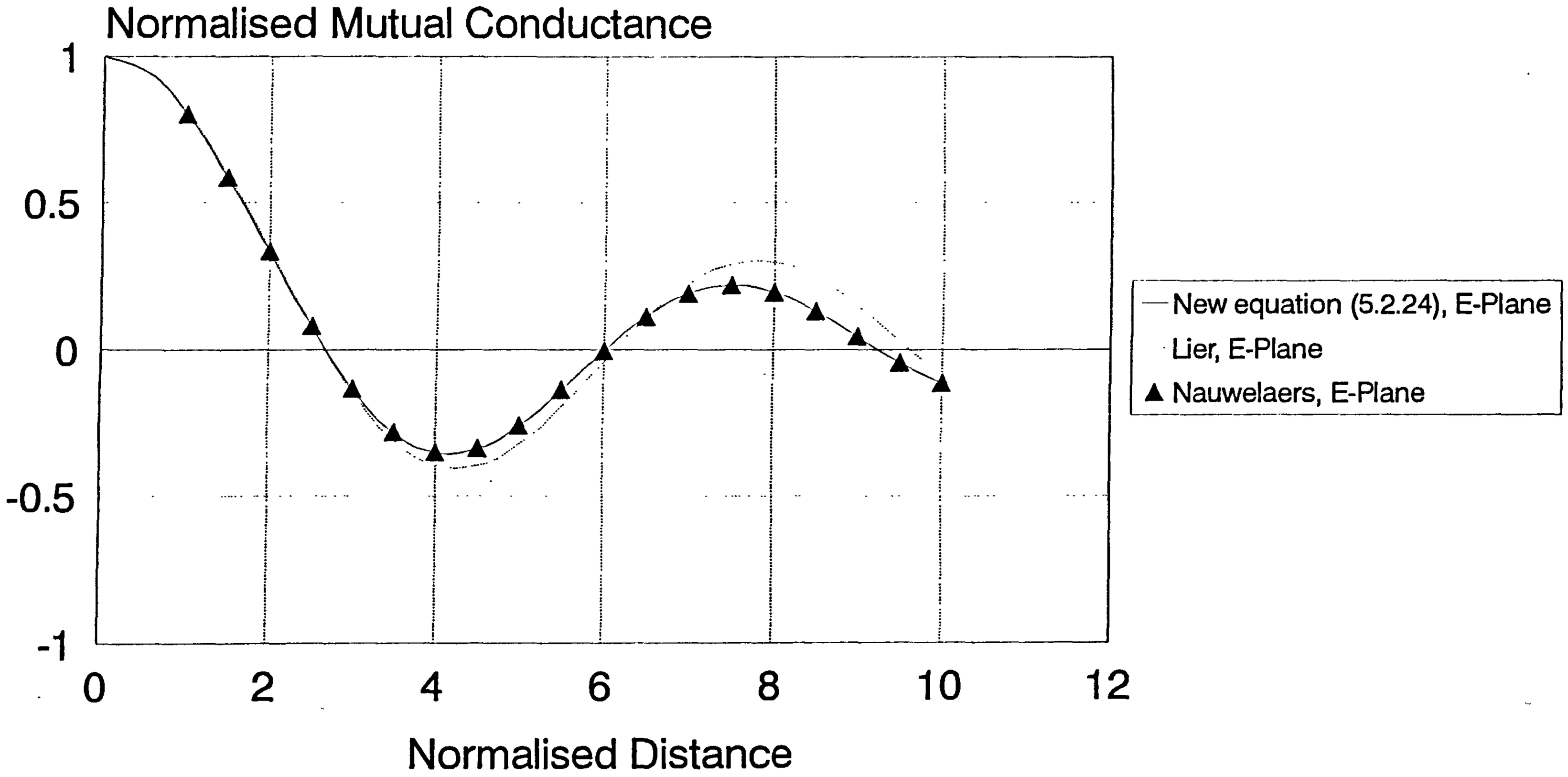

Figure 5.2.3 Mutual Conductance (Gms) (a=3,f=0,m=30)

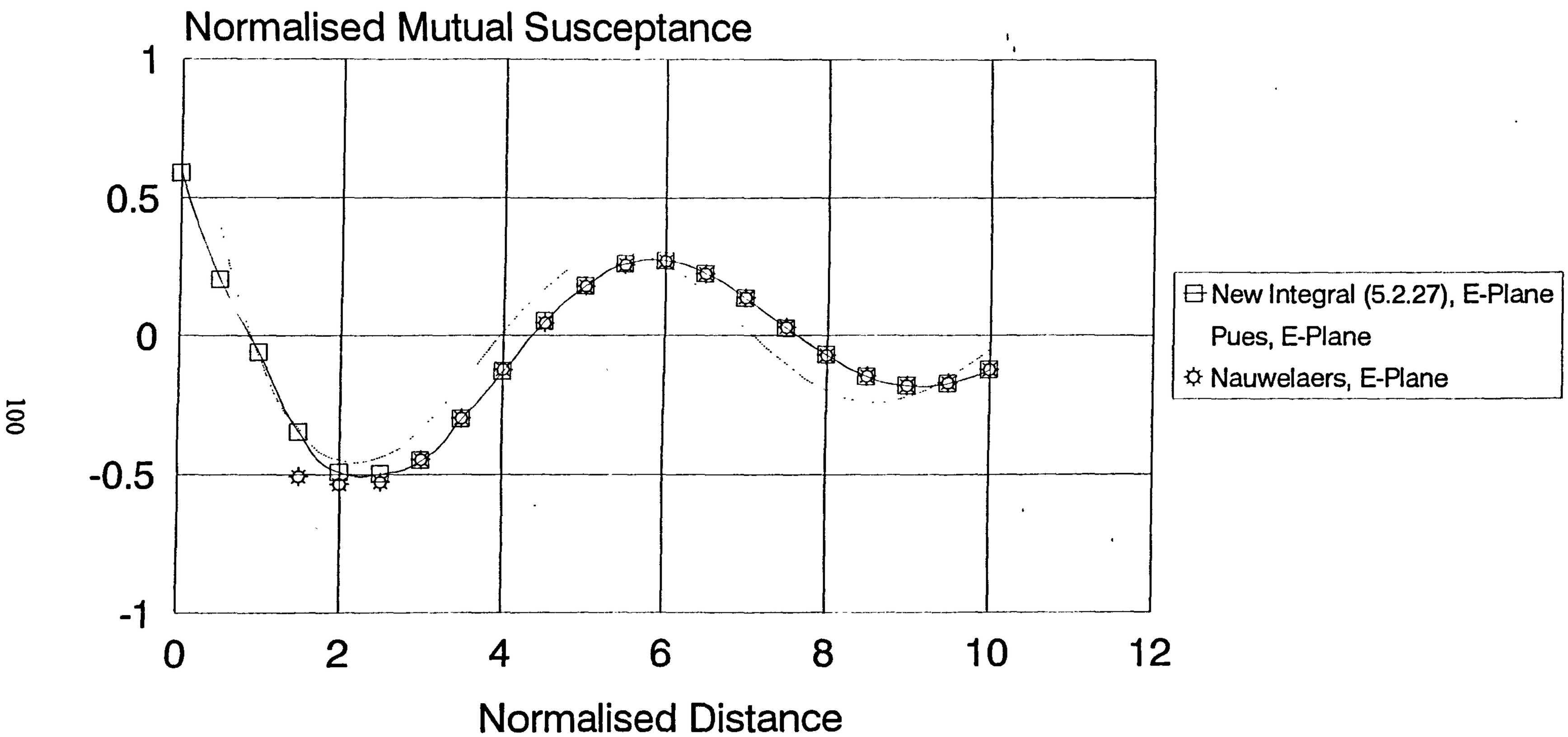

Gs=2.35276E-3, using Equation (5.3.24)

Figure 5.2.4 Mutual Susceptance
(a=3.121,b=0.0238, f=0)

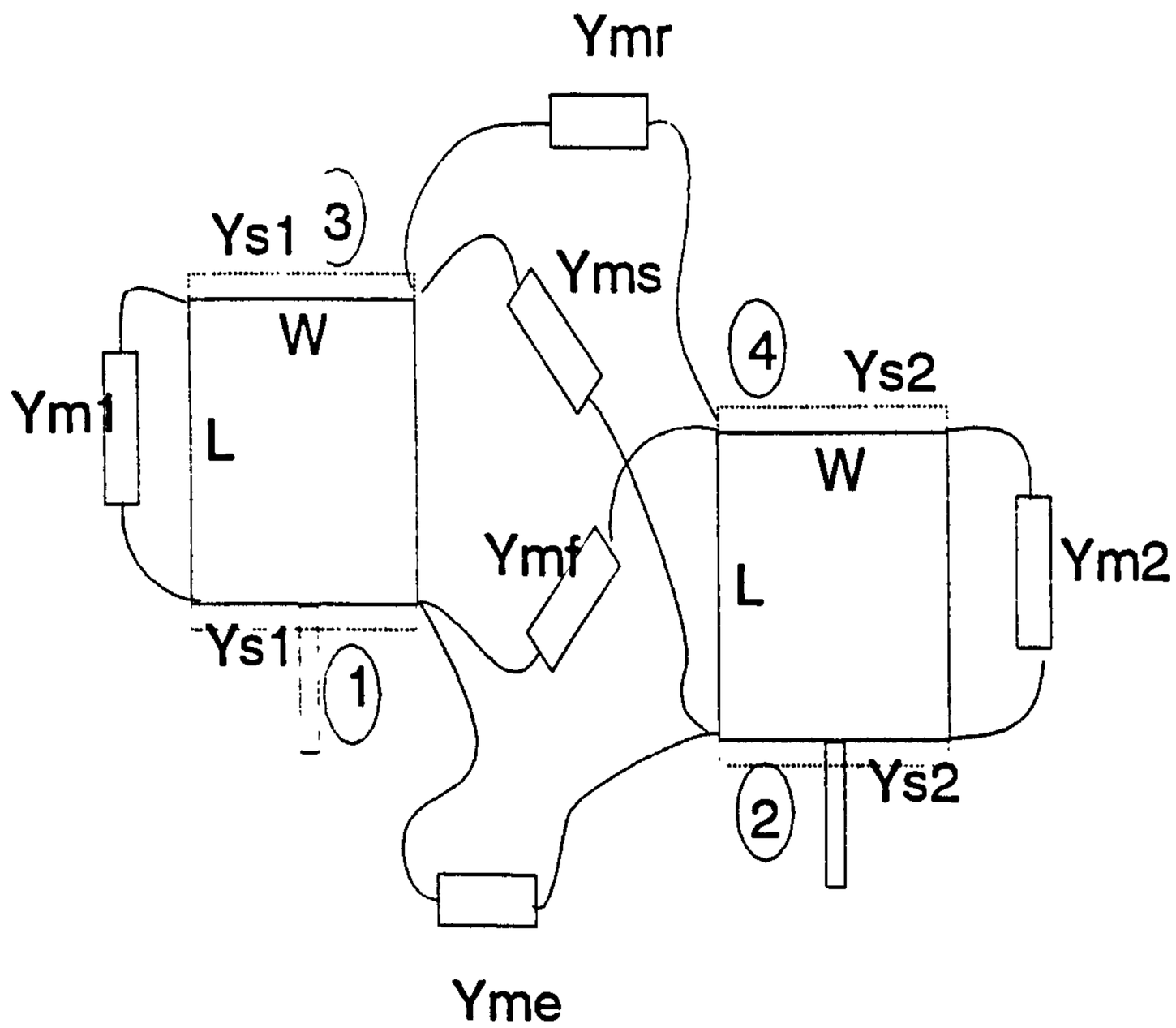

Figure 5.2.5 Self and Mutual admittances of two antennas

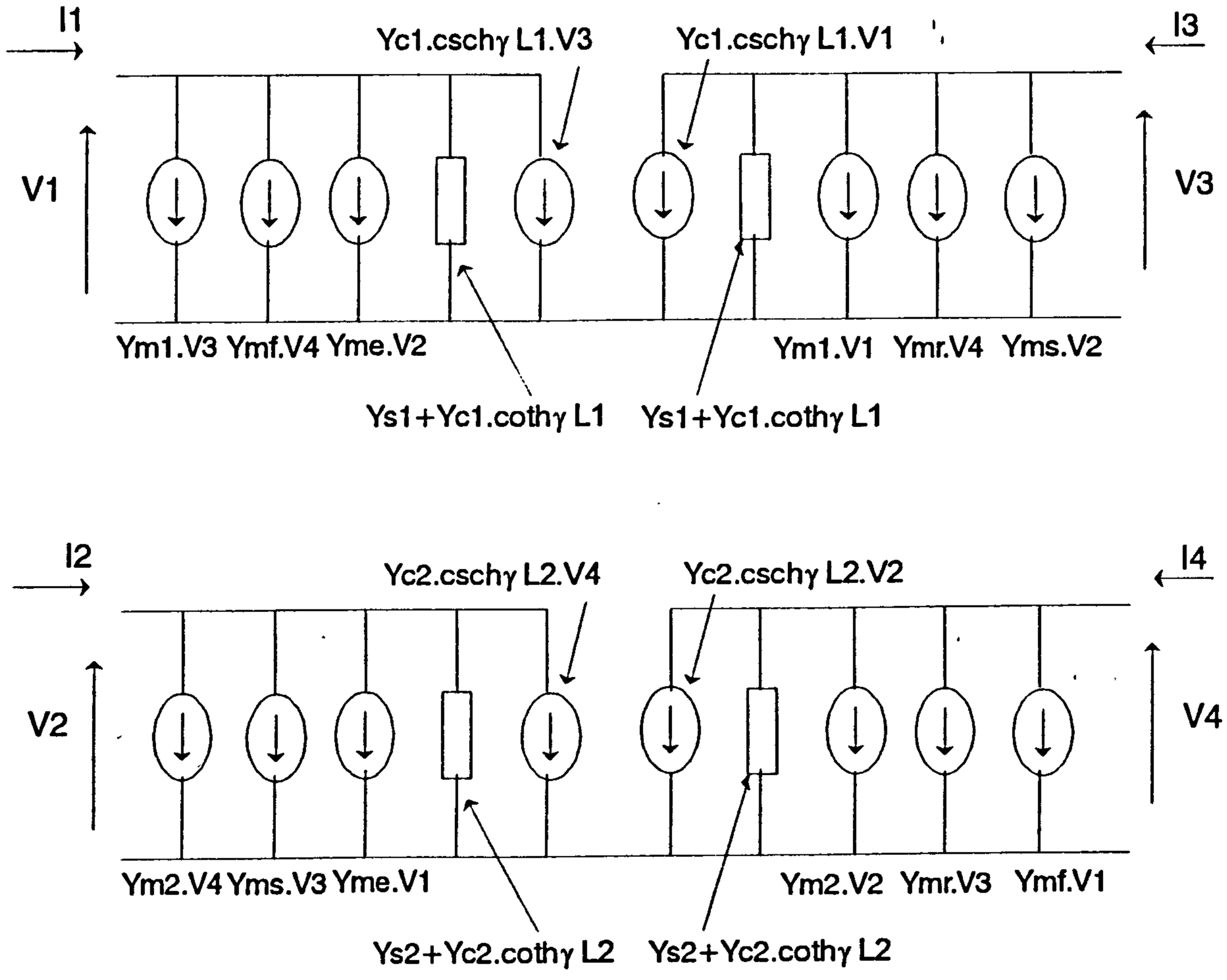

Figure 5.2.6 Equivalent circuit of two antennas

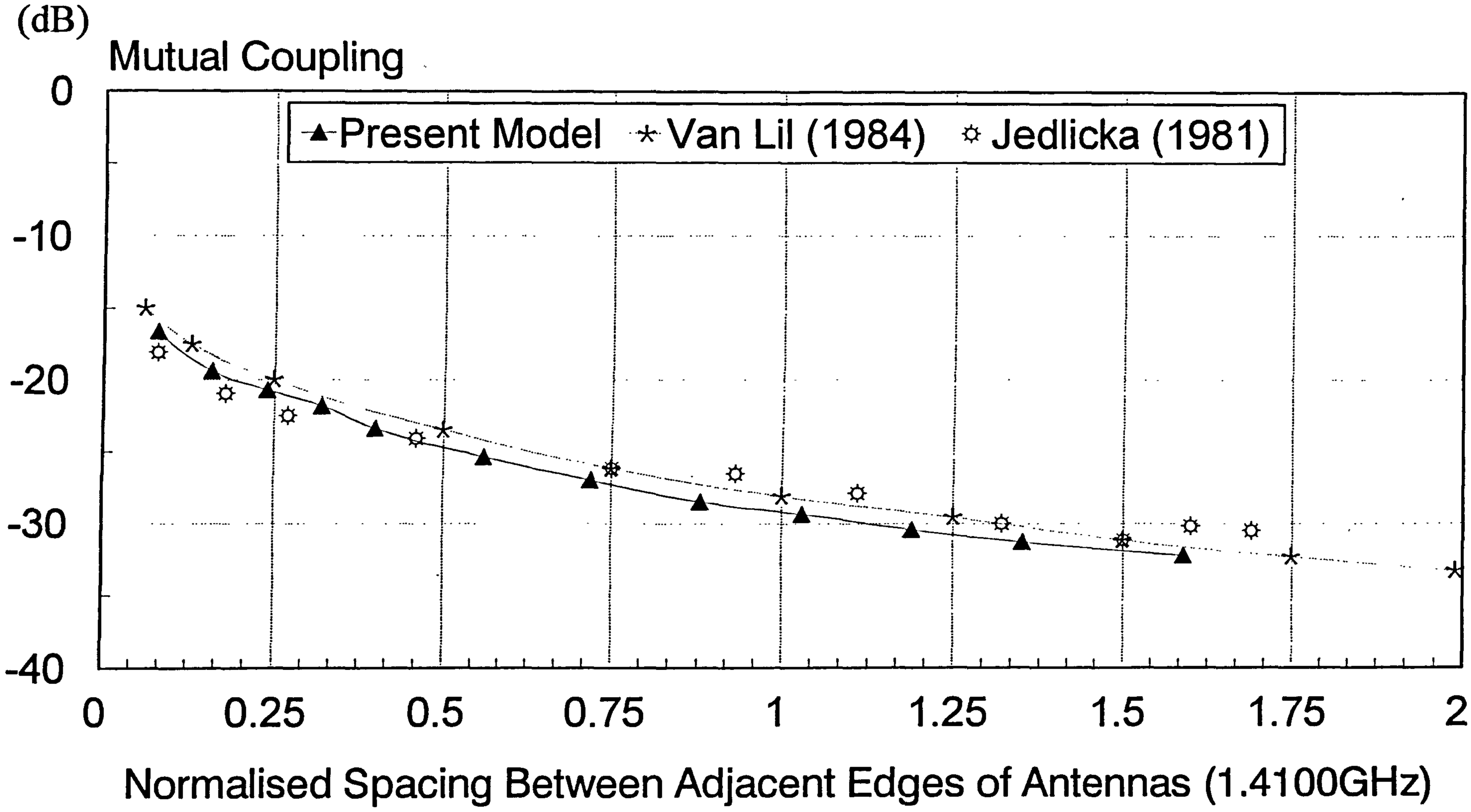

Figure 5.2.7 Mutual Coupling (E-Plane) Using Transmission-Line Model

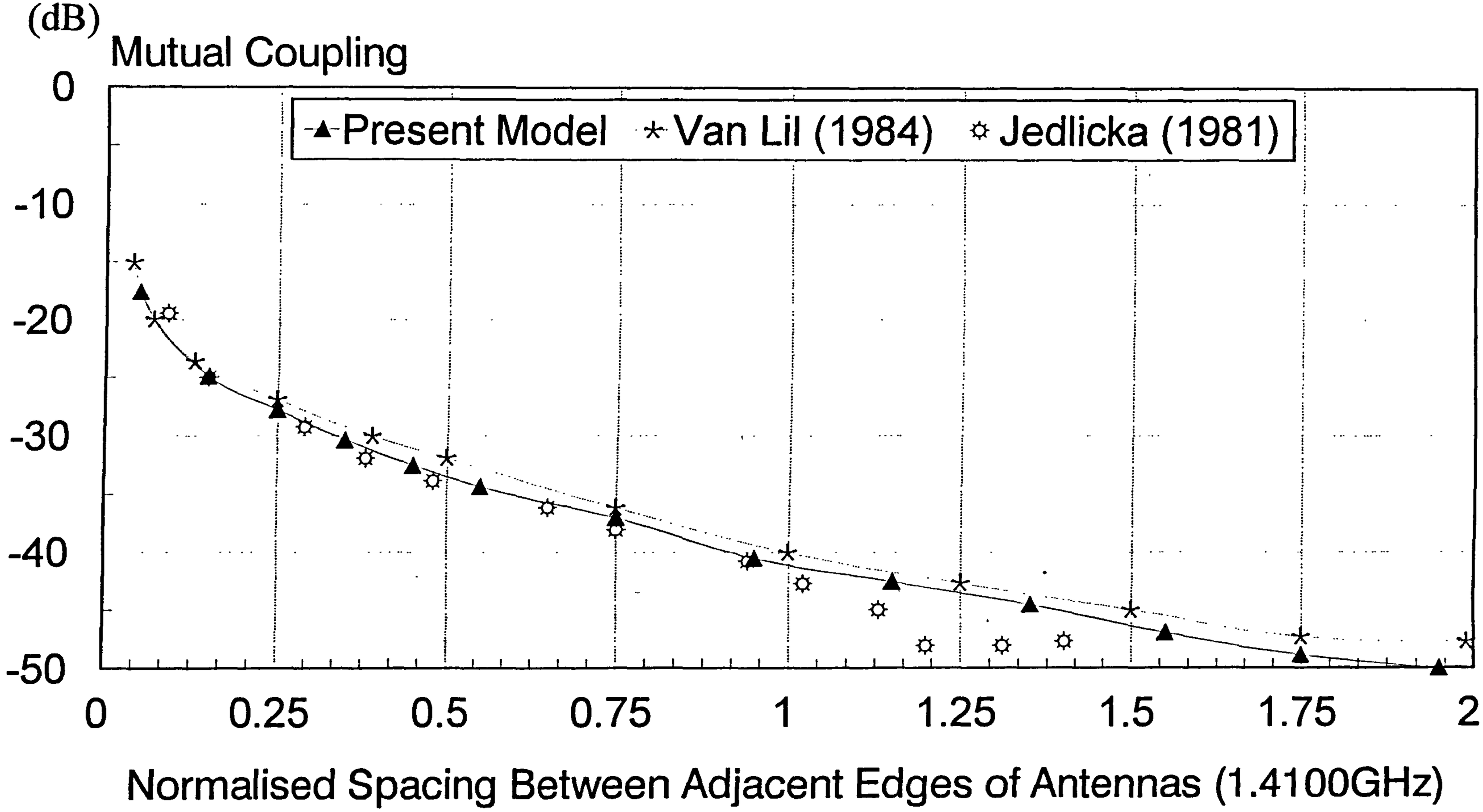

Figure 5.2.8 Mutual Coupling (H-Plane) Using Transmission-Line Model

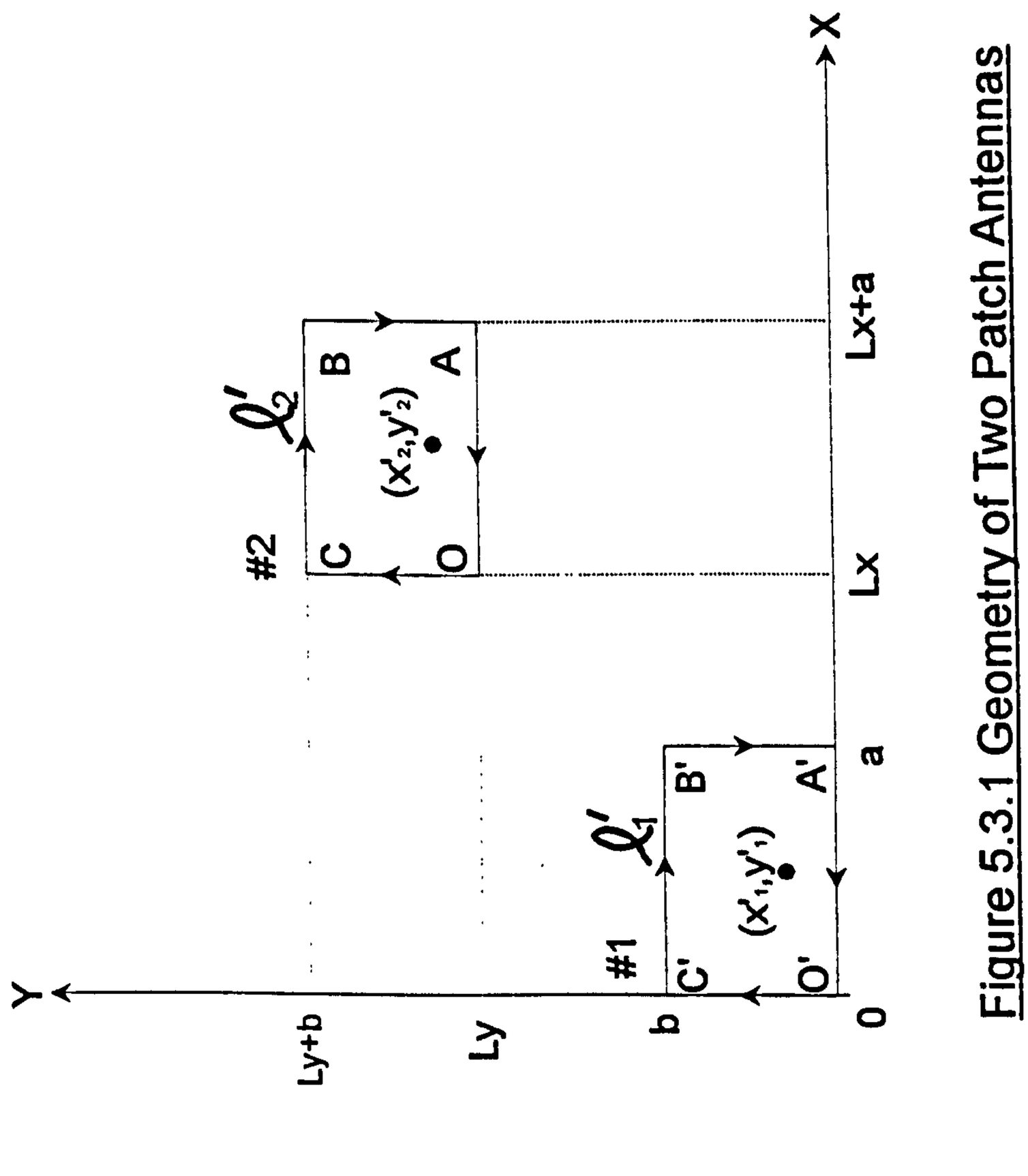

Figure 5.3.1 Geometry of Two Patch Antennas

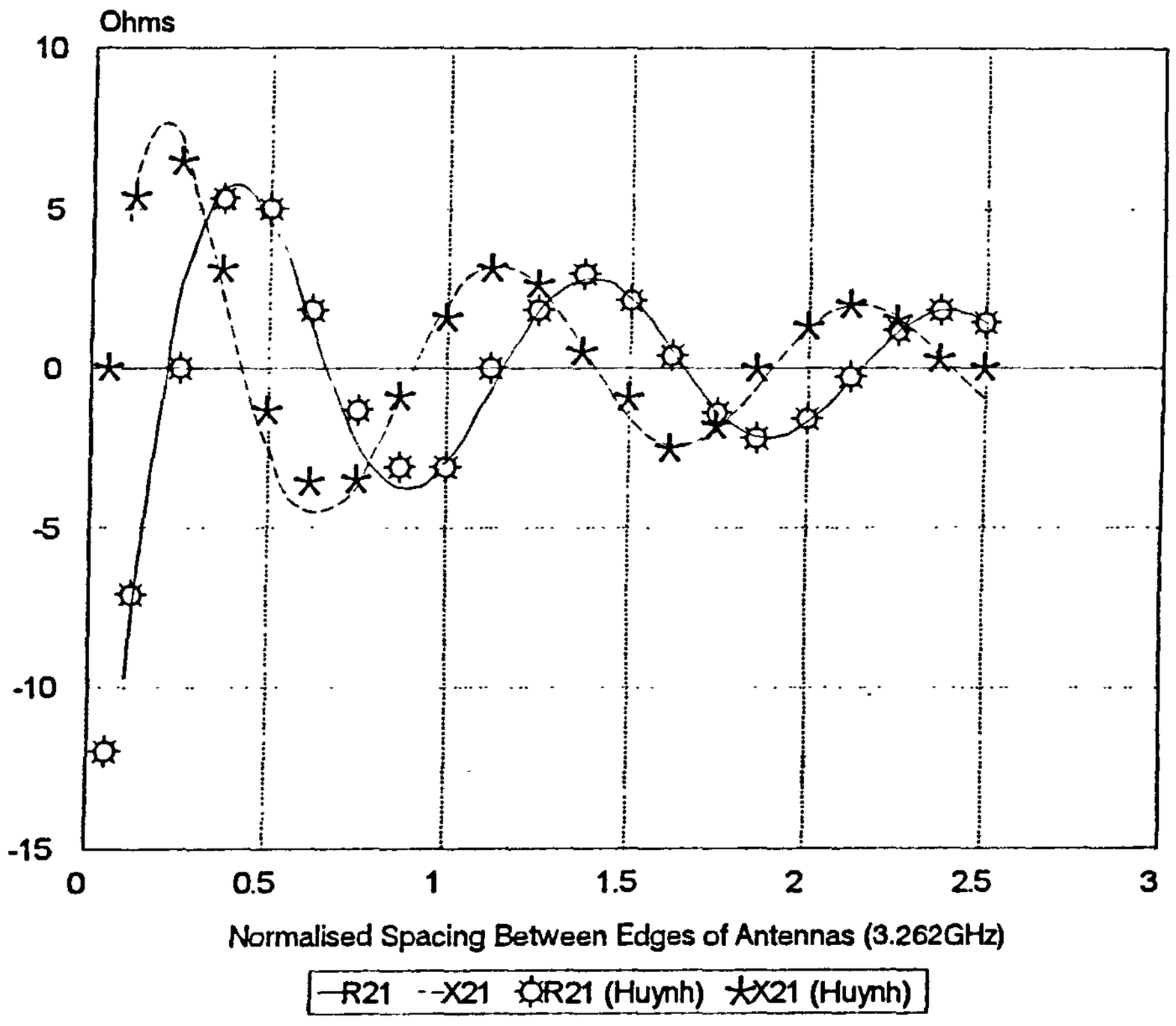

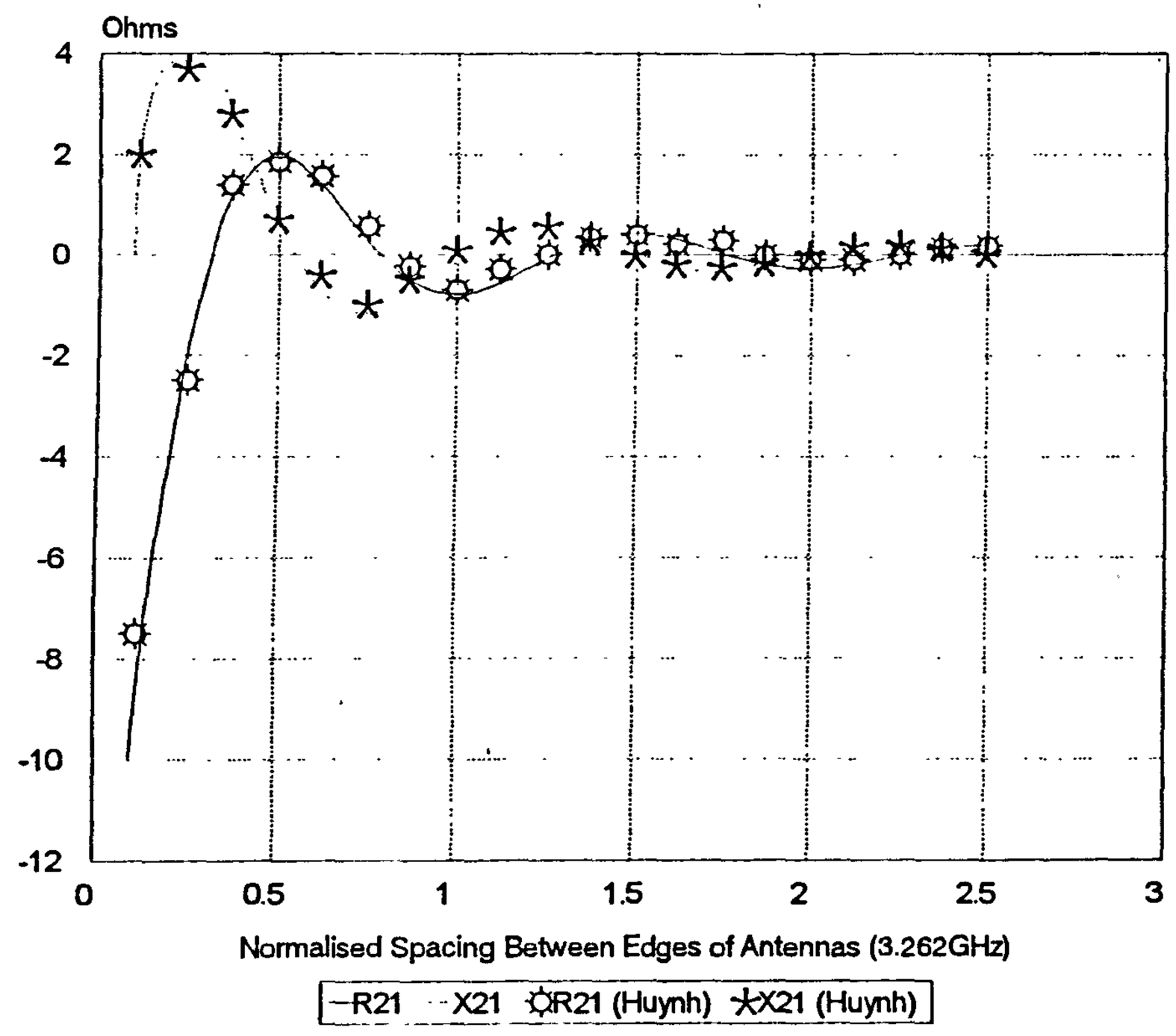

Figure 5.3.2 Mutual Impedance (Case 1)

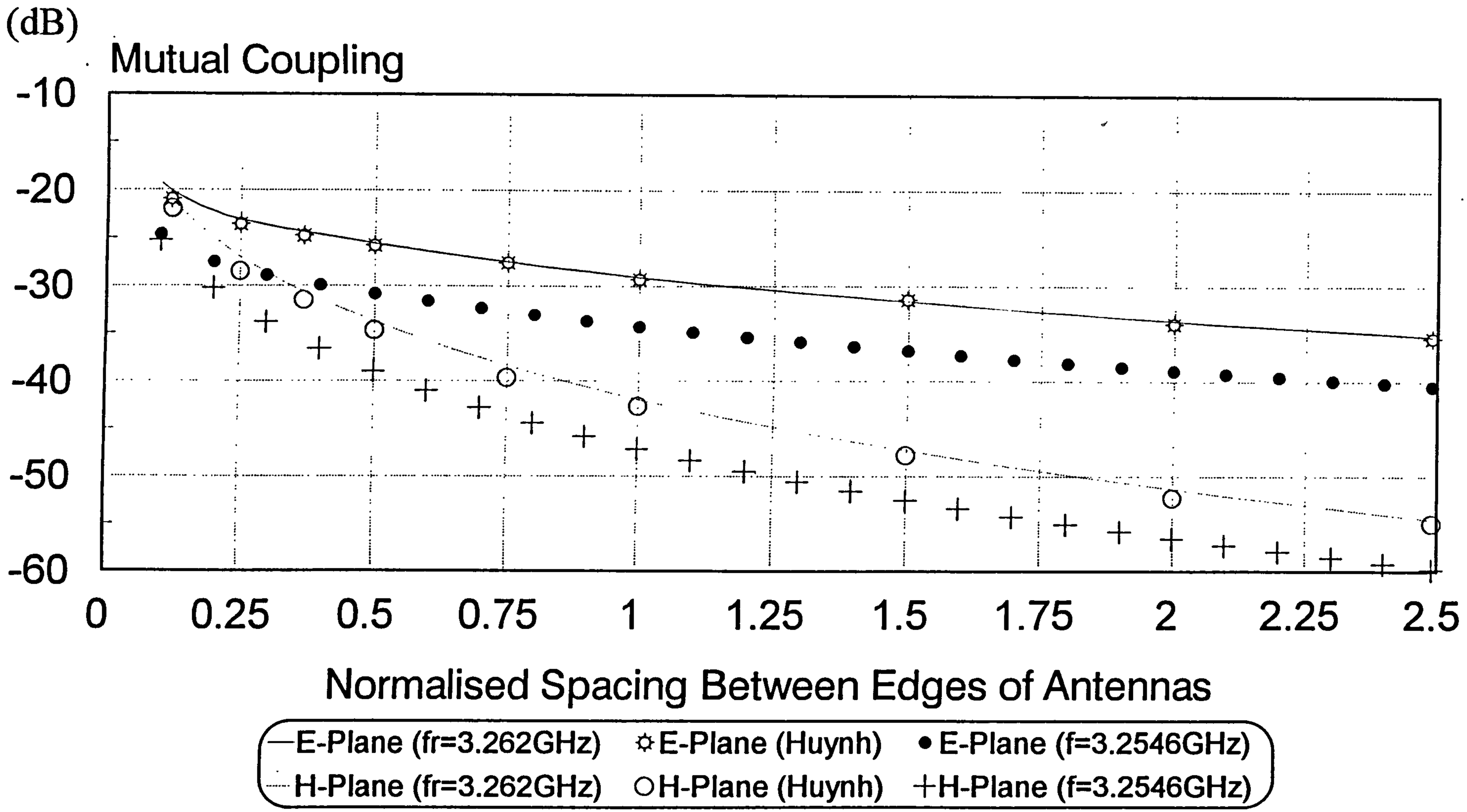

Figure 5.3.3 Mutual Coupling (Case 1), Resonant Frequency = 3.262GHz

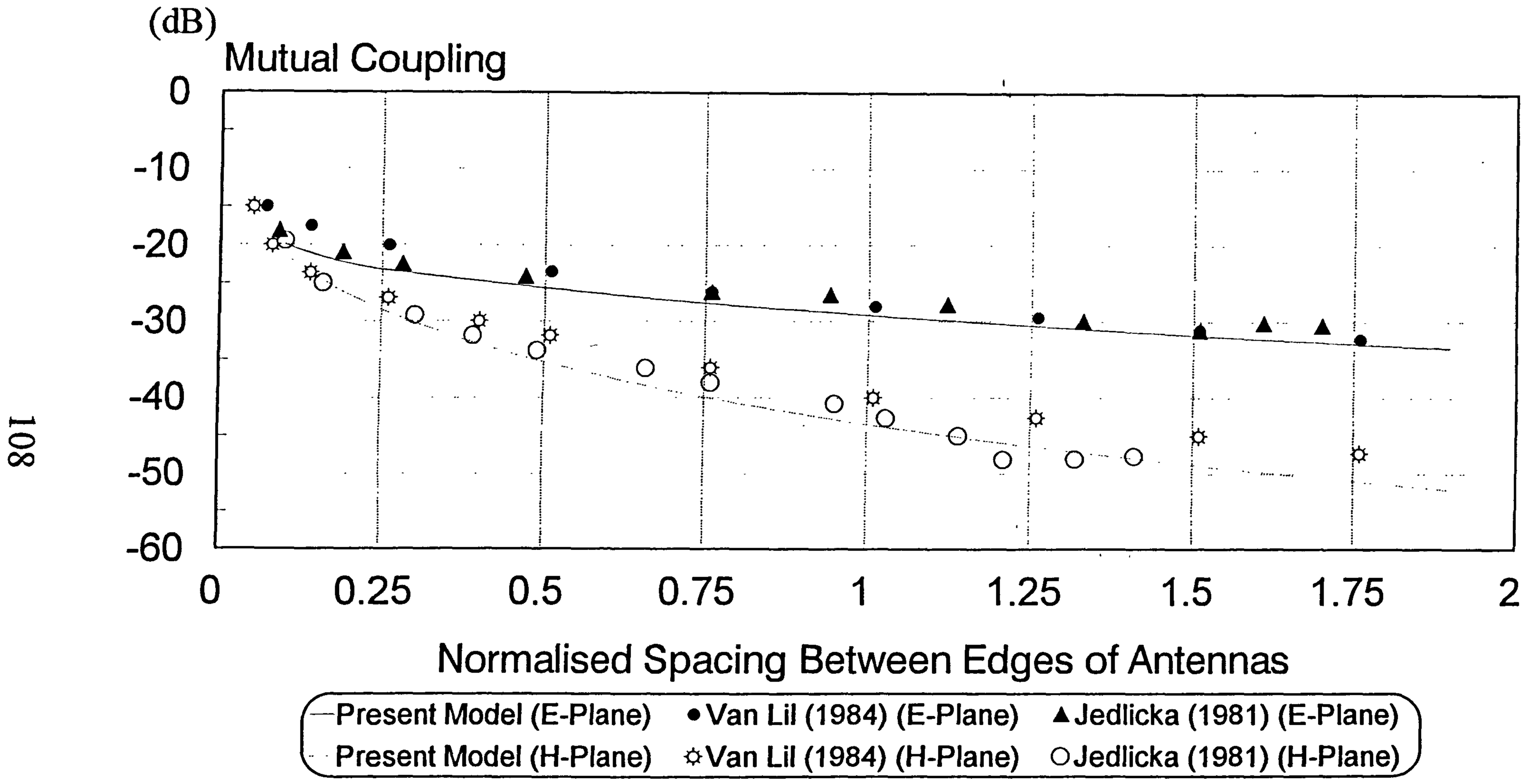

Figure 5.3.4 Mutual Coupling (Case 2)

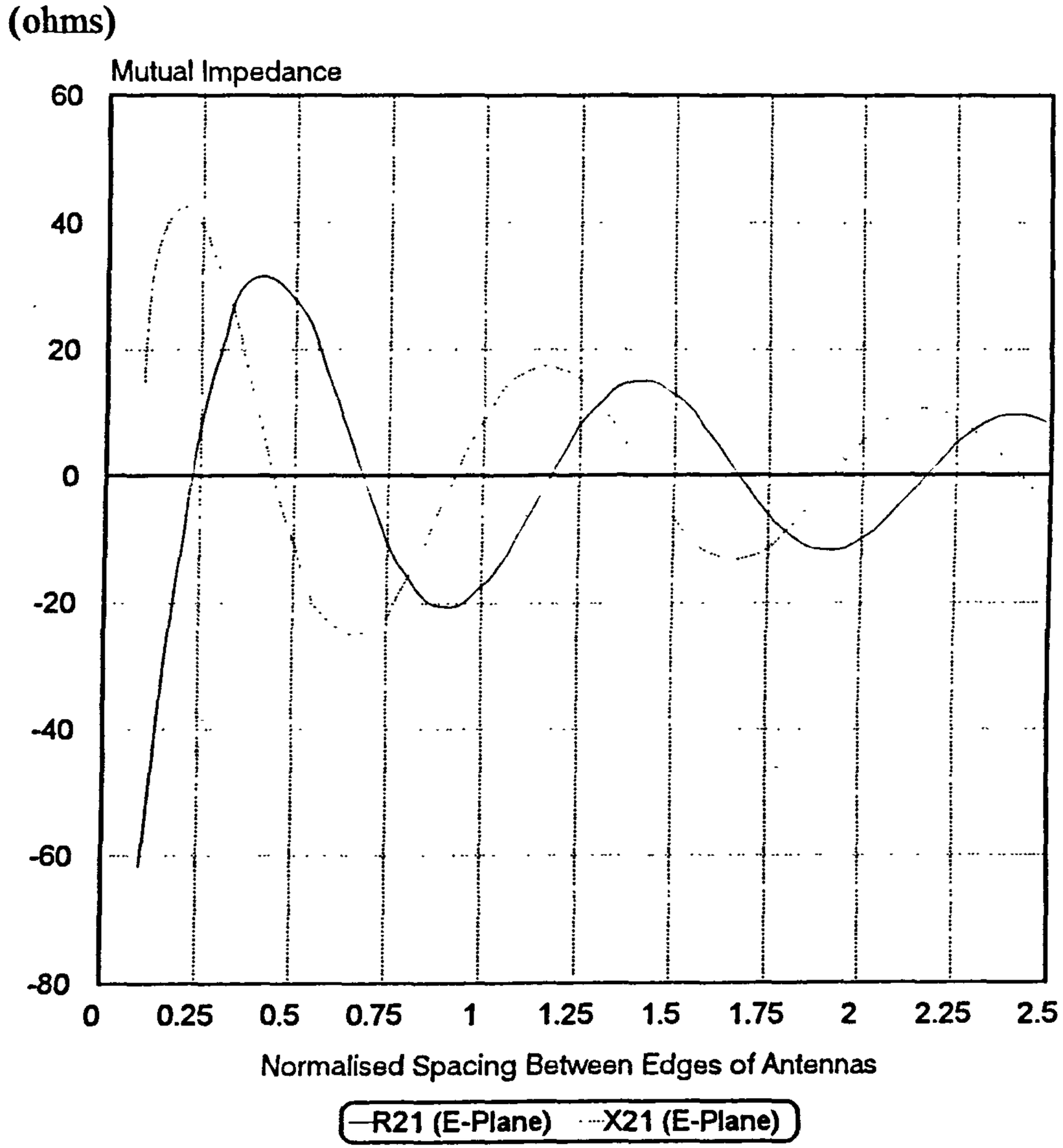

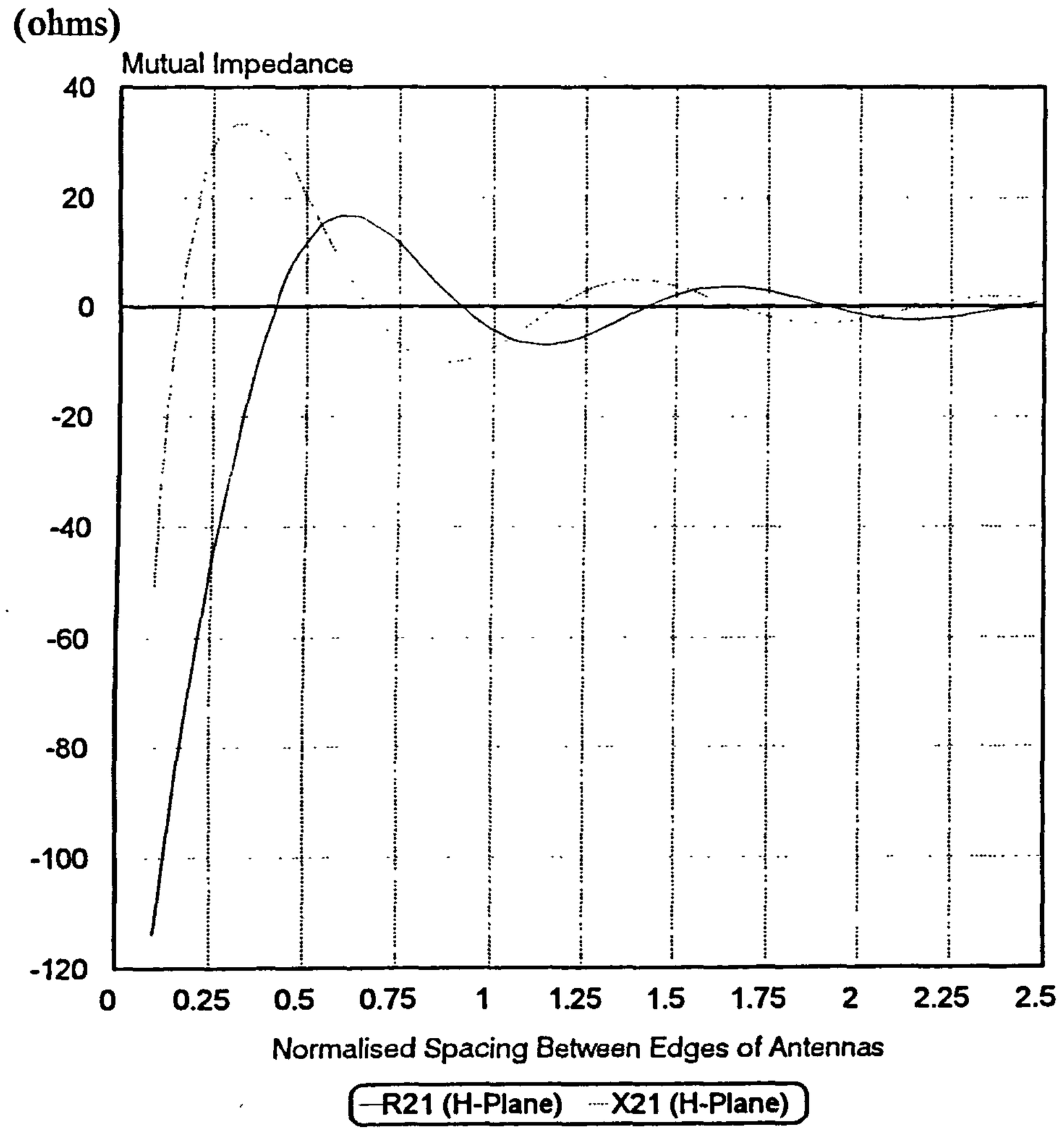

Figure 5.3.5 Mutual Impedance (Case 3)

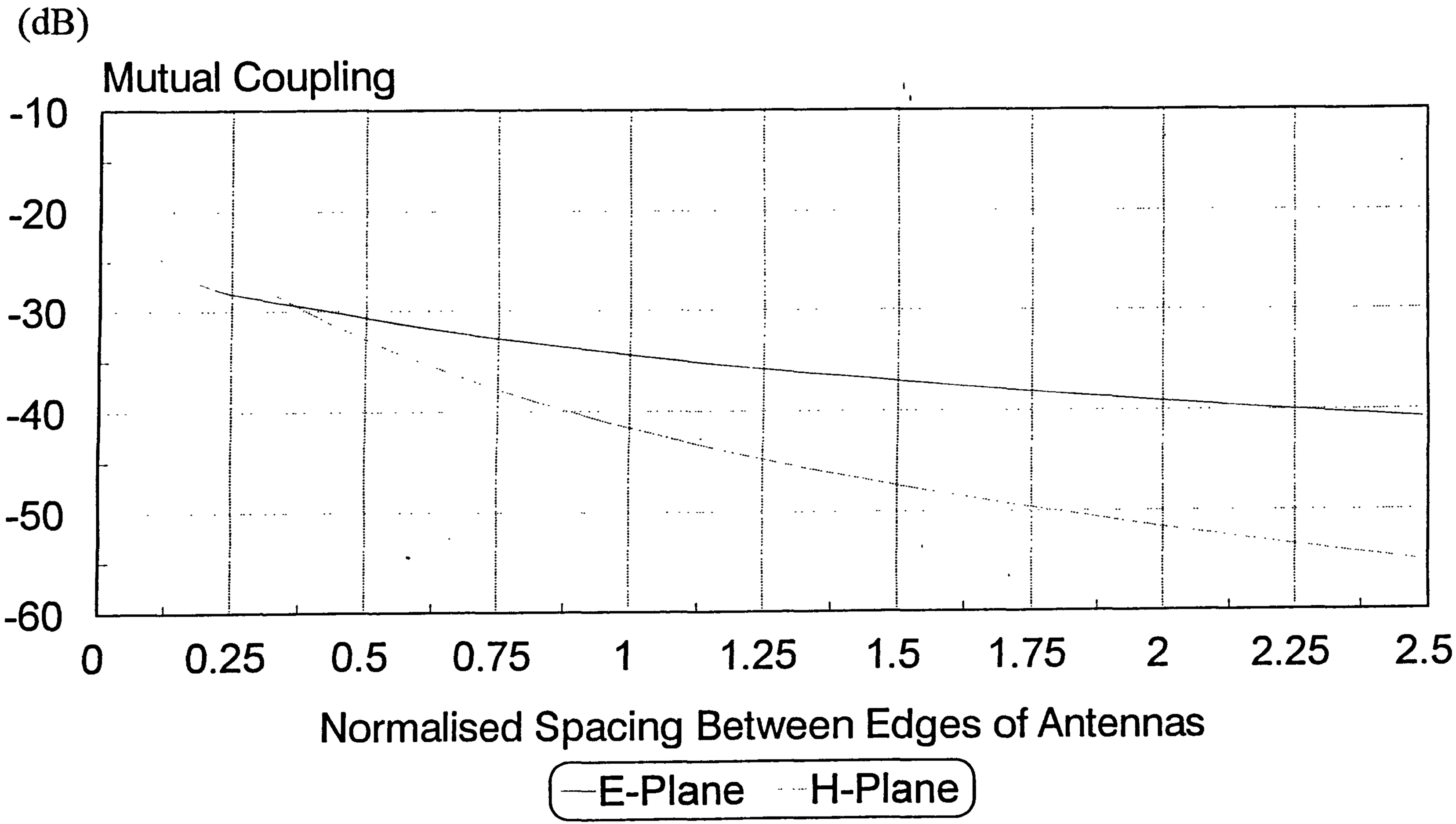

Figure 5.3.6 Mutual Coupling (Case 3)

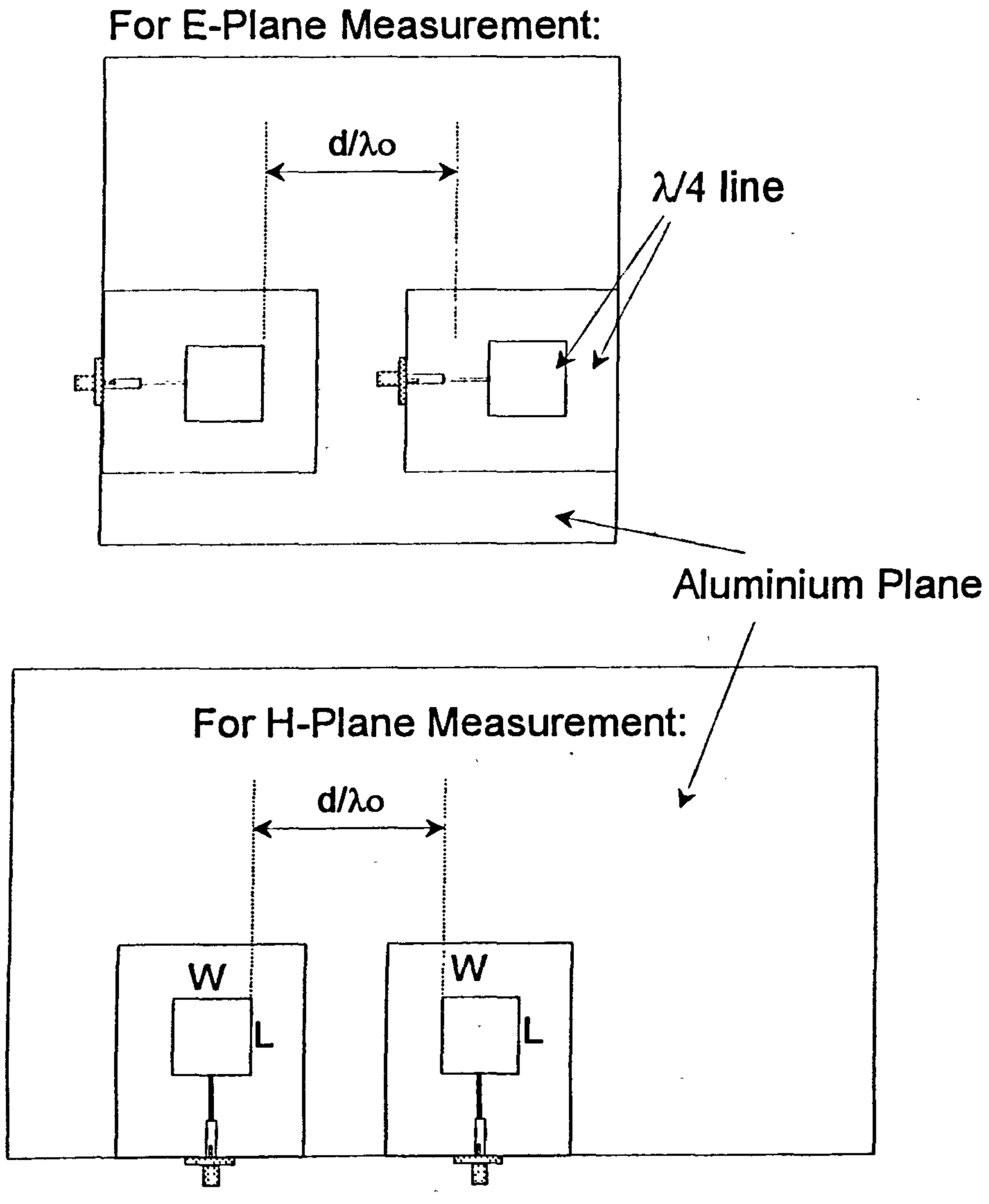

Figure 5.4.1 Measurement of Mutual Coupling

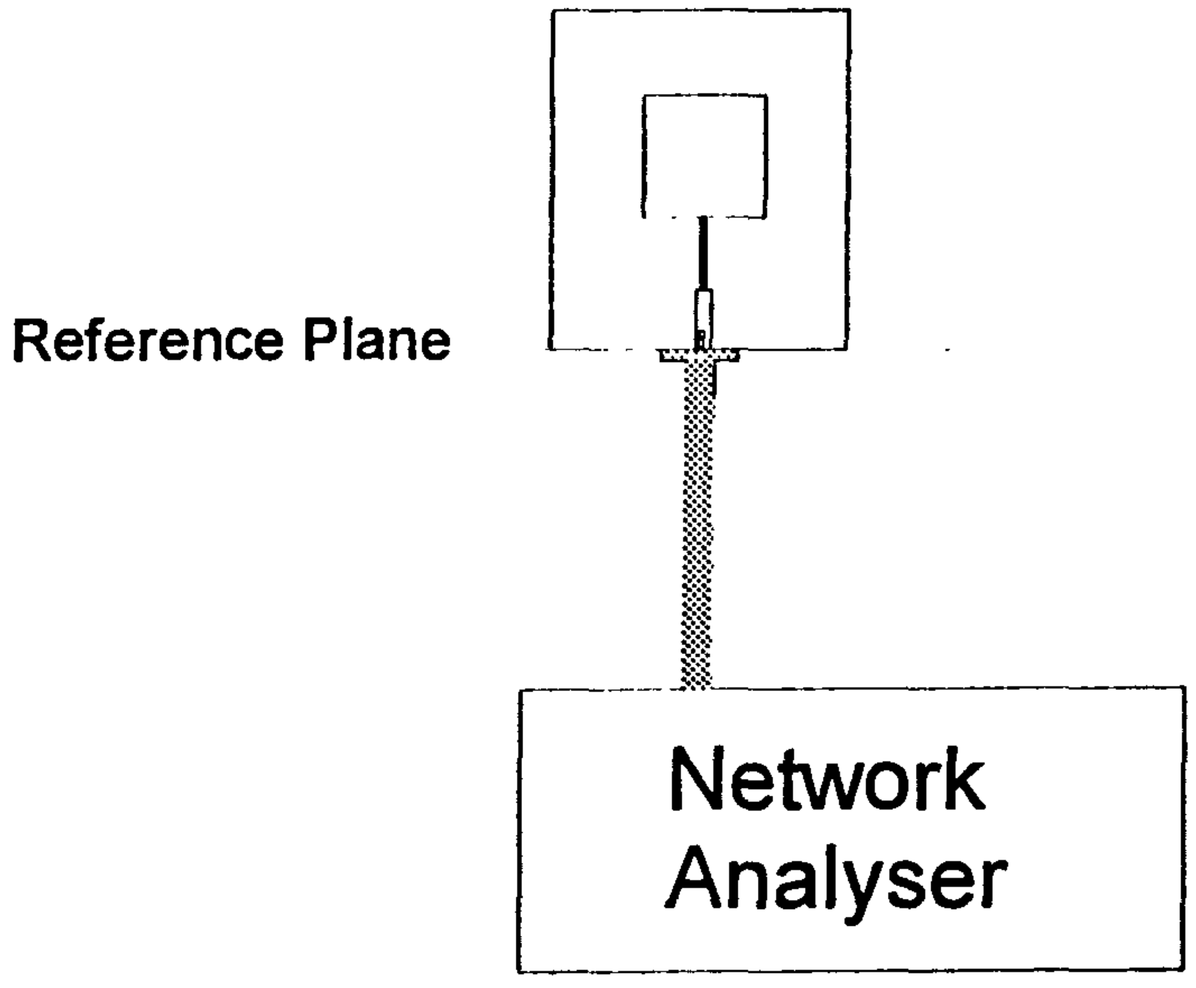

Figure 5.4.2 Measurement of Return Loss

Antenna #1

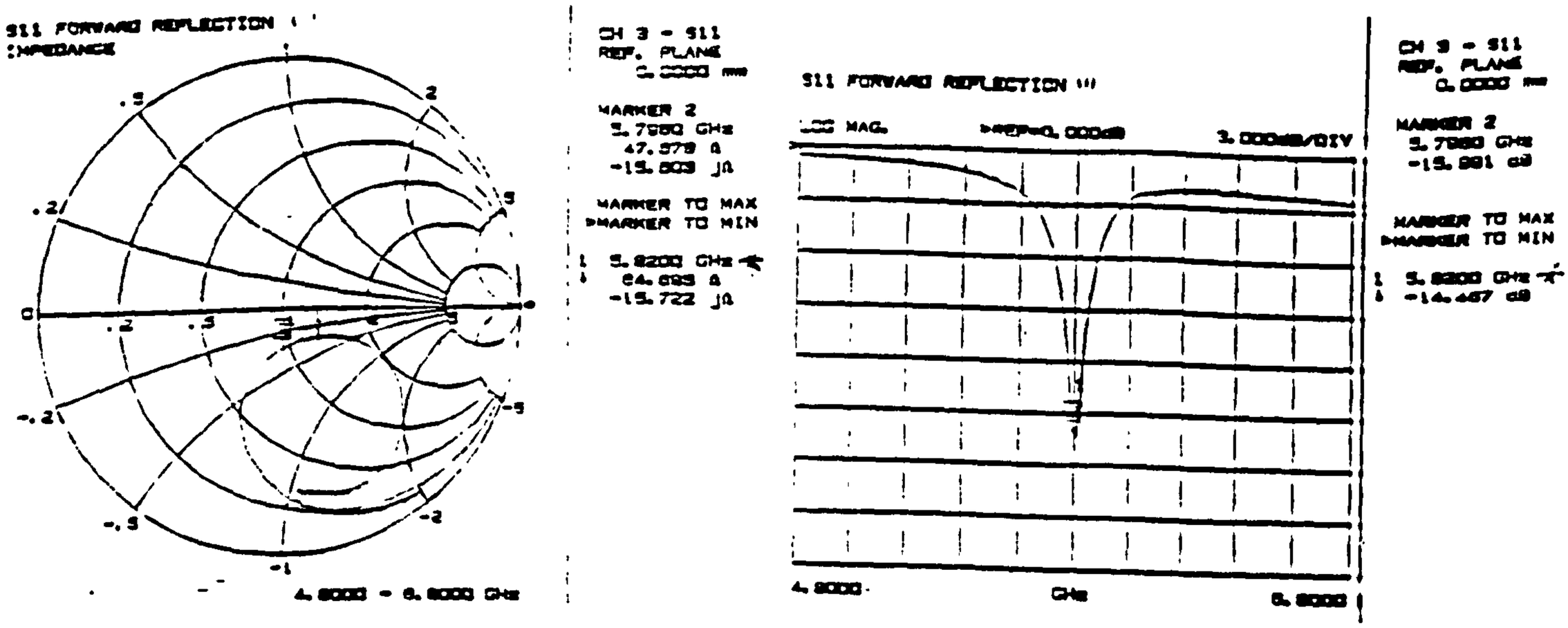

Antenna #2

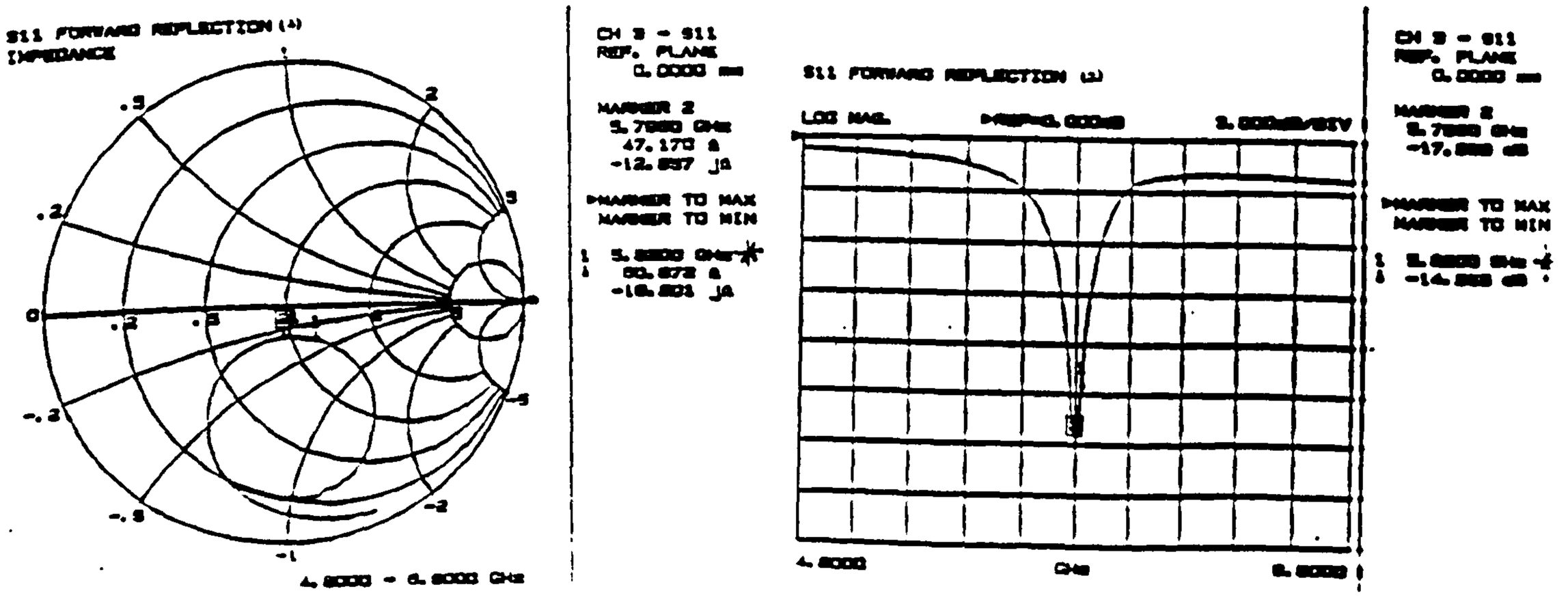

Figure 5.4.3 Return Loss of Two Antennas

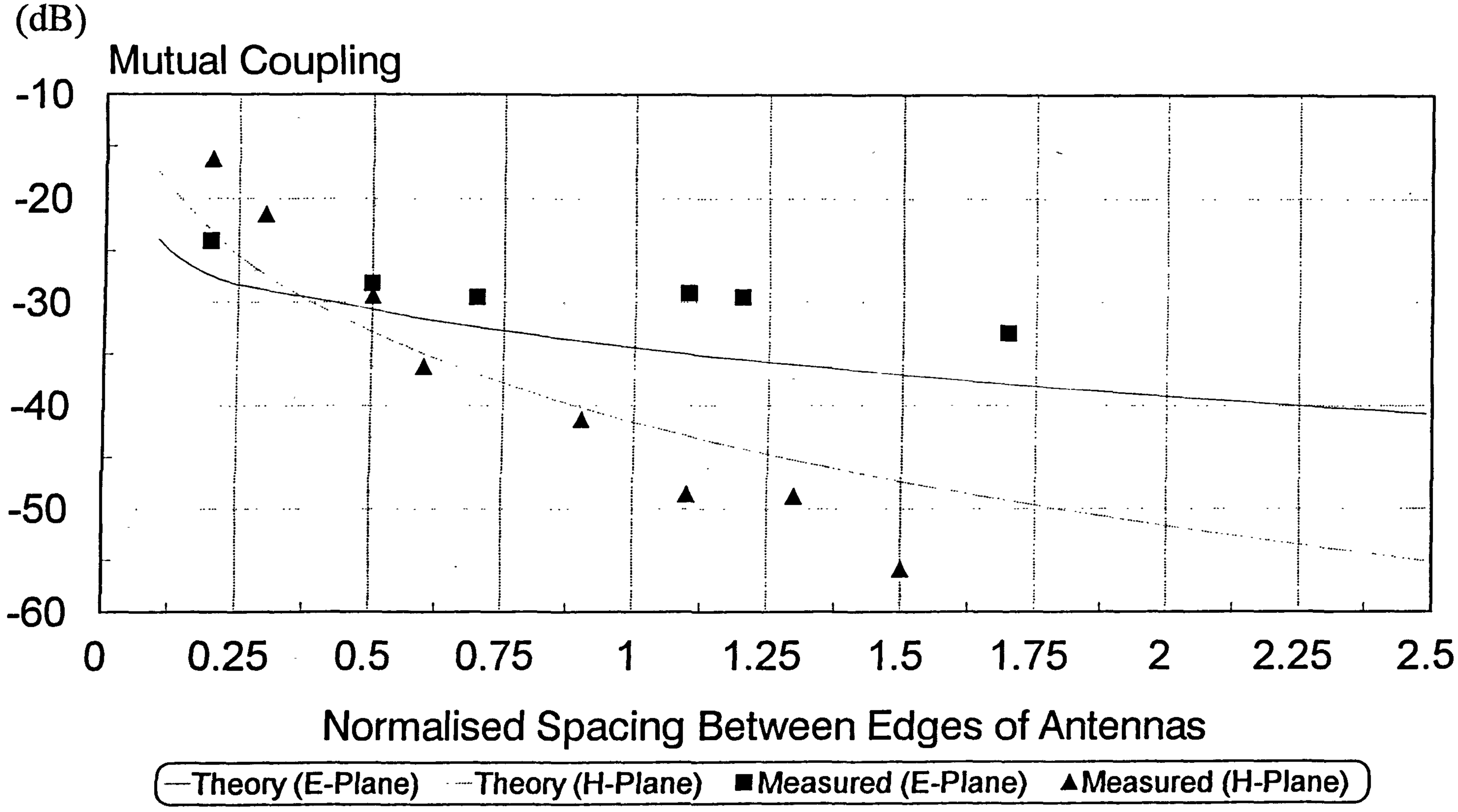

Figure 5.4.4 Measured Mutual Coupling Compared with the Theory

CHAPTER 6

Design and Performance of the RSU Antenna Array

6.1 Introduction

In order to obtain the necessary antenna gain, side lobe level and half-power beamwidth, the patches of the antenna array may have to be located very close to each other and power-fed unevenly. Because of the proximity of the patches it is therefore necessary in any design to include the effect of mutual coupling between patches. Jedlicka (1979), Heberling (1992), Gottwald (1993) and Moss (1993) have examined the effect of mutual coupling on the performance of an antenna array while Carver (1979) also showed how the effect of mutual coupling can be modelled using 'S' parameters.

This chapter examines the parameters, including the effect of mutual coupling between patches, that have to be taken into account in the design of an antenna array using the 'S' parameters. Finally a four by four patch antenna is designed and realised. There is a good agreement between the predicted and measured results of the designed array.

6.2 Design Parameters of an Antenna Array

Radiation Pattern

For a patch element 'i' of a N-element array arrangement shown in figure 6.2.1, the radiation field $E'_{\phi,i}$ is given by (see chapter 4)

$$E'_{\phi,i} = -j\frac{2V_{o,i}}{\pi r}e^{-jk_o r}e^{j\frac{k_o l}{2}\sin\theta\sin\phi}\sin\left(\frac{k_o W}{2}\cos\theta\right)\tan\theta\cos\left(\frac{k_o l}{2}\sin\theta\sin\phi\right) \quad \text{for i=1,2,...,N} \quad (6.2.1)$$

where the effect of mutual coupling between the patches has been neglected.

Mutual coupling between patches affects the input impedance of the array as it causes reflections at the input port of the elements, resulting in a change of excitation voltages. To include this effect, the input slot voltage of each patch $V_{o,i}$ is expressed in the form

$$V_{o,i} = V^+_i + V^-_i = V^+_i(1 + \Gamma_i) \qquad \text{for i=1,2,...,N} \qquad (6.2.2)$$

where Γ_i is the input reflection coefficient of the patch and is a function of the coupling between the patches. The power $P_{rad,i}$ and the electric field $E_{\phi,i}$ radiated by each patch are given by

$$P_{rad,i} = \frac{E'^2_{\phi,i}}{\eta}\left[1-|\Gamma_i|^2\right] \tag{6.2.3}$$

$$E_{\phi,i} = \sqrt{\eta P_{rad,i}} = E'_{\phi,i}\sqrt{1-|\Gamma_i|^2} \tag{6.2.4}$$

where now $E_{\phi,i}$ is the electric field of a single patch antenna which includes the effect of coupling.

Directivity

The directivity $D(\theta,\phi)$ is a measure of the spatial distribution of radiated energy and is defined as the ratio of the power density in the θ,ϕ direction to the average power density radiated. Thus the directivity can be found from the following expression

$$D(\theta,\phi) = \frac{|g(\theta,\phi)f(\theta,\phi)|^2}{\frac{1}{4\pi}\int_0^{2\pi}\int_0^{\pi}|g(\theta,\phi)f(\theta,\phi)|^2\sin\theta d\theta d\phi} \tag{6.2.5}$$

Gain and Efficiency

The directivity as given in equation (6.2.5) assumes that all the energy supplied to the antenna terminals is radiated. However some energy is dissipated or lost within the antenna and its feed network. A good measure of the performance is the actual gain of the antenna in the direction of maximum radiation and is given by

$$G(\theta_m,\phi_m) = \eta D(\theta_m,\phi_m) \tag{6.2.6}$$

where η is the efficiency of the antenna and its feed network.

Beamwidth

The beamwidth of the radiation pattern is determined by the number of elements, the element spacing, the excitation voltage amplitude distribution, and, the element pattern.

Generally for equal excitation voltage distribution, if the spacing between antenna elements is increased the beamwidth will be narrower and the side lobe level will unfortunately be increased. However in order to have a narrow beamwidth and low side lobe level it will be necessary to have an unequal excitation voltage distribution to the individual antenna elements (Parks, 1977).

6.3 Modelling of Mutual Coupling using 'S' Parameters

Mutual coupling affects the input reflection coefficients of each of the patch antennae and hence the antenna gain will be reduced and the polar pattern will be changed. The [S] parameter matrix which represents the mutual coupling between the antenna patches can be expressed in the form (Carver, 1979)

$$\begin{pmatrix} V_1^- \\ V_2^- \\ . \\ . \\ V_N^- \end{pmatrix} = \begin{pmatrix} S_{11} & S_{12} & . & . & S_{1N} \\ S_{21} & S_{22} & . & . & S_{2N} \\ . & . & . & . & . \\ . & . & . & . & . \\ S_{N1} & S_{N2} & . & . & S_{NN} \end{pmatrix} \begin{pmatrix} V_1^+ \\ V_2^+ \\ . \\ . \\ V_N^+ \end{pmatrix} \qquad (6.3.1)$$

where V^- and V^+ are the reflected and incident voltages at each patch, respectively. Assuming a lossless feed-line network and all the incident voltages to the patches are equal, i.e. $V^+_1 = V^+_2 = \ldots = V^+_N$, the input reflection coefficients of each patch can be expressed in the form

$$\begin{aligned} \Gamma_1 &= S_{11} + S_{12} + \ldots + S_{1N} \\ \Gamma_2 &= S_{21} + S_{22} + \ldots + S_{2N} \\ &. \\ &. \\ \Gamma_N &= S_{N1} + S_{N2} + \ldots + S_{NN} \end{aligned} \qquad (6.3.2)$$

6.4 Design and Performance of a 5.8GHz 4*4 Planar Antenna Array

A 5.8GHz circular polarisation antenna array has been designed as shown in figure 6.4.1. Each patch antenna elements has two input feeds located on adjacent sides with a 90° phase difference in order to produce circular polarisation. From the output port of the 3dB two-branch coupler the 50Ω line feeds a pair of 50Ω feed lines using the 35.4Ω quarter

wavelength transformer. These 50Ω lines each feed a pair of 100Ω lines. These 100Ω lines each feed a pair of 100Ω lines using the 70.7Ω quarter wavelength transformer. These 100Ω lines then feed a pair of 75Ω lines using the 61.2Ω quarter wavelength transformer. Finally these 75Ω lines feed the individual antenna patches using the 155Ω quarter wavelength transformer.

Table 6.4.1 shows the relationship of spacing between the patches of a 4*4 array and the 3dB beamwidth and the first side lobe level. In order to satisfy the requirement of the communication zone (see chapter 3), the beamwidth has been chosen as 16° and so the spacing between the patches is then $0.75\lambda_o$.

Resonant frequency: 5.8GHz
Width of a single patch: 16.18mm
H-plane pattern

Element Spacing		-3dB	First Side lobe Level	
λo	(mm)	Beamwidth (°)	(dBi)	at the angles(°)
0.50	25.86	24	-17.37	±44
0.55	28.45	22	-16.47	±40
0.60	31.03	20	-15.83	±36
0.65	33.62	19	-15.37	±33
0.70	36.21	17	-15.01	±31
0.75	**38.79**	**16**	**-14.74**	**±29**
0.80	41.38	15	-14.51	±27
0.85	43.97	14	-14.32	±25
0.90	46.55	14	-14.19	±24
0.95	49.14	13	-14.08	±22
1.00	51.72	12	-13.95	±21

Table 6.4.1 Effect of Element Spacing on 3dB Beamwidth and First Side lobe Level

The radiation pattern for a 4*4 planar antenna array can be derived in the form

$$E_\phi = 2E_{\phi,1}\cos\left[\frac{k_o d_o}{2}(3\cos\theta+3\sin\phi)\right]+2E_{\phi,2}\cos\left[\frac{k_o d_o}{2}(3\cos\theta+\sin\phi)\right]$$

$$+2E_{\phi,3}\cos\left[\frac{k_o d_o}{2}(3\cos\theta-\sin\phi)\right]+2E_{\phi,4}\cos\left[\frac{k_o d_o}{2}(3\cos\theta-3\sin\phi)\right]$$

$$+2E_{\phi,5}\cos\left[\frac{k_o d_o}{2}(\cos\theta+3\sin\phi)\right]+2E_{\phi,6}\cos\left[\frac{k_o d_o}{2}(\cos\theta+\sin\phi)\right]$$

$$+2E_{\phi,7}\cos\left[\frac{k_o d_o}{2}(\cos\theta-\sin\phi)\right]+2E_{\phi,8}\cos\left[\frac{k_o d_o}{2}(\cos\theta-3\sin\phi)\right]$$

(6.4.1)

where, because of the symmetry of the array, the following relationships have been used:

$$E_{\phi,1} = E_{\phi,16}\ ; E_{\phi,2} = E_{\phi,15}; E_{\phi,3} = E_{\phi,14}; E_{\phi,4} = E_{\phi,13};$$
$$E_{\phi,5} = E_{\phi,12}; E_{\phi,6} = E_{\phi,11}; E_{\phi,7} = E_{\phi,10}; E_{\phi,8} = E_{\phi,9}$$

(6.4.2)

For the H-Plane, ϕ=180°, 0°<θ<180° and the total electric field is given by

$$E_\phi = 2\left(E_{\phi,1}+E_{\phi,2}+E_{\phi,3}+E_{\phi,4}\right)\cos\left(\frac{3k_o d_o}{2}\cos\theta\right)+2\left(E_{\phi,5}+E_{\phi,6}+E_{\phi,7}+E_{\phi,8}\right)\cos\left(\frac{k_o d_o}{2}\cos\theta\right)$$

(6.4.3)

while, for the E-Plane, θ=90°, 90°<ϕ<270° and the total electric field is given by

$$E_\phi = 2\left(E_{\phi,1}+E_{\phi,4}+E_{\phi,5}+E_{\phi,8}\right)\cos\left(\frac{3k_o d_o}{2}\sin\theta\right)+2\left(E_{\phi,2}+E_{\phi,3}+E_{\phi,6}+E_{\phi,7}\right)\cos\left(\frac{k_o d_o}{2}\sin\theta\right)$$

(6.4.4)

A computer program which takes into account the effect of coupling has been developed (see Appendix J) and used to predict the radiation pattern for both linear and circular polarisations. The following 'S' parameters for the array (element spacing = 0.75λo) were calculated using the cavity model (see chapter 5):

$S_{1,1} = 0$

$S_{1,2} = 0.03096 \angle -2.59°$, -30.18dB

$S_{1,3} = 0.01639 \angle 71.11°$, -35.71dB

$S_{1,4} = 0.01111 \angle 150.55°$, -39.09dB

$S_{1,5} = 0.02605 \angle 77.27°$, -31.68dB

$S_{1,6} = 0.01389 \angle -92.62°$, -37.15dB

$S_{1,7} = 0.01175 \angle 10.85°$, -38.60dB

$S_{1,8} = 0.00939 \angle 107.16°$, -40.55dB

$S_{1,9} = 0.00600 \angle 157.85°$, -44.44dB

$S_{1,10} = 0.00506 \angle 59.16°$, -45.91dB

$S_{1,11} = 0.00590 \angle -143.67°$, -44.58dB

$S_{1,12} = 0.00624 \angle -12.09°$, -44.10dB

$S_{1,13} = 0.00262 \angle -121.27°$, -51.62dB

$S_{1,14} = 0.00244 \angle 170.64°$, -52.26dB

$S_{1,15} = 0.00301 \angle 9.51°$, -50.44dB

$S_{1,16} = 0.0038 \angle 175.32°$, -48.41dB

Also because of the symmetry of the array, the following relationships can be deduced:

$$S_{1,1} = S_{2,2} = S_{3,3} = \ldots = S_{16,16}$$

$$S_{1,2} = S_{2,3} = S_{3,4} = S_{5,6} = S_{6,7} = S_{7,8} = S_{9,10} = S_{10,11} = S_{11,12} = S_{13,14} = S_{14,15} = S_{15,16}$$

$$S_{1,3} = S_{2,4} = S_{5,7} = S_{6,8} = S_{9,11} = S_{10,12} = S_{13,15} = S_{14,16}$$

$$S_{1,4} = S_{5,8} = S_{9,12} = S_{13,16}$$

$$S_{1,5} = S_{5,9} = S_{9,13} = S_{2,6} = S_{6,10} = S_{10,14} = S_{3,7} = S_{7,11} = S_{11,15} = S_{4,8} = S_{8,12} = S_{12,16}$$

$$S_{1,6} = S_{2,5} = S_{2,7} = S_{3,6} = S_{3,8} = S_{4,7} = S_{5,10} = S_{6,9} = S_{6,11} = S_{7,10} = S_{7,12} = S_{8,11} = S_{9,14} = S_{10,13} = S_{10,15} = S_{11,14} = S_{11,16} = S_{12,15}$$

$$S_{1,7} = S_{2,8} = S_{3,5} = S_{4,6} = S_{5,11} = S_{6,12} = S_{7,9} = S_{8,10} = S_{9,15} = S_{10,16} = S_{11,13} = S_{12,14}$$

$$S_{1,8} = S_{4,5} = S_{5,12} = S_{8,9} = S_{9,16} = S_{12,13}$$

$$S_{1,9} = S_{2,10} = S_{3,11} = S_{4,12} = S_{5,13} = S_{6,14} = S_{7,15} = S_{8,16}$$

$$S_{1,10} = S_{2,9} = S_{2,11} = S_{3,10} = S_{3,12} = S_{4,11} = S_{5,14} = S_{6,13} = S_{6,15} = S_{7,14} = S_{7,16} = S_{8,15}$$

$$S_{1,11} = S_{2,12} = S_{3,9} = S_{4,10} = S_{5,15} = S_{6,16} = S_{7,13} = S_{8,14}$$

$$S_{1,12} = S_{4,9} = S_{5,16} = S_{8,13}$$

$$S_{1,13} = S_{2,14} = S_{3,15} = S_{4,16}$$

$$S_{1,14} = S_{2,13} = S_{2,15} = S_{3,14} = S_{3,16} = S_{4,15}$$

$$S_{1,15} = S_{2,16} = S_{3,13} = S_{4,14}$$

$$S_{1,16} = S_{4,13}$$

(6.4.5)

The individual input reflection coefficients of each patch can be obtained using equation (6.3.2). By substituting equation (6.3.2) into equations (6.2.4) and (6.4.1) the total radiation of the antenna array has been determined.

Effect of Mutual Coupling on Radiation Pattern

Figures 6.4.2 and 6.4.3 (for E and H-plane respectively) show the predicted radiation patterns for linear polarisation with and without mutual coupling being taken into account. It was found that the antenna gain is 0.03dB lower if the mutual coupling is included while the beamwidth and the side lobe level were unchanged.

Figure 6.4.4 shows the effect of mutual coupling on the radiation pattern for circular polarisation (CP). The antenna gain is 0.03dB lower while the beamwidth (16°) and the side lobe level (-12.56dB) were unchanged.

Performance of a 4×4 Antenna Array

The 4*4 Circularly Polarised (CP) antenna array was realised using a RT/Duroid (ε_r=2.33, h=0.79mm) substrate. The measured radiation pattern is shown in figure 6.4.5. The predicted and practical results were summarised in tables 6.4.2 and 6.4.3 together with the antenna gain and axial ratio.

Antenna Gain (η=100%)	Half-Power Beamwidth	Side lobe Level	Axial Ratio
20.28dBi	16°	-12.56dB	0dB

Table 6.4.2 Predicted Results (included mutual coupling)

Antenna Gain	Half-Power Beamwidth	Side lobe Level RHCP, LHCP	Axial Ratio RHCP , LHCP
17.00dBi	15°	-9dB, -11.8dB	1dB , 4.2dB

Table 6.4.3 Practical Results

The measured 'S' parameters of the array are shown in figure 6.4.6 where S_{11} = -20dB and S_{21} = -13.5dB at 5.8GHz.

Good agreement on both the beamwidth and the side-lobe level has been obtained between the practical results and the theory which takes into account the effect of mutual coupling. It was found that the mutual coupling has little effect on the beamwidth and the side lobe level when the spacing between the centres of elements is $0.75\lambda o$. Moreover there is a negligible effect (0.03dB) on the antenna gain. Therefore in practice it is not necessary to include the effect of mutual coupling in the design of antenna array when the spacing between the centres of antenna elements is equal to or greater than $0.75\lambda o$.

6.5 Summary and Conclusions

This chapter has shown how to model the mutual coupling on the performance of an antenna array using 'S' parameters. In order to satisfy the requirement of the range of the communication zone, a circularly polarised 4 by 4 RSU antenna array with a high gain and a narrow beamwidth has been realised. It was shown that the mutual coupling has negligible effect on the performance of the antenna array. Therefore in practice under the constraints of the design parameters, it is not necessary to include the mutual coupling effects.

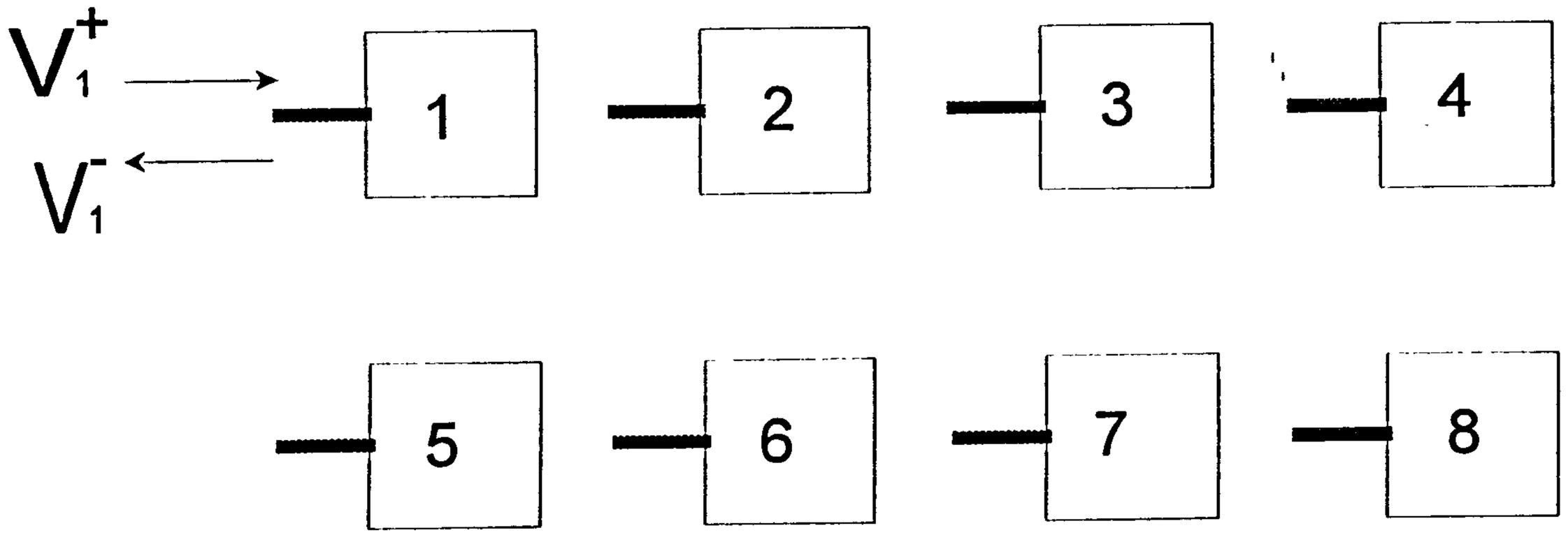

Figure 6.2.1 4*4 Antenna Array

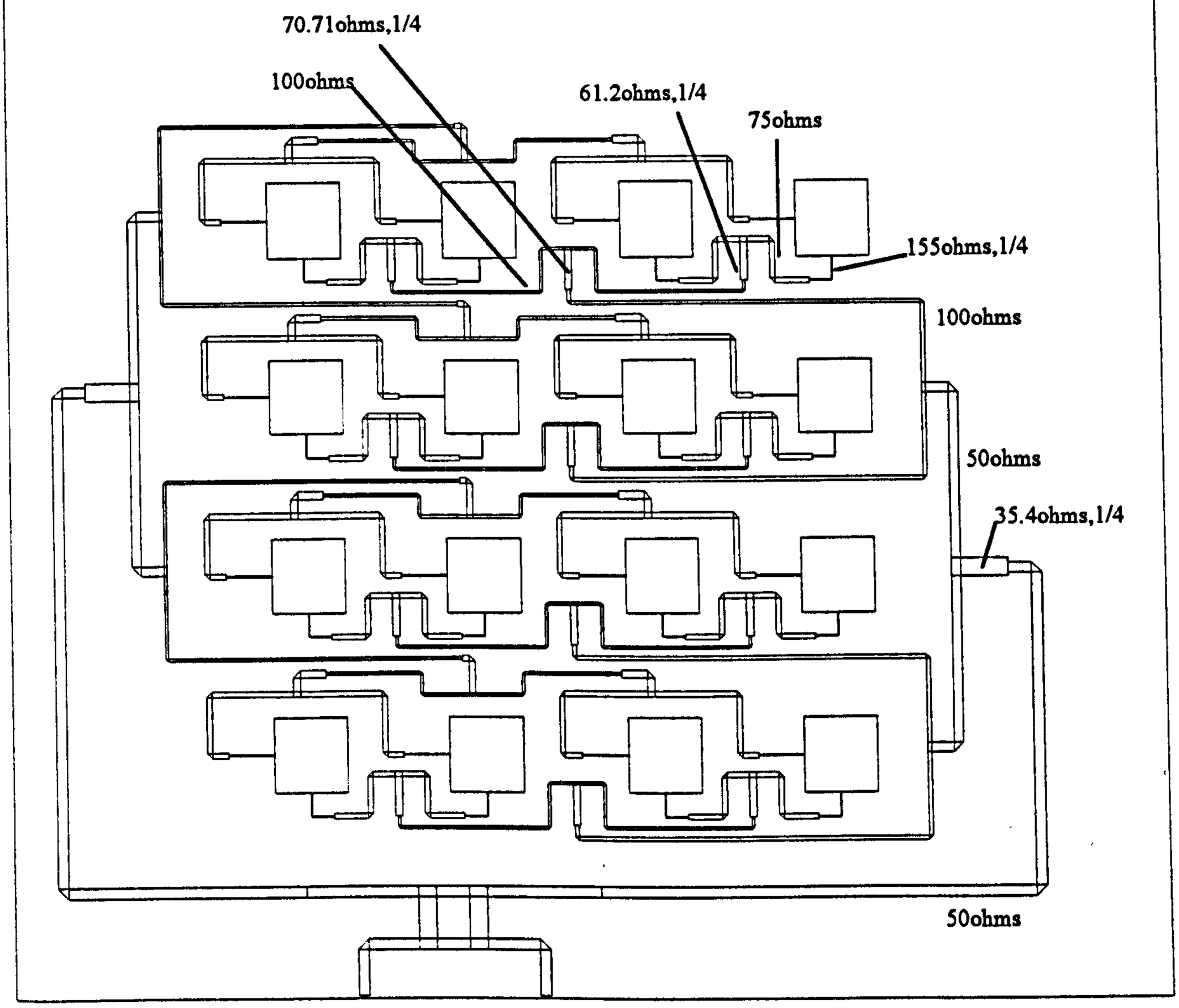

Figure 6.4.1 5.8GHz C.P. Array Antenna with Feed Line Impedance

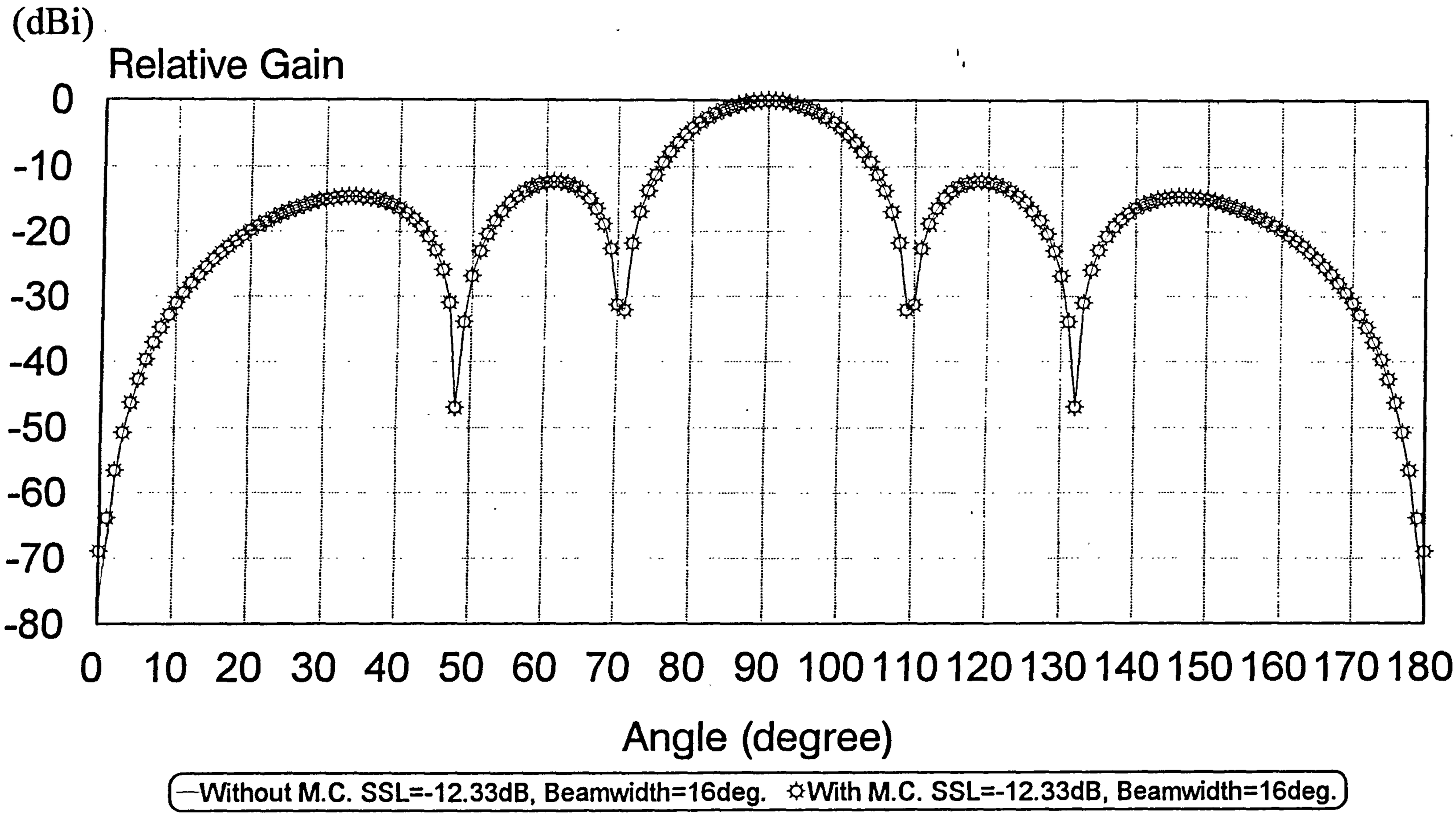

Figure 6.4.2 Radiation Pattern for Linear Polarisation, E-Plane (Simulated)

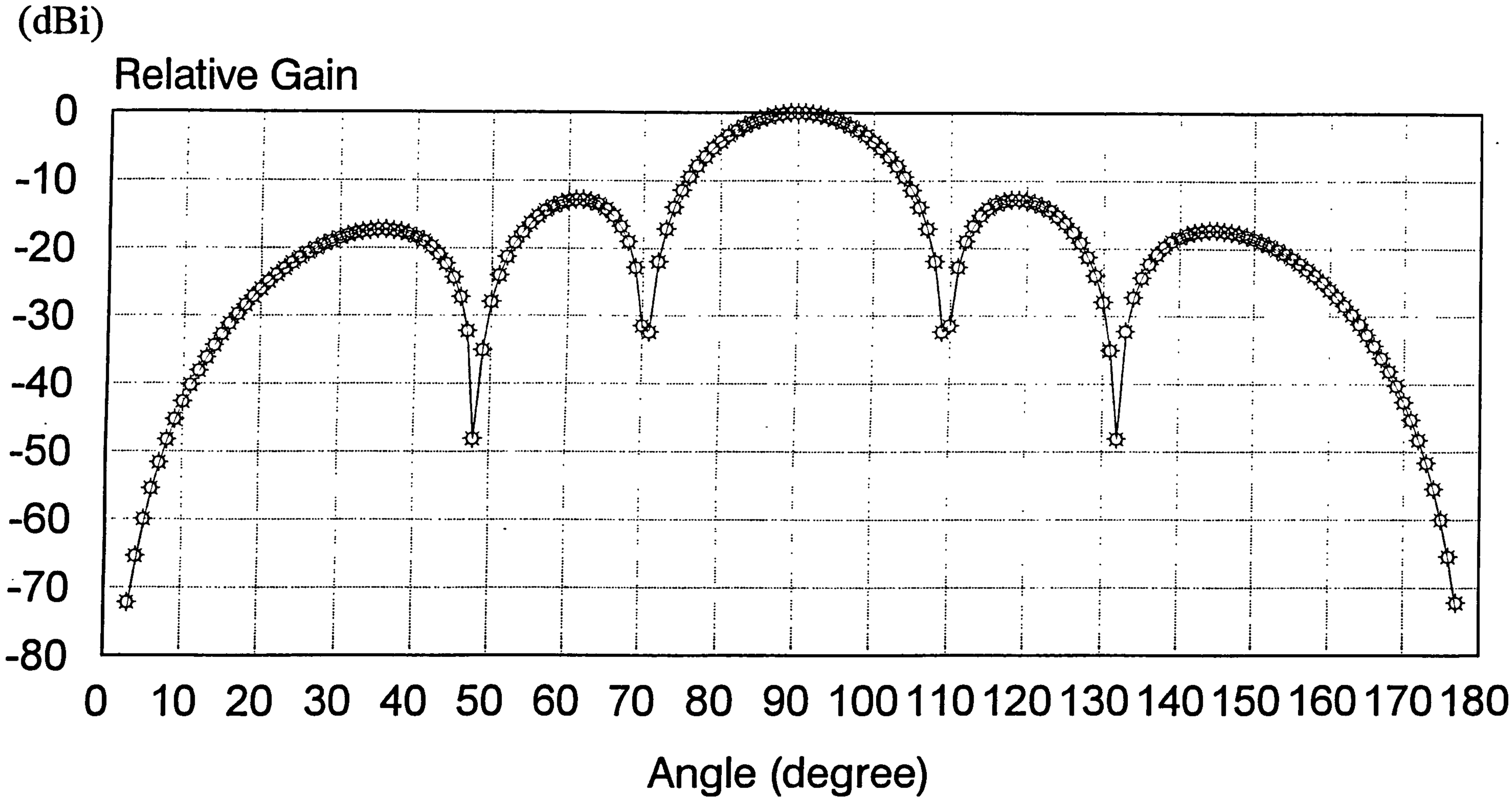

Figure 6.4.3 Radiation Pattern for Linear Polarisation, H-Plane (Simulated)

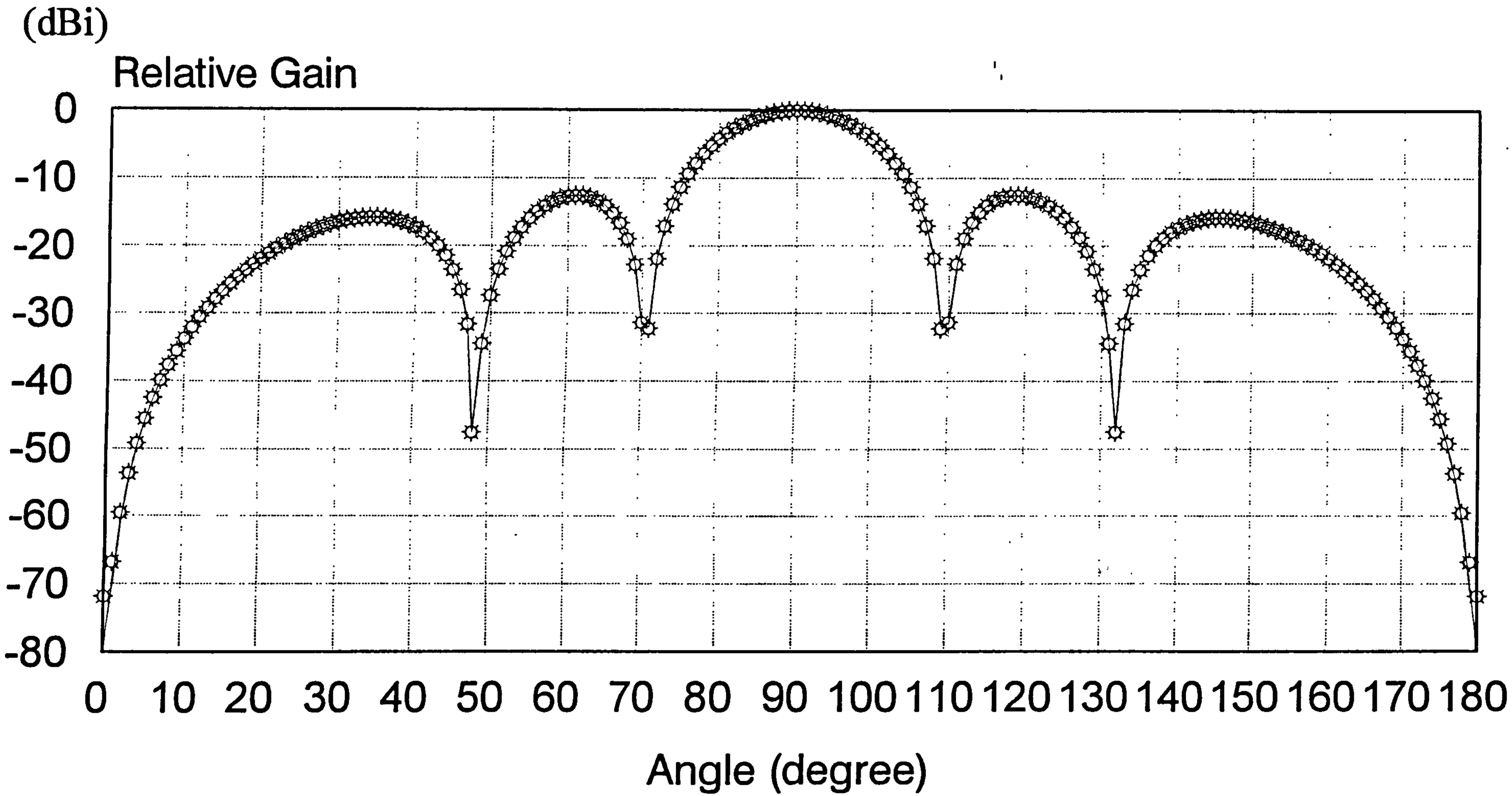

Figure 6.4.4 Radiation Pattern for Circular Polarisation (Simulated)

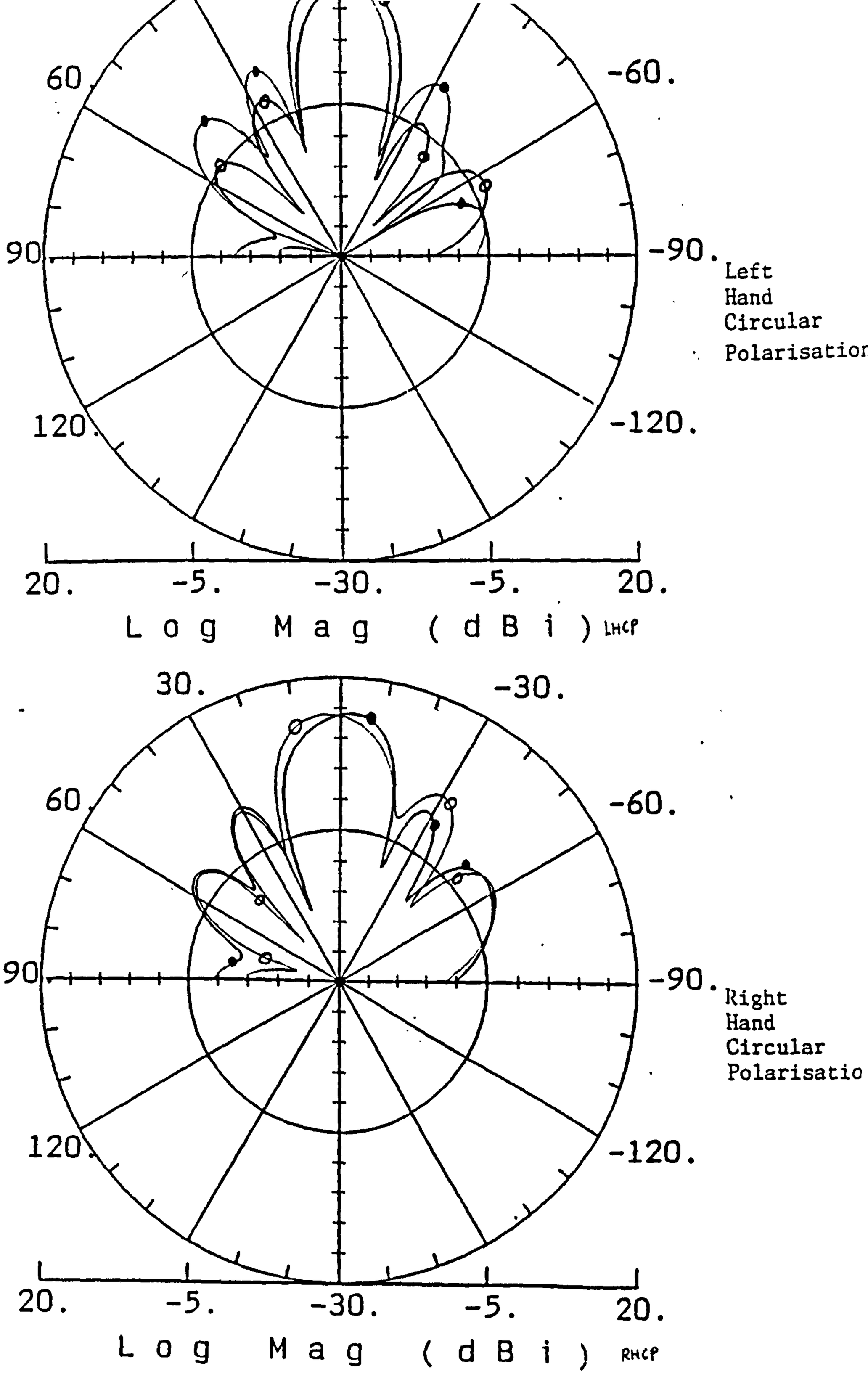

● — Antenna placed horizontally
o — Antenna placed vertically

Figure 6.4.5 Measured Radiation Pattern

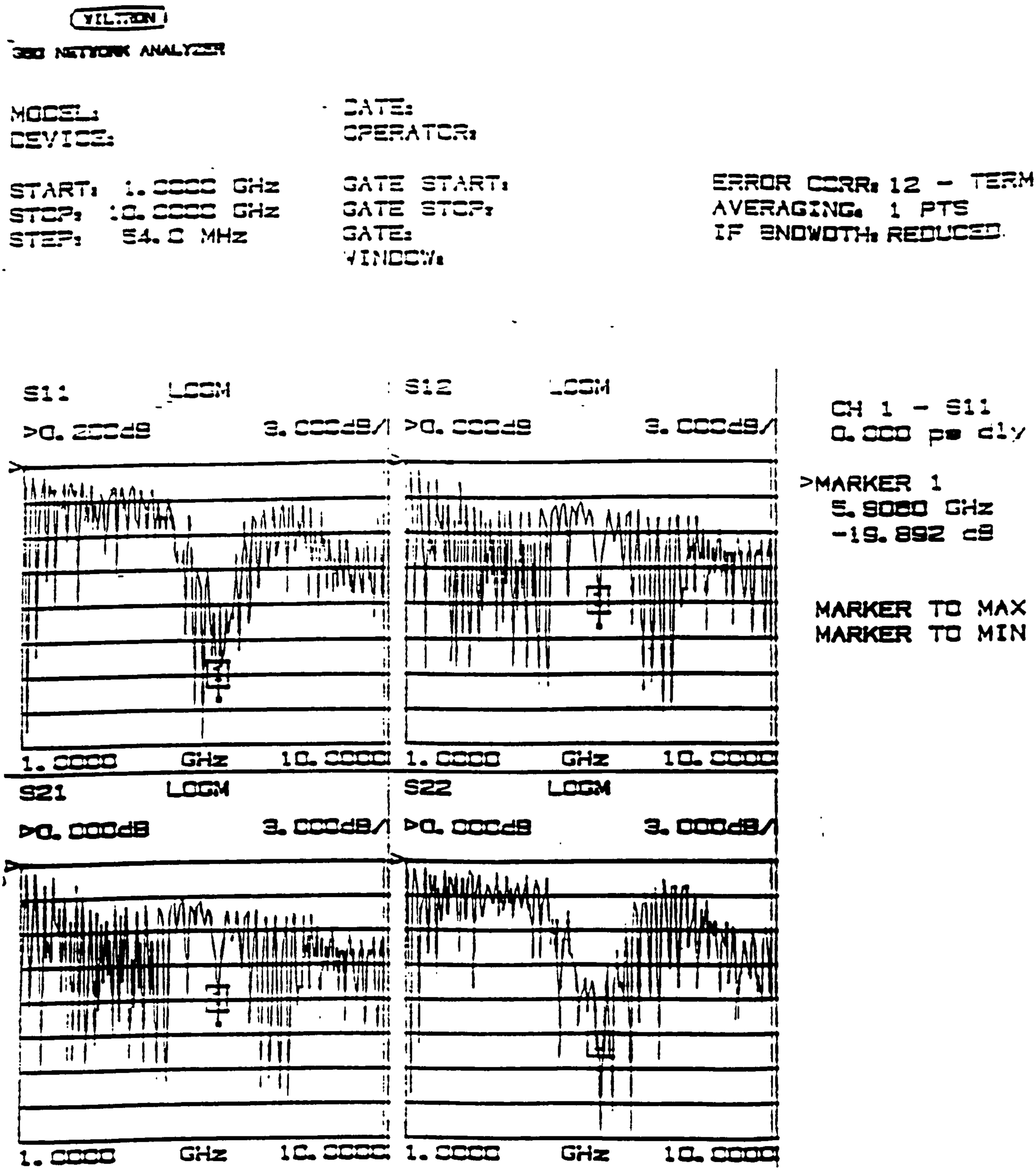

Figure 6.4.6 Measured 'S' Parameters of Antenna Array

CHAPTER 7

Design and Performance of an ASK Detector/PSK Modulator and an Image Rejection Mixer (IRM)

7.1 Introduction

This chapter reviews the theory of an ASK detector and a single-diode PSK modulator. An ASK modulator is used for demodulating the ASK signal transmitted from the RSU in the case of down-link operation. For up-link operation a PSK modulator is used for modulating the microwave carrier. In order to make the OBU simple and inexpensive, a single-diode arrangement is used for the realisation of a combined ASK detector/PSK modulator. Then the theory and performance of an image rejection mixer (IRM) used at the RSU is also presented.

7.2 Review of Diode Detector Theory

Modelling of Diode Characteristic at High Frequencies

The diode equivalent model shown in Figure 7.2.1 consists of a junction resistance and capacitance R_j and C_j, a series resistance R_s and the package parasitics L_1, L_2 and C_1. The diode impedance is given by

$$Z_d = j\omega L_1 + \frac{1}{Y_s + j\omega C_1} \tag{7.2.1}$$

where

$$Y_s = \frac{1 + j\omega C_j R_j}{(R_s + R_j - \omega^2 L_2 C_j R_j) + j\omega\left(L_2 + C_j R_j R_s\right)} \tag{7.2.2}$$

If it is assumed that the diode has an ideal I-V characteristic, the dc voltage-current relationship of a diode is given by (Cowley, 1966)

$$i = I_s\left(e^{\alpha V_j} - 1\right) \tag{7.2.3}$$

where i is the instantaneous diode current, I_s is the diode saturation current, V_j is the voltage across the junction resistor and α is given by

$$\alpha = \frac{e}{nkT} \tag{7.2.4}$$

where n is the ideality factor, e is the electron charge and k is the Boltzmann constant. Since the diode junction resistance R_j is the inverse of the average slope of the I-V curve at the operating point, giving

$$R_j = \left[\left. \frac{di}{dv_j} \right|_{I_o} \right]^{-1} = \frac{1}{\alpha(I_s + I_o)} \tag{7.2.5}$$

where I_o is the bias current. The junction capacitance C_j is given by

$$C_j = \frac{Cjo}{\sqrt{1 - \frac{Vj}{\phi}}} \tag{7.2.6}$$

where

$$V_j = \frac{1}{\alpha} \ln\left(\frac{I_s + I_o}{I_s} \right) \tag{7.2.7}$$

and C_{jo} is the junction capacitance at zero bias and ϕ is the diode work function.

At high frequencies the diode is influenced not only by the junction resistance and junction capacitance, but also by the parasitic components. Therefore, in the design of the ASK detector, a matching circuit is connected to the diode so that the maximum power transfer can be obtained.

Diode Noise

For a biased diode the output noise is a combination of shot noise of the barrier, the thermal noise of the series resistance and the low-frequency noise (called 1/f noise, or, flicker noise). Two assumptions are made (Uhlir, 1963):

1. that the shot and thermal noise are white (its power spectrum is quite flat in the usual output frequency ranges) and
2. that the flicker noise has a 1/f spectrum

The shot noise in bandwidth B generated in a Schottky barrier diode due to the junction resistance is given by Van der Ziel (1970)

$$v_{n1}^2 = 2nkTBR_j\left(\frac{I_o + 2I_s}{I_o + I_s}\right) \tag{7.2.8}$$

and the thermal noise generated in the diode series resistance is given by

$$v_{n2}^2 = 4kTBR_s \tag{7.2.9}$$

Flicker noise varies as 1/f and its value depends on the frequency and bandwidth of the detector and is given by (Bhartia, 1988)

$$v_{n3}^2 = 2nkTR_j f_c \ln\left(1 + \frac{B}{f_L}\right) \tag{7.2.10}$$

where f_L is the lower frequency limit of the measurement bandwidth B, and f_c is the corner frequency which is defined as the frequency where the flicker noise equals the shot noise generated in the junction resistance.

The total noise generated in the diode is therefore

$$v_n^2 = v_{n1}^2 + v_{n2}^2 + v_{n3}^2 = 4kTB\left[R_j \frac{n}{2}\frac{I_o + 2I_s}{I_o + I_s} + R_s + R_j \frac{n}{2}\frac{f_c}{B}\ln\left(1 + \frac{B}{f_L}\right)\right] \tag{7.2.11}$$

The total output noise from the amplifier is then given by

$$v_a^2 = 4kTBG^2\left[R' + R_j \frac{n}{2}\frac{f_c}{B}\ln\left(1 + \frac{B}{f_L}\right)\right] \tag{7.2.12}$$

where

$$R' = R_j \frac{n}{2}\frac{I_o + 2I_s}{I_o + I_s} + R_s + R_a \tag{7.2.13}$$

and R_a is the equivalent noise resistance and G is the gain of the amplifier.

Theory of the Diode Detector

The diode detector includes an input matching network, a dc biasing arrangement, a Schottky barrier diode and a video amplifier. The matching network is used to maximise the absorbed microwave power by the diode while the dc biasing current is used to enable the diode to work in the square-law region for low-level detection and also to produce a reduction of the r.f. and output (video) impedance of the diode. Reducing the r.f. impedance allows an easier realisation of the r.f. matching network and the lower output impedance allows the use of a lower input impedance amplifier. The bandlimited video amplifier is used to convert the detected voltage into the TTL data. Matching the impedance of the diode with that of the video amplifier results in an improvement in the sensitivity of the detector (Oxley,1980 and Siegal,1975). The generalised microwave detector circuit is shown in Figure 7.2.2. Figure 7.2.3 shows the output current resulting from a sinusoidal input applied to the non-linear diode junction. For a small applied ac voltage δV, the application of the Taylor expansion to equation (7.2.3) gives

$$i = i(V_o + \delta V) = i(V_o) + \delta V \left.\frac{di}{dV_o}\right|_{Io} + \left.\frac{\delta V^2}{2!}\frac{d^2 i}{dV_o^2}\right|_{Io} + \ldots \qquad (7.2.14)$$

The voltage sensitivity (β_v) is defined as the open-circuit output voltage divided by the power absorbed in the diode and is given by (appendix K)

$$\beta_v = \frac{\alpha R_j R_L}{2(R_j + R_s)(R_v + R_L)} \left| \frac{R_j Y_s}{(1 + j\omega C_j R_j)[1 + j\omega L_1 (Y_s + j\omega C_1)]} \right|^2 \mathrm{Re}(Z_d) \ \mathrm{Volts/Watts} \qquad (7.2.15)$$

The tangential signal sensitivity (TSS) is used to measure the ability of the detector to detect a signal against a background noise which includes amplifier noise. The TSS is defined as the amount of microwave signal power (below the 0dBm reference level) which is required to produce an output pulse whose amplitude is sufficient to raise the noise fluctuations by an amount equal to the average noise level. The minimum input power is defined as the r.f. input power required to produce an output signal-to-noise ratio of unity (or 0dB) for a bandwidth of 1 Hz.

The voltage signal-to-noise ratio at the output of the detector is given by

$$\frac{S}{N}=\frac{\beta_v P_{in}}{\sqrt{4kTB\left[R'+R_j\frac{n}{2}\frac{f_c}{B}\ln\left(1+\frac{B}{f_L}\right)\right]}} \tag{7.2.16}$$

For a diode with a low flicker noise, it reduces to

$$\frac{S}{N}=\frac{\beta_v P_{in}}{\sqrt{4kTBR'}} \tag{7.2.17}$$

The minimum detectable signal $P_{\min}$ can be determined by letting S/N = 1 (or 0dB) giving

$$P_{\min}=\frac{\sqrt{4kTBR'}}{\beta_v} \tag{7.2.18}$$

TSS can also be illustrated as the condition when the negative noise peaks riding on the detected voltage V_{det} equal the noise peaks when no signal is present as shown in Figure 7.2.4. At the above (tangent) condition

$$V_{pk}=V_{\det}-V_{pk} \quad \text{or} \quad V_{\det}=2V_{pk}=2\sqrt{2}V_n \tag{7.2.19}$$

therefore

$$V_{\det}=\beta_v\, TSS=2\sqrt{2}V_n \tag{7.2.20}$$

The TSS becomes

$$TSS=\frac{2\sqrt{2}V_n}{\beta_v}=\frac{2\sqrt{2}\sqrt{4kTBR'}}{\beta_v}=2\sqrt{2}P_{\min} \tag{7.2.21}$$

or

$$TSS(dBm)=4.5dB+P_{\min}(dBm) \tag{7.2.22}$$

Therefore the TSS is approximately 4.5dB above the minimum detectable signal power $P_{\min}$ when S/N=1 (or 0dB) and from equation (7.2.20)

$$TSS=\frac{V_{\det}}{\beta_v}=\frac{2\sqrt{2}V_n}{\beta_v} \tag{7.2.23}$$

For a bit error rate (BER) of 10^{-6} in the ASK non-coherent detection, the probability P_e of an error is related to $\frac{A}{2\sigma}$ (Shanmugan,pp401) as follows:

$$P_e \approx \int_{-\infty}^{A/2} \frac{1}{\sqrt{2\pi\sigma^2}} \exp\left(-\frac{(r-A)^2}{2\sigma^2}\right) dr = Q\left(\frac{A}{2\sigma}\right) = 10^{-6} \qquad (7.2.24)$$

where A is the peak detected voltage and σ^2 is the r.m.s. noise power. Since $\frac{A}{2\sigma} = 4.75$, $\frac{A}{\sigma} = \frac{\beta_v P_r}{V_n} = 2*4.75 = 9.5$, where P_r is the received power at the input of the detector.

Combining with equation 7.2.23, P_r is given by

$$P_r = 9.5\frac{V_n}{\beta_v} = 9.5\frac{TSS}{2\sqrt{2}} = 3.39TSS \qquad (7.2.25)$$

$$\text{or} \qquad P_r(dBm) = 5.3dB + TSS(dBm) \qquad (7.2.26)$$

Hence the actual received power at the input of the diode detector is required to be approximately 5.3dB above the TSS in order that the BER is 10^{-6} .

Comparison of the TSS Between the Practical and Theoretical Results

The TSS has been evaluated as a function of impedance and bandwidth values of the video amplifier against the biasing current of the diode at both 2.45GHz and 5.8GHz as shown in Figures 7.2.5 and 7.2.6 respectively. As the biasing current is reduced, the diode resistance will be higher than the load resistance so most of the detected voltage appears across the diode rather than across load. However, at higher biasing current, the diode is no longer working at the square-law region. It can be seen that if the biasing current is too high or too low, the TSS is reduced. In addition by limiting the bandwidth of the video amplifier the TSS can also be improved. At 2.45GHz the optimum biasing current is about 200μA giving the TSS equal to -50dBm for a 1kΩ load impedance and a 1MHz bandwidth while at 5.8GHz the optimum biasing current is about 20μA giving a TSS value of -57dBm for a 3.3k Ω load impedance and a 1MHz bandwidth.

In order to compare the measured values of the TSS with the theoretical results, diode

detectors using a HSMS-8101 diode were fabricated and tested at 2.45GHz and 5.8GHz, respectively (the bandwidth of the CRO was 60MHz and the load impedance was 1kΩ). Table 7.2.1 shows the comparison between theoretical and practical results and a fairly good agreement was obtained.

	Theoretical	Practical
TSS (2.45GHz) 200μA	-42dBm	-44dBm
TSS (5.8GHz) 20μA	-48dBm	-50dBm

Table 7.2.1 Comparison of TSS Between Theoretical and Practical Results

7.3 Theory and Design of a Single-Diode PSK Modulator

The diode impedance in 'on' and 'off' conditions at the high frequency is required in the design of a PSK modulator. Since the diode may not appear as a perfect switch, it is necessary to design a matching network to establish that the input reflection coefficients have equal magnitudes and a 180° phase difference with respect to 50Ω resistance of the modulator for both 'on' and 'off' states of the diode.

This section first presents the theoretical and measured values of the diode impedance at high frequencies. An analysis of a non-ideal PSK modulator and the design of the matching network for the PSK modulation is then presented. And finally the performance of a combined ASK detector/PSK modulator is discussed.

Diode Impedance and Measurement

The parameters of the HSMS-8101 diode given by the manufacturer are as follows:

$R_s = 4\Omega$ $L_1 = 1\text{nH}$

$L_2 = 1.3\text{nH}$ $C_1 = 0.22\text{pF}$

$C_{jo} = 0.23\text{pF}$ (junction capacitance at V=0)

$I_s = 90\text{nA}$ (diode saturation current)

$\alpha = e/(nkT)$ $\phi = 0.5$

n = 1.08 (ideality factor) e = 1.6021917E-19 (electron charge)

k = 1.380622E-23 (Boltzmann constant) T = 300K

Using the equation 7.2.1 the theoretical values of the diode impedance varying as a

function of biasing current are shown in Table 7.3.1 at 2.45GHz and 5.8GHz, respectively.

The test-circuit for measuring the impedance of the diode is shown in Figure 7.3.1. A network analyser was used to determine the impedance of the diode. However in order to obtain the impedance it is necessary to include the effect of the 50Ω line offset, as it is not possible to connect the network analyser directly to the diode terminals. Table 7.3.1 shows the measured impedance of the diode at both 2.45GHz and 5.8GHz along with the theoretical values. They are also shown on the Smith Chart in Figure 7.3.2(a) and (b).

As can be seen the theoretical and practical results are consistent over the range of bias current used. In order to produce PSK modulation it is necessary to continuously switch the diode current 'On' and 'Off'. From the results shown on the Smith Chart (Figure 7.3.2) the bias current required to switch the diode 'On' is 8mA. The corresponding reflection coefficients are shown in Table 7.3.2.

Biasing Current	Diode Impedance (Zd) (Ω) at 2.45GHz (Theoretical)	Diode Impedance (Zd) (Ω) at 2.45GHz (Measured)	Diode Impedance (Zd) (Ω) at 5.8GHz (Theoretical)	Diode Impedance (Zd) (Ω) at 5.8GHz (Measured)
0 μA	*1.19 - j 123.56*	*6.50 - j 169.99*	*1.63 - j 9.21*	*1.05 - j 20.68*
20μA	14.60 - j 108.35	11.10 - j 155.98	5.53 - j 0.50	1.09 - j 12.76
40μA	26.46 - j 103.02	15.55 - j 153.17	8.93 + j 1.06	2.11 - j 11.14
60μA	36.99 - j 96.88	20.65 - j 150.79	12.20 + j 2.28	3.09 - j 9.89
80μA	46.02 - j 89.84	24.57 - j 148.74	15.36 + j 3.44	4.02 - j 8.82
100μA	53.47 - j 82.18	28.99 - j 146.53	18.42 + j 4 64	5.09 - j 7.76
1mA	34.65 + j 28.54	87.69 - j 25.93	55.07 + j 74.35	52.05 + j 62.67
2mA	20.34 + j 34.36	45.99 + j 22.95	40.93 + j 97.81	51.36 + j 140.58
3mA	15.20 + j 35.59	22.71 + j 35.08	32.38 + j 104.56	37.78 + j 155.35
4mA	12.58 + j 36.05	15.67 + j 37.09	27.39 + j 107.35	30.66 + j 160.01
5mA	10.99 + j 36.28	12.82 + j 37.65	24.21 + j 108.78	26.12 + j 161.85
6mA	9.93 + j 36.41	11.46 + j 37.83	22.01 + j 109.63	23.09 + j 159.64
7mA	9.18 + j 36.49	10.52 + j 37.97	20.41 + j 110.17	20.47 + j 161.18
8mA	*8.61 + j 36.54*	*9.90 + j 38.02*	*19.19 + j 110.54*	*19.27 + j 161.63*
9mA	8.16 + j 36.59	9.45 + j 38.09	18.23 + j 110.81	18.58 + j 162.33
10mA	7.81 + j 36.61	9.13 + j 38.13	17.46 + j 111.02	18.38 + j 162.56

Table 7.3.1 Diode Impedance (2.45GHz and 5.8GHz)

Biasing Current	Measured Reflection Coefficients (2.45GHz)	Measured Reflection Coefficients (5.8GHz)
0mA 'off'	Γ_1=0.980∠-32.7°	Γ_1=0.965∠-135.0°
8mA 'on'	Γ_2=0.779∠104.1°	Γ_2=0.936∠34.0°
Amplitude difference: Phase difference:	$\Delta\Gamma$=1.99dB $\Delta\phi$=136.8°	$\Delta\Gamma$=0.27dB $\Delta\phi$=169°

Table 7.3.2 Diode Reflection Coefficients (2.45GHz and 5.8GHz)

Analysis of a Non-Ideal PSK Modulator

This section examines the effect of amplitude and phase error of the reflection coefficients on the non-ideal PSK modulator in terms of the bit error rate (BER). Consider a PSK signal in the form

$$v(t) = f(t)\cos(\omega_o t + \phi(t)) + n(t) \tag{7.3.1}$$

with a phase error $\Delta\phi = \phi_1 - \phi_0 + 180°$ and amplitude error $k = d_1/d_0$. The bandlimited noise can be expressed as (Schwartz, p.365)

$$n(t) = r(t)\cos(\omega_o t + \theta(t)) \tag{7.3.2}$$

where $x(t) = r(t)\cos\theta(t)$ and $y(t) = r(t)\sin\theta(t)$. In the synchronous demodulation as shown in Figure 7.3.3, the output voltage is given by

$$v_0(t) = v(t) \bullet \cos\omega_0 t = f(t)\cos\phi(t) + x(t) = \begin{cases} d_1\cos\phi_1 & \text{for '1'} \\ d_0\cos\phi_0 & \text{for '0'} \end{cases} + x(t) \tag{7.3.3}$$

The equation 7.3.3 can be expressed as

$$v_0(t) = \begin{cases} d_1\cos\phi_1 & \text{for '1'} \\ -d_0\cos(\phi_1 - \Delta\phi) & \text{for '0'} \end{cases} + x(t) \tag{7.3.4}$$

Assuming the error has a normal distribution (thermal noise only) as shown in Figure 7.3.4 the probability of error for '0' and '1' are given by

$$P_{e0} = \int_{0}^{\infty} p\left(x + d_0 \cos(\phi_1 - \Delta\phi)\right) dx \tag{7.3.5}$$

$$P_{e1} = \int_{-\infty}^{0} p\left(x - d_1 \cos\phi_1\right) dx \tag{7.3.6}$$

respectively. Equations 7.3.5 and 7.3.6 can be expressed as

$$P_{e0} = \int_{0}^{\infty} \frac{\exp\left(-\frac{\left(x + d_0 \cos(\phi_1 - \Delta\phi)\right)^2}{2\sigma^2}\right)}{\sqrt{2\pi\sigma^2}} dx = \frac{1}{2} erfc\left(\frac{d_0 \cos(\phi_1 - \Delta\phi)}{\sqrt{2}\sigma}\right) \tag{7.3.7}$$

$$P_{e1} = 1 - \int_{0}^{\infty} \frac{\exp\left(-\frac{\left(x - d_1 \cos\phi_1\right)^2}{2\sigma^2}\right)}{\sqrt{2\pi\sigma^2}} dx = \frac{1}{2} erfc\left(\frac{d_1 \cos\phi_1}{\sqrt{2}\sigma}\right) \tag{7.3.8}$$

The bit error rate $BER = P_0 P_{e0} + P_1 P_{e1}$. Assuming $P_0 = P_1 = 0.5$ the BER was derived as

$$BER = \frac{1}{4}\left[erfc\left(\frac{d_0 \cos(\phi_1 - \Delta\phi)}{\sqrt{2}\sigma}\right) + erfc\left(\frac{d_1 \cos\phi_1}{\sqrt{2}\sigma}\right)\right] \tag{7.3.9}$$

or

$$BER = \frac{1}{4}\left[erfc\left(\sqrt{\frac{E_b}{\eta_o}} \frac{1}{k} \cos\Delta\phi\right) + erfc\left(\sqrt{\frac{E_b}{\eta_o}}\right)\right] \tag{7.3.10}$$

where the amplitude error is equal to $20\log_{10}\left(\frac{d_1}{d_2}\right) = 20\log(k)$.

For an ideal case where $d_0 = d_1 = A$ and $\Delta\phi = 0°$ ($\phi_1 = 0°$ and $\phi_0 = 180°$) the bit error rate (BER) is given by

$$BER = \frac{1}{2} erfc\left(\sqrt{\frac{E_b}{\eta_o}}\right) \tag{7.3.11}$$

The relation between the BER and the amplitude error and phase error is shown in Figures 7.3.5 and 7.3.6. Further the relation between the BER and the combined amplitude-phase error is shown in Figure 7.3.7. In order to maintain the reflection coefficients of equal magnitude and phase difference of 180° between 'on' and 'off' conditions, it is necessary to have a matching network, as is demonstrated in Table 7.3.2 (page 84).

It is also shown that the phase error has less effect on the bit error rate compared to the amplitude error. It is however more important to have an equal amplitude rather than an exact 180° phase difference for a PSK modulator.

Design and Performance of the PSK Modulator

Three different matching networks as shown in Figure 7.3.8 can be used to transform the terminating impedances Z_1 and Z_2 into the reflection coefficients Γ_1 and Γ_2 at the output. Z_1 and Z_2 correspond to the impedances of the diode in its 'off' and 'on' state. The design procedure is based on the work by Atwater (1980). Γ_1 and Γ_2 must satisfy the condition

$$\Gamma_1 (Z_1) = e^{j\phi} \Gamma_2 (Z_2) \qquad (7.3.12)$$

where ϕ is the value of phase shift. The equation 7.3.12 can be expressed as

$$\frac{Z_1 - Z_m}{Z_1 + Z_m^*} = e^{j\phi} \frac{Z_2 - Z_m}{Z_2 + Z_m^*} \qquad (7.3.13)$$

The expressions for calculating the values of Z_m are shown in the Appendix L. Once the virtual impedance Z_m is calculated from Z_1, Z_2 and ϕ, the parameters of the different matching networks can be calculated and are summarised below:

a) Quarter-Wavelength Double-Stub Transformer (Fig. 7.3.8(a))

If Zm is expressed as follows,

$$Z_m = Z_o / (g_m + jb_m) \qquad (7.3.14)$$

then the electrical lengths of the two stubs are

$$\theta_1 = \mp \tan^{-1} \sqrt{\frac{1-g_m}{g_m}} \tag{7.3.15}$$

$$\theta_2 = \tan^{-1}[-b_m \mp \sqrt{g_m(1-g_m)} \tag{7.3.16}$$

where θ_2 is the length of the stub nearer the termination.

b) Transmission Line Transformer (Fig. 7.3.8(b))

Characteristic impedance

$$Z'_{om} = \sqrt{Z_o \frac{(R_m Z_o - R_m^2 - X_m^2)}{(Z_o - R_m)}} \tag{7.3.17}$$

Electrical length

$$\theta_m = \tan^{-1} \sqrt{\frac{(Z_o - R_m)}{Z_o X_m^2}(R_m Z_o - R_m^2 - X_m^2)} \tag{7.3.18}$$

c) Tandem 3/8 - Wavelength Network (Fig. 7.3.8(c))

The characteristic impedance of the 45° section is Z_m, and the 90° section has a characteristic impedance

$$Z_m = \sqrt{R_m^2 + X_m^2} \tag{7.3.19}$$

$$Z_{om} = \sqrt{\frac{Z_o R_m Z_m}{(Z_m - X_m)}} \tag{7.3.20}$$

The phase shift circuit was designed for the frequency of 2.45GHz and a phase shift ϕ =180° using an HSMS-8101 diode. The impedance of the diode in its 'on' and 'off' states was measured in order to determine the design parameters Z_1 and Z_2. Measured values of the 'off' and 'on' state impedances obtained were as follows:

Z_1=12.86-j165.62 (Ω) at I_B=0mA 'Off', and Z_2=9.97+j38.88 (Ω) at I_B=8mA 'On'

and hence Z_m was calculated as (see Appendix L)

$$Z_m=102.06-j50.43\ (\Omega),\ \text{and}\ \ g_m=0.3937\ \ b_m=0.1949$$

By using Z_m , the parameters of the three different matching networks were determined and the results are summarised below:

a) Quarter-wavelength double-stub transformer: $\theta_1= +51.14°$ and $\theta_2= +16.37°$,
b) Transmission line transformer: $Z'_{om}=86.87\Omega$ and $\theta_m= 60.86°$,
c) Tandem 3/8 - wavelength network: $Z_m= 113.84\Omega$ and $Z_{om}= 59.47\Omega$.

The matching networks for the three topologies have been modelled and the dimensions of the line optimised. They were fabricated on RT/Duroid $\varepsilon r=2.20$, h=1.57mm, tand=0.0012. The circuit layouts are shown in Figure 7.3.9(a) to (c). Both the simulated and the practical results are shown in Table 7.3.3.

	'SuperCompact' Simulation				Measurement			
	Γ1 (Off)	Γ2 (On)	ΔΓ	Δϕ	Γ1 (Off)	Γ2 (On)	ΔΓ	Δϕ
A	-1.76dB	-1.02dB	0.74dB	180.2°	-0.70dB	-1.14dB	0.52dB	183.5°
B	-0.98dB	-0.98dB	0dB	180.2°	---	---	---	---
C	-1.01dB	-1.00dB	0.01dB	181.8°	---	---	---	---

Table 7.3.3 Comparison of a 2.45GHz PSK modulators Between Theoretical and Measured Results

It was found that the topologies B and C did not agree with the theory (the results are not shown since the discrepancy was too great). In order to get near 180° phase shift and equal magnitudes of Γ_1 and Γ_2, it was necessary to fine tune the length of the matching line. The discrepancy may be due to the difficulty of soldering the pin of the diode to a precise position on the very thin microstrip line. However the topology (a) (double-stub matching network) gave good results namely $\Delta\Gamma$=0.52dB and $\Delta\phi$=183.5°.

In order to obtain a better virtual r.f. ground for the diode the $\lambda/4$ rectangular patch was replaced with a radial stub as shown in Figure 7.3.10. The measured coefficients for 'Off' and 'On' states were:

$$\Gamma_1 = -0.93dB\angle -55° \quad \text{and} \quad \Gamma_2 = -0.99dB\angle 124.5°$$

or $\Delta\Gamma$=0.04dB and $\Delta\phi$=179.5°.

The same method was used for 5.8GHz and in this case it was found that topologies A and C have extreme L/W ratios which are hard to realise. Matching network B was selected with length L=15mm and width W=4.1mm. Then the matching network with the diode was built and tested using network analyser. It was found that the reflection coefficient of the 'on' state is practically independent of the biasing current in the range 6-10 mA.

The measured reflection coefficients for 'on' and 'off' states were:

$$\Gamma_1 = -1.604dB\angle -119.25° \quad \text{and} \quad \Gamma_2 = -1.729dB\angle 59.74°$$

or $\Delta\Gamma$=0.125dB and $\Delta\phi$=178.99°.

Single Diode ASK Detector/PSK Modulator

The PSK modulator has also been used as an ASK detector. Switching the diode between 0mA and 8mA allows the diode to function as a PSK modulator. Biasing the diode at 20μA allows the diode to function as an ASK detector. The matching network is designed for the diode acting as a PSK modulator which results in a mismatch in the ASK detector. The resultant TSS will be degraded by the factor

$$-10\log_{10}\left(1-\left|\Gamma_{PSK,in}\right|^2\right) \text{dB} \qquad (7.3.21)$$

where $\Gamma_{PSK,in}$ is the input reflection coefficient of the PSK modulator which is functioning as an ASK detector.

The 2.45GHz PSK modulator was then tested as an ASK detector whose TSS was degraded from -50dBm to -45dBm due to the mismatch of the matching network. For the 5.8GHz PSK modulator, the measured TSS was also degraded from -52dBm to -48dBm.

7.4 Theory of an Image Rejection Mixer (IRM)

The image rejection mixer (IRM) consists of two broadband mixers, together with a common local oscillator and four phase shifters as shown in Figure 7.4.1. The basic element of the mixer is two broadband single balanced mixers consisting of a 3dB coupler and two

diodes as shown in Figure 7.4.2(a). The equivalent circuit for analysis is shown in Figures 7.4.2(b) to (d). The advantages of using the single balanced mixer are that the local oscillator (pump) and signal ports are isolated and that the local oscillator noise is suppressed (Saleh, 1971). The two diodes are connected so that on a positive half cycle of the local oscillator waveform only one diode is in forward conduction whilst the other is effectively switched off. On a negative half-cycle the process is reversed. This means that there is 180° phase difference between the operation of the two pairs. The Fourier series for the resistance of the resistive diode is therefore given by

$$r_+(t) = R_o + 2\sum_{n=1}^{\infty} R_n \cos n\omega_p t \tag{7.4.1}$$

and

$$r_-(t) = R_o + 2\sum_{n=1}^{\infty} (-1)^n R_n \cos n\omega_p t \tag{7.4.2}$$

where r_+ and r_- are the diode resistance in the Fourier series form for the positive and negative half cycles of the local oscillator waveform, respectively. ω_p is the pump (local oscillator) frequency. From Figure 7.4.2(d) the output current $I_{if}(t)$ is given by

$$I_{if}(t) = i_1(t) - i_2(t) \tag{7.4.3}$$

and

$$i_1(t) + i_2(t) = 2i_s(t) \tag{7.4.4}$$

from equations (7.4.3) and (7.4.4)

$$i_1(t) = i_s(t) + \frac{I_{if}(t)}{2} \tag{7.4.5}$$

and

$$i_2(t) = i_s(t) - \frac{I_{if}(t)}{2} \tag{7.4.6}$$

It can then be shown that the signal voltages ($v_s(t)$) and the i.f. currents ($i_s(t)$) at all possible frequencies in the circuit are given by

$$v_s(t) = \frac{4r_+(t)r_-(t)}{r_+(t)+r_-(t)} i_s(t) + \frac{2[r_-(t)-r_+(t)]}{r_+(t)+r_-(t)} v_{if}(t) \qquad (7.4.7)$$

and

$$I_{if}(t) = \frac{2[r_-(t)-r_+(t)]}{r_+(t)+r_-(t)} i_s(t) + \frac{4}{r_+(t)+r_-(t)} v_{if}(t) \qquad (7.4.8)$$

In these equations the voltage at the input is restricted to contain only the components at signal frequency and the output current contains only the component at i.f. frequency.

For the IRM it is necessary that the following conditions are satisfied.

1. There can be no net image power transfer between two identical mixers. The image recovery must only be due to the cancellation of image voltages (or currents) generated by each individual mixer at the input port in order to prevent any power loss at this frequency. In other words this creates short or open circuit terminations for the images.
2. The mixers are both 'broadband' and the theoretical minimum conversion loss of each mixer is 3dB since this divides the input r.f. power equally between i.f. and image frequencies.

As far as the image rejection mixer is concerned, by suitable choice of phase shifters, the broadband properties of the two mixers (which would normally lead to a minimum conversion loss 3dB) can be modified so that dissipation of power at the image frequency in the input termination is avoided.

In realising a practical circuit using two mixers together with phase shifters, the design must satisfy the following requirements:

1. The signal and local oscillator phase shifts must combine to produce either image voltage or image current cancellation at the input port;
2. The signal at the image frequency should generate i.f. voltages from the I and Q- mixer channels and these voltages will cancel each other out; and
3. The signal at the r.f signal frequency should generate i.f. voltages from the mixers at the I and Q- channels, which are then combined to give a maximum i.f. power output.

The image rejection mixer reflects any image frequency component appearing at the r.f. terminals of the mixer back to the diode for reconversion to i.f. which is in phase with the original generated i.f. signal. The angles α_1 and α_2 shown in Figure 7.4.1 must be chosen so that the input impedance of the mixers at image frequency are either open or short circuited.

Consider the input signal (which in complex form is valid for AM, DSB, SSB and NBFM as shown in Figure 7.4.3) as

$$V_s = \sum_{all\ s} a_s \left[e^{j(\omega_s t + \phi_s)} + e^{-j(\omega_s t + \phi_s)} \right] \tag{7.4.9}$$

The input signals after a phase shift by α_1 or α_2 and fed into 'I' and 'Q' mixers become,

$$V_{sI} = \sum_{all\ s} a_s \left[e^{j(\omega_s t + \phi_s - \alpha_1)} + e^{-j(\omega_s t + \phi_s - \alpha_1)} \right] \tag{7.4.10}$$

$$V_{sQ} = \sum_{all\ s} a_s \left[e^{j(\omega_s t + \phi_s - \alpha_2)} + e^{-j(\omega_s t + \phi_s - \alpha_2)} \right] \tag{7.4.11}$$

The output of the local oscillator after a phase shift of β for the 'I' channel becomes

$$V_{oI} = a_p \left[e^{j(\omega_p t - \beta)} + e^{-j(\omega_p t - \beta)} \right] \tag{7.4.12}$$

while for the 'Q' channel it is

$$V_{oQ} = a_p \left[e^{j\omega_p t} + e^{-j\omega_p t} \right] \tag{7.4.13}$$

The Fourier series for the conductance of the diodes of the two mixers is given by:

$$g(t)_I = g_0 + g_1 \left(e^{j(\omega_p t - \beta)} + e^{-j(\omega_p t - \beta)} \right) + g_2 \left(e^{j2(\omega_p t - \beta)} + e^{-j2(\omega_p t - \beta)} \right) + \ldots \tag{7.4.14}$$

$$g(t)_Q = g_0 + g_1 \left(e^{j\omega_p t} + e^{-j\omega_p t} \right) + g_2 \left(e^{j2\omega_p t} + e^{-j2\omega_p t} \right) + \ldots \tag{7.4.15}$$

The output current (or voltage) of the mixer i(t)=v.g(t) (or v(t)=i.R(t)) can be separated into different frequency components at the i.f. and image frequencies as shown below

I-Channel:

$$\left(I_{i.f.}\right)_I = K_1 \sum_{all\ s} a_s \left[e^{j\left((\omega_p - \omega_s)t - \phi_s + \alpha_1 - \beta\right)} + e^{-j\left((\omega_p - \omega_s)t - \phi_s + \alpha_1 - \beta\right)} \right] \tag{7.4.16}$$

$$\left(I_{im}\right)_I = K_2 \sum_{all\ s} a_s \left[e^{j\left((2\omega_p - \omega_s)t - \phi_s + \alpha_1 - 2\beta\right)} + e^{-j\left((2\omega_p - \omega_s)t - \phi_s + \alpha_1 - 2\beta\right)} \right] \tag{7.4.17}$$

Q-Channel:

$$\left(I_{i.f.}\right)_Q = K_1 \sum_{all\ s} a_s \left[e^{j\left((\omega_p - \omega_s)t - \phi_s + \alpha_2\right)} + e^{-j\left((\omega_p - \omega_s)t - \phi_s + \alpha_2\right)} \right] \tag{7.4.18}$$

$$\left(I_{im}\right)_Q = K_2 \sum_{all\ s} a_s \left[e^{j\left((2\omega_p - \omega_s)t - \phi_s + \alpha_2\right)} + e^{-j\left((2\omega_p - \omega_s)t - \phi_s + \alpha_2\right)} \right] \tag{7.4.19}$$

where K_1 and K_2 are constants representing the Fourier coefficients of the non-linear device (mixer diode). K_2 is smaller than K_1 as K_2 is derived from the 2nd harmonic of the conductance waveform.

In considering the image signal which is generated from the two single balanced mixers, the total phase shift for the image signal is given by:

$$\pm j\left[\left(2\omega_p - \omega_s\right)t - \phi_s + \alpha_1 - 2\beta\right] \pm j\left[\left(2\omega_p - \omega_s\right)t - \phi_s + \alpha_2\right]$$

$$= \pm j\left[\theta_1 + \alpha_1 - 2\beta\right] \pm j\left[\theta_1 + \alpha_2\right] \tag{7.4.20}$$

where $\theta_1 = \left(2\omega_p - \omega_s\right)t - \phi_s$. The phasor diagram of the image signal in the 'I' and 'Q' channels is shown in Figure 7.4.4 and the condition for the image signal to cancel is

$$\left(\theta_1 + \alpha_1 - 2\beta\right) - \left(\theta_1 + \alpha_2\right) = n\pi, \quad \text{n} = 1,3,5,\ldots \tag{7.4.21}$$

giving,

$$\left(\alpha_1 - \alpha_2\right) - 2\beta = n\pi \tag{7.4.22}$$

Taking $\beta=\pi/2$,

$$\left(\alpha_1 - \alpha_2\right) = m\pi, \quad \text{m}=0,2,4,\ldots \tag{7.4.23}$$

Therefore, a condition to create an open circuit at the node 0 is

$$\alpha_1 - \alpha_2 = 0 \quad \text{and} \quad \beta = \frac{\pi}{2} \tag{7.4.24}$$

and

$$(I_{im})_I + (I_{im})_Q = 0 \tag{7.4.25}$$

The image currents cancel each other out at the node 0 and no power is dissipated in the source conductance.

Considering the phase components of i.f. outputs at channels I and Q after a phase shift of γ the following result is obtained:

$$\pm j\left[(\omega_p - \omega_s)t - \phi_s + \alpha_1 - \beta\right] \pm j\left[(\omega_p - \omega_s)t - \phi_s + \alpha_2 - \gamma\right]$$

$$= \pm j\left[\theta_2 + \alpha_1 - \beta\right] \pm j\left[\theta_2 + \alpha_2 - \gamma\right] \tag{7.4.26}$$

where $\theta_2 = (\omega_p - \omega_s)t - \phi_s$. The phasor diagram for the I.F. in 'I' and 'Q' channels is shown in Figure 7.4.5. The vector sum is a maximum when the two vectors are in phase so that

$$\theta_2 + \alpha_1 - \beta = \theta_2 + \alpha_2 - \gamma \tag{7.4.27}$$

giving $\gamma = \pi/2$. Therefore the i.f. current at the output port (after phase shifted by $\pi/2$ for Q-channel) is given by

$$(I_{i.f.})_I + (I_{i.f.})_Q \angle -90° = (I_{i.f.})_I + (I_{i.f.})'_Q$$

$$= K_1 \sum_{all\ s} a_s \left[e^{\pm j\left((\omega_p - \omega_s)t - \phi_s + \alpha_1 - \frac{\pi}{2}\right)} + e^{\pm j\left((\omega_p - \omega_s)t - \phi_s + \alpha_2 - \frac{\pi}{2}\right)} \right]$$

$$= 2K_1 \sum_{all\ s} a_s e^{\pm j\left((\omega_p - \omega_s)t - \phi_s + \alpha_1 - \frac{\pi}{2}\right)} \tag{7.4.28}$$

As the current (voltage) at the node 0 is zero, the image of the I and Q-channels will be reflected back to the mixers and converted into intermediate frequencies. The i.f. outputs for I and Q channels after the second mixing (indirect i.f.) are given below.

<u>I-Channel:</u>

$$\left((I_{im})_I\right)_{i.f.} = (I_{im})_I * g(t)_I$$

$$= K_3 \sum_{all\ s} a_s\, e^{\pm j\left((\omega_p-\omega_s)t-\phi_s+\alpha_1-\beta\right)}$$

$$= K_3 \sum_{all\ s} a_s\, e^{\pm j\left((\omega_p-\omega_s)t-\phi_s+\alpha_1-\frac{\pi}{2}\right)} \qquad (7.4.29)$$

<u>Q-Channel:</u>

$$\left((I_{im})_Q\right)_{i.f.} = (I_{im})_Q * g(t)_Q$$

$$= K_3 \sum_{all\ s} a_s\, e^{\pm j\left((\omega_p-\omega_s)t-\phi_s+\alpha_2\right)} \qquad (7.4.30)$$

The value of K_3 is smaller than K_2 and K_1. After a phase shift of $\gamma = \pi/2$ for $\left((I_{im})_Q\right)_{i.f.}$:

$$\left((I_{im})_Q\right)'_{i.f.} = K_3 \sum_{all\ s} a_s\, e^{\pm j\left((\omega_p-\omega_s)t-\phi_s+\alpha_1-\frac{\pi}{2}\right)} \qquad (7.4.31)$$

Thus the total output current can be obtained by

$$I_{out} = \left(I_{i.f}\right)_I + \left(I_{i.f}\right)'_Q + \left((I_{im})_I\right)_{i.f.} + \left((I_{im})_Q\right)'_{i.f.} \qquad (7.4.32)$$

direct conversion	direct conversion	indirect conversion	indirect conversion

When an input signal at image frequency is applied to the mixer the resulting spectrums are shown in Figure 7.4.6. With the IRM parameters $\alpha_1 = \alpha_2$, $\beta = \pi/2$ and $\gamma = \pi/2$, the i.f. and image outputs of the mixers are as follows:

I-Channel:

$$\text{i.f.:} \quad \left(I_{i.f.}\right)_I = K_1 \sum_{all\ s} a_s\, e^{\pm j\left((\omega_s-\omega_p)t+\phi_s-\alpha_1+\beta\right)} \tag{7.4.33}$$

$$\text{image:} \quad \left(I_{im}\right)_I = K_2 \sum_{all\ s} a_s\, e^{\pm j\left((2\omega_p-\omega_s)t-\phi_s+\alpha_1-2\beta\right)} \tag{7.4.34}$$

Q-Channel:

$$\text{i.f.:} \quad \left(I_{i.f.}\right)_Q = K_1 \sum_{all\ s} a_s\, e^{\pm j\left((\omega_s-\omega_p)t+\phi_s-\alpha_2\right)} \tag{7.4.35}$$

$$\text{image:} \quad \left(I_{im}\right)_Q = K_2 \sum_{all\ s} a_s\, e^{\pm j\left((2\omega_p-\omega_s)t-\phi_s+\alpha_2\right)} \tag{7.4.36}$$

The sum of the two currents is zero i.e.

$$\left(I_{im}\right)_I + \left(I_{im}\right)_Q = 0 \tag{7.4.37}$$

Since the open-circuit condition is created at the node '0' the image frequency components will be reflected back to the mixers for a second mixing. The re-converted i.f. components after second mixing are given by

I-Channel:

$$\left(\left(I_{im}\right)_I\right)_{i.f.} = \left(I_{im}\right)_I * g(t)_I$$

$$= K_3 \sum_{all\ s} a_s\, e^{\pm j\left((\omega_s-\omega_p)t+\phi_s-\alpha_1+\frac{\pi}{2}\right)} \tag{7.4.38}$$

Q-Channel:

$$\left(\left(I_{im}\right)_Q\right)_{i.f.} = \left(I_{im}\right)_Q * g(t)_Q$$

$$= K_3 \sum_{all\ s} a_s\, e^{\pm j\left((\omega_s-\omega_p)t+\phi_s-\alpha_1\right)} \tag{7.4.39}$$

For the Q-channel after a phase shift of $\gamma = \pi/2$ expressions for $\left(I_{i.f.}\right)_Q$ and $\left(\left(I_{im}\right)_Q\right)_{i.f.}$ become

$$\left(I_{i.f.}\right)_Q^{'} = K_1 \sum_{all\ s} a_s\, e^{\pm j\left((\omega_s-\omega_p)t+\phi_s-\alpha_1-\frac{\pi}{2}\right)} \tag{7.4.40}$$

$$\left(\left(I_{im}\right)_Q\right)_{i.f.}^{'} = K_3 \sum_{all\ s} a_s\, e^{\pm j\left((\omega_s-\omega_p)t+\phi_s-\alpha_1-\frac{\pi}{2}\right)} \tag{7.4.41}$$

Thus the total output current can be obtained.

$$I_{out} = \underbrace{\left(I_{i.f}\right)_I}_{\text{direct conversion}} + \underbrace{\left(I_{i.f}\right)_Q^{'}}_{\text{direct conversion}} + \underbrace{\left(\left(I_{im}\right)_I\right)_{i.f.}}_{\text{indirect conversion}} + \underbrace{\left(\left(I_{im}\right)_Q\right)_{i.f.}^{'}}_{\text{indirect conversion}} \tag{7.4.42}$$

$= 0$

The signal at the image frequency is cancelled at the output of the image rejection mixer. The mathematical analysis has shown that by choosing suitable phase shifts the IRM will rejects the image signal.

Performance of the IRM

In the last section it has been shown that the phase shift parameters of the image rejection mixer must be $\alpha_1 = \alpha_2$, $\beta = \gamma = \pi/2$ in order to reject the components generated at the image frequency and to maximise the components generated at the signal frequency. Therefore the r.f. signal fed into the mixers I and Q must be in phase while the local oscillator signal fed into the mixers must be 90° out of phase. An IRM operating at 5.8GHz has been designed and fabricated on RT/Duroid 6010, (ε_r = 10.5, h=1.27mm) and is shown in Figure 7.4.7. The following tests were carried out on the IRM.

LO-RF Leakage

The test set-up for measuring the LO-RF Leakage (the power leakage between the LO port and the RF port) is shown in Figure 7.4.8 and the measured LO leakage was +13.58dB.

The Effect of Local Oscillator Power Level on the Conversion Loss

The test set-up is shown in Figure 7.4.9. Conversion loss is defined as the ratio between the r.f. input power against the output i.f. power. Figure 7.4.10 shows the conversion loss

against the LO power level for I and Q-channels. Conversion loss decreases as the LO power level increases but the converstion loss increases if the LO power level is too high because of the mismatch of the diode impedance. The minimum conversion loss of 6.52dB was obtained at LO=+12dBm for I channel.

Effect of DC Biasing Current

In order to investigate the biasing current effect on the conversion loss the mixer was modified as shown in Figure 7.4.11. By biasing the mixer diodes there is a reduction of the LO power level. However an increase in the noise figure results in an increase in the conversion loss. Figures 7.4.12 and 7.4.13 show the effect of biasing current on the conversion loss for the LO power levels equal to +5dBm, 0dBm, -5dBm and -10dBm for I and Q-Channels respectively.

The measured results were summarised as follows:

1. LO-RF leakage: 13.58dB
2. Conversion Loss (LO=+10dBm, RF=-45.81dBm) : 7.04dB (I-Channel) and 7.52dB (Q-channel)

7.5 Conclusions

This chapter has presented the theory and performance of the diode detector, the PSK modulator and the image rejection mixer (IRM). The tangential signal sensitivity (TSS) which characterises the performance of an ASK detector has been derived using a diode model which includes the parasitics. It was found that a biasing current, a matching network and a video amplifier with a narrow bandwidth are required to optimise the TSS.

An analysis for a non-ideal PSK modulation has been presented. It was found that the phase error has little effect on the bit error rate compared with the effect of the amplitude error. Therefore it was concluded that it is very important to maintain the equal amplitude property of the PSK modulator in order to have a good PSK modulation.

In order to simplify the circuitry of the On-Board Unit the single diode approach was attempted. First a matching network was designed in order to maximise the PSK modulator's performance. The PSK modulator was then used as an ASK detector and it was found that the TSS was degraded due to the mismatch of the PSK matching network.

Finally the analysis of the IRM using a phasing technique was presented. The mixer consists of a phase shifter realised by a 3dB two-branch coupler and two broadband single balanced mixers realised by a 3dB two-branch coupler with two diodes for each mixer. A mixer has been fabricated and tested and good performance has been achieved. It has also been shown in practice that it is possible to reduce the local oscillator power level by employing a biasing condition for the diodes.

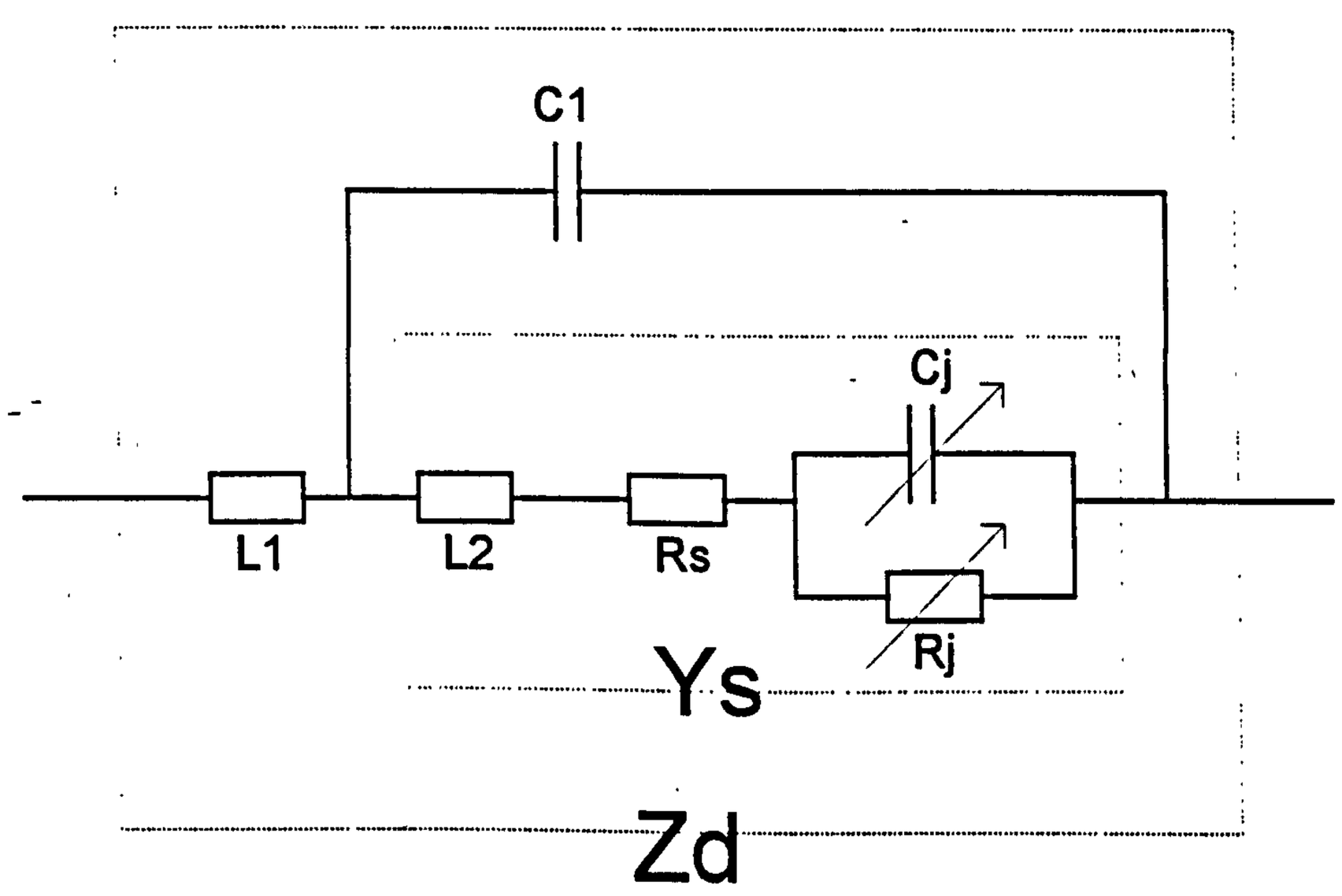

Figure 7.2.1 Diode Equivalent Circuit (HSMS-8101)

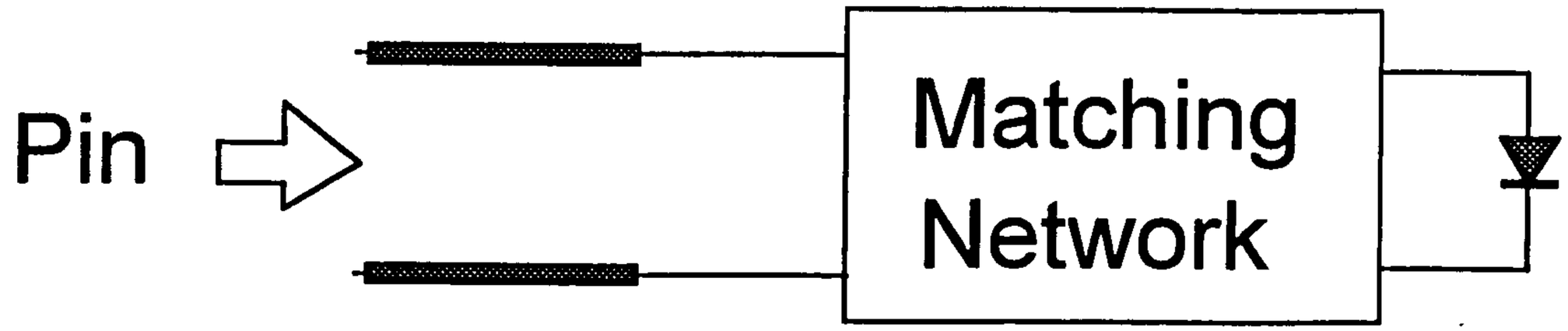

R.F.Circuit

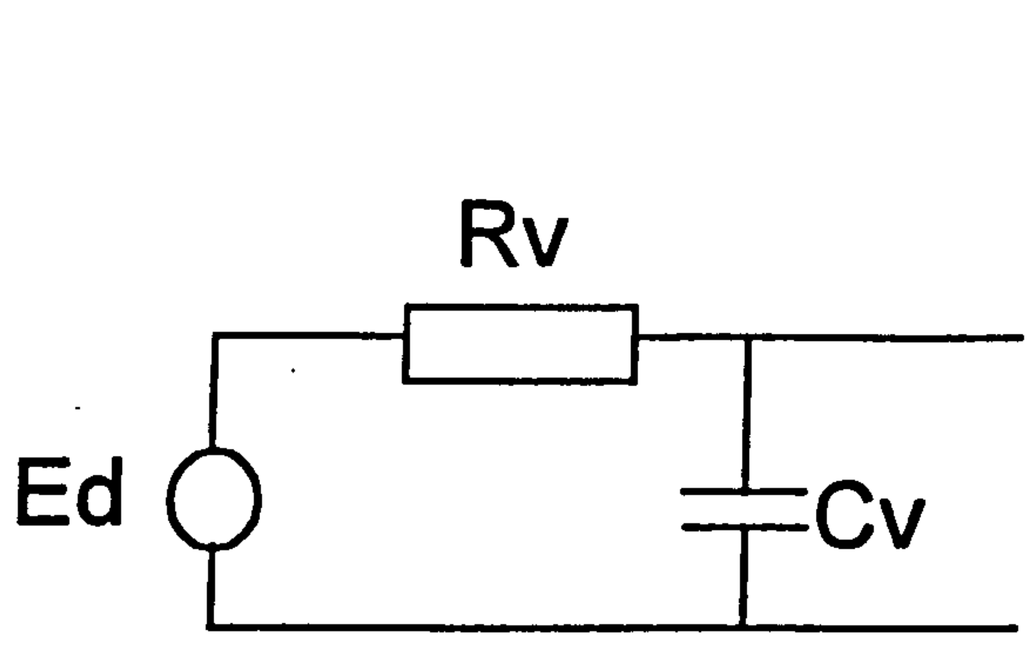

Video Circuit

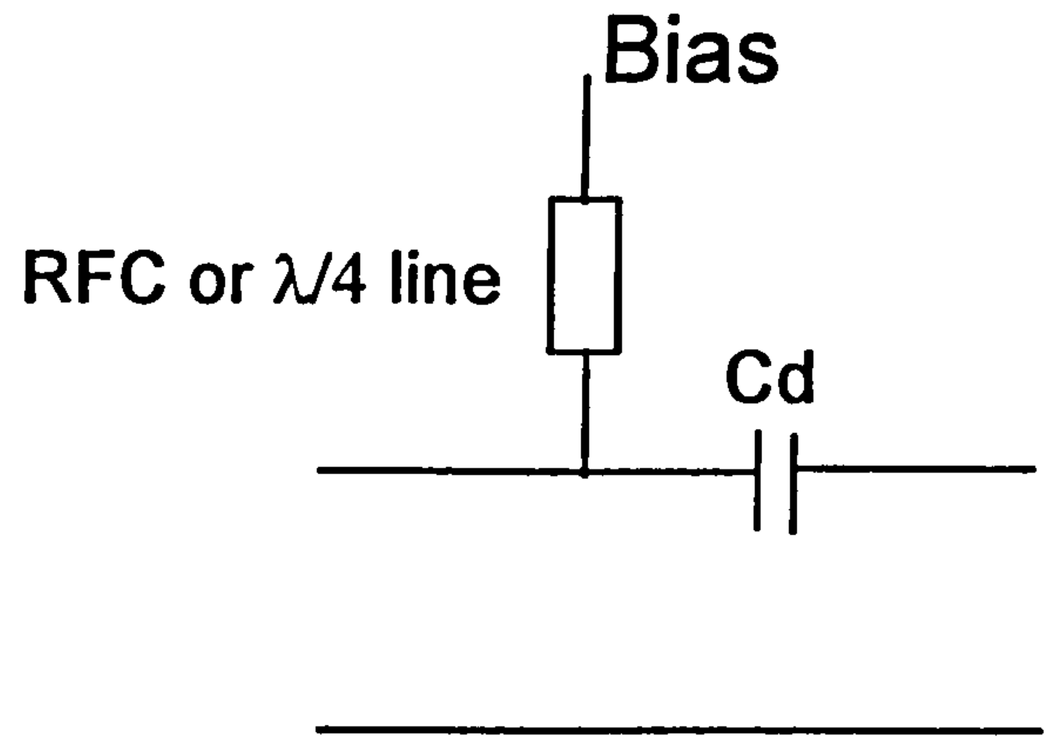

Bias Circuit

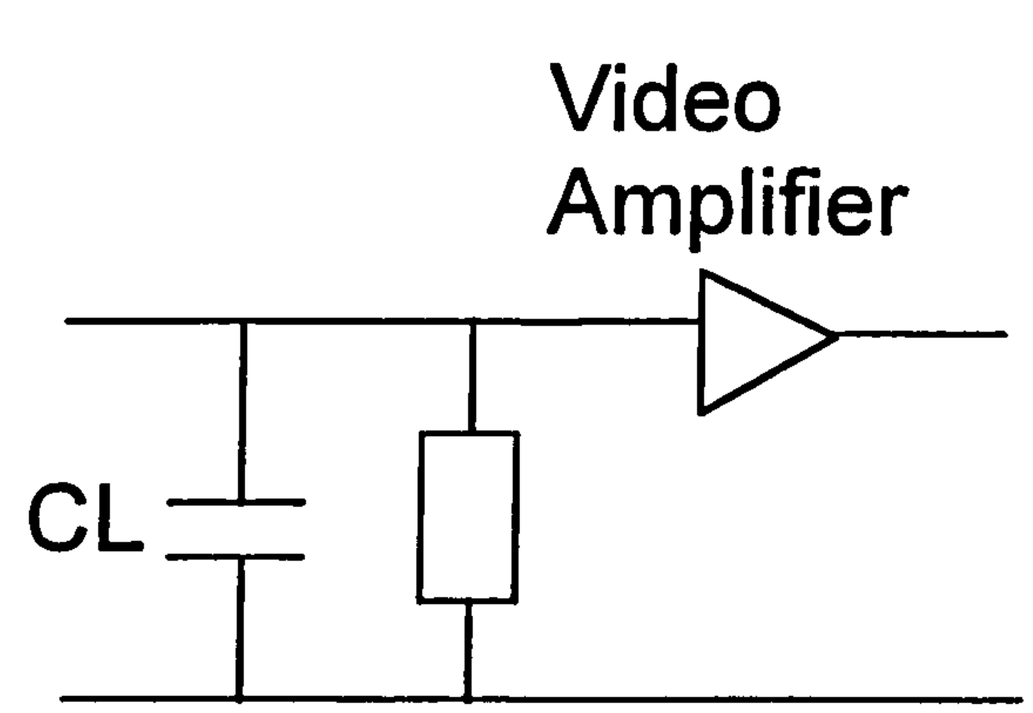

Video Load Circuit

Figure 7.2.2 Generalised Detector Circuit

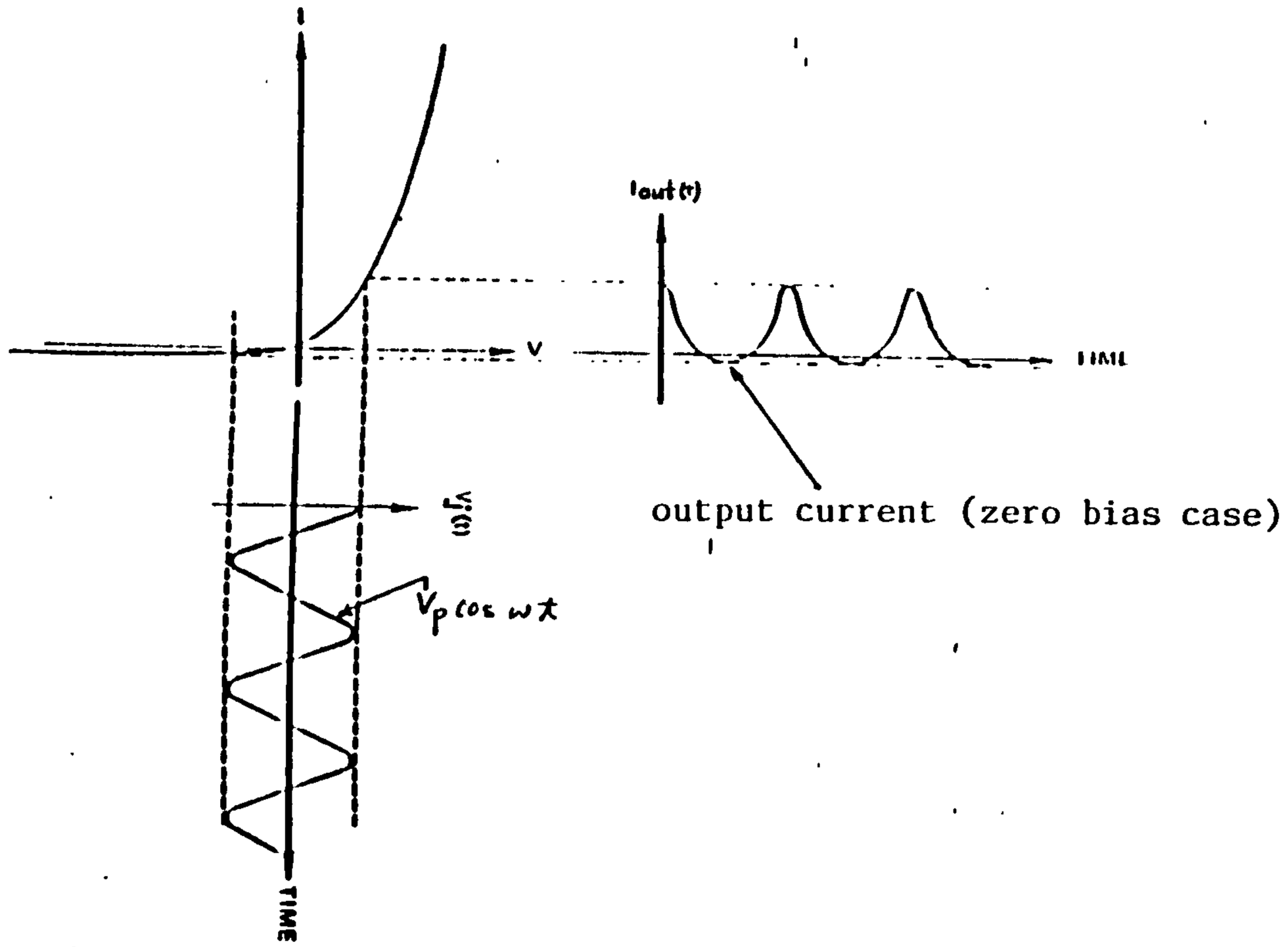

Figure 7.2.3 Input-Output Signals for a non-linear device

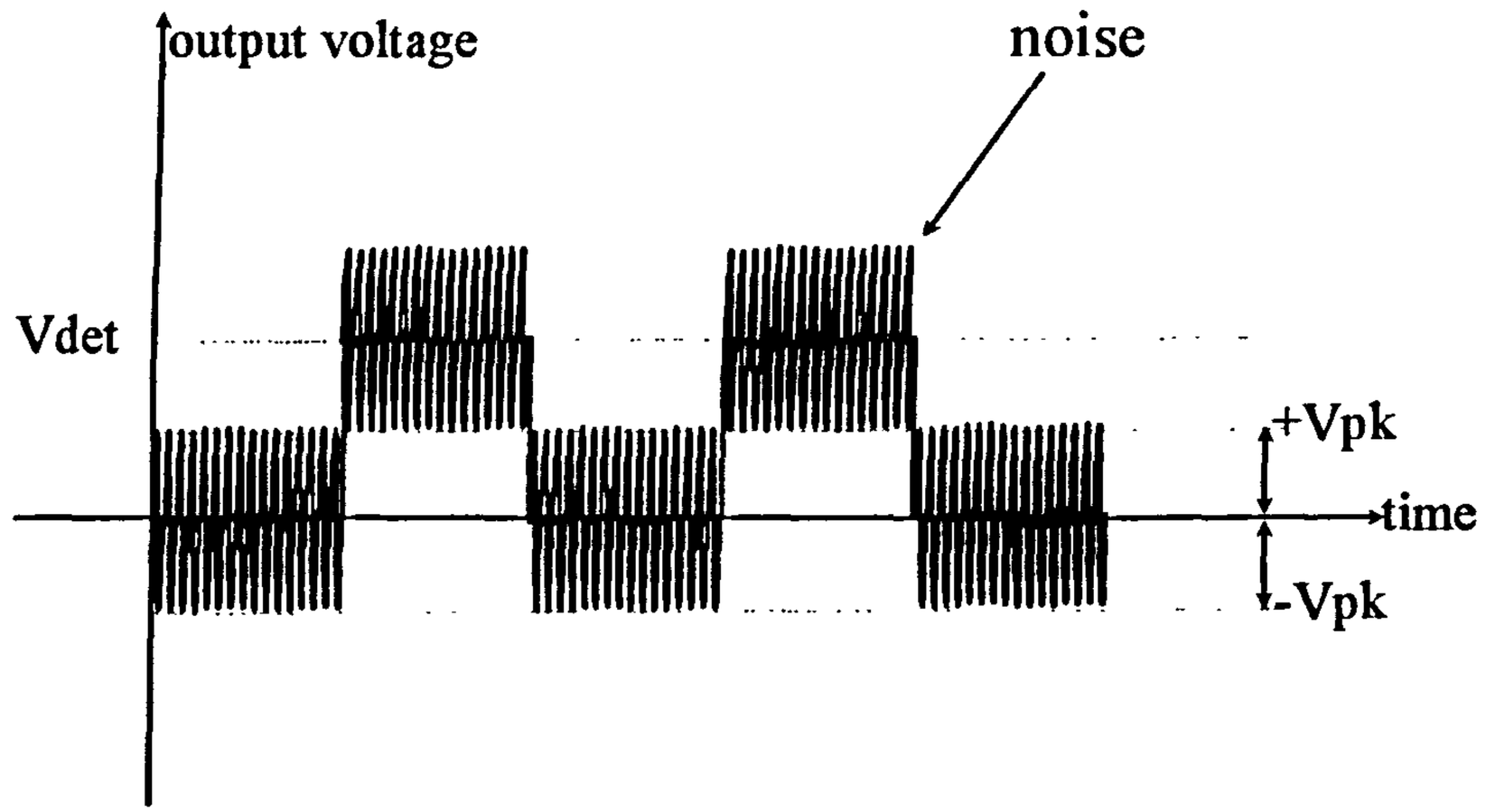

Figure 7.2.4 Condition for tangential signal sensitivity (TSS)

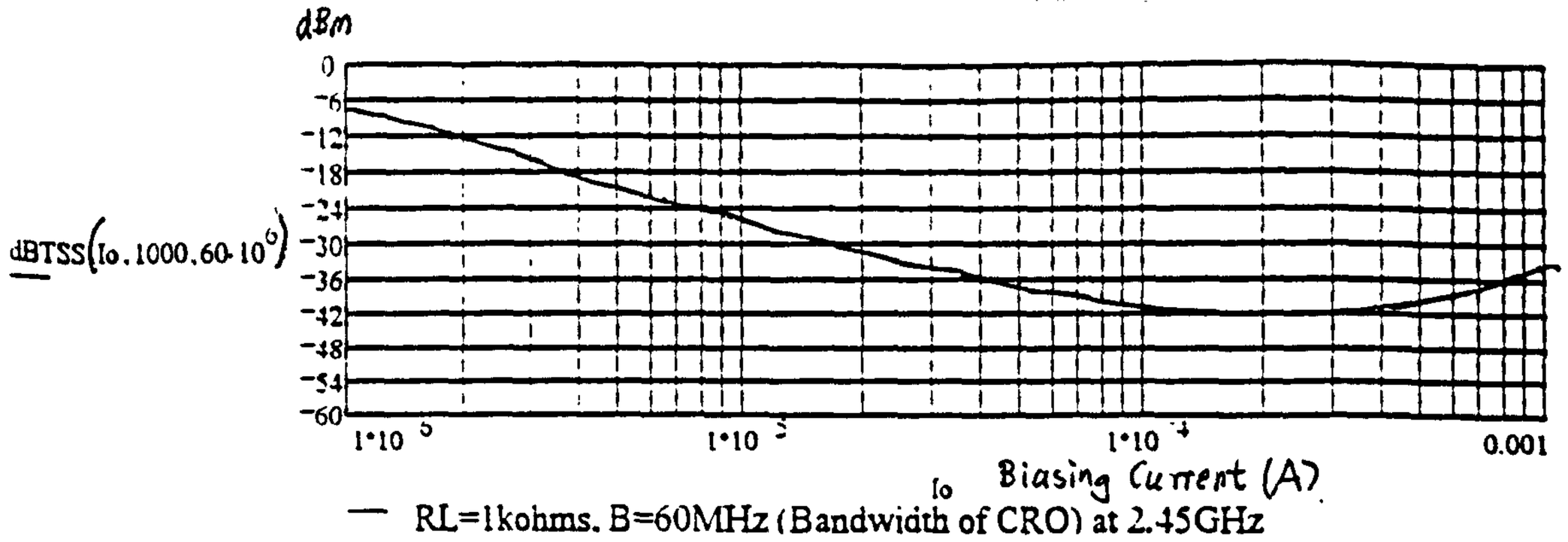

— RL=1kohms. B=60MHz (Bandwidth of CRO) at 2.45GHz

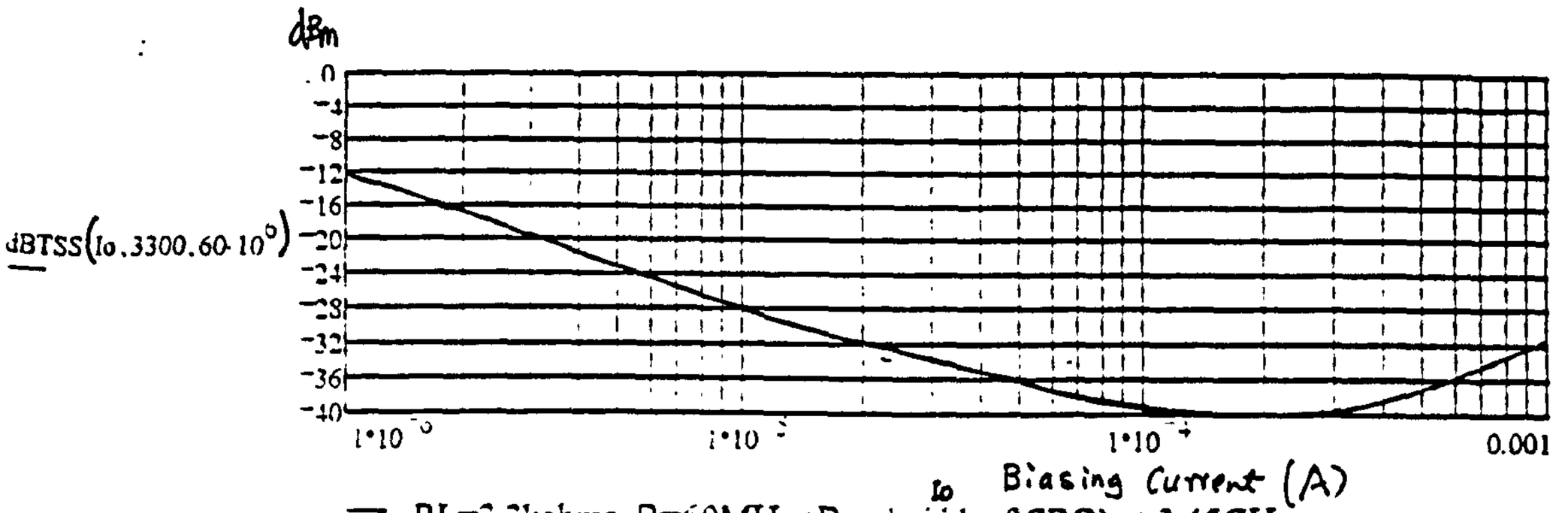

— RL=3.3kohms. B=60MHz (Bandwidth of CRO) at 2.45GHz

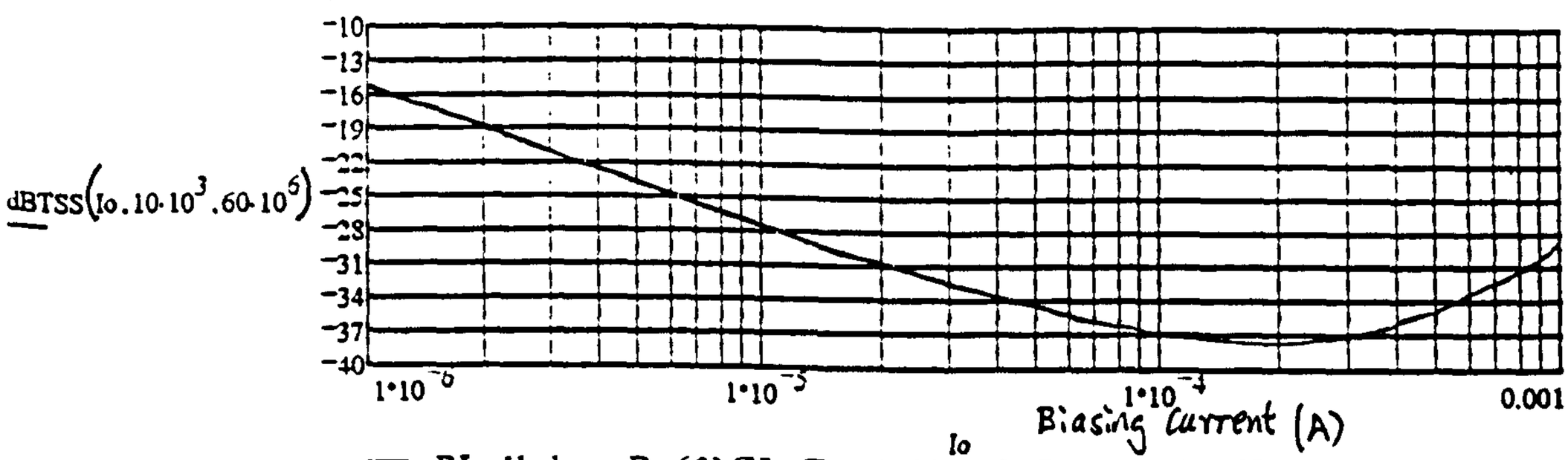

— RL=1kohms. B=60MHz (Bandwidth of CRO) at 2.45GHz

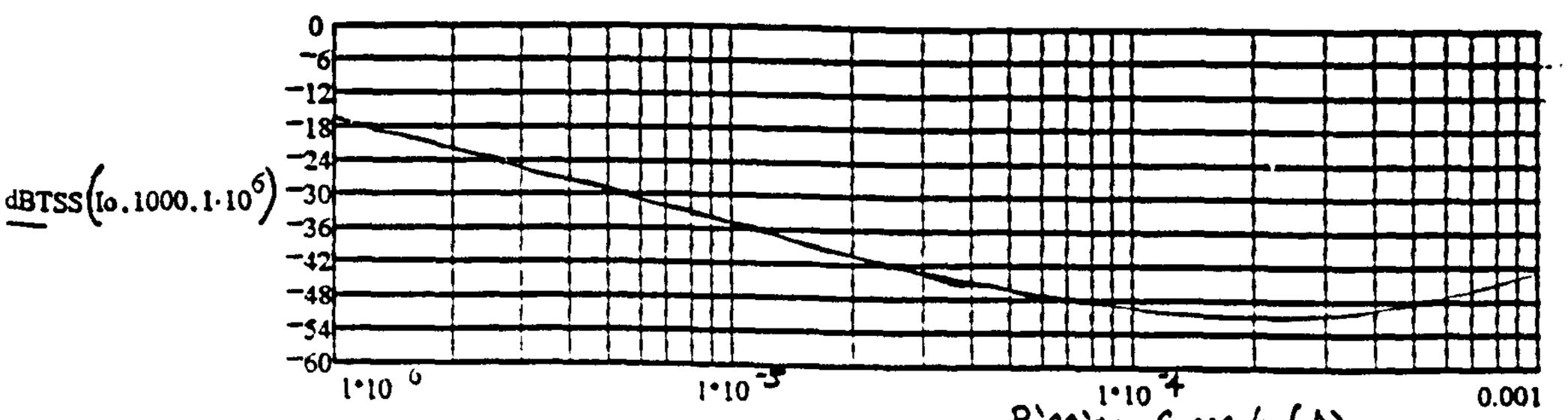

— RL=1kohms. B=1MHz (Bandwidth of Video Amplifier) at 2.45GHz

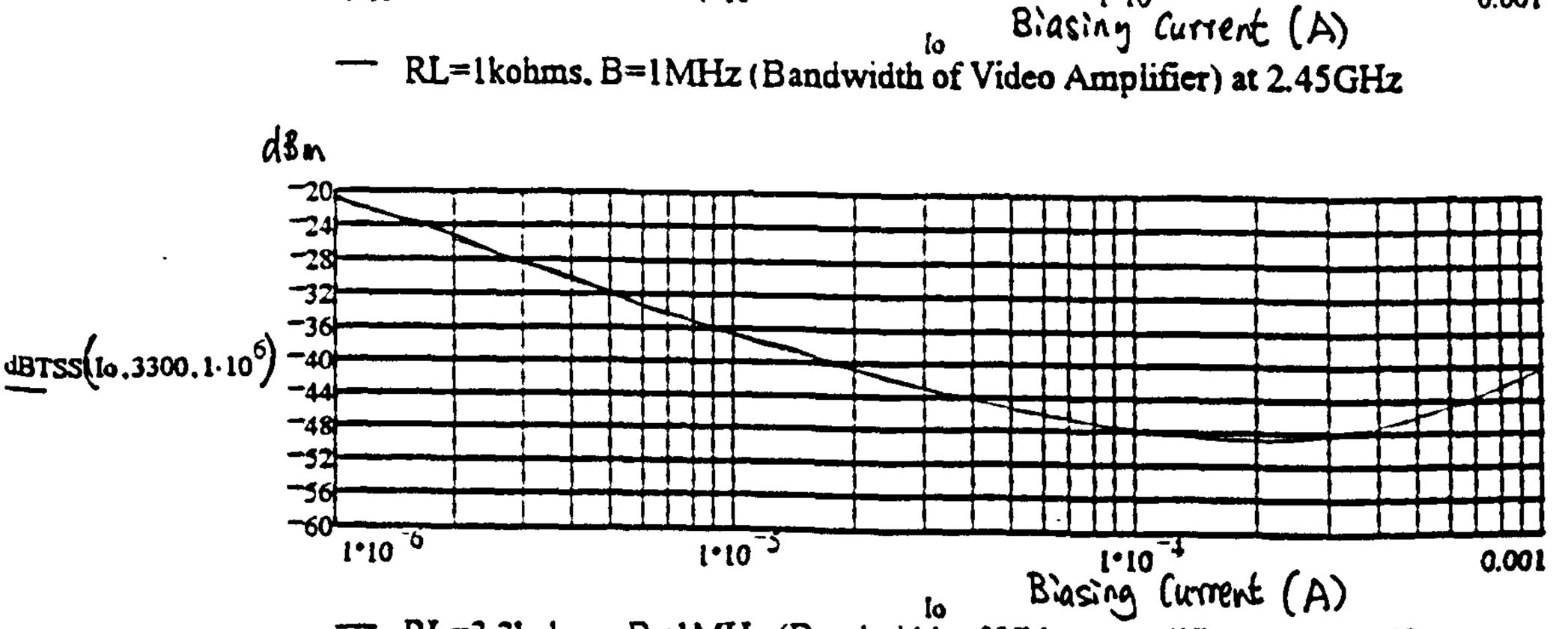

— RL=3.3kohms. B=1MHz (Bandwidth of Video Amplifier) at 2.45GHz

Figure 7.2.5 Tangential Signal Sensitivity (TSS) at 2.45GHz

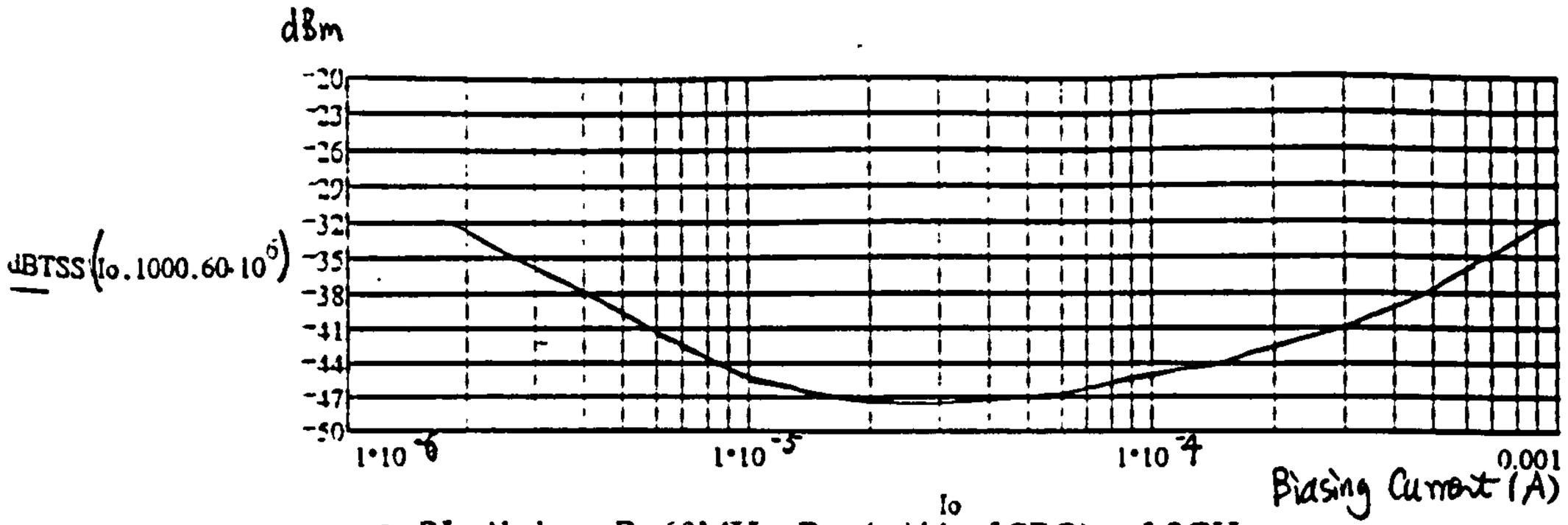

— RL=1kohms. B=60MHz (Bandwidth of CRO) at 5.8GHz

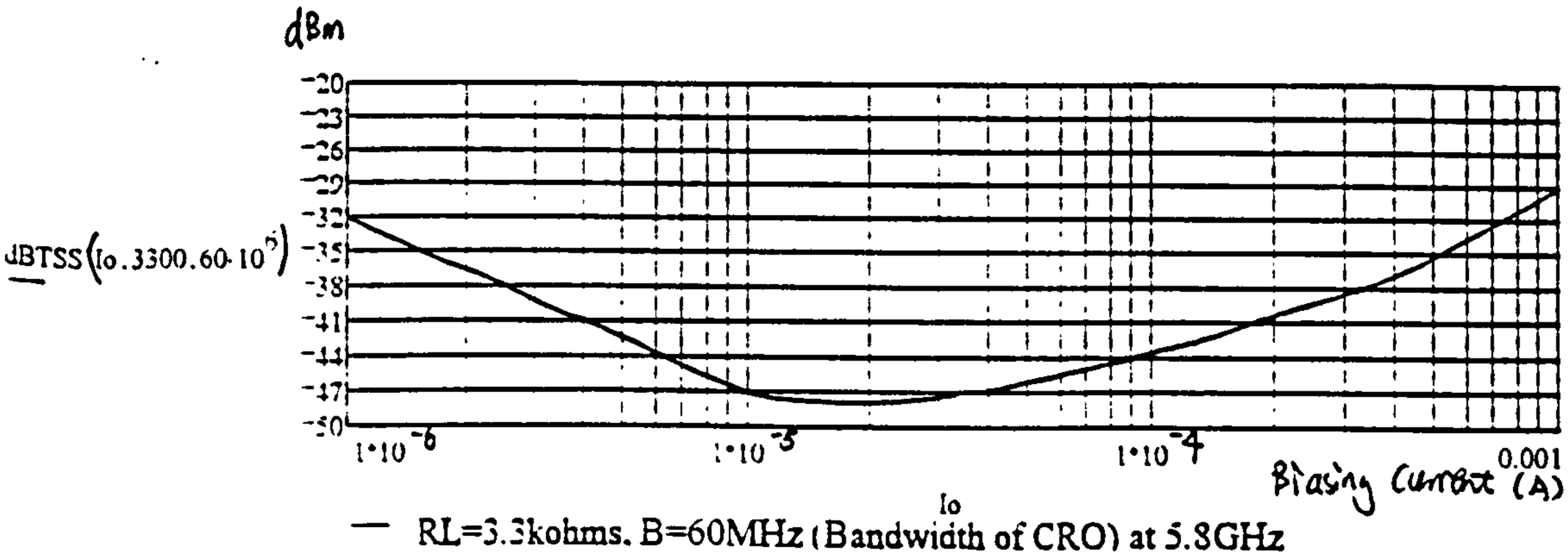

— RL=3.3kohms. B=60MHz (Bandwidth of CRO) at 5.8GHz

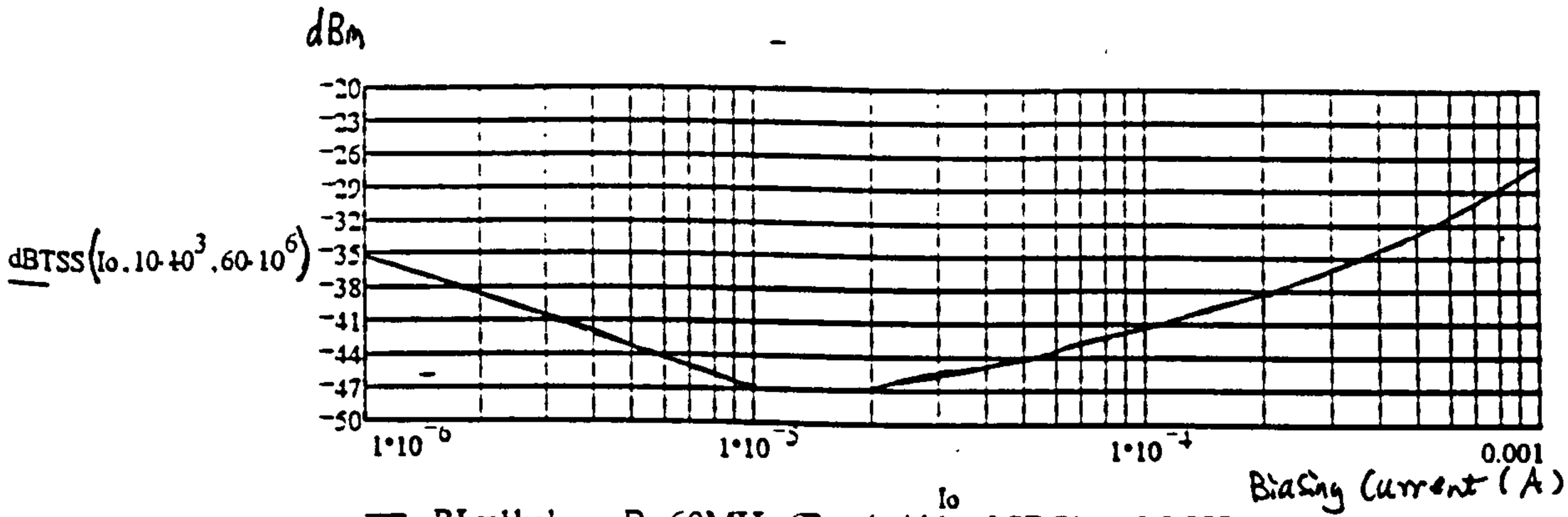

— RL=1kohms. B=60MHz (Bandwidth of CRO) at 5.8GHz

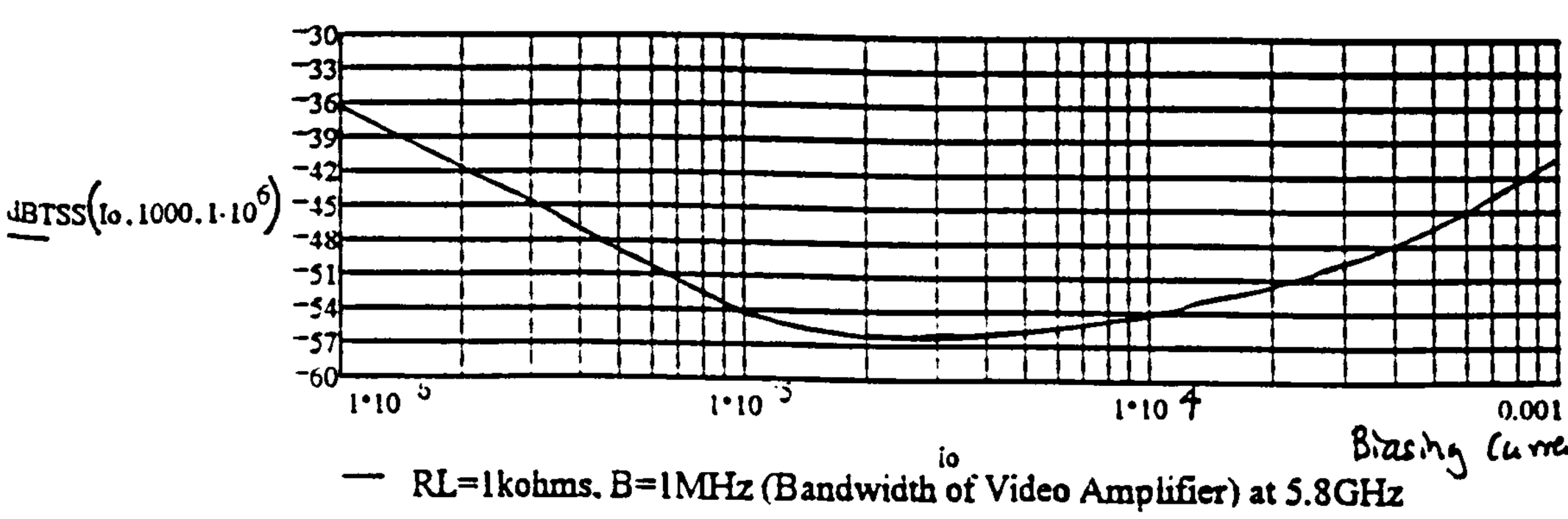

— RL=1kohms. B=1MHz (Bandwidth of Video Amplifier) at 5.8GHz

— RL=3.3kohms. B=1MHz (Bandwidth of Video Amplifier) at 5.8GHz

Figure 7.2.6 Tangential Signal Sensitivity (TSS) at 5.8GHz

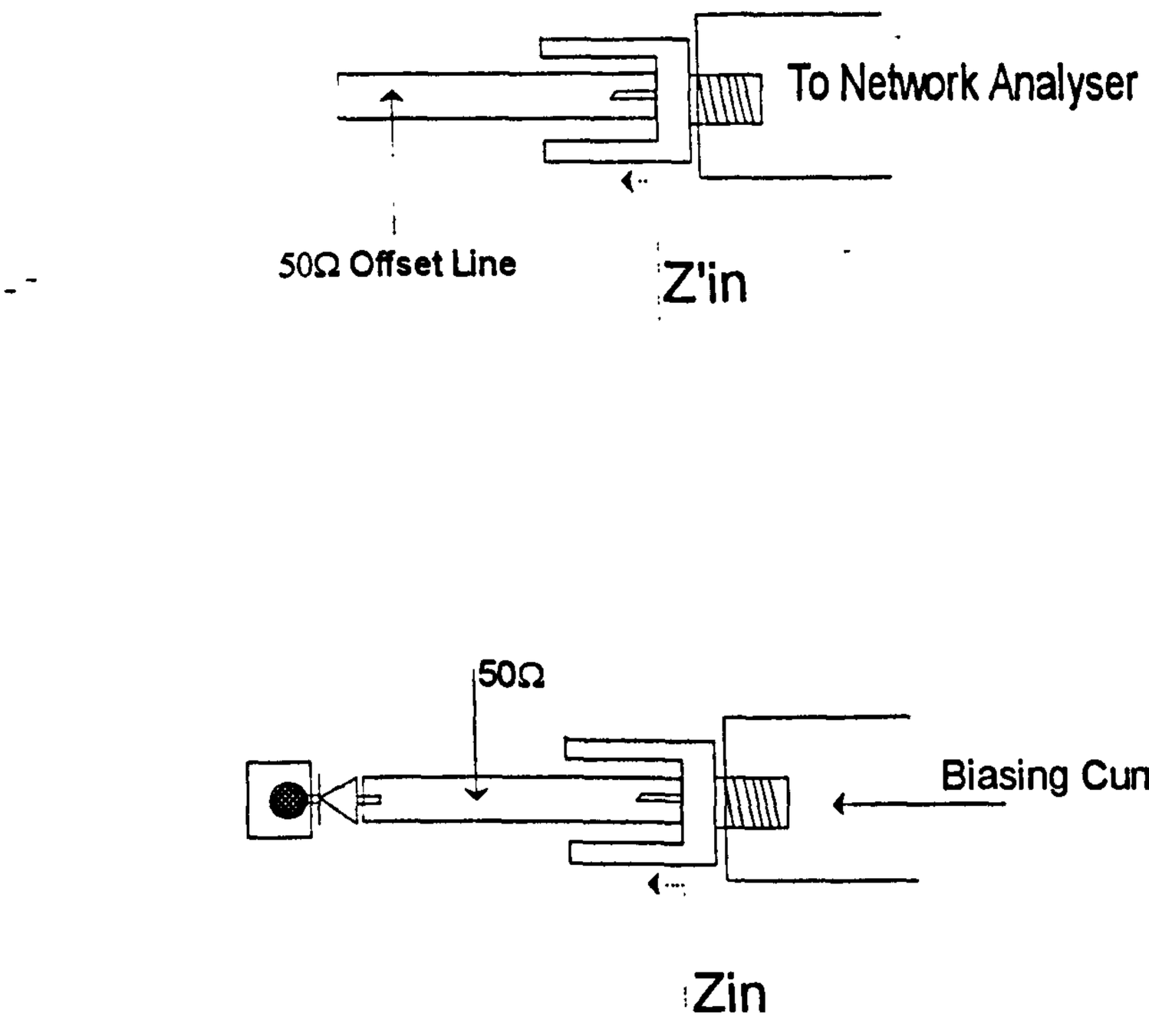

Figure 7.3.1 Diode Impedance (Zd) Measurement

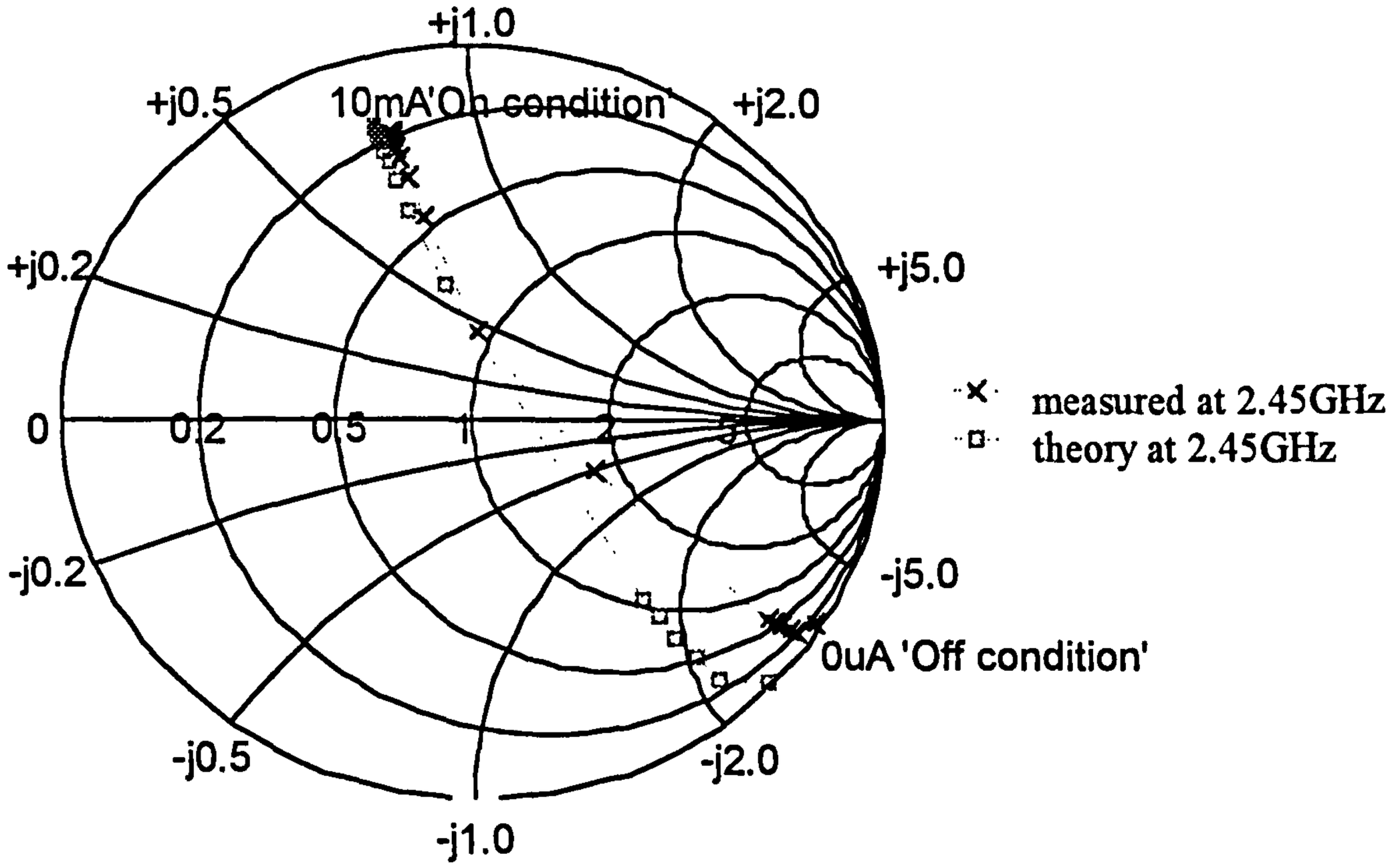

Figure 7.3.2(a) Diode impedance at 2.45GHz

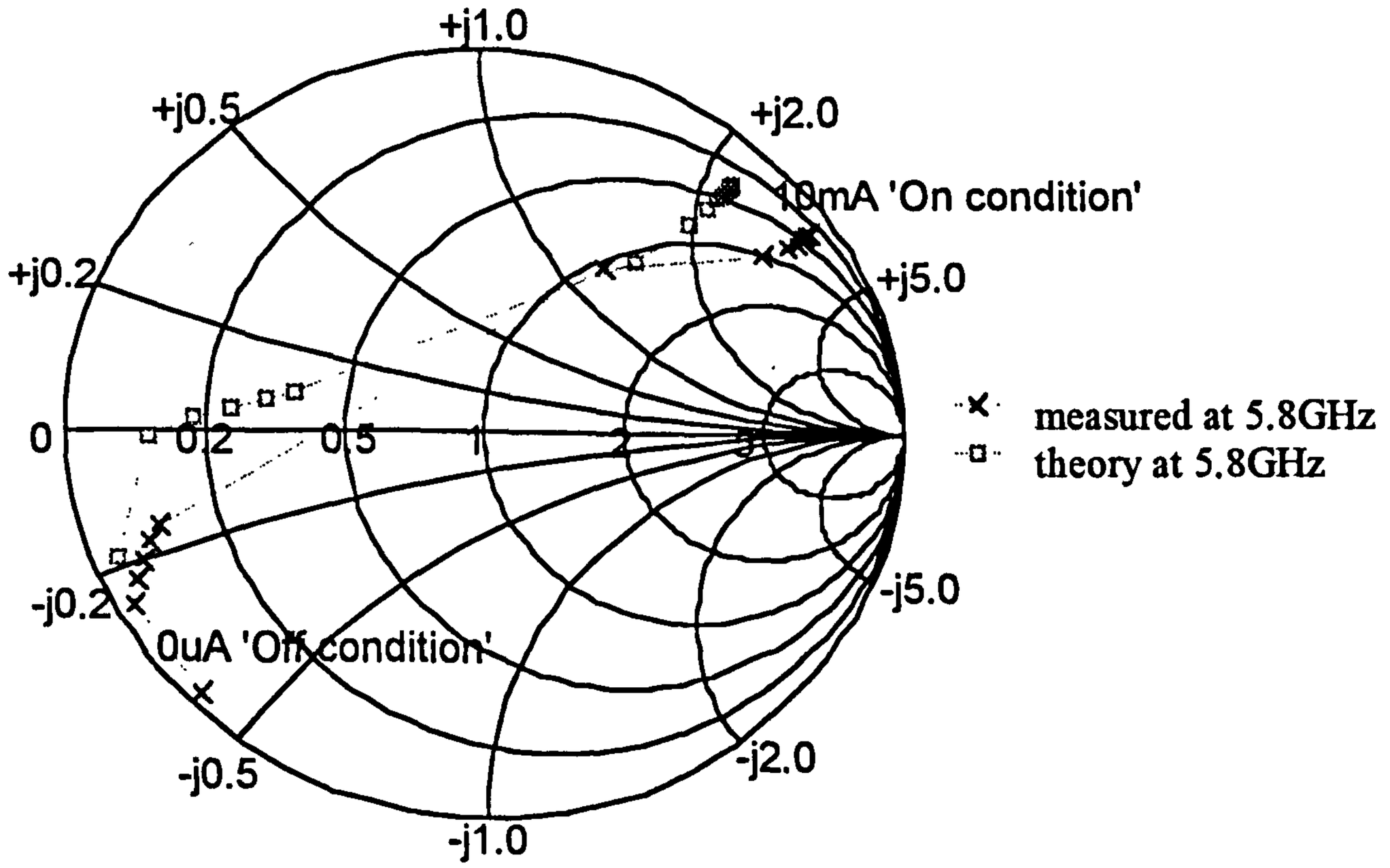

Figure 7.3.2(b) Diode impedance at 5.8GHz

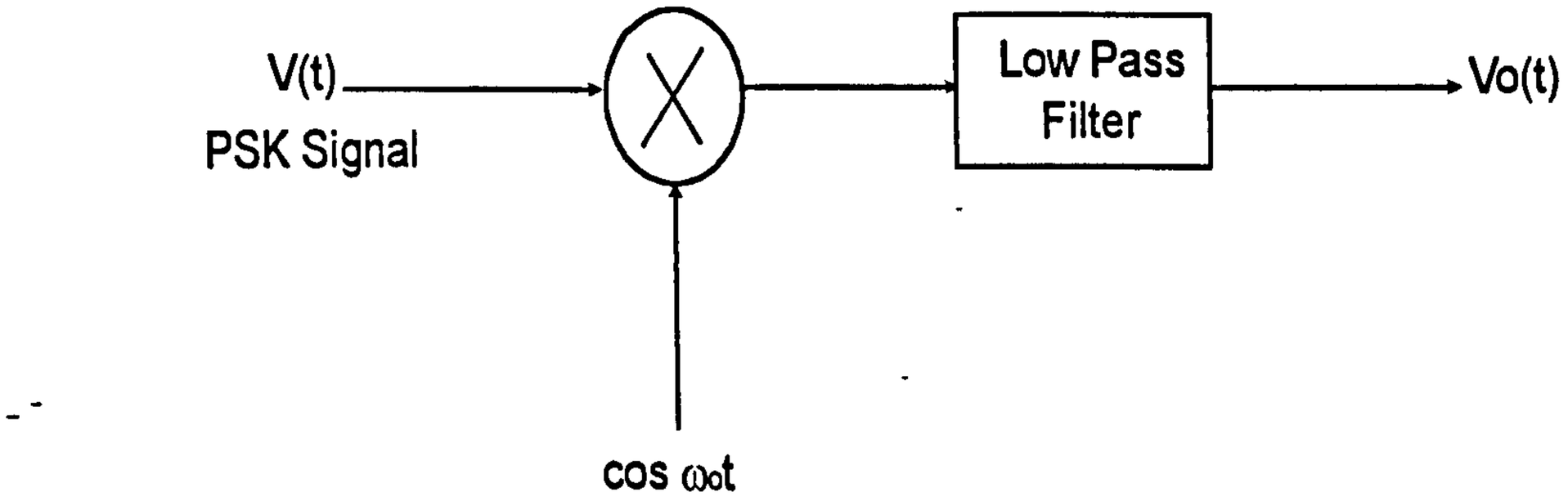

Figure 7.3.3 Synchronous Detection

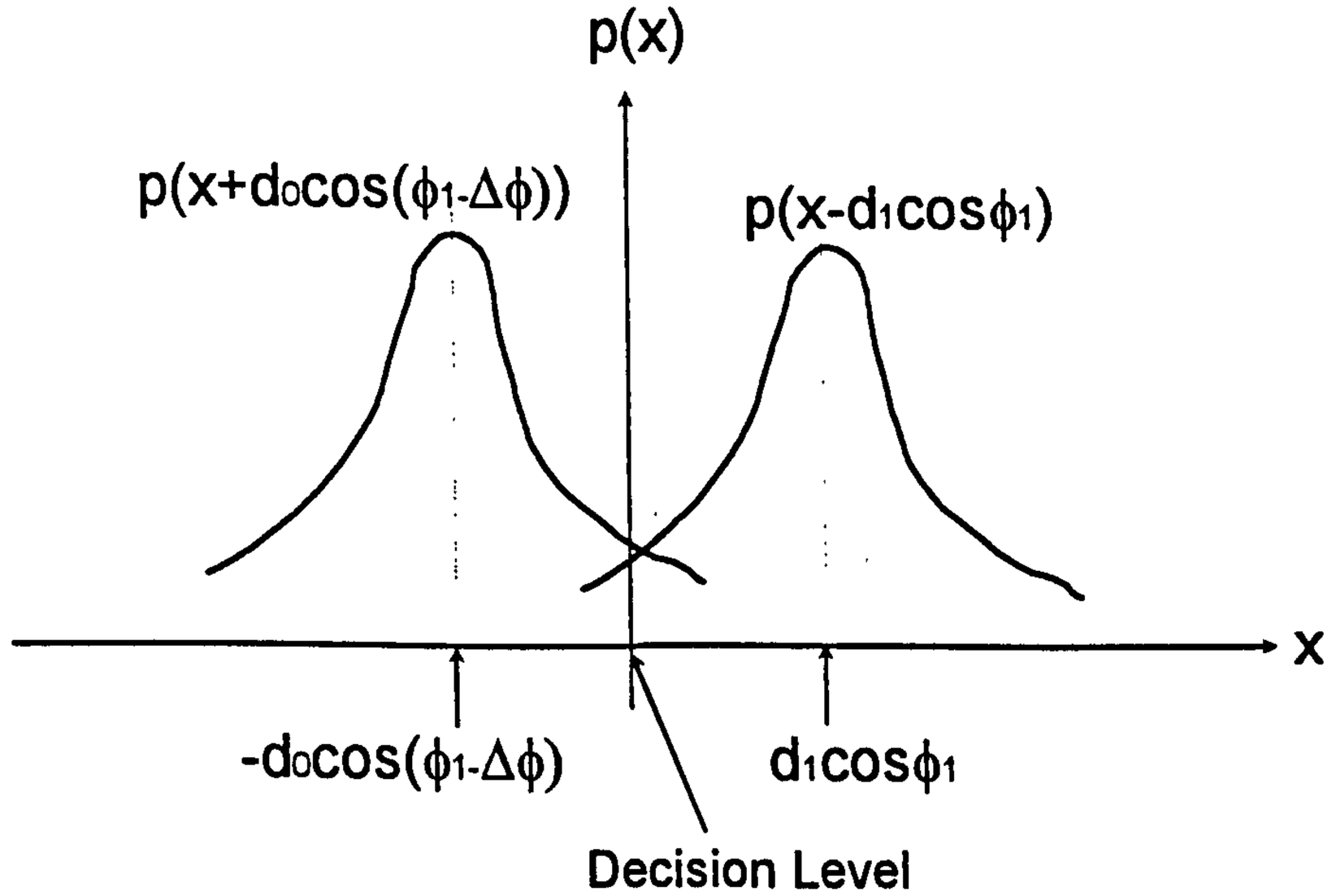

Figure 7.3.4 Error Distribution

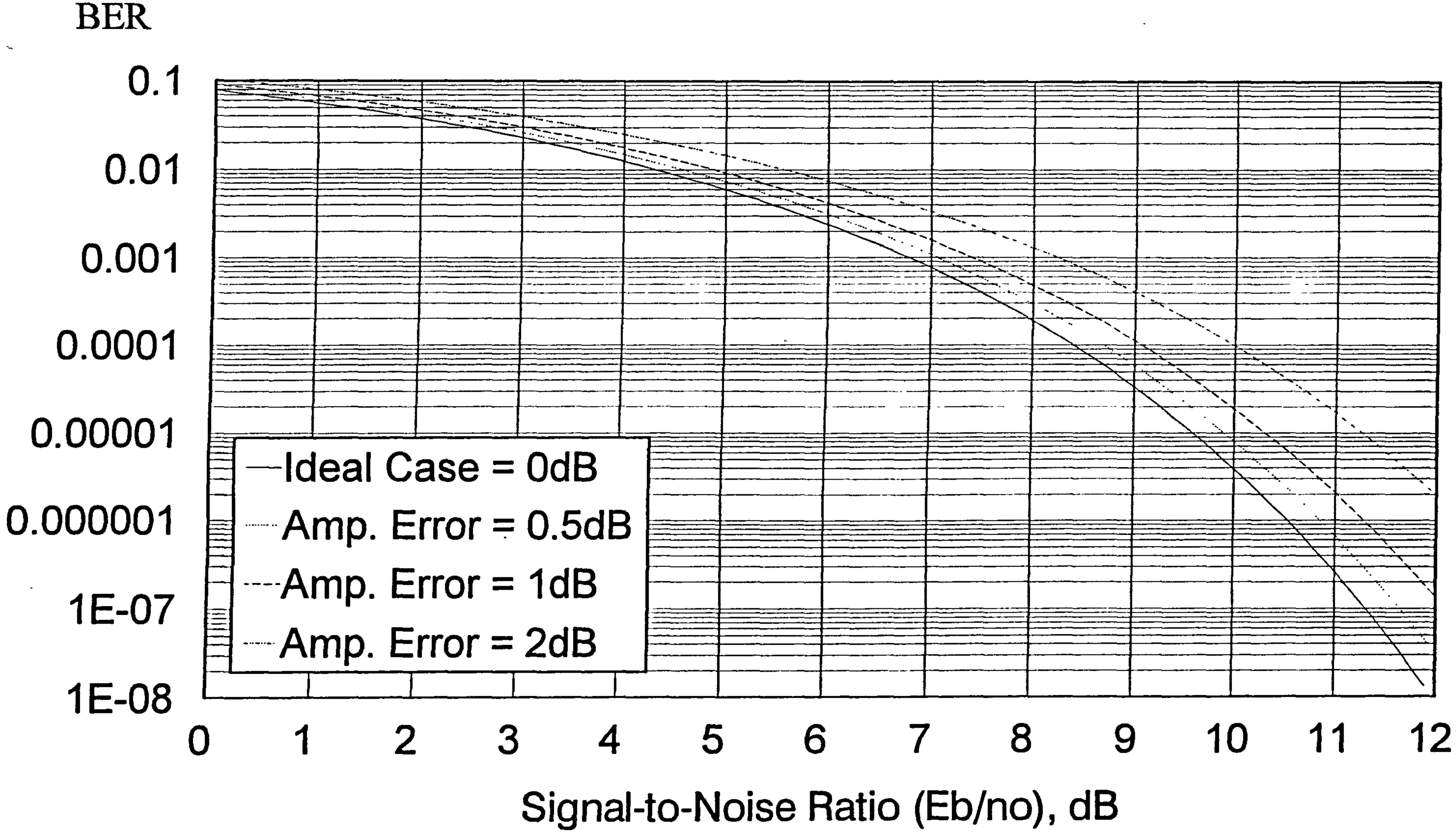

Figure 7.3.5 Bit Error Rate on the Effect of Amplitude Error (Phase Error=0)

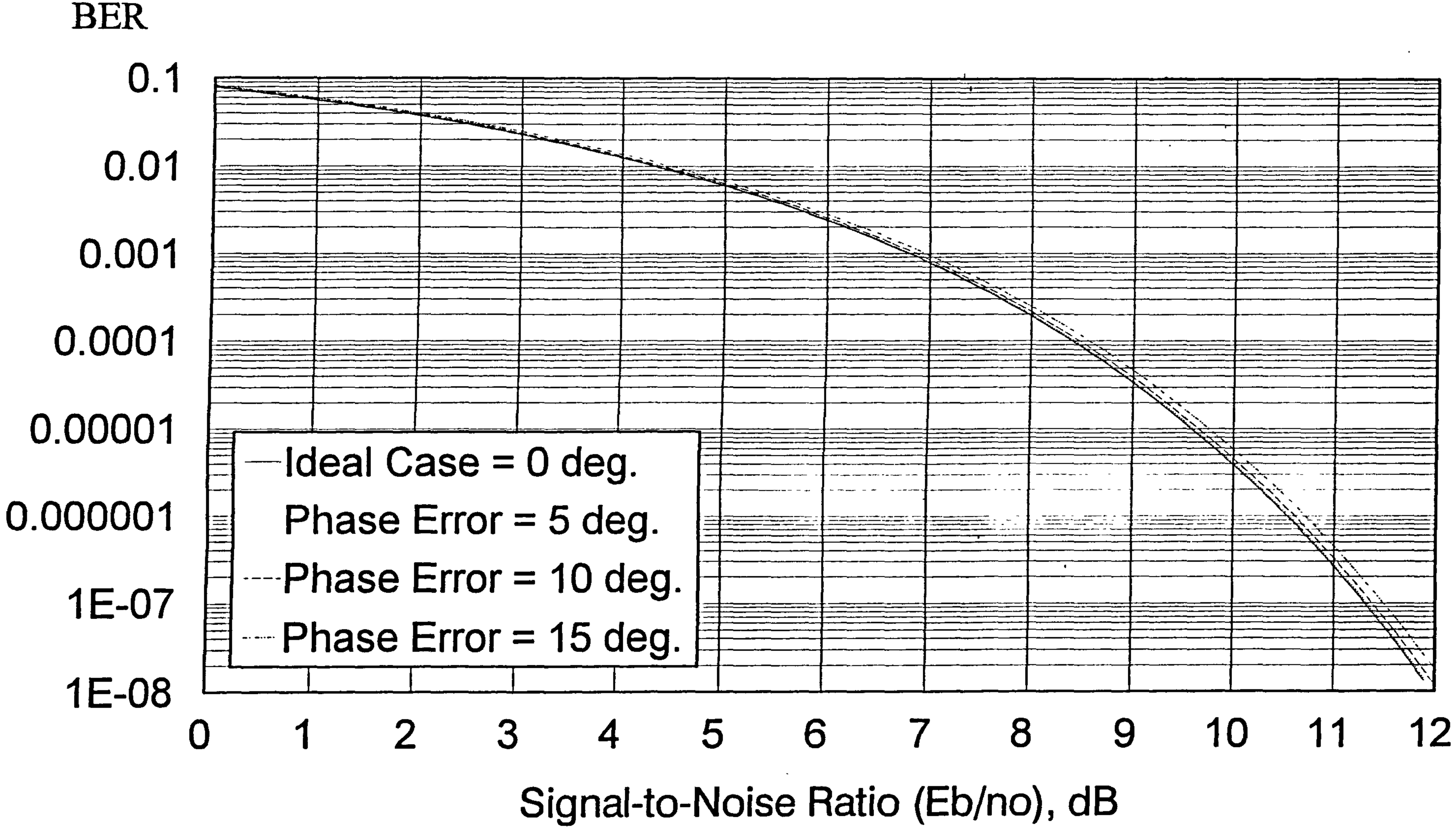

Figure 7.3.6 Bit Error Rate on the Effect of Phase Error (Amplitude Error=0dB)

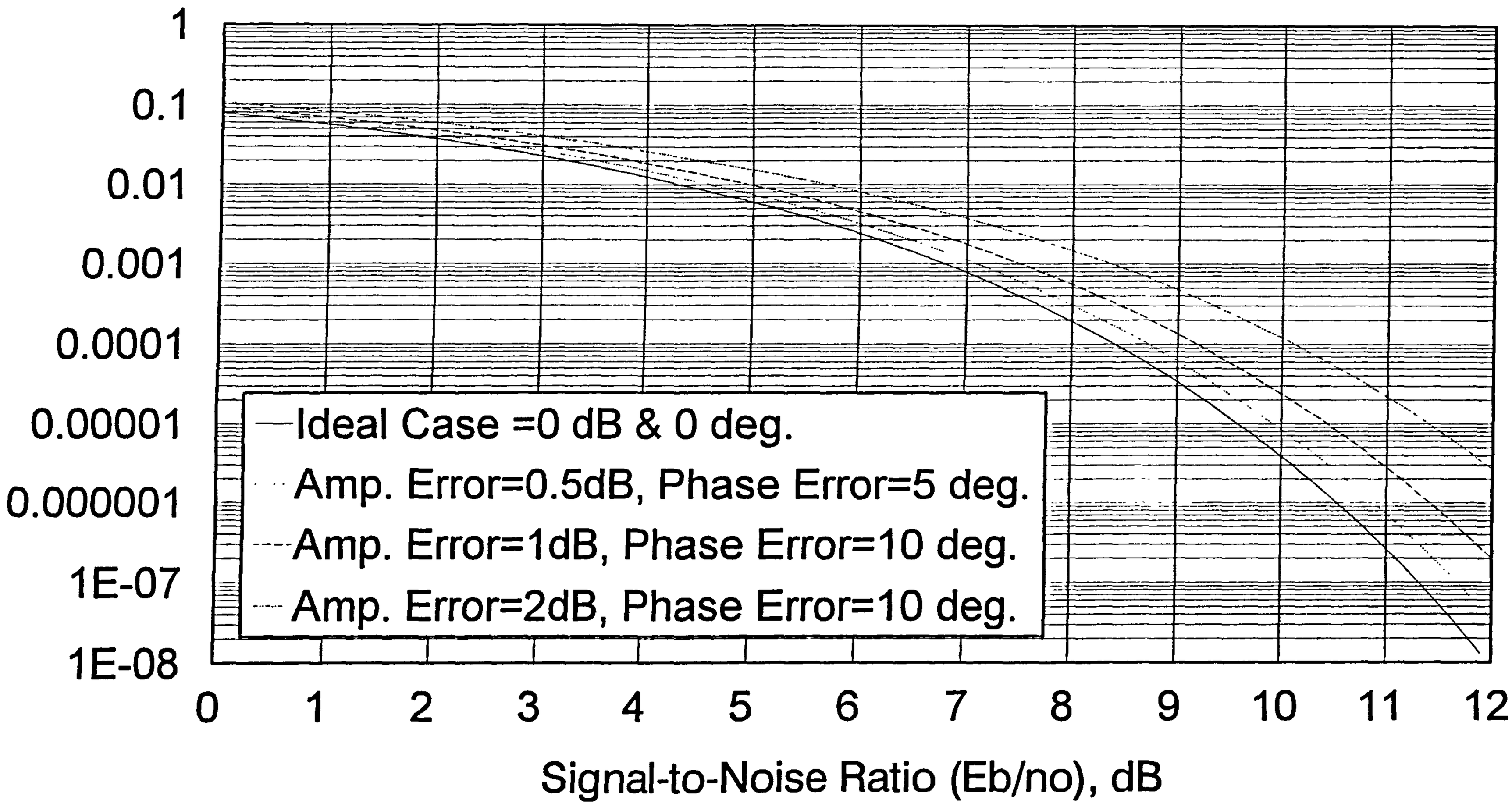

Figure 7.3.7 Bit Error Rate on the Effect of Amplitude and Phase Error

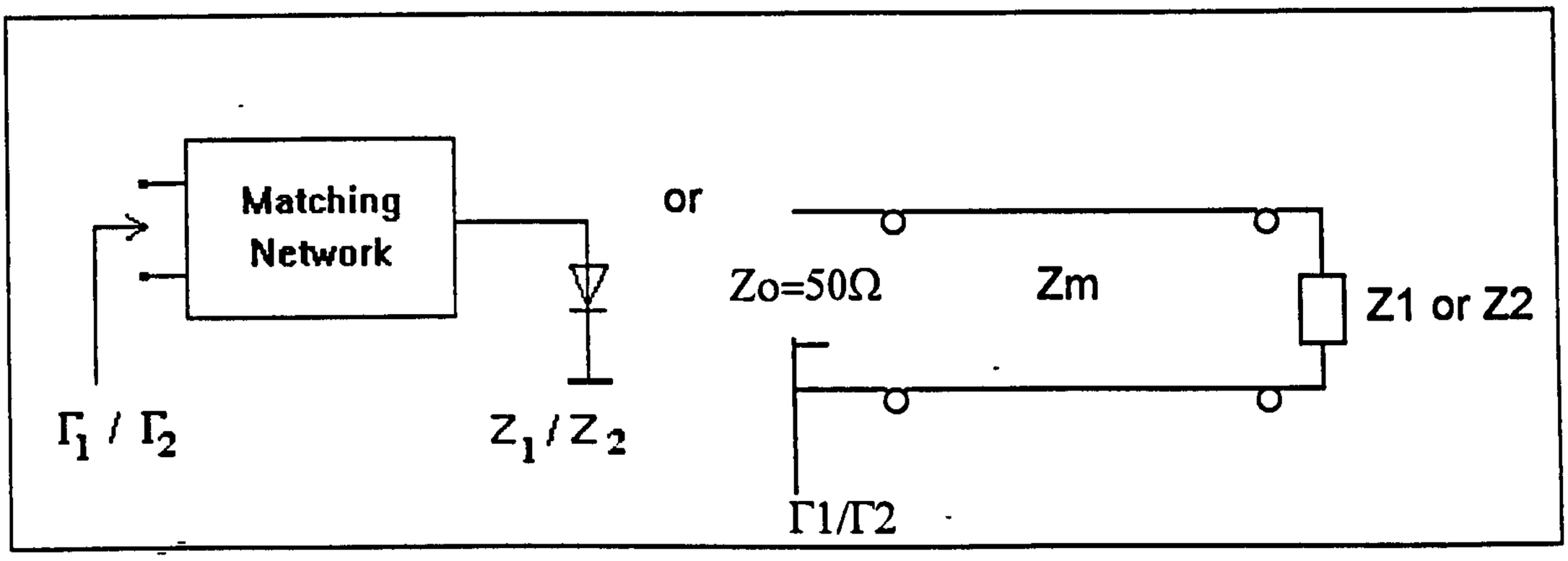

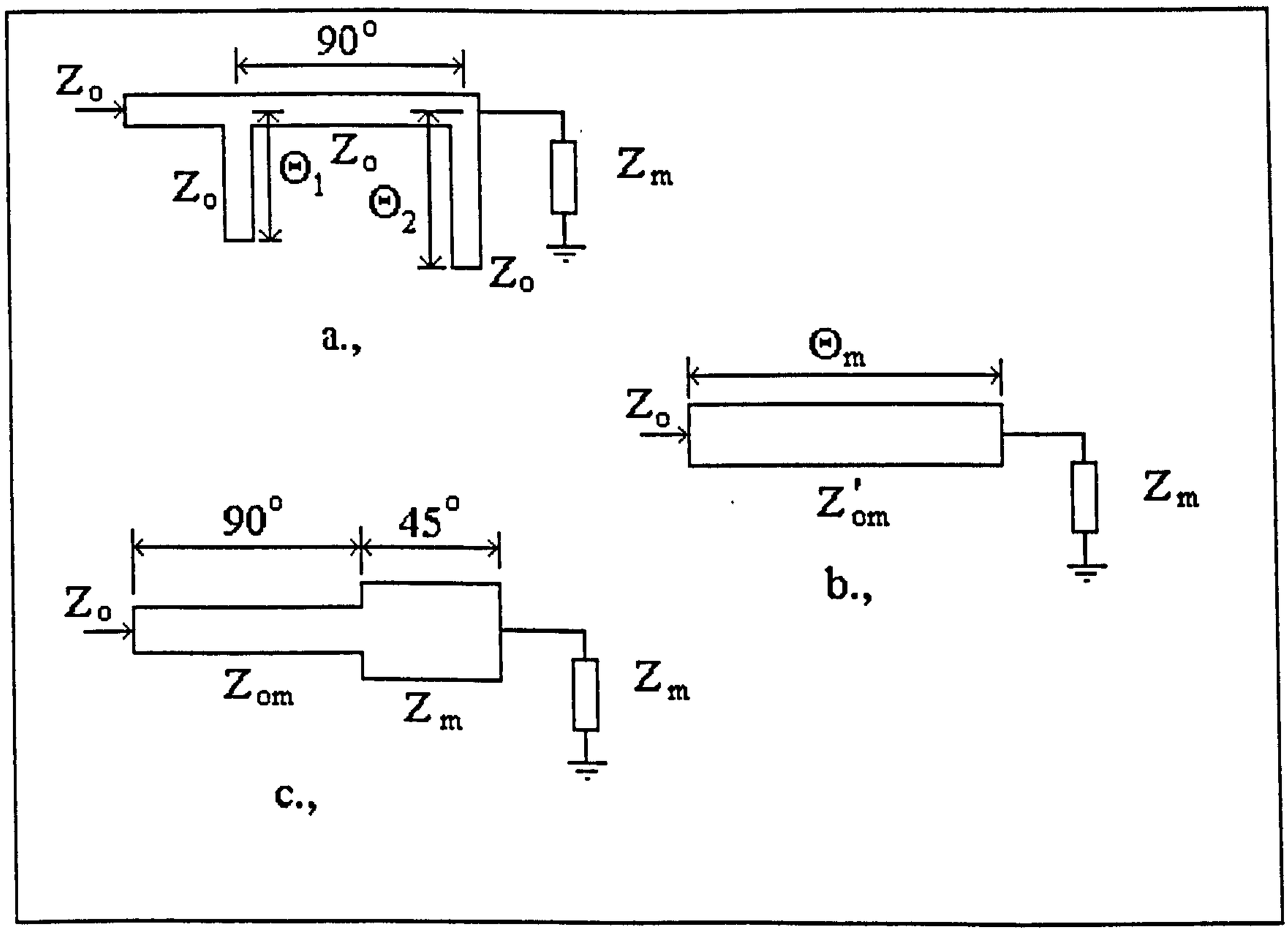

Figure 7.3.8 Matching Networks for PSK Modulator Design

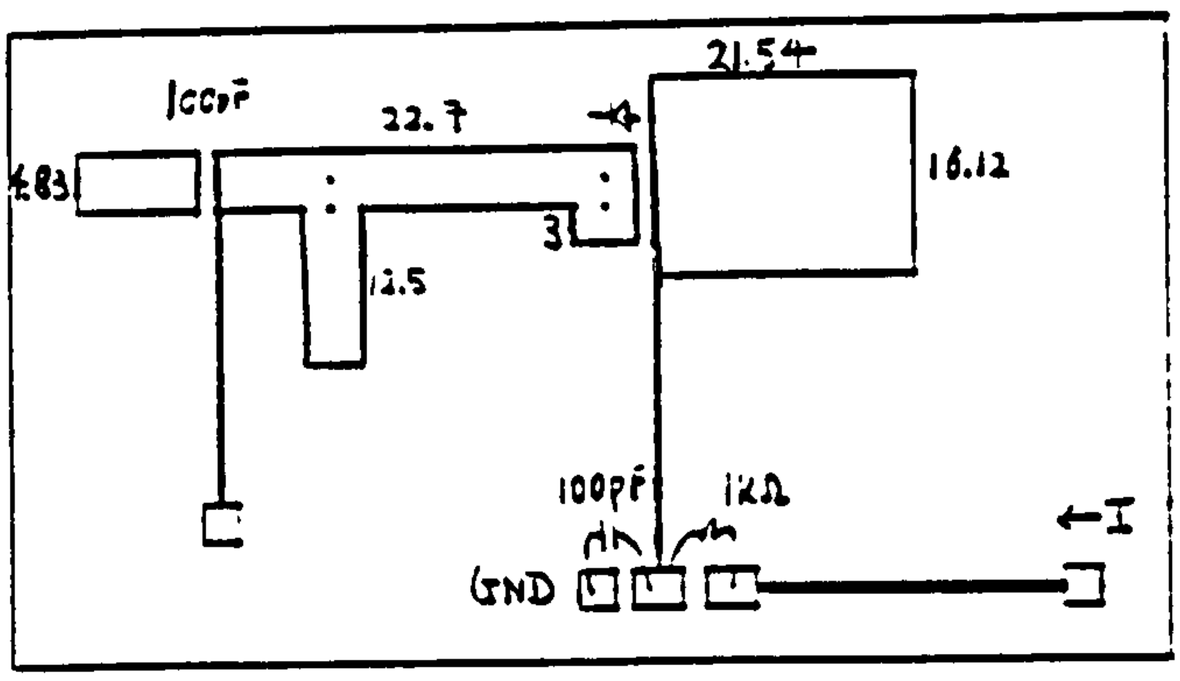

A. Quarter-Wavelength Double-Stub Transformaer

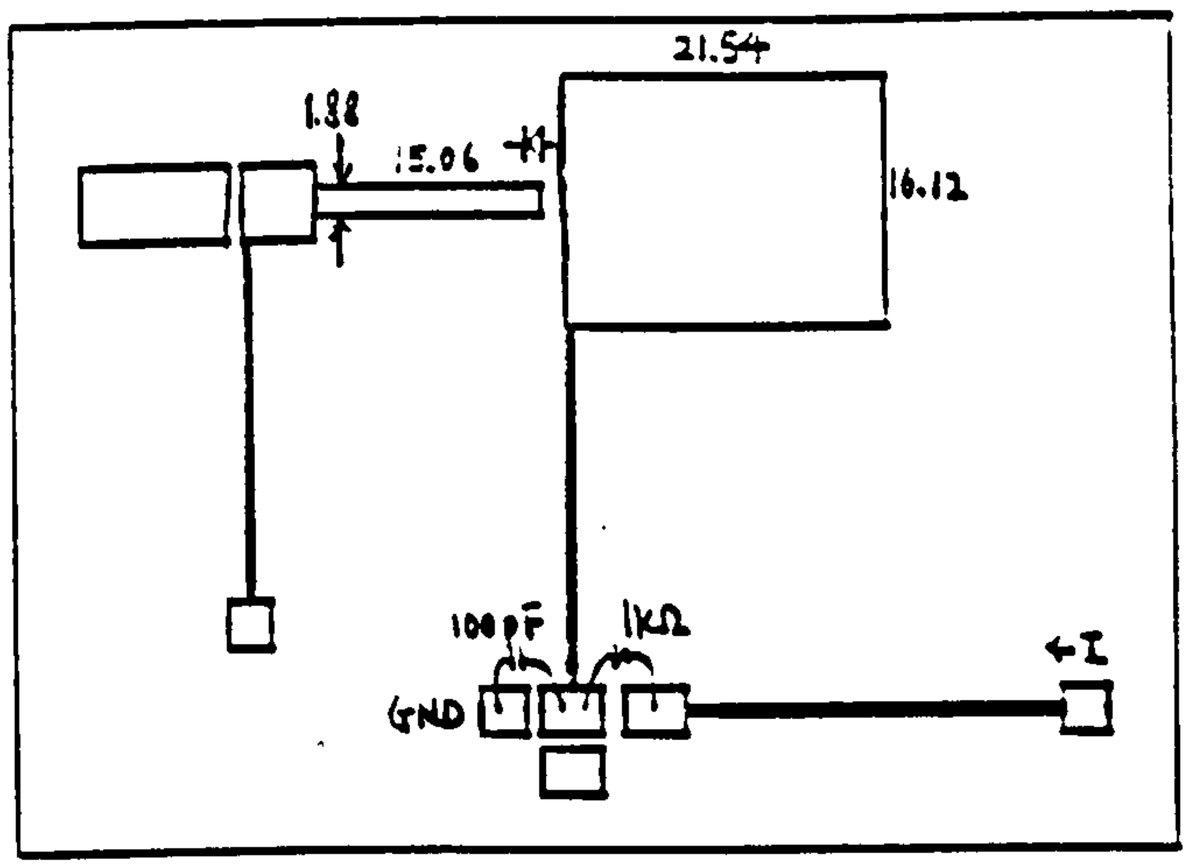

B. Transmission Line Transformer

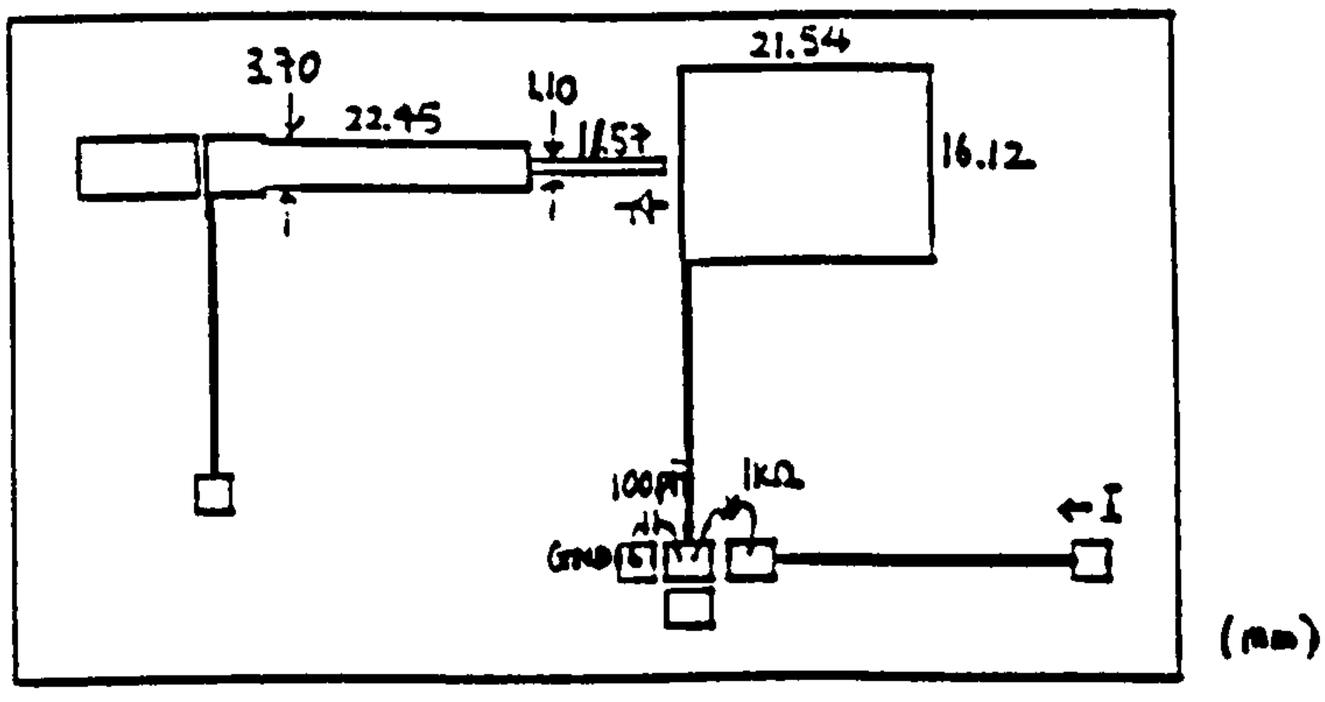

C. Tandem 3/8 - Wavelength Network

Figure 7.3.9 Matching Networks for PSK Modulator

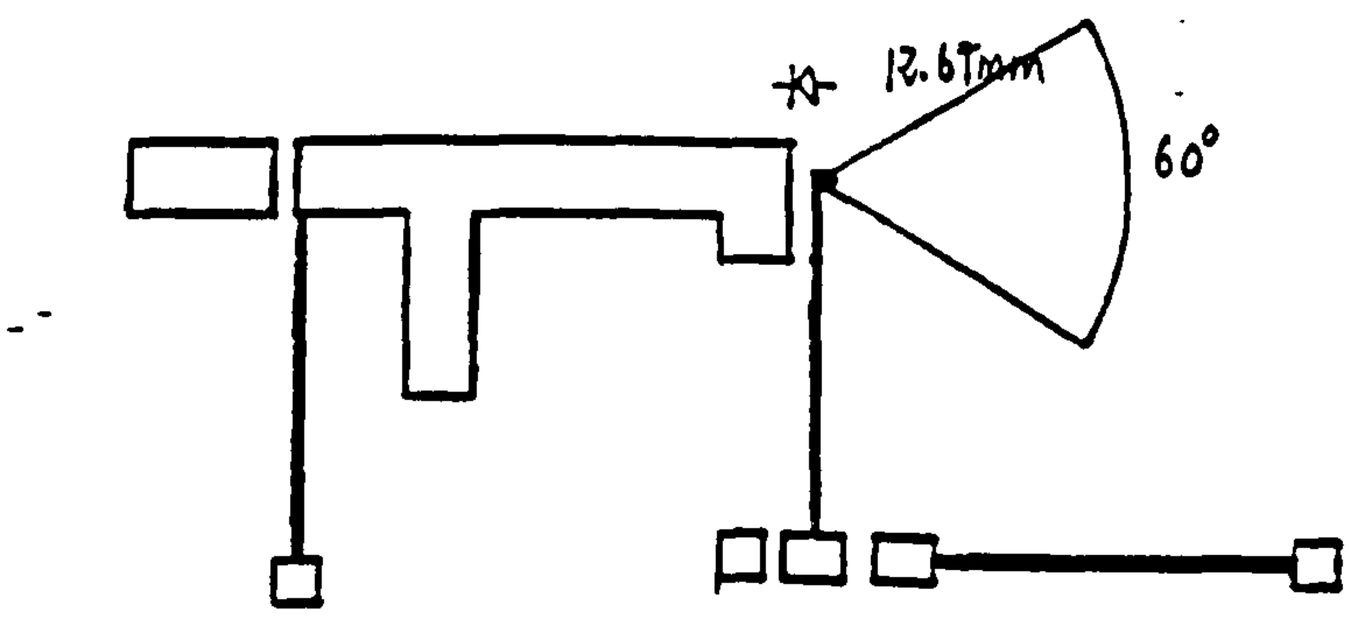

Figure 7.3.10 Quarter-Wavelength Double-Stub Transformer Using Radial Stub

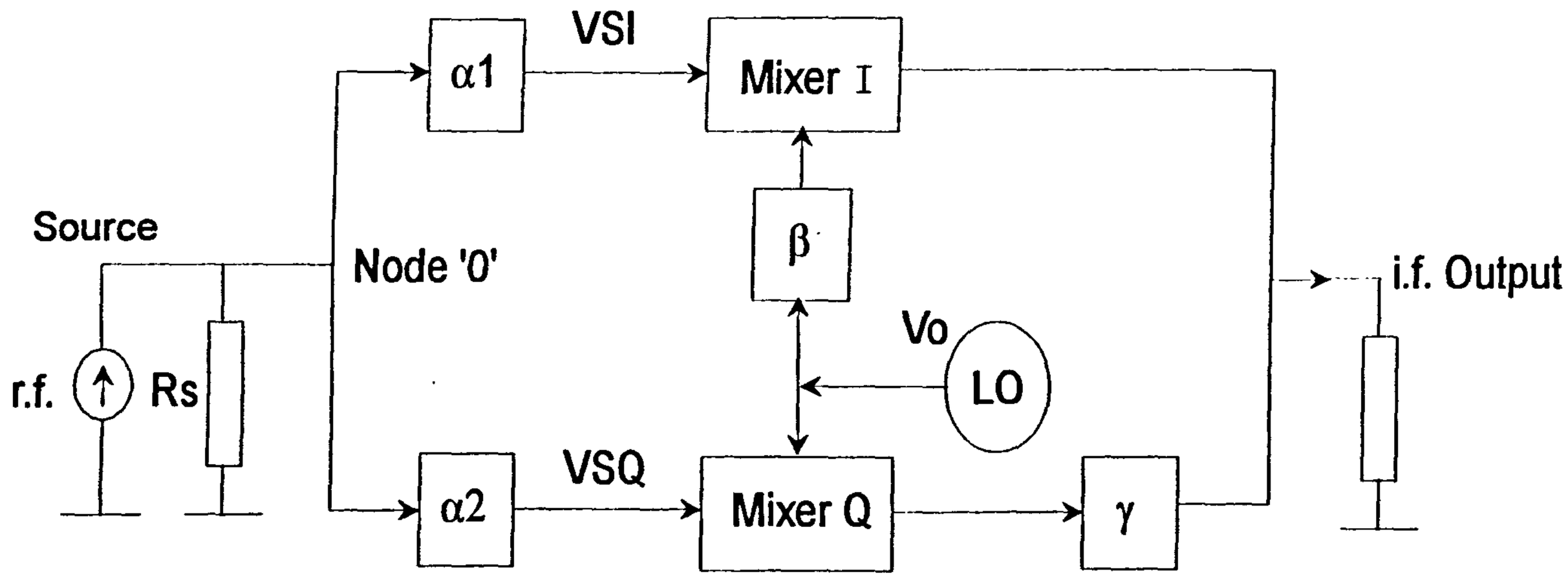

Figure 7.4.1 Block Diagram of an Image Rejection Mixer

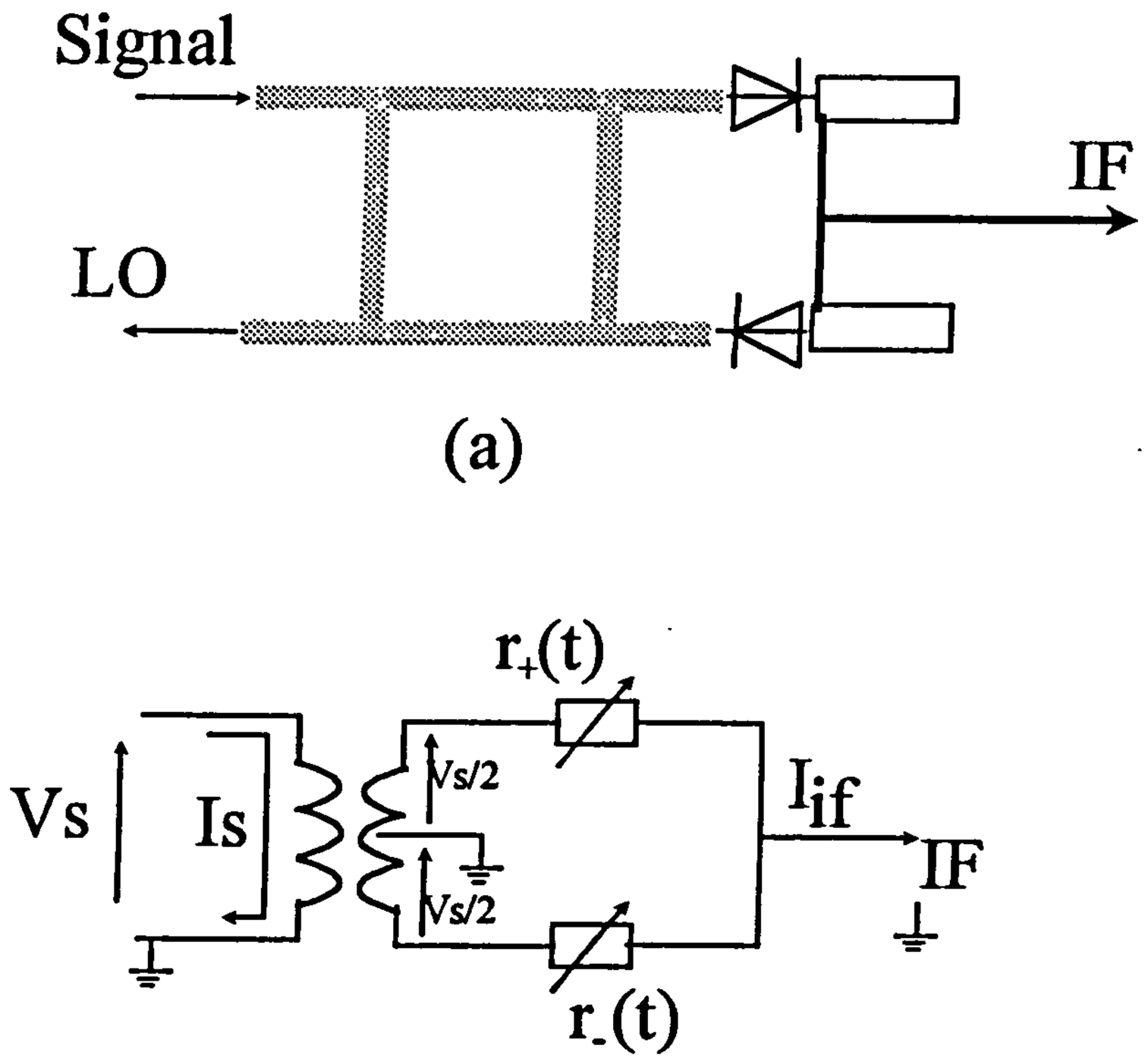

Figure 7.4.2 Single Balanced Mixer

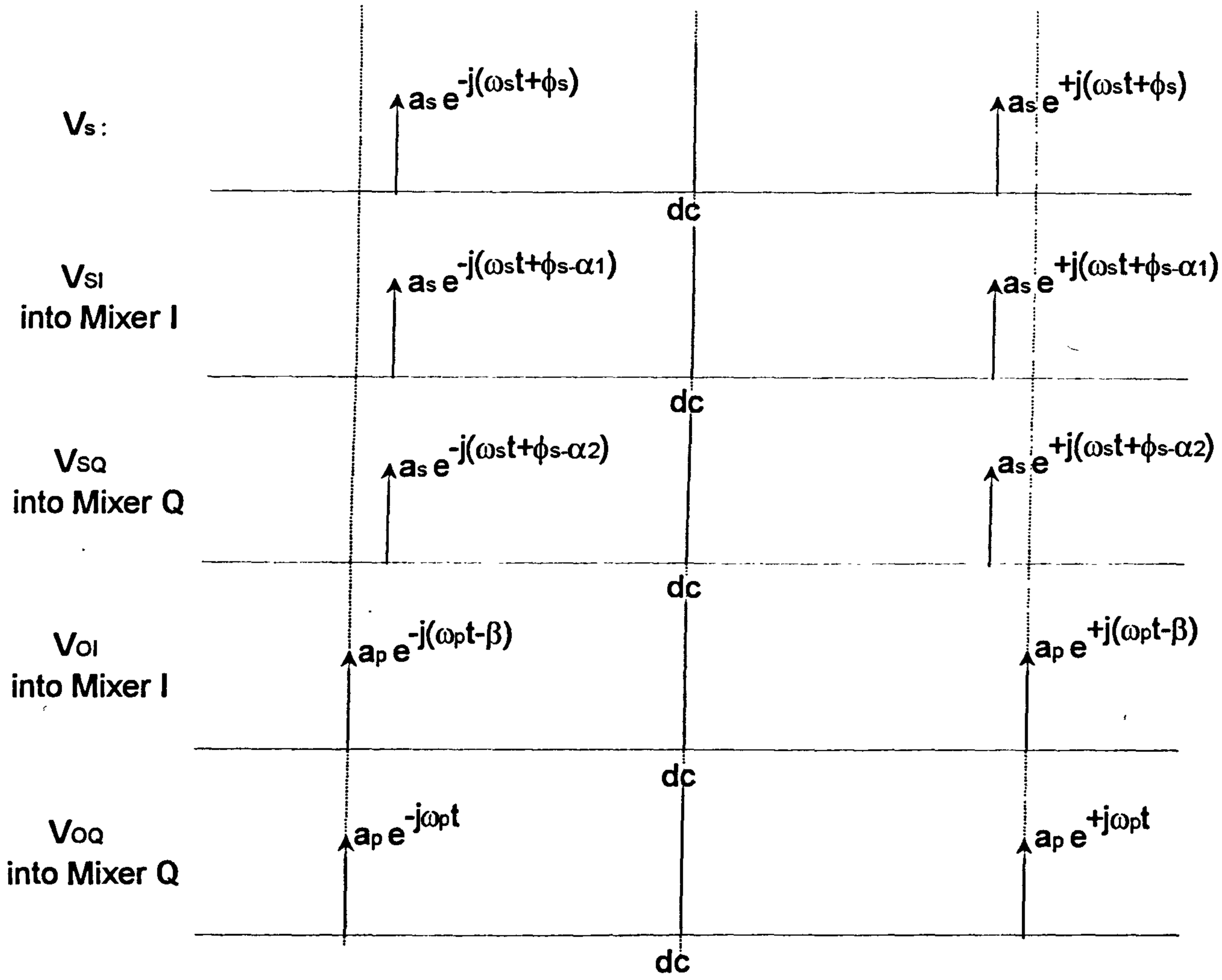

Figure 7.4.3 Spectrums of the V_{SI}, V_{SQ}, V_{OI} & V_{OQ}, V_S as an Input Signal at R.F. Signal Frequency

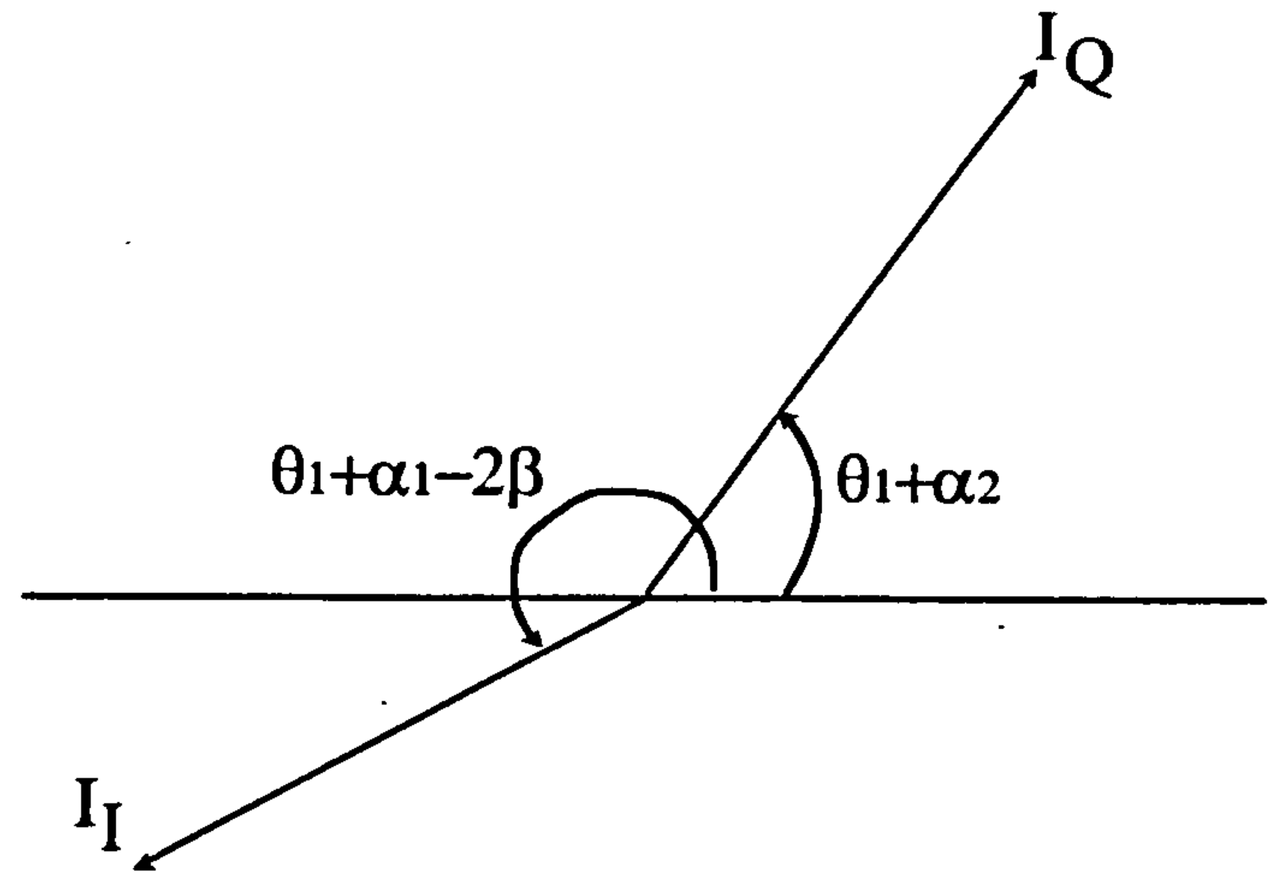

Figure 7.4.4 Phase Relationship of the Image Signals

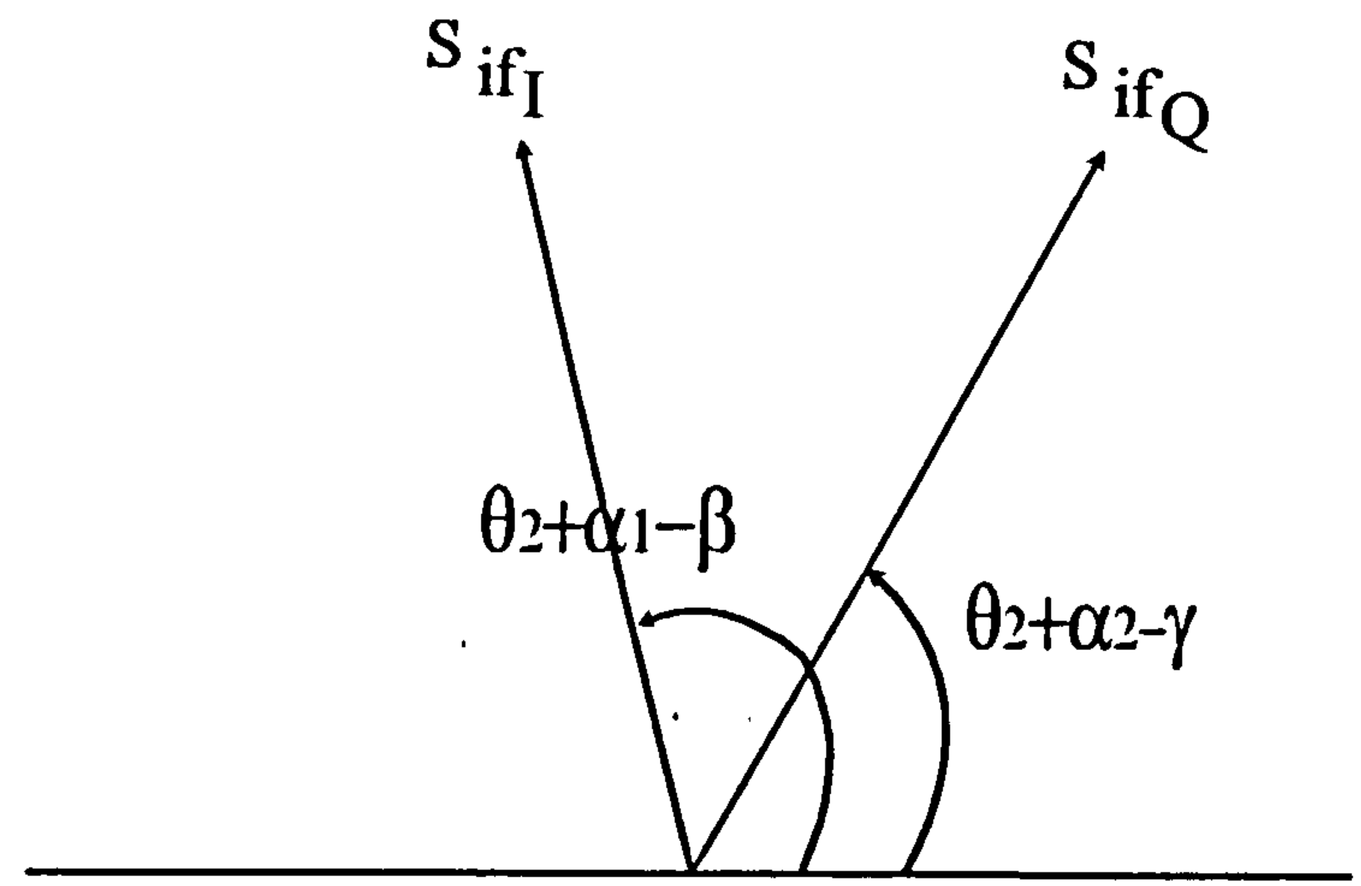

Figure 7.4.5 Phase Relationship of the IF Signals

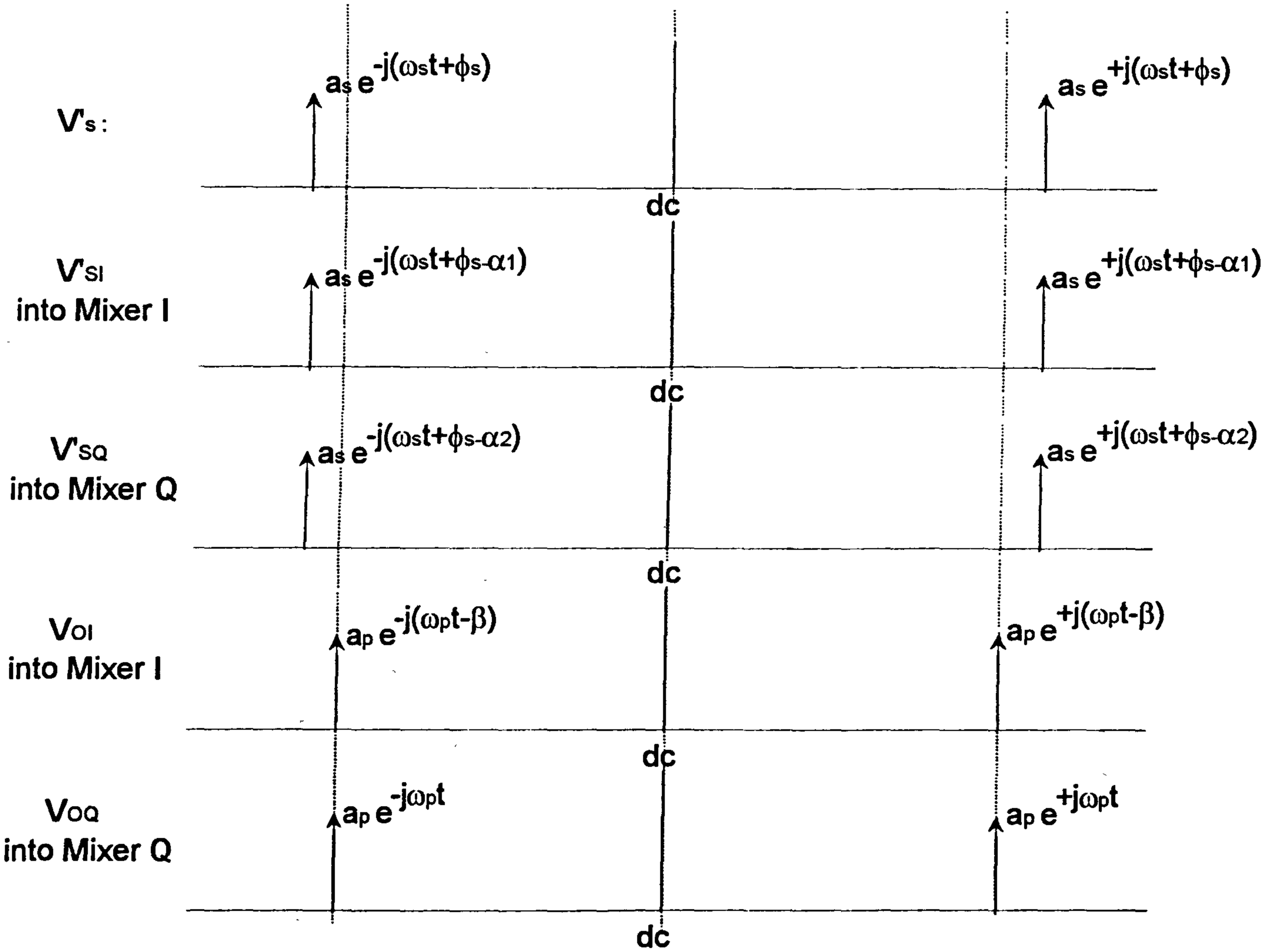

Figure 7.4.6 Spectrums of the V'_{SI}, V'_{SQ}, V_{OI} & V_{OQ} V'_s as an Input Signal at Image Frequency

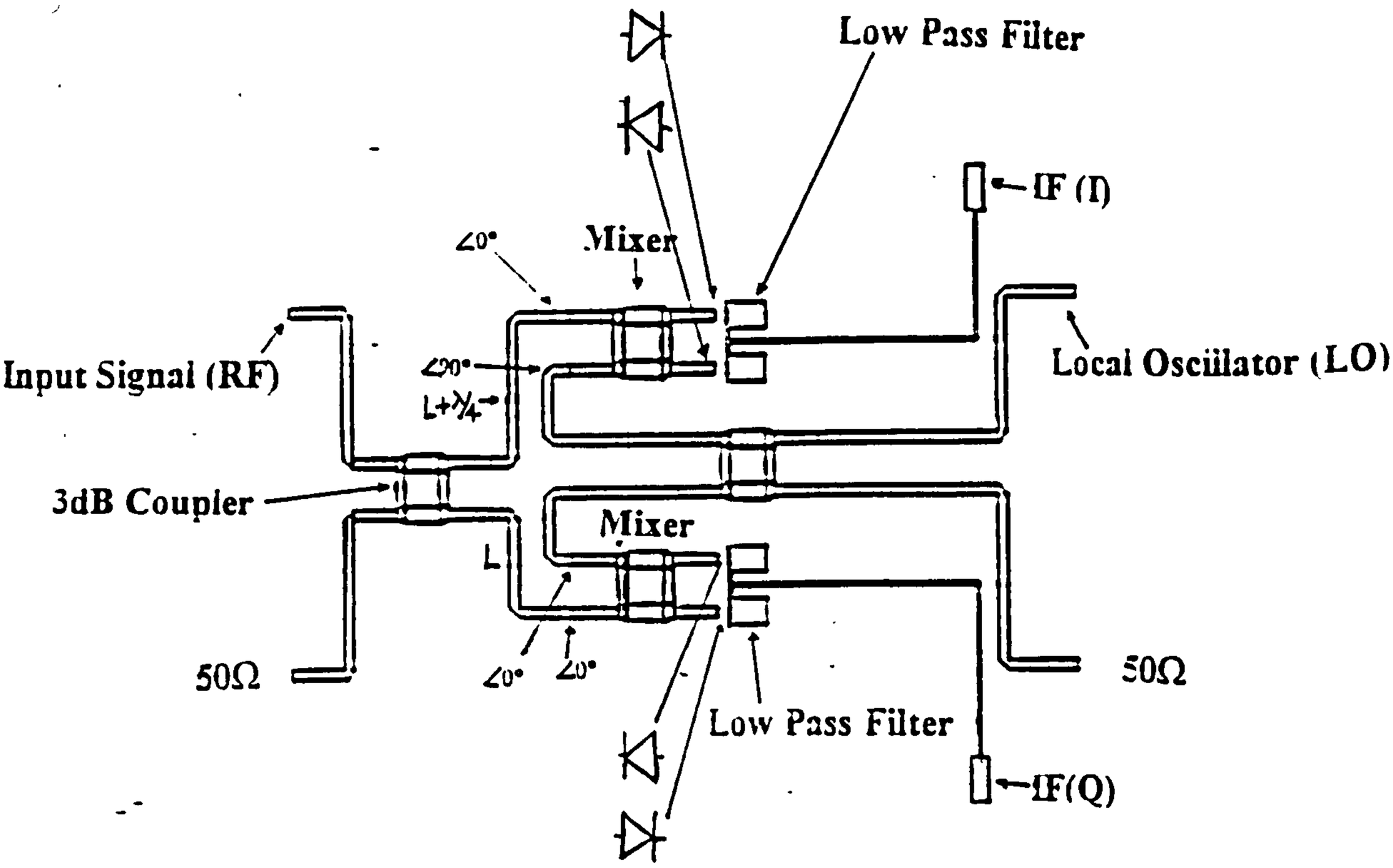

Figure 7.4.7 5.8GHz Image Rejection Mixer Circuit Layout

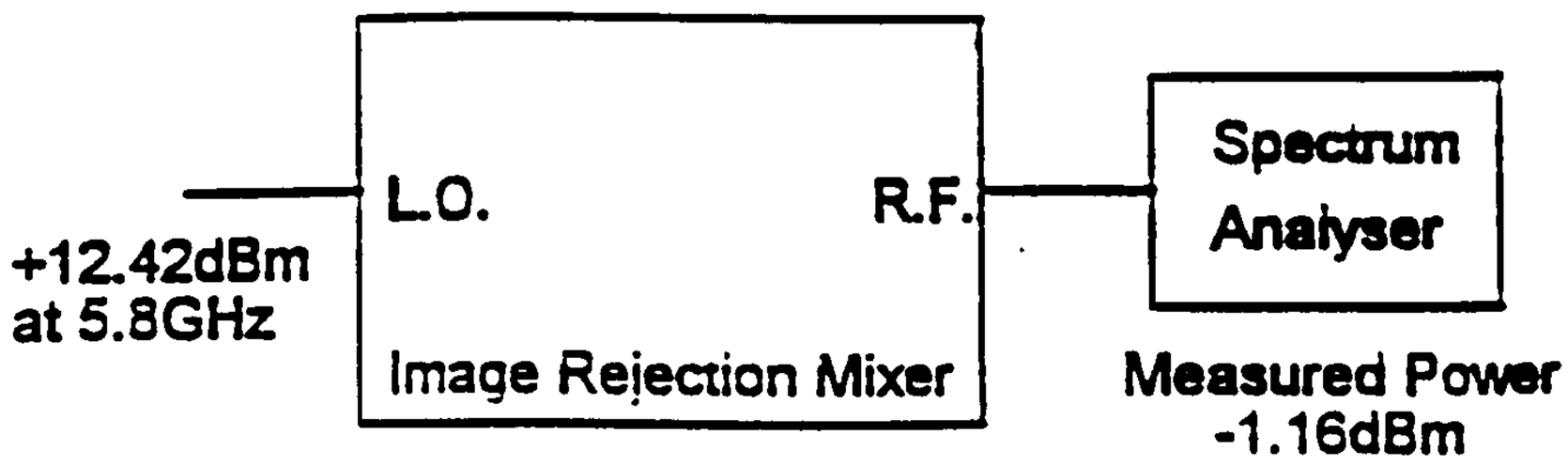

Figure 7.4.8 Test Set-up for LO-RF Leakage Measurement

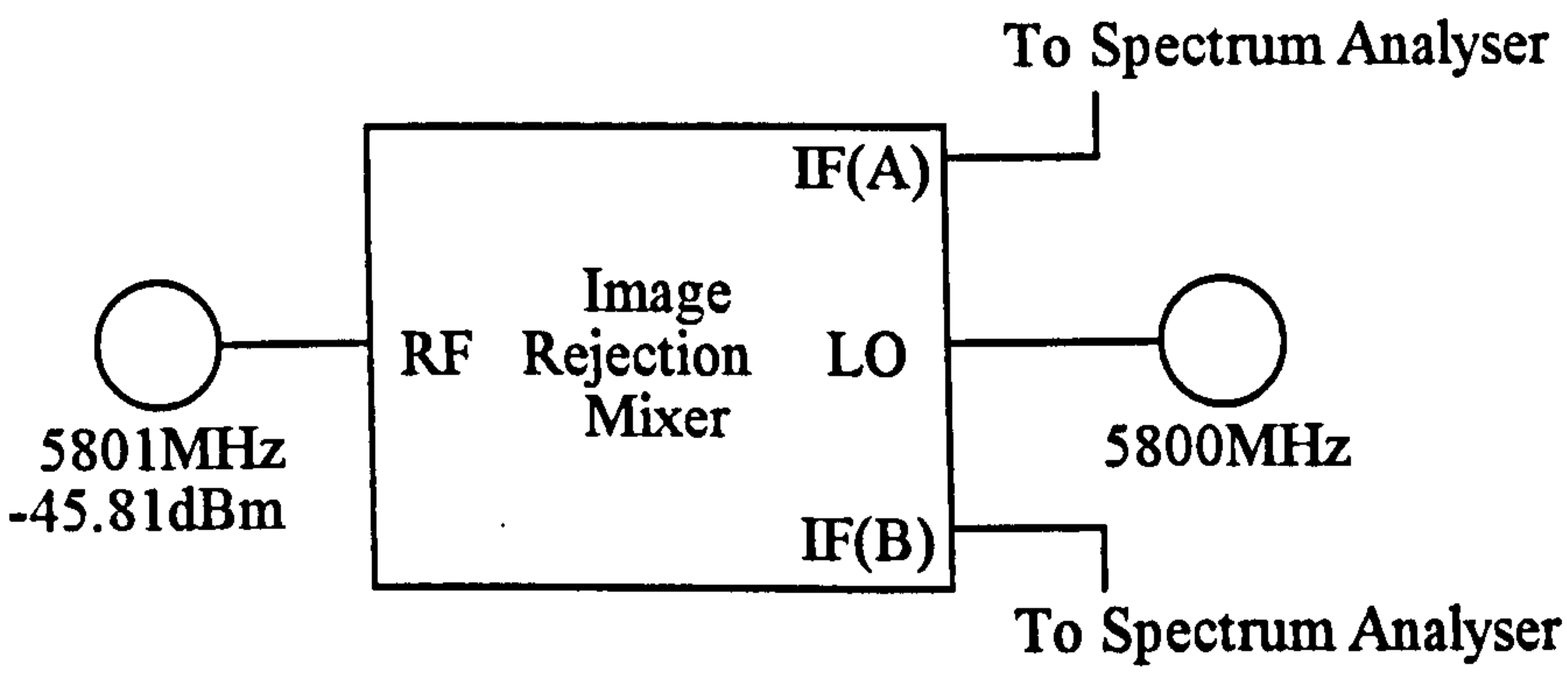

Figure 7.4.9 Test Set-up for Conversion Loss Measurement

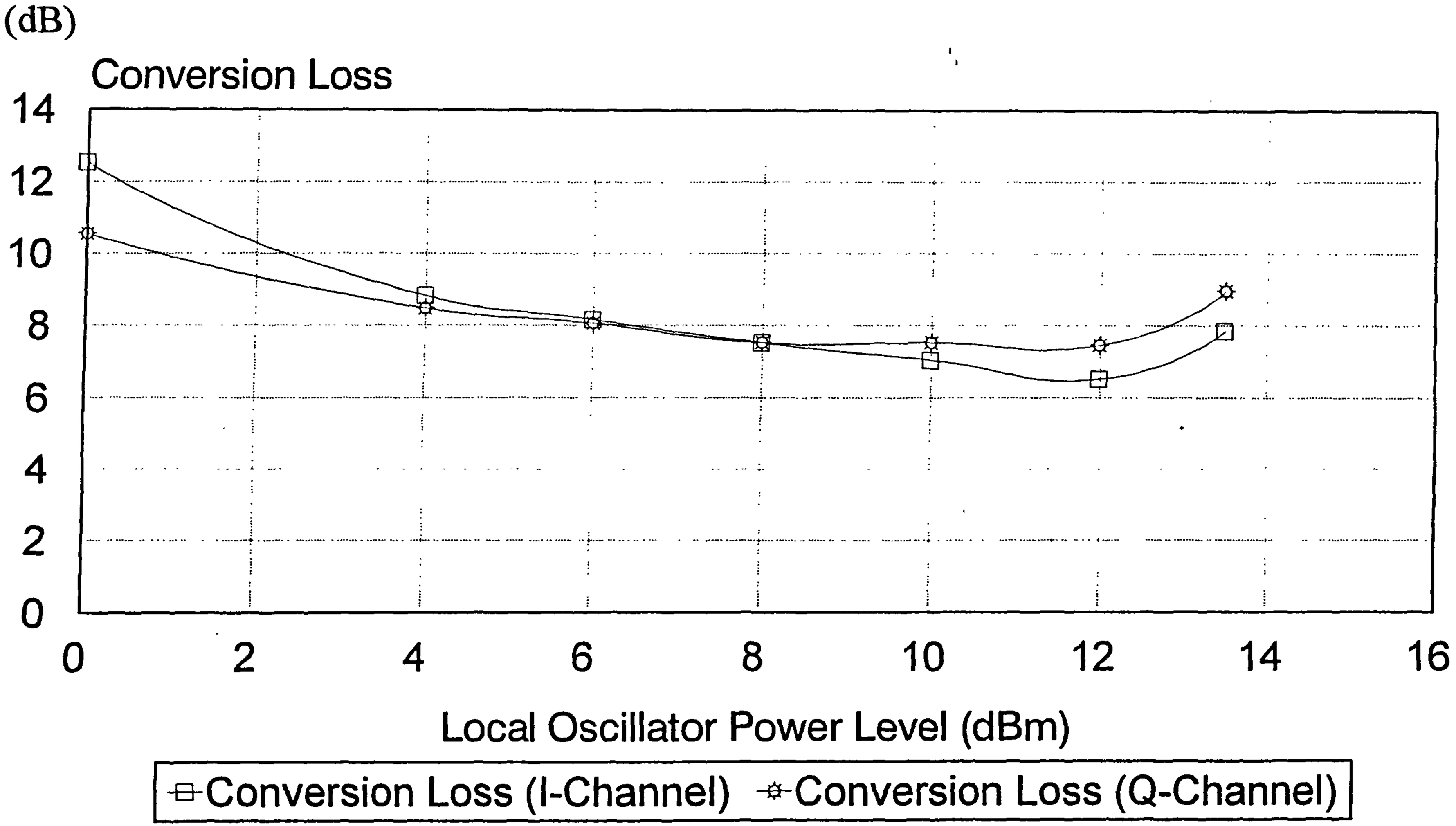

Figure 7.4.10 Conversion Loss against Local Oscillator Power Level

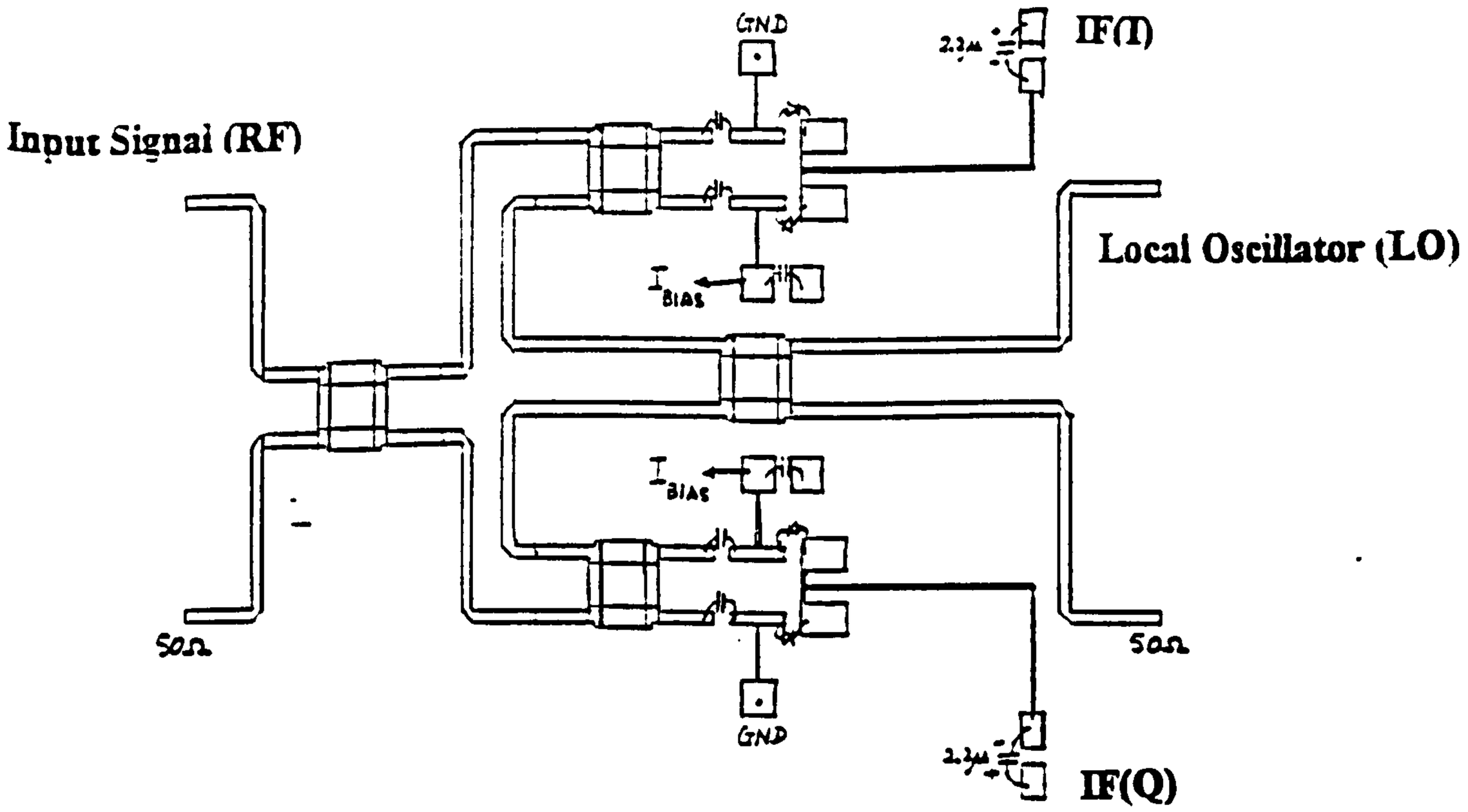

4F : 100pF

Figure 7.4.11 5.8GHz Image Rejection Mixer Circuit Layout with Biased Condition

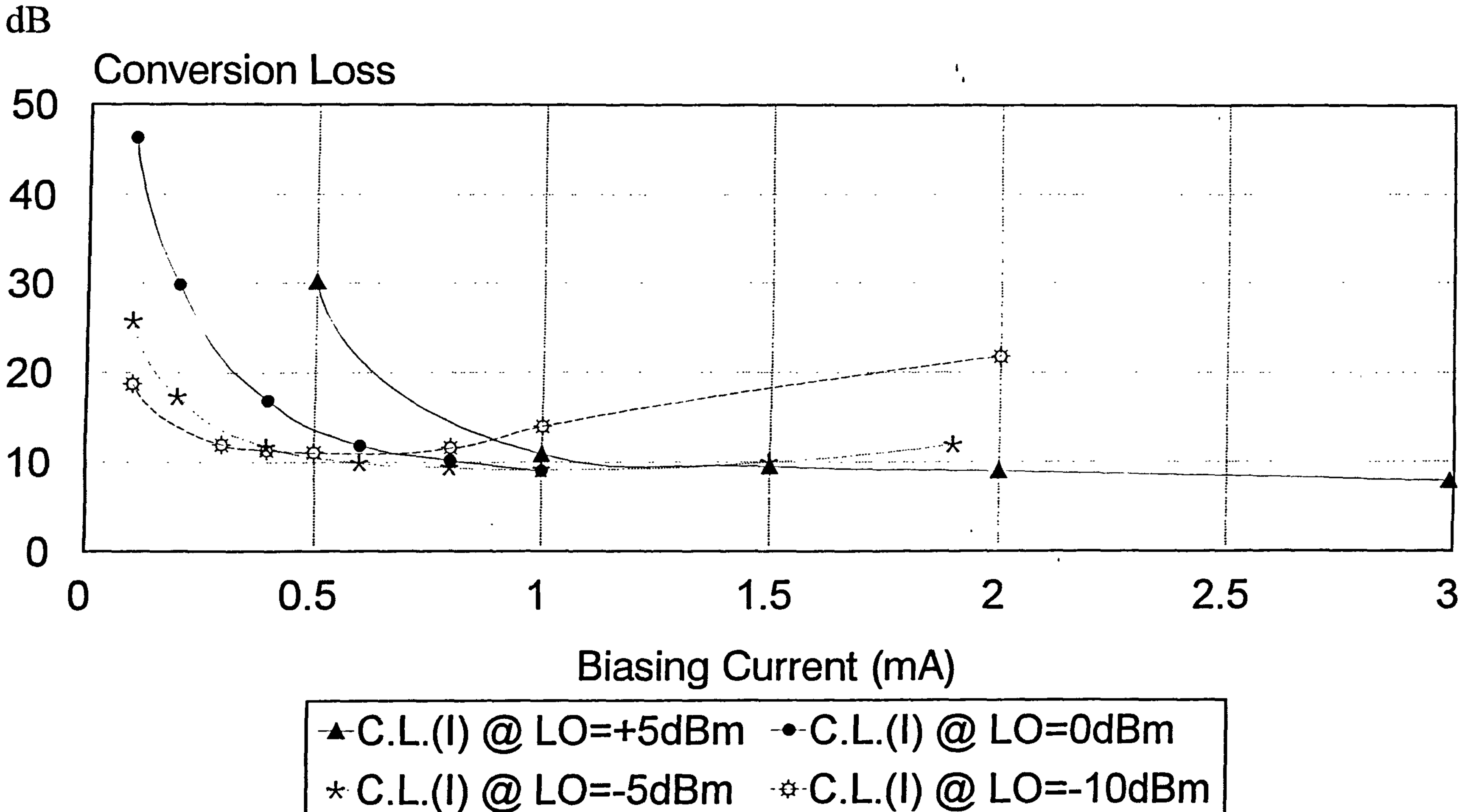

Figure 7.4.12 Conversion Loss (C.L.) on the Effect of Biasing Current for I-Channel

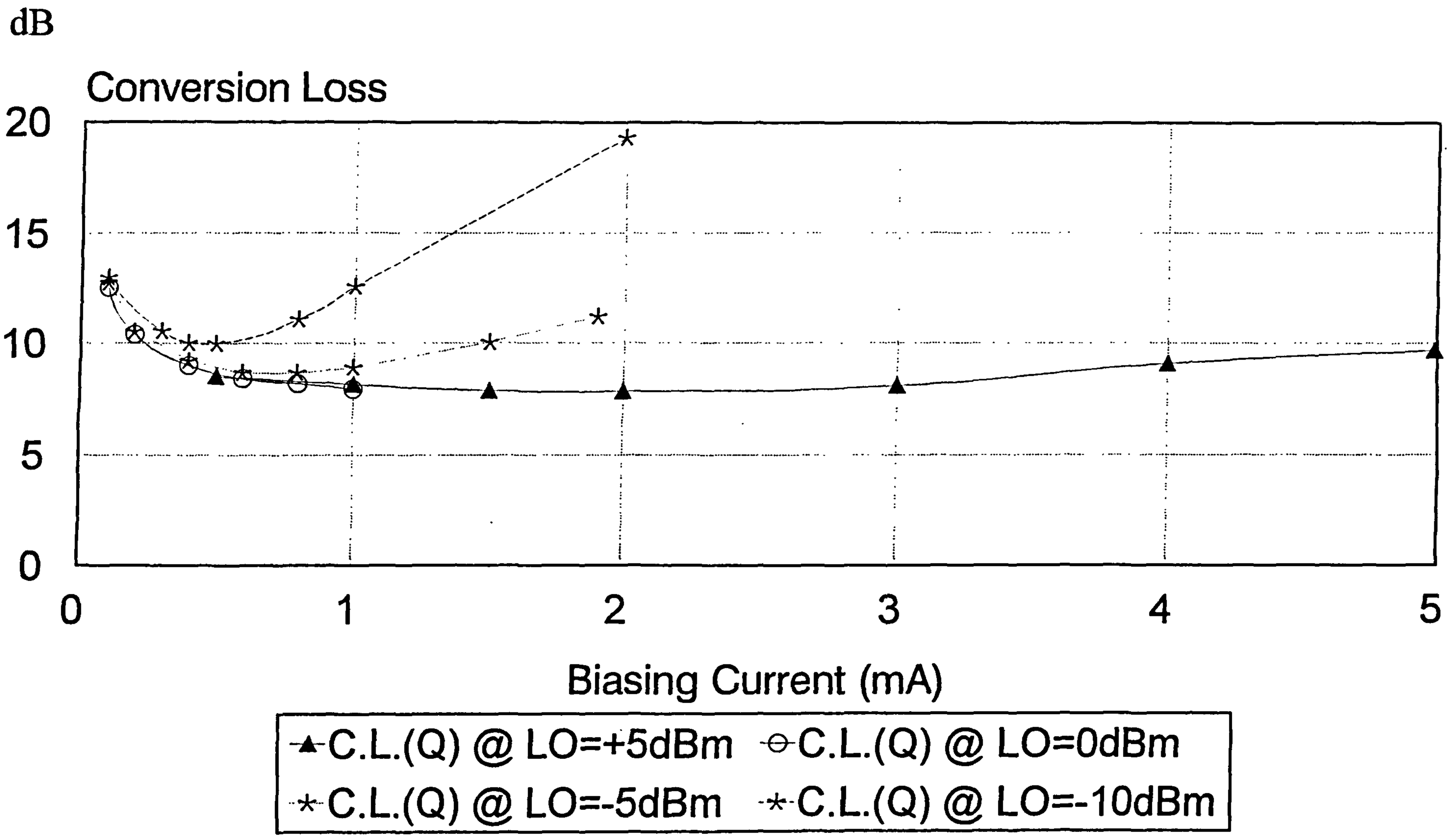

Figure 7.4.13 Conversion Loss (C.L.) on the Effect of Biasing Current for Q-Channel

CHAPTER 8

Design and Performance of the Two-Way Communication System

8.1 Introduction

This chapter presents the design of the OBU and the RSU. The design studies included the case when the same circular polarisations were employed for both down and up-link communication and also when a right hand circular polarisation was employed for the up-link communication with a left hand polarisation for the down link communication. The results of practical measurements for both up and down-link in terms of field strengths are then presented. It was found that there is a good correlation between the practical and the theoretical results.

8.2 On-Board Unit Design

Option 1 - Using Different Circular Polarisations (CP)

As discussed in Chapter 3, for the down-link operation, an ASK signal is transmitted from the RSU to the OBU using the left-hand CP. In the case of up-link, the RSU transmits a pure CW-signal, which is modulated by the OBU. The modulated signal is then re-radiated back to the RSU using the right-hand CP.

One way of implementing the above communication procedure is to use a two-diode arrangement as shown in figure 8.2.1. In the case of the down-link, the ASK signal with the left-hand CP is demodulated using a diode detector. For the up-link operation, the CW-signal is PSK-modulated by a DPSK 1MHz sub-carrier signal using a second diode which is optimised for PSK modulation. The modulated signal is then re-radiated back to the RSU with the right-hand CP. The detailed design of the ASK detector and the PSK modulator has been presented in Chapter 7.

If an extra gain is needed in order to increase the communication range, it is necessary to add an amplifier at the OBU (an amplfier costs about £25 each). The CW-signal is amplitude-modulated (DSB modulation) by a DPSK 1MHz sub-carrier signal at the OBU as shown in figure 8.2.2. The DSB modulator is basically a switching amplifier. The carrier wave is modulated by the sub-carrier which is modulated by baseband signal. By switching the r.f. surface-mounted amplifier, the DSB signal can be obtained. However, care must be taken in the design of the OBU layout to prevent any possible electromagnetic oscillations

taking place between the two antennae at the OBU.

Option 2 - Using Same CP

Figure 8.2.3 shows the OBU for the use of the same polarisation. For down-link operation, an ASK signal is transmitted from the RSU to the OBU using the left-hand CP. In the case of the up-link the OBU transmits a pure CW-signal which is DPSK modulated by the OBU. The modulated signal is then re-radiated back to the RSU using the left-hand CP. A single diode which costs about £1 each is used to implement both the ASK detection and the PSK modulation. Since the received power in up-link communication is much weaker than that in down-link communication (see chapter 3), a matching network optimised for the BPSK modulator circuit (for up-link) was first developed to ensure that the reflection coefficients are equal in magnitude and a 180° out of phase when the diode is switched between 'On' and 'Off' conditions. This circuit was then tested as an ASK detector (see chapter 7). Using a single diode arrangement this makes the OBU circuitry simpler and less expensive to build than using either of the other two arrangements since only one diode and one antenna are required.

8.3 Road Side Unit Design

The RSU generally consists of two microstrip antenna arrays, a microwave oscillator, a mixer, a 10dB coupler, a low noise amplifier (LNA), an i.f. amplifier and detection circuit. The RSU block diagram is shown in figure 8.3.1. For the down-link operation the ASK signal with Manchester encoding was used because it requires simple circuitry (i.e. a diode detector and a video amplifier) at the OBU for demodulation . For the up-link operation, BPSK modulation on the microwave carrier was used. In order to reduce low frequency noise of the mixer diodes and to use only one microwave oscillator at the RSU, a DPSK 1MHz sub-carrier was employed (see chapter 3).

To demodulate the DSB signal, the received signal at the RSU is synchronously demodulated using an image rejection mixer (IRM) which removes the carrier frequency and one of the sidebands of the amplitude modulated carrier. This is done in order to overcome the fading of the signal due to the motion of the vehicle with respect to the RSU (see chapter 3). The output from the mixer is then again demodulated in order to recover the data transmitted from the OBU.

The specifications of the RSU's sub-units operating at both the frequencies of 5.8GHz and 2.45GHz are shown in table 8.3.1(a)-((f).

Oscillator	
5.8GHz	2.45GHz
Dielectric Resonant Oscillator (DRO)	Cavity Free Running Oscillator

Table 8.3.1(a) Oscillator

10dB Coupler		
	5.8GHz	2.45GHz
Substrate:	RT/Duroid 6006,ε_r=10.5,h=1.27mm	RT/Duroid 6006,ε_r=6,h=1.27mm
Input/Output VSWR:	1.54:1 max	1.03:1 max
Main beam coupling:	-2.86dB	-0.68dB
Coupled beam:	-10.05dB	-10.74dB

Table 8.3.1(b) 10dB Coupler

SPST Switch		
	5.8GHz	2.45GHz
Substrate:	RT/Duroid 6006,ε_r=6,h=1.27mm	RT/Duroid 6006,ε_r=6,h=1.27mm
SPST chip:	Alpha AS006M1-1	Alpha AS006M1-1
Input/Output VSWR:	1.58:1 max	1.07:1 max
Insertion loss:	-5.24dB	-1.8dB
Isolation:	-34.02dB	-30.9dB

Table 8.3.1(c) SPST Switch

Image Rejection Mixer (IRM)		
	5.8GHz	2.45GHz
Substrate:	RT/Duroid 6010,ε_r=10.5,h=1.27mm	RT/Duroid 6010,ε_r=10.5,h=1.27mm
Diodes (x4):	HP HSMS-8101	HP HSMS-8101
LO level:	+10dBm	+10dBm
Conversion loss:		
I-Channel:	7.04dB	6.8dB
Q-Channel:	7.52dB	6.6dB
LO-RF leakage:	13.58dB	36dB
I.F. frequency:	1MHz	1MHz

Table 8.3.1(d) Image Rejection Mixer

Low Noise Amplifier (LNA)		
	5.8GHz	2.45GHz
Small Signal Gain:	30dB	30dB
Output Power (1dB GCP):	5dBm	20dBm
Noise Figure:	2.2dB max, 1.9dB typ	2dB max, 1dB typ
Manufacturer:	Celeritek	Microwave Amplifier Ltd.

Table 8.3.1(e) Low Noise Amplifier

RSU Antenna Array		
	5.8GHz	2.45GHz
Substrate:	RT/Duroid 5870,ε_r=2.33,h=0.79mm	RT/Duroid 5880,ε_r=2.2,h=1.57mm
Antenna Gain	17dBi	13dBi
Input VSWR:	1.22:1 max	1.01:1 max
Axial Ratio:		
Left-hand CP:	4.2dB	1dB
Right-hand CP:	1dB	2.22dB
Half-Power Beamwidth:	15	30°
Side-lobe Level:	-9dBc max	-12dBc max

Table 8.3.1(f) RSU Antenna Array

8.4 Performance of the Two-Way Microwave System

The measurement set-up, as shown in figure 8.4.1, has the roadside unit in an overhead gantry position at a height of 4.5m and the on-board unit (OBU) in the top centre of the vehicle windscreen at a height of 1.2m. The test vehicle is a Ford Sierra saloon car.

Measurements were carried out with the RSU at angles of orientation of both 60° and 45° with the vehicle travelling in the central position on the road. In order to carry out the measurements of the down-link signal strength the RSU was set-up to transmit a constant 125kHz square wave. In the vehicle the output of the diode detector was amplified and fed to a storage oscilloscope which recorded a voltage level corresponding to the signal strength. It should be noted that due to the square law response of the diode detector the output voltage is proportional to the received power.

The measurement set-up for the up-link was essentially the same as the down-link except that the OBU was set to transmit a constant string of zero's whilst the signal strength at the roadside unit was monitored. For the up-link measurements the output was taken from the output of the I.F. amplifier. In both cases the oscilloscope was triggered at distance of 15m from the roadside unit.

Practical Results

Down-Link

The results given in Figure 8.4.2 are for the roadside unit at an angle of 60° with the vehicle travelling in the centre of the beacon while figure 8.4.3 shows the results with the roadside unit at an angle of 45°. Comparing the results in figures 8.4.2 and 8.4.3 shows that with the RSU at 45° the maximum received signal strength is stronger, as compared to the case when it is at 60°, however, the length of the communication zone is reduced.

Up-Link

The results given in figure 8.4.4 show the up-link signal strengths with the test vehicle travelling in the centre of the road and the RSU at an angles of both 60° and 45°. These results show, as with the corresponding down-link measurements, that with the RSU at 45° the signal strength reaches a higher peak but the duration of the communication zone is reduced, as compared to the case when the RSU is at 60°.

RSU Radiation Power Levels

Measured results are presented of the radiation power levels at the road surface produced by the RSU transmission, when set to down-link mode as shown in figure 8.4.5, with the RSU at angles of 60° and 45°. It should be noted that the measurements obtained are of relative power, with 0dB corresponding to the background noise level and it was found that 15dB being the minimum signal strength required for reliable down-link communication.

The results presented have illustrated the signal strengths, for both up- and down-link, within the communication zone of the system. Assuming the reliable communication can be obtained when the signal level exceeds the background noise level, then down-link communication can be maintained for approximately 7m and 4m with the RSU set to 60° and 45°, respectively. By comparison the theoretical results for the down-link communication zone with the 60° and 45° orientations of the RSU were 6.9m and 3.8m respectively and good agreement has been obtained.

Measurement of the projected power levels on the surface of the road illustrated the different 'foot prints' that were obtained with the RSU at both 60° and 45°, these results being consistent with the signal strength measurements. The results are also consistent with the predicted results presented in chapter 3.

Much of the microwave design study in the present work has been incorporated into the microwave modules used in extensive field tests in five cities in the Europe under the ADEPT:V2026 project. The locations were Göteborg (Sweden), Thessaloniki (Greece), Cambridge (UK), Lisbon (Portugal) and Trondheim (Norway). It was shown that the system fully met the requirements on the technical aspect. They are

- system performance,
- reliability and durability,
- security,
- compatibility, and
- handling.

8.5 Summary

The design and development of the OBU and the RSU has been presented. Manchester encoded ASK modulation was employed for down-link operation while 1MHz DPSK sub-carrier was used in up-link mode. This was achieved by using a single diode arrangement for both PSK modulation and ASK detection at the OBU. Since the received power in up-link mode is much weaker than that in down-link, it is necessary to ensure that the matching network of the diode is optimised for the PSK modulation. A matching network optimised for the PSK modulator circuit was first developed and this circuit was then tested as an ASK detector in order to make the OBU simple and inexpensive to build. By using a single diode arrangement, the cost for the OBU has been reduced by approximately £60 (using two-amplifier arrangement) down to approximately £6 (using single diode approach).

Finally the system has been evaluated in terms of signal strengths for down and up-link operations. It was found that the measured communication zone is in agreement with the predicted results. The measured down-link communication zones were approximately 7m and 4m with the RSU oriented at 60° and 45° compared with the theoretical values of 6.9m and 3.8m respectively.

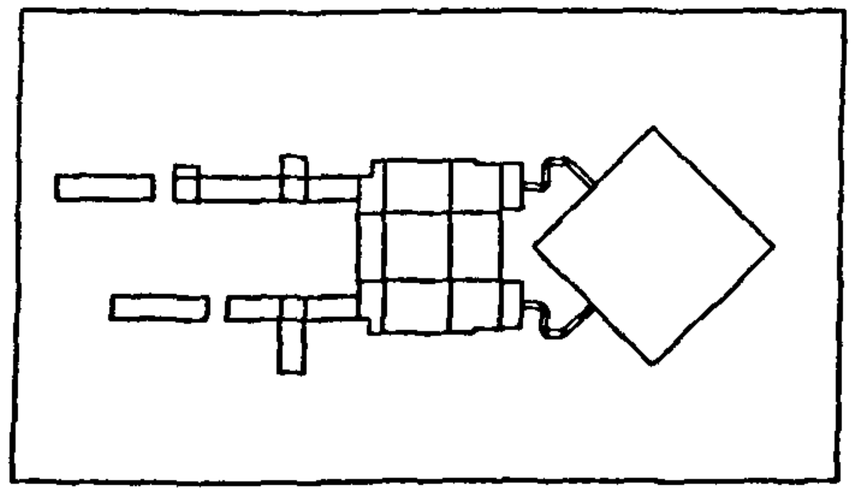

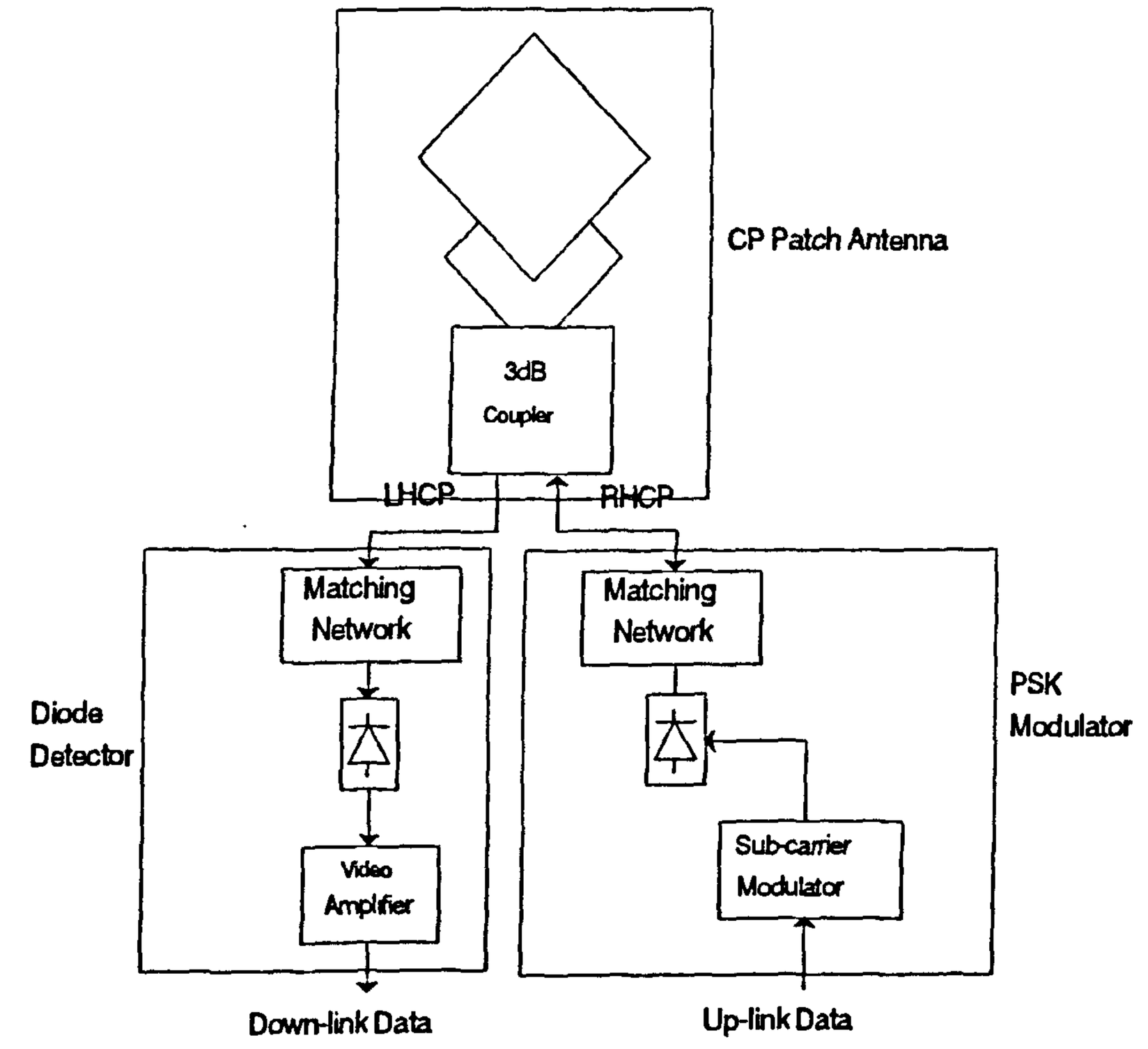

Figure 8.2.1 OBU Layout using two diodes

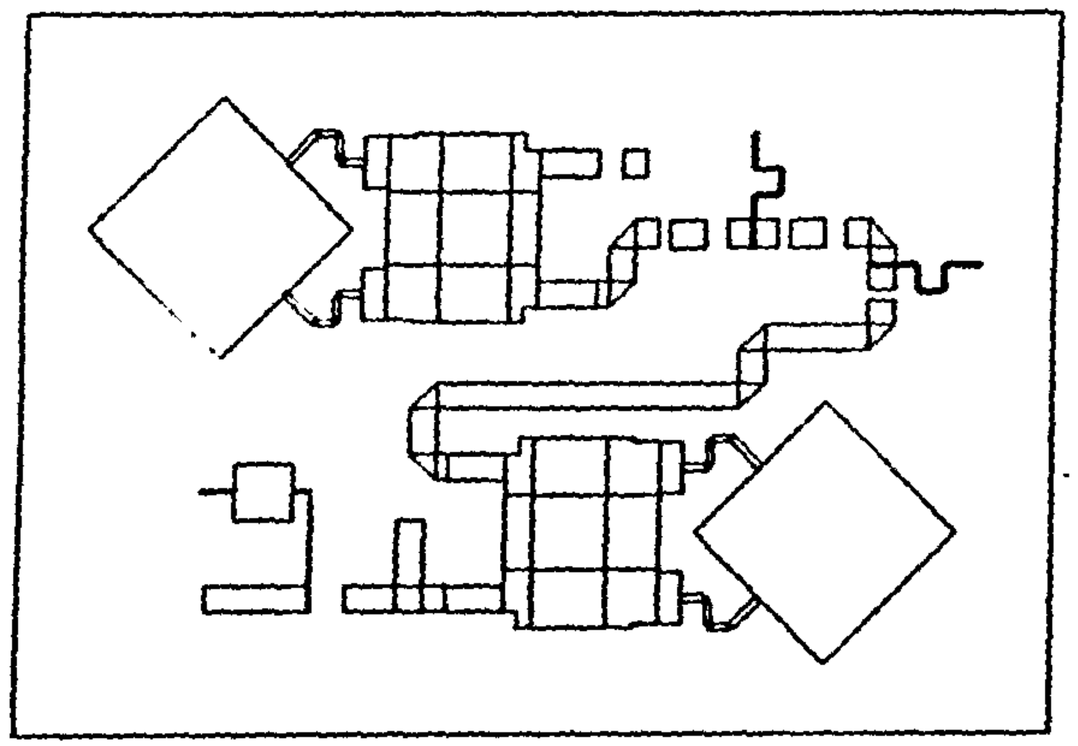

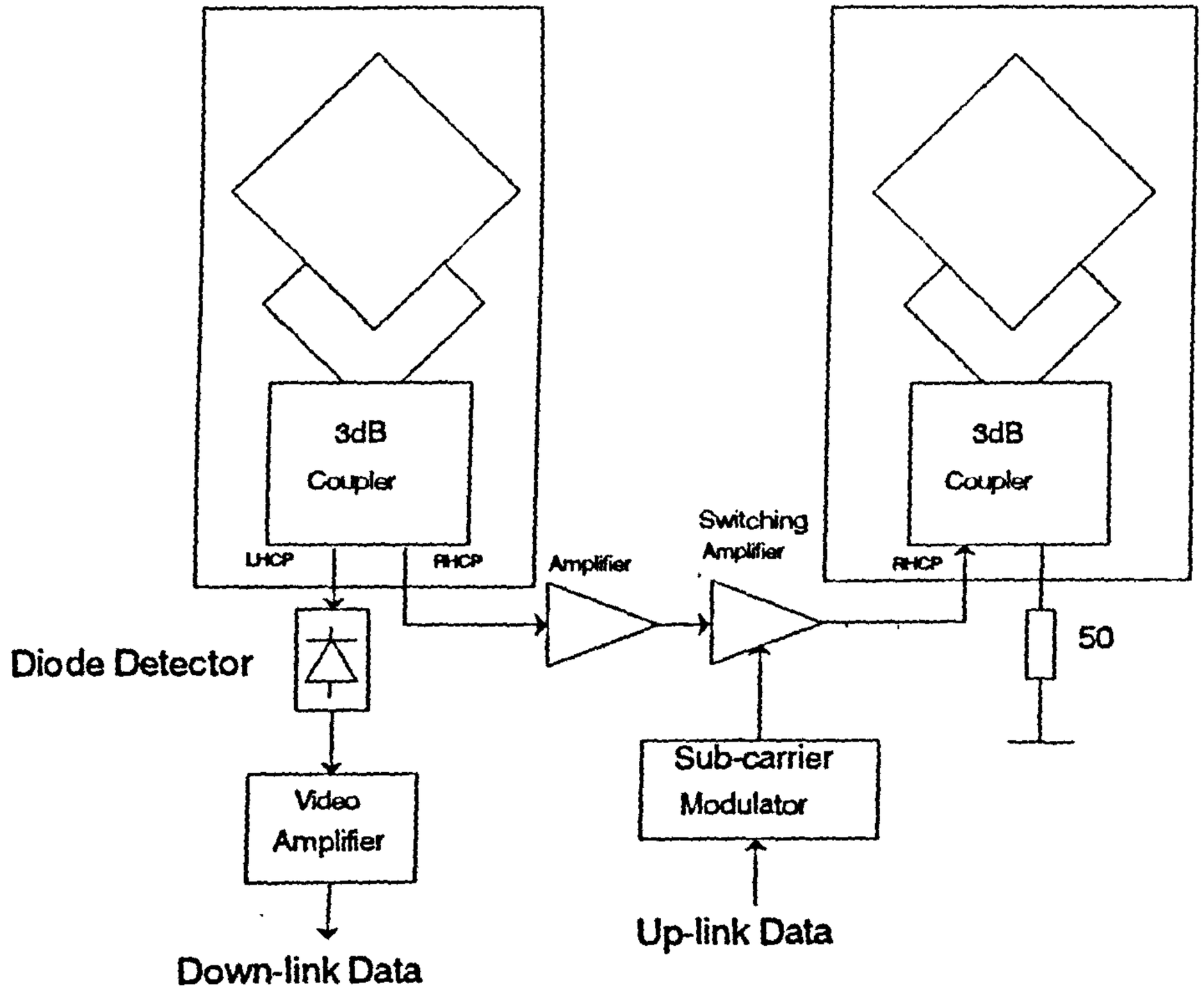

Figure 8.2.2 OBU Layout using an amplifier

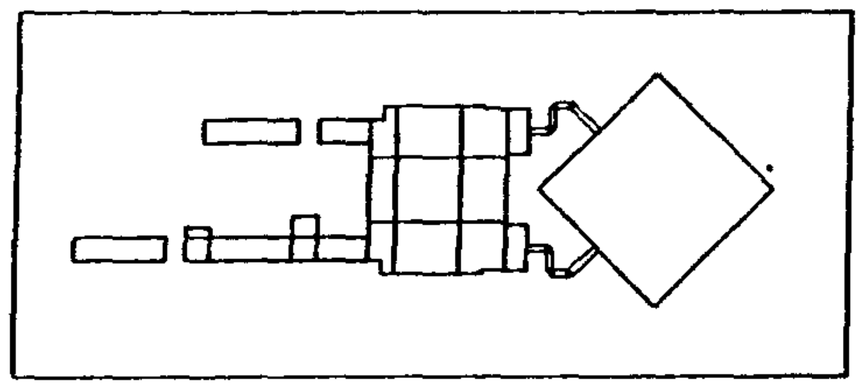

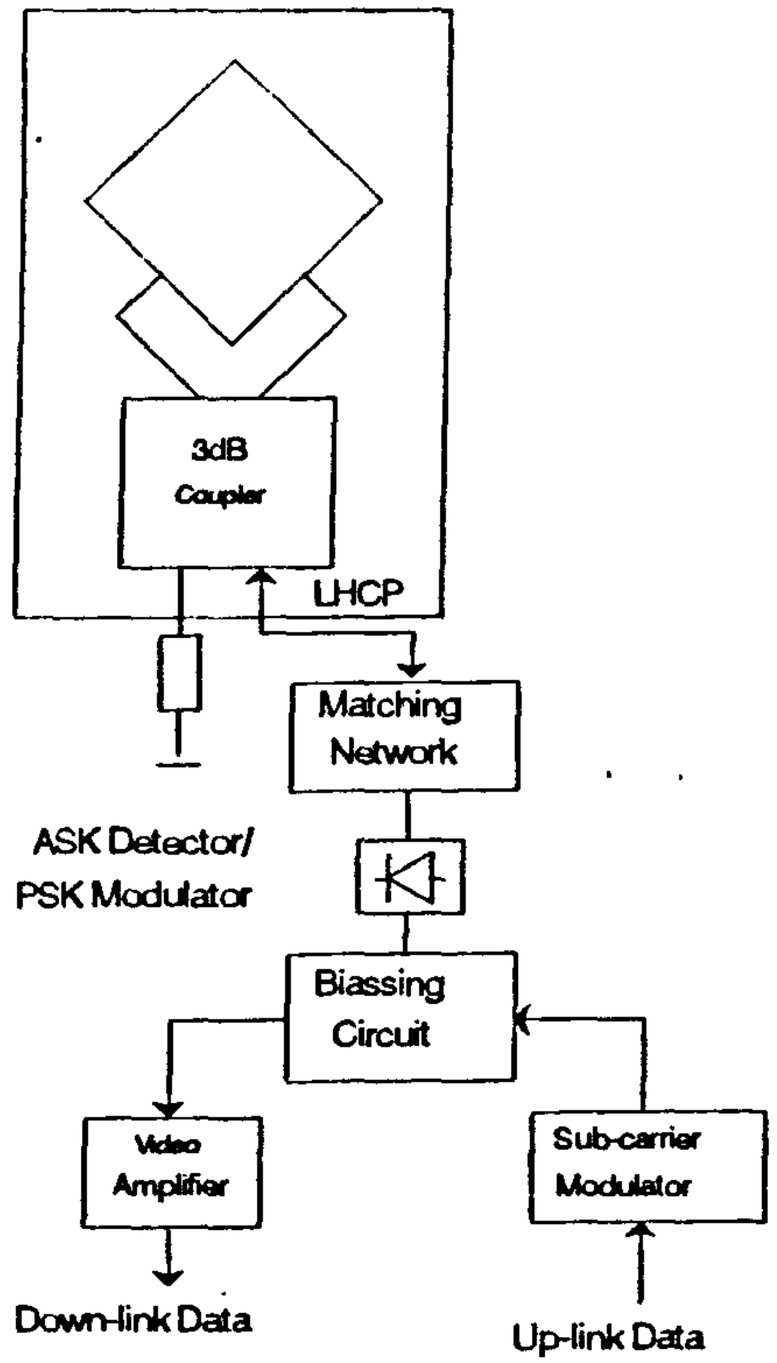

Figure 8.2.3 OBU Layout using a single diode

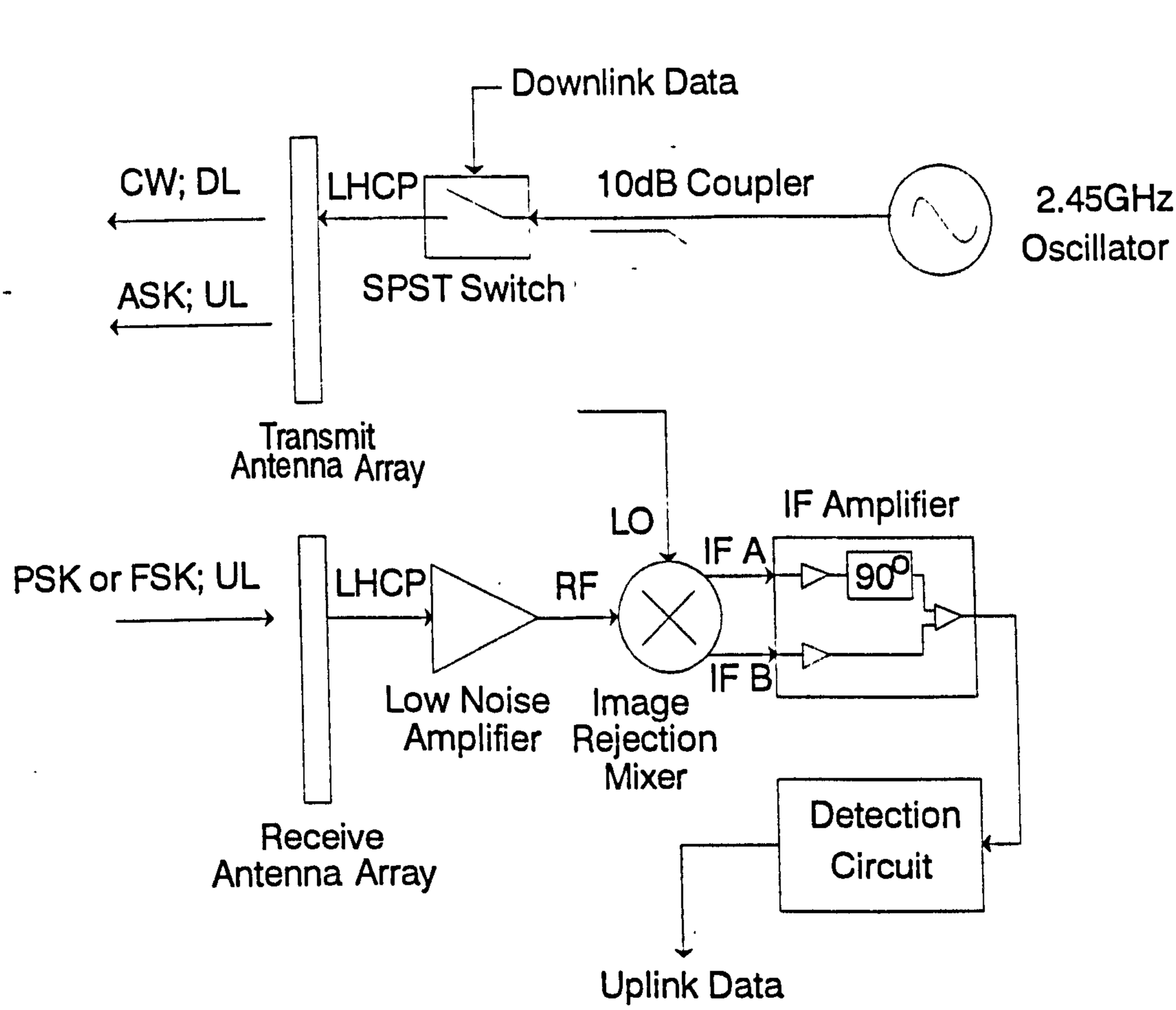

Figure 8.3.1 Block diagram of the Road Side Unit

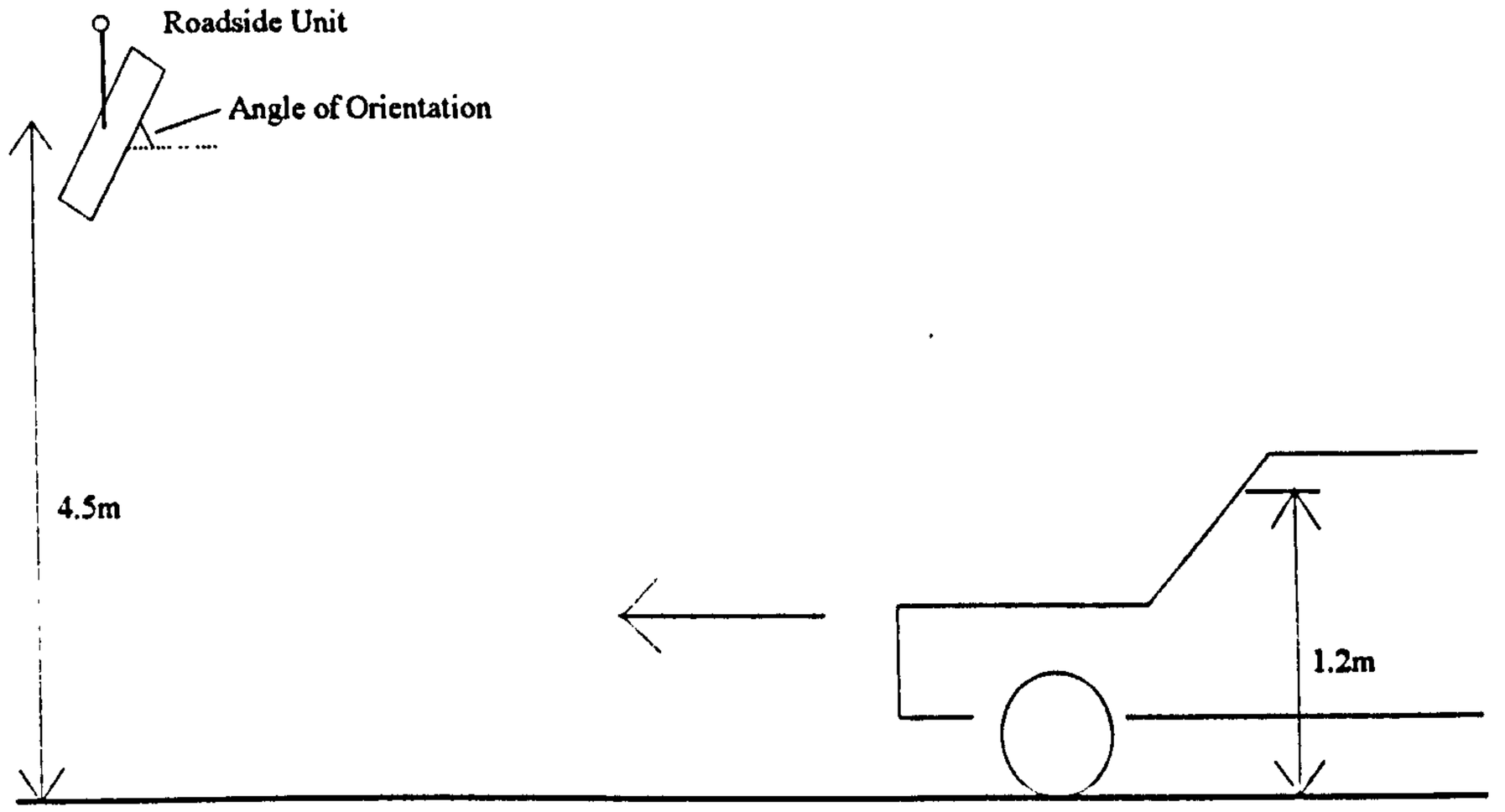

(a) Side View

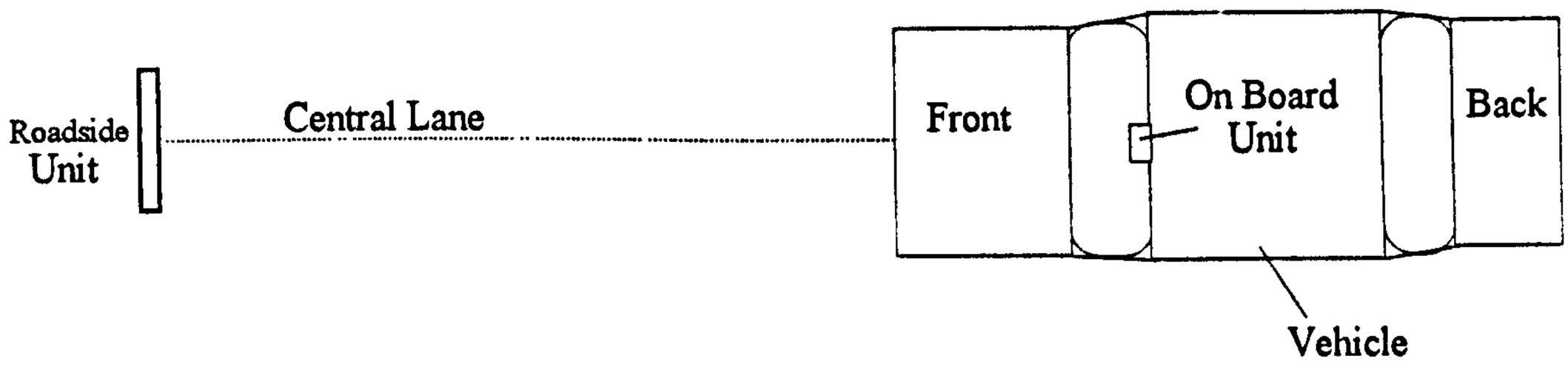

(b) Top View

Figure 8.4.1 Practical Measurement Arrangement

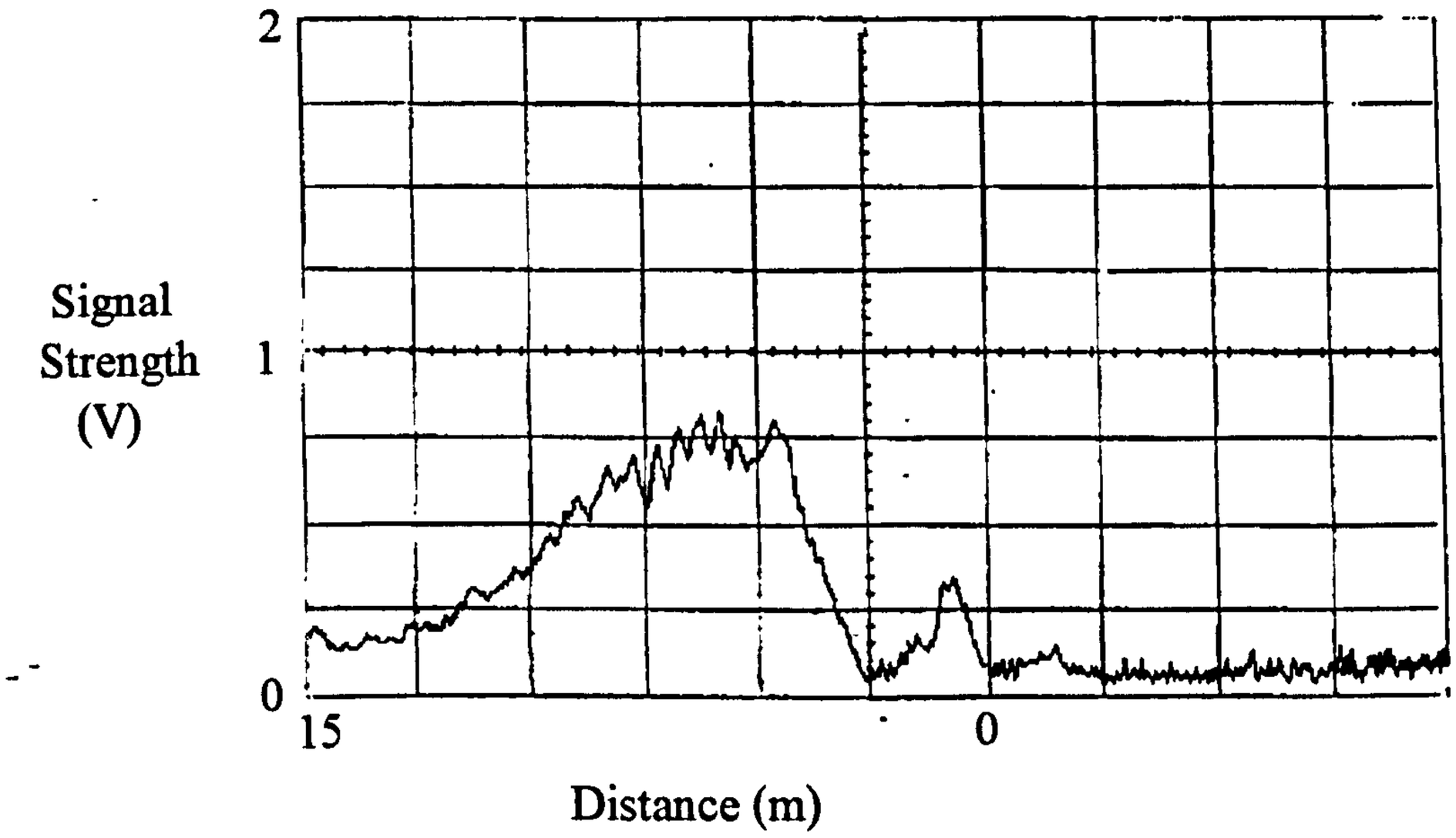

Figure 8.4.2 Down-Link Signal Strength Measurement Results, RSU at 60°

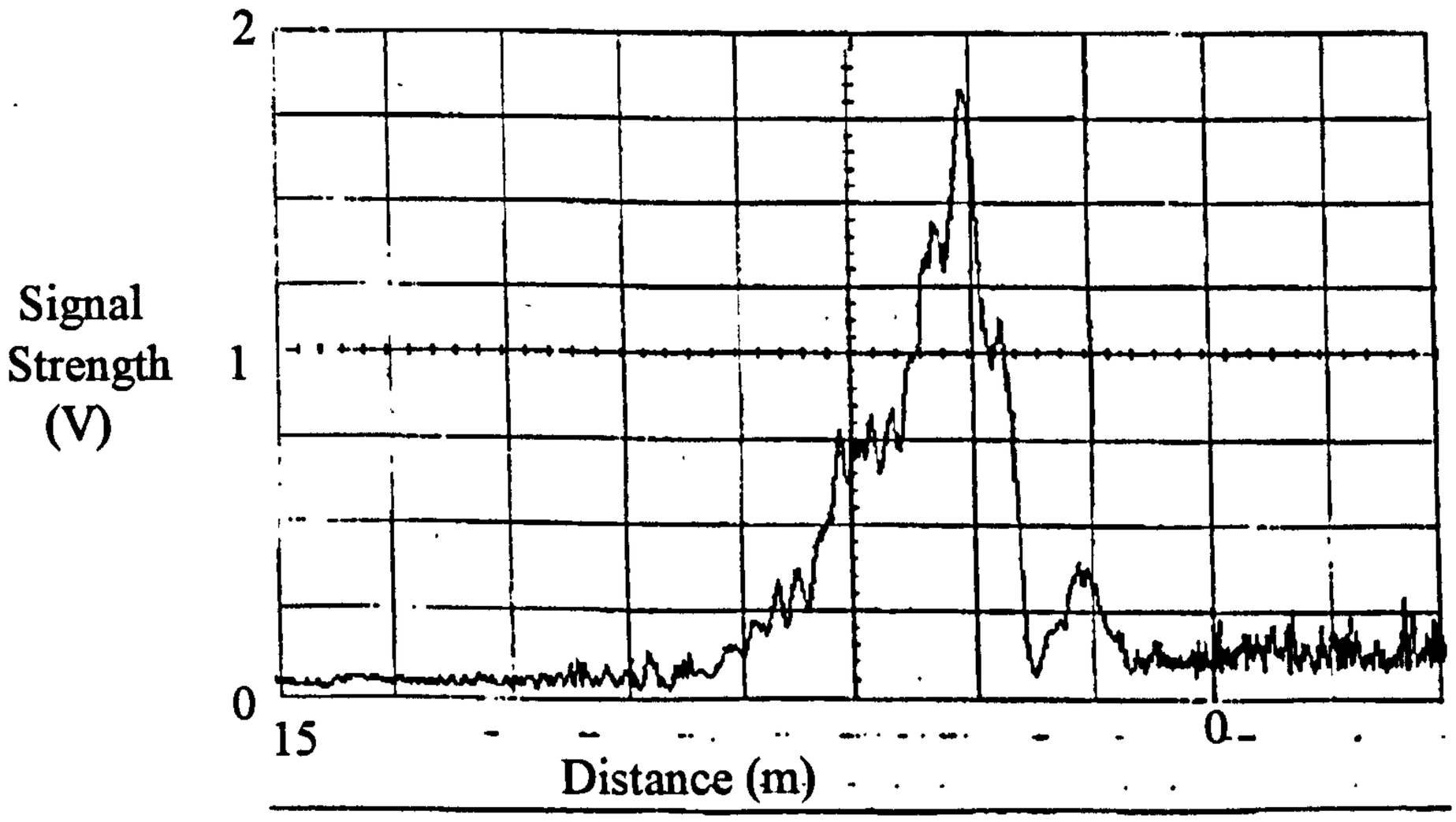

Figure 8.4.3 Down-Link Signal Strength Measurement Results, RSU at 45°

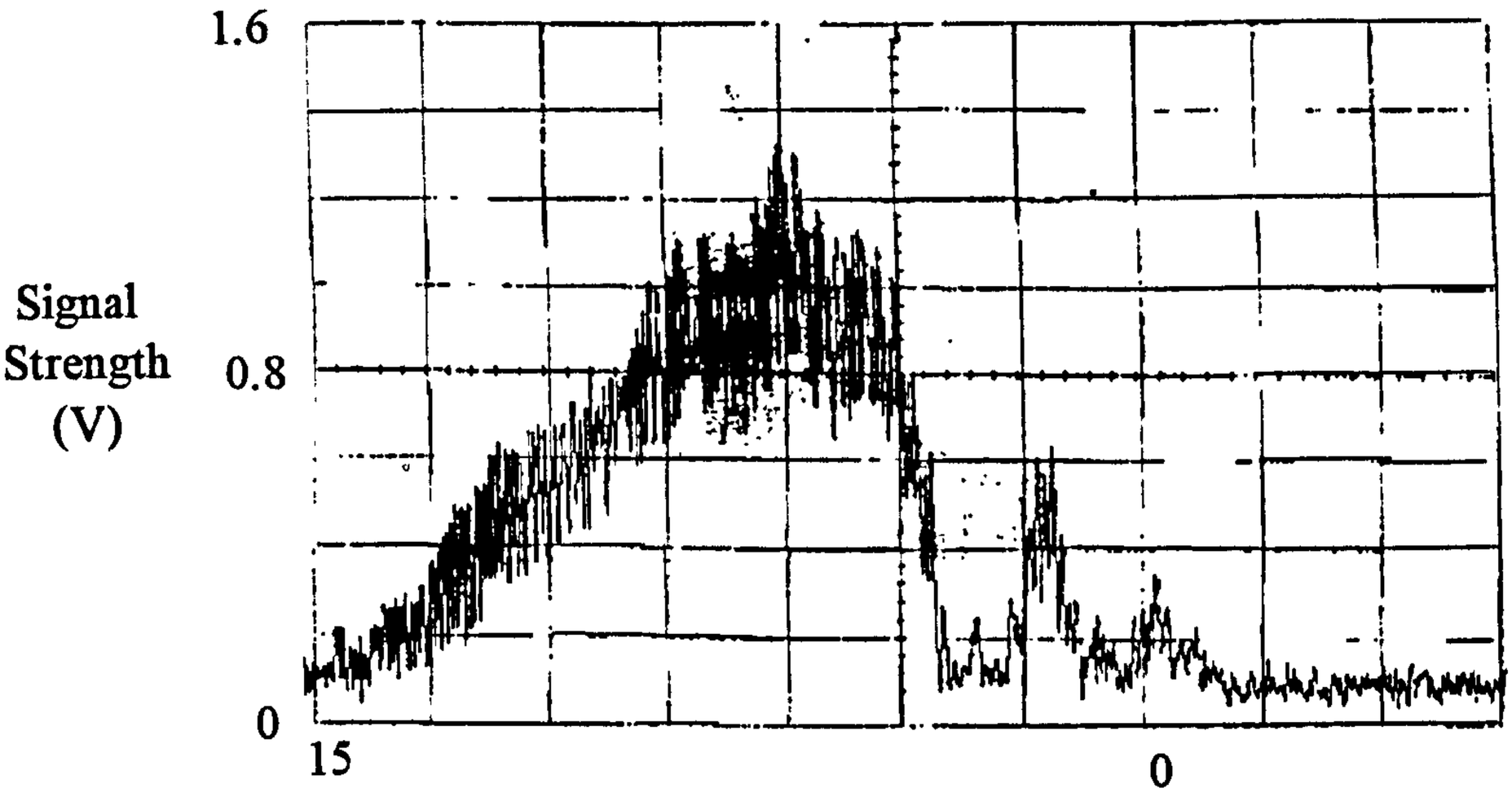

(a) RSU at 60°

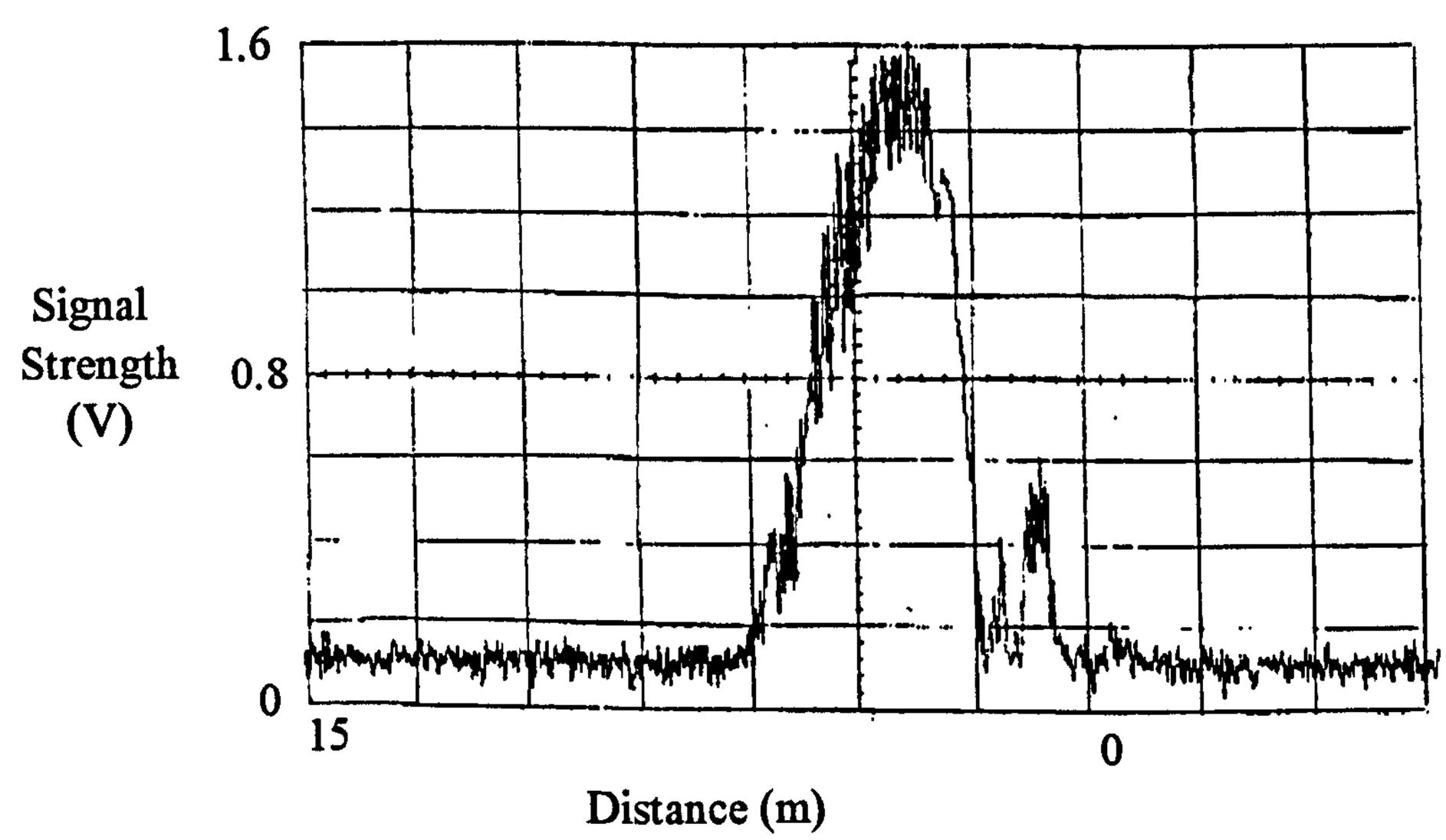

(b) RSU at 45°

Figure 8.4.4 Up-Link Signal Strength Measurements with the Test Vehicle

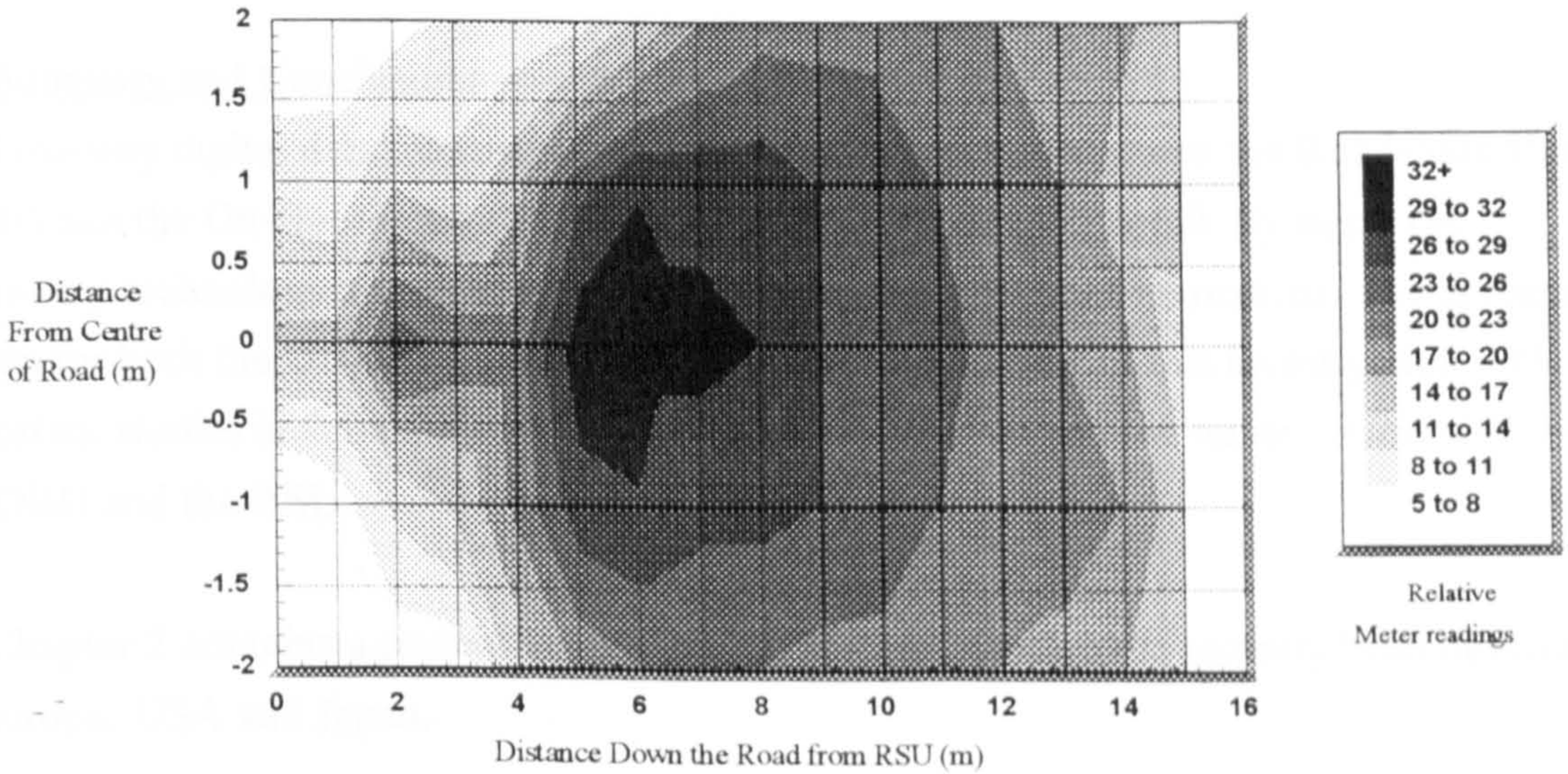

(a) RSU at an Angle of 60

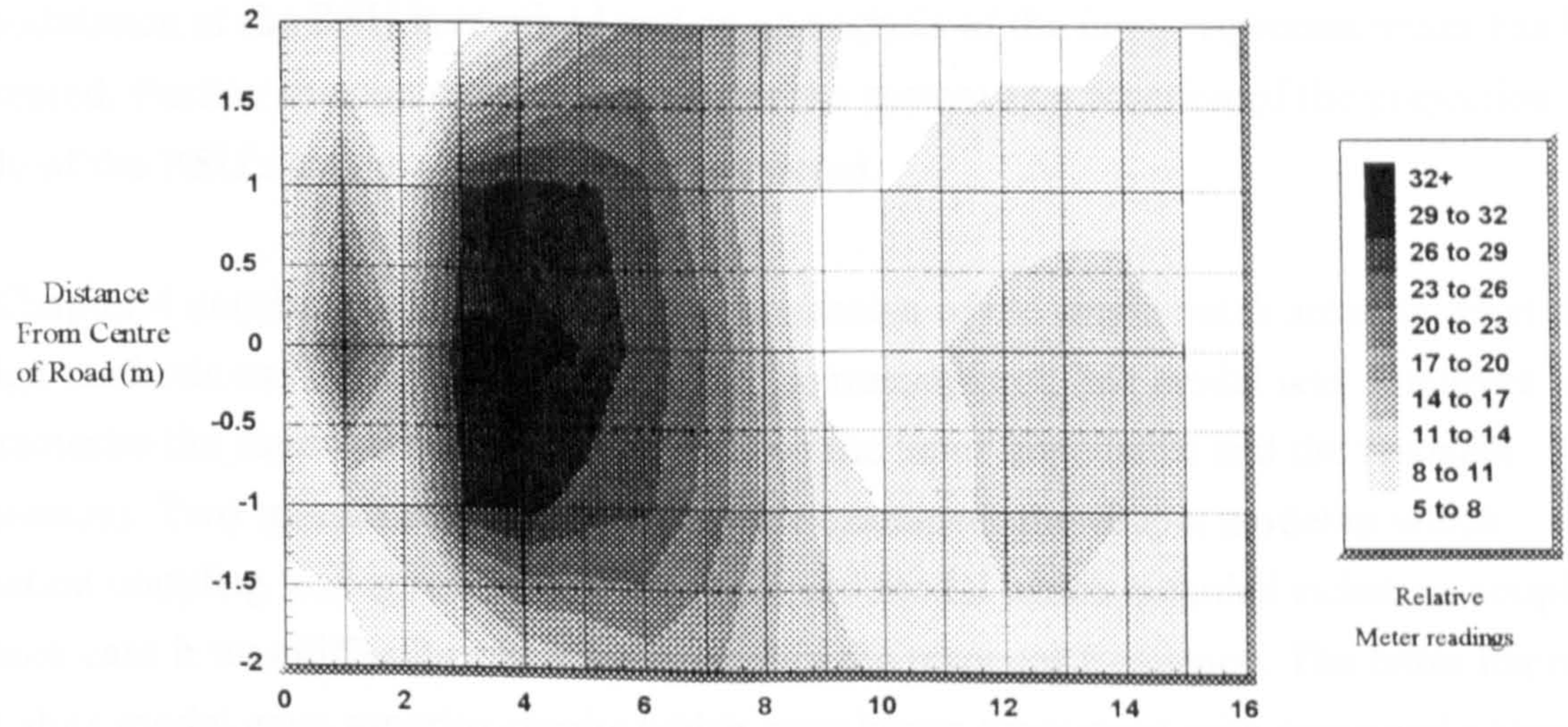

(b) RSU at an Angle of 45

Figure 8.4.5 Projected Power Levels on the Road Surface with the RSU in Down-Link Mode

CHAPTER 9

Conclusions and Further Work

9.1 Summary and Conclusions

Two-way digital data microwave communication systems between the Road-Side Unit (RSU) and the On-Board unit (OBU) have been investigated in detail. By using the microstrip technology a very light weight and compact OBU can be realised. The antenna design for both the OBU and the RSU constitutes a major part of this investigation. Other important studies include the PSK modulator/ASK detector and the mixer circuitry for both the OBU and the RSU.

Chapter 2 contains a review of a number of systems which have recently been developed in Europe, USA and Japan.

Chapter 3 is concerned with the specifications of the system for the down and up-link operations. It is easier to produce a double side-band signal by using either a single diode or a switching amplifier at the OBU. In either case an image rejection mixer for the demodulation at the RSU is required and so an analysis of the image rejection mixer has been presented. Further the communication zone of the system as a function of the projection angle of the RSU's antenna has also been predicted.

Chapter 4 contains an investigation into the design of the single patch antenna. First the design methods and models were reviewed. The transmission line model was employed to characterise the single patch antenna (mainly on the input impedance and the resonant frequency). Two transmission line models were examined, the simple model in which radiation coupling was ignored, and, the improved model which included radiation coupling. In each case it was difficult to accurately predict the resonant frequency. The latter improved two slots model gave superior results which gave better agreement with measured values. Finally a circular polarised OBU antenna was developed and it performed well in practice.

In the design of the planar array antenna mutual coupling between adjacent patches may affect the performance of the antenna. Two approaches to the analysis of the mutual coupling have been presented in Chapter 5 - the transmission line model (TLM) and the Cavity Model. For the TLM the mutual admittance between two radiating slots is required to predict the mutual coupling. For the mutual susceptance the Nauwelaers (1985) formula was

in fact divergent. This was because it neglected the width of the radiating slots. A new formulation of the expression for the mutual susceptance was obtained which included the slot widths. However the mathematical integration involved proved difficult because of the poor convergence properties of the integrand. In respect of the mutual conductance a new computational formula was derived which proved to be more accurate and computationally efficient. Moreover this formula did not involve Bessel functions and it was preferred to the formula given by Nauwelaers (1985).

In respect of the Cavity Model the formulation by Huynh (1992) was studied and the necessary specific analysis required for the present study has been presented. The above formulation is in terms of a line integral contained within another line integral which takes into account all the field interactions between the two antennae. The integration evaluates the interaction of each segment of the antenna #1 in turn with each segment of the antenna #2. There are total of sixteen interactions involved giving rise to sixteen double integrations.

Practical measurements for the mutual coupling between two antennae at 5.8GHz have also been carried out and the results were compared with the predicted results using both the transmission line model and Cavity Model, respectively.

Chapter 6 is concerned with the design of the RSU antenna array working at 5.8GHz using [S] parameters to model the mutual coupling between antenna elements. In order to obtain the required beamwidth (15°) of the antenna, it was found necessary to make the spacing between the centres of adjacent patches to be $0.75\lambda_0$. It was found that the mutual coupling has a negligible effect for this spacing. Thus it was concluded that it is <u>not</u> necessary to take the mutual coupling into account in the design of the RSU antenna. A 4 by 4 antenna array has been used successfully. As a result of the work done in Chapter 6, a paper has been published in the IEE Colloquium Proceedings (11 June 1993).

In chapter 7 the design and performance of the ASK Detector, PSK Modulator and the image rejection mixer have been presented. The equation for the tangential signal sensitivity (TSS) which characterises the performance of the detector has been derived. In order to make the OBU design simple, a single diode arrangement was employed. First a matching network was designed to maximise the performance of the PSK modulator. It was then used as an ASK detector. The TSS was degraded due to the mismatch of the PSK matching

network. Further, an analysis for a non-ideal PSK modulation has also been presented. It was shown that in order to maintain the signal-to-noise ratio of 10.5dB to 11dB the amplitude that can be tolerated is approximately 0.5dB and the phase error that can be tolerated is about 10 . It was found that it is very important to maintain the equal amplitude rather than exact 180 phase difference of the reflection coefficients in the design of the PSK modulator. As a result of the work done in the design of the single-diode arrangement for the PSK modulator and the ASK detector at the OBU, a paper is to be presented in the 24th European Microwave Conference (5-8 September 1994).

Further the mathematical analysis of an image rejection mixer using a phasing technique has also been presented. The mixer was then built and tested and a good performance was achieved. It was also found possible to reduce the Local Oscillator power level for the mixer by applying a biasing condition to the mixer diodes.

Chapter 8 is concerned with the development and testing of the two-way communication system. By using the same polarisation for both down and up-link operations, a simple design of both the OBU and the RSU was achieved. As a result of the work done in the design of the microwave transponder a paper is to be presented in the Microwaves 94 Conference and Exhibition (25-27 October 1994).

Finally, a field test was carried out to evaluate the system and it was found that the measured communication zone are in good agreement with the theory.

As a result of the work done in the design of the communication system, two reports have been published in the Commission of the European Communities R & D Programme documents (November 1992 and May 1994).

9.2 Suggestions for Further Work

The work below identifies the areas for further investigations and research. In order to further reduce the size and the cost for the On-Board Unit it is suggested that the CP antenna which consists of a square patch and a 3dB two-branch coupler on the same side of the microwave board may be replaced by the following alternatives:

1. To use an aperture coupling: The microstrip antenna to be formed on a separated dielectric substrate above the ground plane and the two structures electromagnetically coupled through an electrically small aperture in the ground plane between them. With the two-layer design, the antennae to be located on a separated substrate, which not only will reduce the unwanted radiations from the feed line network but also reduce the size of the OBU. Moreover, aperture coupling obviates problems associated with probe feeds at microwave frequencies, such as complexity of construction and large probe self-reactance.

2. To use a square patch antenna with a rectangular slot on the main diagonal to produce circular polarisation; this design does not need a feed line network (i.e. a 3dB coupler) to generate a 90° phase shift between the vertical and the horizontal components of the signal. Therefore a structure for the OBU which is simple and small in size can be achieved.

3. To employ two patches in order to form an array; this enables the polar pattern to have a narrower beamwidth. This will result in the increase of the antenna gain which in turn would increase the communication range.

4. To attach the microstrip patch antenna on the inside of windscreen of the vehicle; this is to investigate the possible degradation of the circular polarisation property of the signal on transmission through the windscreen in terms of the vertical and horizontal components of the signal.

5. To investigate the polarisation arrangement; the degree of interference between adjacent systems in the multi-lane situation may be influenced by the polarisations used for up and down-link operations. It is therefore necessary to examine the reflections due to the road

surface and nearby vehicle bodies in order to decide whether different or the same polarisation should be used for up and down-link operations.

REFERENCES

Abbound, F.and Damiano, J.P. et al (1988).'Simple Model for the Input Impedance of Coax-fed Rectangular Microstrip Patch Antenna for CAD'. Proc. IEE, Vol. 135- H, No. 5, Oct. 1988, p.323-326.

Alwater, H.A. (1980).'Reflection Coefficient Transformations for Phase-Shift Circuits'. IEEE Trans. MTT-28, June 1980, p.563-567.

AMTECH. (1989).'AMTECH: Corporate Overview'. The AMTECH Corporation, Jan. 1989.

Alwater, H.A. (1980).'Reflection coefficient transformations for phase-shift circuits'. IEEE Trans.-MTT-28, June 1980, p.563-7.

Autostrade S.p.A. (1991).'Telepass, toll-payment without stopping, central department for information'. Florence, Italy.

Bahl, I.J. and Bhartia, P. (1988).'Microwave Solid-State Circuit Design'. John Wiley & Sons, Chapter 11, p.540-600.

Bahl, I.J. and Bhartia, P.(1980).'Microstrip Antenna'. Artech House.

Balanis, C.A. (1982).'Antenna Theory - Analysis and Design'. John Wiley & Sons Inc.

Bhandal, A.S. and Richardson, M.J. (1992).'Future Applications for Short Range Vehicle/Roadside Communications Links'. IEE Colloquium on Prometheus and Drive, 15th Oct. 1992, p.7/1-5.

Bic, J.C. and Duponteil, D. et al (1991).'Elements of Digital Communication'. Chapter 8-Distortions and Perturbations, John Wiley & Sons, p.328-331.

Blume, G. and Ohler, M. et al (1992).'Automatic fee collection as an integrated part of a conclusive RTI-System'. IEE Colloquium on Toll System, 2nd Oct 1992, p.7/1-8.

REFERENCES

Blythe, P.T. and Hills, P.J. (1992).'Pricing and Monitoring ELectronically of Automobiles-The DRIVE project PAMELA-3: The field-trials and the future plans for the PAMELA system'. Traffic Engg & Control, Nov. 1992, p.614-8.

Bogen, K. (1989).'KOFRI (Queue-Free), Non-Stop Toll Payment System - A Brief Description'. Technical Paper, Micro-Design, Selbu, Norway.

Braegas, P. (1980).'Function, Equipment, and Field Testing of a Route Guidance and Information System for Drivers (ALI)'. IEEE Trans. VT-29, p.216-225.

Carver, K.R. (1979).'Mathematical Modelling of Mutual Coupling Between Antennas'. PSL Tech Note EM79-1, Physical Science Laboratory, New Mexico State University, Sep. 1979.

Carver, K.R. and Coffey, E.L. (1979).'Theoretical Investigation of the Microstrip Antenna'. Technical Report, PT-00929, Physical Science Laboratory, New Mexico State University, Las Cruces, NM, USA, Jan. 1979.

Catling, I. and Harbord, B.J. (1985).'Electronic Road Pricing in Hong Kong: the Technology'. Traffic Eng and Control, Dec. 1985, p.608-615.

Chan, T.K., Korolkiewicz, E. and Armstrong, R. (1993).'Design of a Microstrip Antenna Array for a Short Range Two-Way Microwave System'. IEE Colloquium on 'Validation and Application of Design Tools for Antennas', 11th June 1993, p.8.1-8.8.

Cowley, A.M. and Sorensen, H.O. (1966).'Quantitative Comparison of Solid-State Microwave Detectors'. IEEE Trans. MTT-14, Dec. 1966, p.588-602.

Dadds, A.F. and Stocker, B.J. et al (1991).'Final Report on the Design of the PAMELA Roadside Unit and Transponder'. DRIVE project V1030 PAMELA, Deliverable-ME13.

Datta, S. 'Surface Acoustic Wave Devices'. Prentice-Hall.

Davies, P. and Ayland, N. (1989a).'The Heavy Vehicle Electronic Licience Plate (HELP) Programme'. ISATA 20th Int. Symp., Itay.

REFERENCES

Davies, P., Ayland, N. et al (1989b).'Automatic Vehicle Identification for Non-Stop Toll Collection - the Virginia Experience'. Proc. of IEE Int. Conf. Road Traffic Monitoring, UK, p.133-137.

Dawson, J.A.L. and Brown, F.N. (1985).'Electronic Road Pricing in Hong Kong: 1. A fair to go?'. Traffic Engg & Control, Nov. 1985, p.522-529.

Derneryd, A.G. (1976).'Linearly Polarised Microstrip Antennas'. IEEE Trans. Antennas and Propagation, AP-24, p.846-851.

Derneryd, A.G. (1978).'A Theoretical Investigation of the Rectangular Microstrip Antenna Elements.' IEEE Trans. AP-26, p.532-535.

Demuynck, F. and Van de Capelle, A. (1992)'.Higher Order Modes in Microstrip Antenna Design via the Transmission Line Model'. Electronics Letters, 27th August, Vol. 28, p.1732-1734.

Enoksen, R. (1992).'Microwave Specification, OSI layer 1. Technical explanations'. DRIVE-ATT Project ADEPT, Micro-Design A/S.

Foote, R.S. (1980).'Automatic Vehicle Identification: Tests and Applications in the late 1970s". IEEE Trans. VT-29, p.226-9.

Gottwald, G. and Wiesbeck, W. (1993).'Influence of Mutual Coupling and Feed Network on Directivity and Gain'. 8th International Conference on Antenna and Propagation, Conference No. 370, March, 1993.

Guttenberger, M. and Mierzwiak, K.H. et al (1993).'Microstrip Array Antenna for an Automatic Road Pricing System'. 23rd European Microwave Conference, Spain, 6-9 September, 1993.

Hammer, P., Van Bouchaute, D. et al (1979).'A Model for Calculating the Radiation Field of Microstrip Antennas'. IEEE Trans. AP-27, No.2, Mar. 1979, p.267-270.

REFERENCES

Hammerstad, E.O. (1975).'Microstrip Handbook'. Division of Telecommunication, NTNF (The Royal Norwegian Council for Scientific and Industrial Research).

Harrington, R.F. (1961).'Time-Harmonic Electromagnetic Waves'. McGraw-Hill.

Heberling, D. and Winterfield, C. (1992).'Investigations on Mutual Coupling Effects in Polarimetric Conformal Patch - Arrays'. International Conference Radar 92, Conference Publication 365, 12-13 October, 1992.

Holmes, R.F. (1992).'Recent Developments in toll collection facilities at the Dartford River Crossing'. IEE Colloquium on Toll Systems, 2nd Oct. 1992, p.3/1-3.

Howson, D.P. and Gardiner, J.G. (1972).'Image Cancelling Mixers'. Electronics Letters, Vol. 8, No. 14, Jul. 1972, p.352-354.

Huynh, T. and Lee, K.F. et al (1992).'Mutual Coupling Between Rectangular Microstrip Patch Antennas'. Microwave and Optical Technology Letters, Vol. 5, No.11, Oct. 1992, p.572-576.

James, J.R.; Hall, P.S. and Wood, C. (1981).'Microstrip Antenna Theory and Design'. IEE, Peter Peregrinus.

James, J.R. and Hall, P.S. (1989).'Handbook of Microstrip Antennas'. Peter Peregrinus Ltd.

Jedlicka, R.P. and Carver, K.R. (1979).'Mutual Coupling Between Microstrip Antennas'. Proc. of the Workshop on Printed Circuit Antenna Technology, New Mexico State University, Oct.

Jedlicka, R. and Carver, K. (1981).'Measured mutual coupling between microstrip antennas'. IEEE Trans. Antenna and Propagation, AP-29, Jan. 1981, p.147-9.

Jeffery, D.J. and Russam, K. et al (1987a).'Electronic Route Guidance by AUTOGUIDE'. Proc. TRAFFEX'87.

REFERENCES

Jeffery, D.J. (1987b).'Information Technology Applications in Transport'. Edited by P. Bonsai and M. Bell, VNU Science Press, Utrecht.

JTMTA. (1986).'Research and development of AutoMobile Traffic Information and Control System'. The Japan Traffic Management Technology Association.

Kirschning, M.; Jansen, R. and Koster, N.(1981).'Accurate Model for Open End Effect of Microstrip Lines'. Electronics Letters, Vol. 17, p.123-125.

Korolkiewicz, E. (1991).'The Evaluation of the 2.45GHz Microwave Communication Link'. DRIVE project V1030 PAMELA, Deliverable-ME12.

Koshi, M. (1989).'Development of the advanced vehicle-road information systems in Japan, (the CACS project and after)'. Proc. JSK Int Symp, Tokyo, Nov. 1989, p.10-9.

Lewin, L. (1960).'Radiation form Discontinuities in Stripline'. Proc. IEE, Vol. 107c, p.163-170.

Lier, E. (1982).'Improved Forumlas for Input Impedance of Coax-fed Microstrip Patch Antennas.' IEE Proc. H, Vol. 129, p.161-164.

Lier, E. and Jakobsen, K. (1983).'Rectangular Microstrip Patch Antennas with Infinite and Finite Ground Plane Dimensions'. IEEE Trans. AP-31, Nov. 1983, p.978-984.

MITI. (1977).'The Comprehensive Automatic Traffic Control System: A General Description of the Pilot System'. Agency of Industrial Science and Technology, Ministry of International Trade and Industry (MITI), Japan.

Morgan, D.V. and Howes, M.J. (1980).'Microwave Solid State Devices and Applications'. Chapter 14 by Oxley, T.H., p.222-247.

REFERENCES

Moss, N.I. and Griffiths, H.D. (1993).'A Linear and Planar Array Simulation Program for a Macintosh Personal Computer'. 8th International Conference on Antenna and Propagation, March, 1993.

Murphy, M.T. (1990).'Passive 8-16GHz MMIC Image-Reject Mixer'. 12th annual GaAs IC Symp Tech Digest 1990, 7-10 Oct. 1990, p.117-20.

Munson, R.E. (1974).'Conformal Microstrip Antennas and Microstrip Phased Arrays'. IEEE Trans. AP-22, p.74-78.

Nauwelaers, B. and Van de Capelle, A. (1985).'Formulas for the Calculation of Mutual Coupling Between Rectangular Microstrip Antennas'. Proc. Int. Conf. Ant. and Prop., Coventry, p.99-102.

Nauwelaers, B (1993).'Private Communication'.

Okamoto, H. (1989).'Traffic Control in Japan and the development of the advanced mobile traffic information and communication system (AMTICS)'. Proc. JSK Int. Symp., Tokyo, Nov. 1989, p.22-7.

Okamoto, H. and Hase, M. (1990).'The progress of AMTICS - Advanced Mobile Traffic Information and Communication System'. Proc. CONVERGENCE 90, Oct. 1990, p.217-24.

Okamoto, H. and Hase, M. (1991).'Evaluation of the 2nd AMTICS pilot test in Osaka, Japan'. Proc. the 24th ISATA, May 1991, p.381-9.

Oxley, T.H. (1980).'Microwave Solid State Devices and Applications'. Edited by Morgan, D.V. and Howes, M.J., Chapter 14, p.222-247.

Oxley, T.H. and Lord, J.F. et al (1971).'Image Cancelling Mixers'. Proc. of European Microwave Conference.

Parks, F.G. and Bailey, M.C. (1977).'A Low Sidelobe Microstrip Array'. IEEE AP-S Symposium, Sanford, USA, p.77-80, 1977.

REFERENCES

Philips. (1987a).'PREMID: Introduction'. Philips Industrial Automation, 9498-739-068-12.

Philips. (1987b).'PREMID: How Microwave can make Custom Production Profitable'. Philips Industrial Automation, 9498-739-061-12.

Philips. (1987c).'PREMID: Automatic Charging of Tolls'. Philips Industrial Automation, 9498-739-072-12.

Plessey. (1985).'Automatic Vehicle Identification Systems'. Plessey Control System, Publication 8153.

Pozer, D. (1982).'Input impedance and mutual coupling of rectangular microstrip antennas'. IEEE Trans Antennas and Propagation, AP-30, Nov. 1982, p.1191-6.

Pozer, D. and Targonski, S. (1990).'Axial Ratio of Circularly Polarized Antennas with Amplitude and Phase Errors'. Antenna Designer's Notebook, IEEE Antennas and Propagation Magazine, Vol. 32, Oct. 1990, p.45-46.

Pues, H. and Van de Capelle, A. (1982).'Improved Transmission Line Model for the Rectangular Microstrip Antenna'. Proc. of the 7th Colloquium on Microwave Communications, Budapest, Hungary, p.343-346.

Pues, H. and Van de Capelle, A. (1983).'Accurate Transmission-Line Model for the Transmission-Line Model for the Rectangular Microstrip Antenna'. Catholic University of Louvain Internal Report.

Pues, H. and Van de Capelle, A. (1984)'.Accurate transmission-line model for the rectangular microstrip antenna'. Proc. IEE, Vol.131, Pt.H, No.6, Dec. 1984, p.334-340.

Richards, W.F. and Lo, Y.T. et al (1981).'An Improved Theory for Microstrip Antennas and Applications'. IEEE Trans. on Antennas and Propagation, Vol. AP-29, Jan. 1981, p.38-46.

REFERENCES

RACACT. (1975).'Comprehensive Automobile Control System'. Research Association for Comprehensive Automobile Control Technology, Preliminary report.

Razban, T. and Lemaitre, R. et al (1987).'Passive Transponder Card System'. Microwave Journal, Oct. 1987, p.135-146.

Redding, R.T. (1988). 'The use of SAIC ARRTS for Automatic Vehicle Location and Control for the Ottawa-Carleton Regional Transit-Commission'. SAIC, Ottawa, Final Report, May.

Rose, T. (1993).'Intelligent Vehicle Highway Systems: Going Places Fast'. Microwave Journal, May 1993, p.172-8.

Rumsey, V.H. (1954).'The Reaction Concept in Electromagnetic Theory'. Physics Review, ser. 2, Vol. 94, No. 6, 15 June 1954.

Sabounghi, R.L. (1991).'Intelligent Vehicle Highway System - The Universal Close-Range Road/Vehicle Communication System Concept - The Enhanced AVI and Its CVO Applications'. VNIS'91 Vehicle Navigation and Info System Conf. Proc. P-253, Vol. 2, p.957-67.

Saleh, A.A.M. (1971).'Theory of Resistive Mixers'. The M.I.T. Press.

Schwartz, M. (1981).'Information Transmission, Modulation, and Noise'. McGraw Hill, p.432.

Shanmugam, K.S. (1979).'Digital and Analog Communication Systems'. John Wiley & Sons, p.416.

Shibano, Y. and Ikeda, J. et al (1991).'Development of a road automobile communication system (RACS)'. Sumitomo Electric Technical Review, Jan. 1991, Part 31, p.105-12.

Siegal, B. and Pendleton, E. (1975).'Zero Bias Schottky Barrier Diodes as Microwave Detectors'. Microwave Journal, Vol. 18, September, p.40-43.

REFERENCES

Sisodia, M.L. and Raghuvanshi, G.S. (1987).'Microwave Circuits and Passive Devices'. John Wiley & Sons, p.345.

Skadsheim, A . (1988).'PREMID Toll System - Project Description', Philips A/S, Oslo, Norway.

TCC. (1988).'Route Guidance Information Systems Draft Standard for the Road-Vehicle Communication Link'. Dept. of Transport, TCC Div. UK.

TNO/TDP. (1989).'Evaluation of an Infrared and a Microwave Data -Transmission System for Electronic Toll Payment'. Project Rekening Rijiden, Rijkswaterstaot, Netherlands.

Torrey, H.C. and Whitmer, C.A. (1948).'Crystal Rectifiers'. Vol. 15, M.I.T. Rad. Laboratory Ser New York, McGraw Hill.

Tsuzawa, M. and Okamoto, H. (1989a).'Overview of AMTICS'. ISATA, 20th Int. Symposium, Italy.

Tsuzawa, M. and Okamoto, H. (1989b).'Advanced mobile traffic information and communication system - AMTICS'. Conf. Rec. of VNIS'89, Sep. 1989, p.475-83.

Uhlir, A. (1963).'Characterisation of Crystal Diodes for Low-Level Microwave Detection'. Microwave Journal, p.59-67.

Van de Capelle, A. (1989).'Handbook of Microstrip Antennas'. edited by James, J.R. and Hall, P.S., Peter Peregrinus Ltd., Vol. 1, Chapter 10, p.537.

Van de Ziel, A. (1970).'Noise in Solid State Devices and Lasers'. Proc. of IEEE, Vol. 58, Augest, p.1178-1206.

Van Lil, E.H. and Van de Capelle, A.R. (1980).'Approximate coupling formulas for the the coupling between microstrip resonator antennas'. Proc. of the 10th European Microwave Conf., Poland, p.127-131.

REFERENCES

Van Lil, E.H. and Van de Capelle, A.R. (1984).'Transmission Line Model for mutual coupling between microstrip antennas'. IEEE Trans. Antennas and propagation, AP-32, Aug. 1984, p.816-821.

Yumoto, N. (1979a).'Outline of the CACS Pilot Test Scheme'. 58th Annual Meeting of the TRB, Washington DC.

Yumoto, N. and Ihara, H. et al (1979b).'Outline of the comprehensive automobile traffic control pilot test system'. Tran. Res. Rec. 737, Nat. Acad. Sci., p.113-121.

APPENDICES

A. 'Pascal' program to predict the communication zone

B. 'TouchStone' model for the dummy network in the OBU antenna design

C. Nauwelaers algorithms for mutual admittance

D. 'Pascal' program to evaluate the Nauwelaers algorithms

E. Expansions for G_{12} (f=0)

F. Derivation of mutual conductance

G. Pues equations for mutual susceptance (E-Plane)

H. Lier equations for mutual conductance (E-Plane)

I. Derivation of mutual impedance using cavity model

J. 'Pascal' program to predict the radiation pattern including mutual coupling

K. Derivation of diode detector voltage sensitivity

L. Matching network for phase shifter

M. List of Publications

Appendix A - 'Pascal' Program to Predict the Communication Zone

```
PROGRAM Projection_RSU_Array(INPUT,OUTPUT);
{
  Author: T.K.Chan
  Date  : 10th March 1993

  File name: RSUARRAY.PAS

  This progamme is to calculate projection of radiation pattern from
  RSU antenna onto road for the horizontal distance along away from the
  RSU antenna. Thus the power level recevied at the obu for downlink
  and at the rsu for uplink is then calculated and stores in files,
  namely Pr_obu.dat and Pr_rsu.dat.
}
const pi=3.1415; c=3e8; step=36; max_limit=100;
var
  i,theta_o:integer; answer:char;
  h_o,x_o,r_o,f,EIRP,Pt,Grsu,Gobu,Ld,Lu : real;
  { RSU antenna radiation pattern }
  P_ant: packed array [0..step] of real;
  { Communicaton Range }
  r:packed array [0..step] of real;
  x:packed array [0..step] of real;
  Pr_obu:packed array [0..step] of real;
  Pr_rsu:packed array [0..step] of real;

procedure input_data;
begin
    writeln('Do you want to use the default Radiation Pattern of');
    write  ('the RSU antenna? '); readln(answer);
    if (answer='n') or (answer='N') then
    begin
    writeln('Input radiation pattern of RSU antenna in dB (5 deg. per step');
    for i:= 0 to step do
     begin
       write('angle (',i*10/2-90:5:1,') :'); readln(P_ant[i]);
       P_ant[i]:=exp(P_ant[i]*ln(10)/10); {converted from dB}
     end
end
else
begin
  P_ant[0]:=-30; P_ant[10]:=-26; P_ant[20]:=-4;  P_ant[30]:=-17;
  P_ant[1]:=-28; P_ant[11]:=-19; P_ant[21]:=-10; P_ant[31]:=-20;
  P_ant[2]:=-24; P_ant[12]:=-17; P_ant[22]:=-19; P_ant[32]:=-26;
  P_ant[3]:=-22; P_ant[13]:=-19; P_ant[23]:=-19; P_ant[33]:=-29;
```

```
 P_ant[4]:=-19; P_ant[14]:=-34; P_ant[24]:=-16; P_ant[34]:=-28;
 P_ant[5]:=-18; P_ant[15]:=-12; P_ant[25]:=-16; P_ant[35]:=-26;
 P_ant[6]:=-17; P_ant[16]:=-4;  P_ant[26]:=-22; P_ant[36]:=-25;
 P_ant[7]:=-18; P_ant[17]:=-1;  P_ant[27]:=-34;
 P_ant[8]:=-22; P_ant[18]:=0;   P_ant[28]:=-21;
 P_ant[9]:=-34; P_ant[19]:=-1;  P_ant[29]:=-17;
 for i:= 0 to step do
   P_ant[i]:=exp(P_ant[i]*ln(10)/10); {converted from dB}
end;
write('height of the RSU antenna (m): '); readln(h_o);
write('the projection angle, theta_o, (deg.): '); readln(theta_o);
write('Input Operating frequency (Ghz): '); readln(f); f:=f*1e9;
write('Input RSU antenna gain (dBi): '); readln(Grsu);
write('Input OBU antenna gain (dBi): '); readln(Gobu);
write('Input EIRP (W): '); readln(EIRP);
write('Input the total fixed losses for Downlink (dB): '); readln(Ld);
write('                          for Uplink (dB): ');readln(Lu);
Grsu:=exp(Grsu*ln(10)/10);
Gobu:=exp(Gobu*ln(10)/10);
Ld:=exp(Ld*ln(10)/10);
Lu:=exp(Lu*ln(10)/10);
Pt:=EIRP/Grsu;
end;

procedure calculate;
var theta, beta:real;
begin
    x_o:=h_o*sin(theta_o)/cos(theta_o); writeln('x_o=',x_o);
    r_o:=sqrt(h_o*h_o+x_o*x_o);        writeln('r_o=',r_o);
    for i:=0 to step do
    begin
        theta:=i*10/2-90;
        beta:=theta_o+theta;
        if ( (beta>0) or (beta=0) ) and (beta<90) then
        begin
        r[i] := h_o/cos((theta_o+i*10/2-90)*pi/180);
    end else
    if (theta_o>(i*10/2-90)) then r[i]:=h_o else r[i]:=max_limit;
    x[i]:=sqrt(r[i]*r[i]-h_o*h_o);
    writeln(i,' ',r[i],' ',x[i]);
end;
for i:= 0 to (((90-theta_o) div 5)-1) do P_ant[i]:=0;
for i:=0 to step do
begin
```

```
if P_ant[i]=0 then begin Pr_rsu[i]:=-200; Pr_obu[i]:=-200 end else
begin
{Power received at OBU (Downlink)}
Pr_obu[i]:=Pt*Grsu*Gobu*sqr(c/f/4/pi/r[i])*P_ant[i]/Ld;
Pr_obu[i]:=10*ln(Pr_obu[i]/0.001)/ln(10); {in dBm}
{Power received at RSU (Uplink)}
Pr_rsu[i]:=Pt*sqr(Grsu*Gobu)*sqr(sqr(c/f/4/pi/r[i]))*sqr(P_ant[i])/Lu;
Pr_rsu[i]:=10*ln(Pr_rsu[i]/0.001)/ln(10); {in dBm}
writeln(Pr_obu[i],' ',Pr_rsu[i]);
    end;
    end;
end;

procedure output_data;
var dat:text; name:string[12];
begin
    name:='Pr_OBU.dat';
    assign(dat,name);
    rewrite(dat);
    for i:=0 to step do writeln(dat,x[i]);
    for i:=0 to step do writeln(dat,Pr_obu[i]);
    close(dat);
    name:='Pr_RSU.dat';
    assign(dat,name);
    rewrite(dat);
    for i:=0 to step do writeln(dat,x[i]);
    for i:=0 to step do writeln(dat,Pr_rsu[i]);
    close(dat);
end;

begin
    input_data;
    calculate;
    output_data;
end.
```

Appendix B - TouchStone Model for the Dummy Network in the OBU Antenna Design

```
!OBUANT1.CKT
!5.8GHZ CP ANTENNA AT OBU
!SUBSTRATE 5870
DIM
    FREQ GHZ
    LNG MM
    ANG DEG
VAR
    X1#0 6.40506 15
    X2#0 6.12003 15
    WW1#4.2 4.57416 4.6
    WW2#5 5.01063 5.3
    WW3#2 2.47253 2.5
CKT
    MSUB ER=2.33 H=0.79 T=0.0355 RHO=0.709 RGH=0
    TAND TAND=0.0012

    MLIN 1 2 W=4.44 L=5
    MTEE 4 2 3 W1^WW2 W2=4.44 W3^WW1
    MLIN 3 5 W^WW1 L^X1
    MTEE 6 7 5 W1=4.44 W2^WW2 W3^WW1
    MLIN 6 8 W=4.44 L=5
    MLIN 4 12 W^WW2 L^X2
    MLIN 7 15 W^WW2 L^X2
    MTEE 11 12 10 W1=2.28 W2^WW2 W3^WW3
    MTEE 15 13 14 W1^WW2 W2=2.28 W3^WW3
    MLIN 10 14 W^WW3 L^X1
    MLIN 11 9 W=2.28 L=5
    MLIN 13 16 W=2.28 L=5
    DEF4P 9 16 8 1 C1

    C1 1 2 3 4
    RES 3 0 R=31.25
    RES 4 0 R=31.25
    DEF2P 1 2 C2

    C1 1 2 3 4
    RES 3 0 R=51.03
    RES 3 5 R=30.62
    RES 4 0 R=51.03
    RES 4 6 R=30.62
    DEF4P 1 2 5 6 C3
OUT
    C3 DB[S11] GR1
```

```
    C3 DB[S21] GR1
    C3 DB[S31] GR1
    C3 DB[S41] GR1
    C3 ANG[S31] GR1
    C3 ANG[S41] GR1

FREQ
    STEP 5.8
    SWEEP 5 6.6 0.08
OPT
    C3 DB[S11]<-30
    C3 DB[S21]<-30
    C3 DB[S31]=-9.201
    C3 DB[S41]=-9.201
```

Simlulated Results:

FREQ-GHZ	DB[S11] C3	DB[S21] C3	DB[S31] C3	DB[S41] C3	ANG[S31] C3	ANG[S41] C3
5.00000	-9.342	-12.292	-9.175	-11.232	105.750	-171.323
5.08000	-10.207	-12.903	-9.124	-10.930	100.307	-175.211
5.16000	-11.205	-13.633	-9.088	-10.641	94.833	-179.341
5.24000	-12.367	-14.506	-9.067	-10.371	89.346	176.306
5.32000	-13.735	-15.558	-9.062	-10.123	83.862	171.751
5.40000	-15.371	-16.837	-9.070	-9.900	78.396	167.019
5.48000	-17.383	-18.422	-9.091	-9.707	72.963	162.137
5.56000	-19.967	-20.443	-9.121	-9.543	67.572	157.136
5.64000	-23.537	-23.153	-9.160	-9.412	62.227	152.042
5.72000	-29.077	-27.117	-9.203	-9.312	56.932	146.883
5.80000	-34.317	-33.718	-9.250	-9.244	51.681	141.684
5.88000	-27.731	-35.003	-9.298	-9.208	46.469	136.468
5.96000	-22.970	-27.966	-9.346	-9.202	41.286	131.255
6.04000	-19.857	-23.761	-9.392	-9.227	36.121	126.065
6.12000	-17.582	-20.946	-9.437	-9.280	30.963	120.915
6.20000	-15.798	-18.870	-9.481	-9.360	25.801	115.824
6.28000	-14.333	-17.249	-9.525	-9.468	20.626	110.807
6.36000	-13.094	-15.939	-9.569	-9.600	15.432	105.879
6.44000	-12.022	-14.856	-9.615	-9.756	10.215	101.058
6.52000	-11.082	-13.947	-9.664	-9.934	4.976	96.357
6.60000	-10.249	-13.177	-9.717	-10.132	-0.284	91.792

Appendix C - Nauwelaers Algorithms for Mutual Admittance

Mutual Conductance (G_m):

By expanding the sinc function in its McLaurin series G_m is given by

$$G_m(a,c,f) = \frac{a^2}{3\pi\eta_o}\sum_{m=0}^{\infty}(-1)^m 3\left[\frac{EH_m(c,f) - EH_{m+1}(c,f)}{(2m+2)!}\right]a^{2m} \tag{C.1}$$

where

$$EH_m(c,f) = \sum_{i=0}^{m}\left(eh_m^i . f^{2i}\right)\left(\frac{j_{m+i}(r)}{r^{m+i}}\right) \tag{C.2}$$

$$r = \sqrt{c^2 + f^2} \tag{C.3}$$

$$eh_0^0 = 1, \quad eh_0^j = 0\ (j \neq 0), \quad eh_m^{-1} = 0, \quad eh_{m+1}^i = \left(eh_m^i - \frac{eh_m^{i-1}}{2i-1}\right)(2m+1) \tag{C.4}$$

$$j_0(r) = \frac{\sin r}{r} \quad \& \quad j_1(r) = \frac{\sin r - r.\cos r}{r^2} \tag{C.5}$$

$$j_m(r) = \frac{2m-1}{r} j_{m-1}(r) - j_{m-2}(r) \tag{C.6}$$

where $j_m(r)$ are spherical Bessel functions of the first kind and order m.

The series converge for $\sqrt{c^2 + f^2} > 1$.

Mutual Susceptance (B_m):

(1) For $c^2 + f^2 > a^2$:

$$B_m(a,c,f) = \frac{a^2}{3\pi\eta_o}\sum_{m=0}^{\infty}(-1)^m 3\left[\frac{EH_m(c,f) - EH_{m+1}(c,f)}{(2m+2)!}\right]a^{2m} \tag{C.7}$$

where

$$EH_m(c,f) = -\sum_{i=0}^{m}\left(eh_m^i . f^{2i}\right)\left(\frac{y_{m+i}(r)}{r^{m+i}}\right) \tag{C.8}$$

$$r = \sqrt{c^2 + f^2} \tag{C.9}$$

$$eh_0^0 = 1, \quad eh_0^j = 0 \ (j \neq 0), \quad eh_m^{-1} = 0, \quad eh_{m+1}^i = \left(eh_m^i - \frac{eh_m^{i-1}}{2i-1} \right)(2m+1) \tag{C.10}$$

$$y_0(r) = -\frac{\cos r}{r} \quad \& \quad y_1(r) = -\frac{\cos r + r.\sin r}{r^2} \tag{C.11}$$

$$y_m(r) = \frac{2m-1}{r} y_{m-1}(r) - y_{m-2}(r) \tag{C.12}$$

where $y_m(r)$ are spherical Bessel functions of the second kind and order m.

(2) For $c^2 + f^2 < a^2$ and $f = 0$:

$$B_m(a,c,0) = B_m(1,\frac{c}{u},0).\frac{G_s(a)}{G_s(1)}.CF(a,c) \tag{C.13}$$

where $u = 1.0086 - 0.00772a - 0.00085a^2$

$G_S(a)$: self conductance of the slot

($W=a/\beta_0=(a.\lambda_0)/(2.\pi)$, W=width of the patch)

$G_S(1)$: self conductance as $W = 1/\beta_0 = \lambda_0/(2.\pi)$

$$CF = 1 + \frac{(a-1)^{2.55}}{1000} + 0.016(a-1)(c-3.5) + \frac{sign(c-3.7)|c-3.7|^{5.5}\left(25.03 - |a-3.6|^{3.37}\right)1.49}{10000} \tag{C.14}$$

This is valid only for $1 < a < 5$ and $1.2 < c < a+0.1$.

Appendix D - Pascal Program to Evaluate the Nauwelaers Algorithms

Evaluate Gms(a,c,f)

```
Program Nauwelaers(input,output);
{
   To evaluate Gms(a,c,f) using Bart Nauwelaers algorithms

   The series can converge alright
   06/09/93 by T.K. CHAN
}
Const
  pi  = 3.141592654;
  eta = 376.9911184;

Var
  N    :integer;
  a,c,f :real;

Function Power(x:real; y:integer):real;
{ x to the power of y; Power(2,3):=8 }
var k:integer; d0:real;
begin
   if y=0 then power:=1 else
   begin
      d0:=1;
      for k := 1 to y do
      begin
         d0:=x*d0
      end;
      power:=d0
   end;
end;

Function fact(n:integer):real;
{ To calculate factorial of n }
begin
   if n>33 then writeln('Overflow Error in factorial') else
   if n=0 then fact:=1 else
   fact:=n*fact(n-1)
end;

Function j(m:integer; r:real):real;
{ To evaluate 1st kind spherical Bessel function }
```

Appendix D - Pascal Program to Evaluate the Nauwelaers Algorithms

```
{ Input:  ym(x) <---> y(m,r)                    }
Begin
    if (m=0) then j:=sin(r)/r else
    if (m=1) then j:=(sin(r)-r*cos(r))/(r*r) else
    begin
        j:=(2*m-1)*j(m-1,r)/r - j(m-2,r)
    end
end;

Function eh(m:integer; i:integer):real;
Begin
    if (m=0) and (i=0) then eh:=1 else
    if (m=0) and (i<>0) then eh:=0 else
    if (i=-1) then eh:=0 else
    begin
        eh:=( eh(m-1,i)-eh(m-1,i-1)/(2*i-1) )*(2*m-1)
    end
end;

Function EHH(n:integer; c:real; f:real):real;
var i   :integer;
   d0,r:real;
Begin
    r := sqrt(c*c +f*f);
    d0 := 0;
    for i := 0 to n do
    begin
        d0:=eh(n,i)*Power(f,2*i)*j(n+i,r)/Power(r,n+i) + d0;
    end;
    EHH:=d0;
end;

Function Gms(a:real; c:real; f:real):real;
var m :integer;
   d1:real;
Begin
writeln;
d1 := 0;
for m := 0 to N do
begin
    d1:= Power(-1,m)*3*(EHH(m,c,f)-EHH(m+1,c,f))/fact(2*m+2)*
        Power(a,2*m) + d1;
    writeln('m=',m,': Gms= ',d1*a*a/(3*pi*eta));
end;
```

```
    Gms:= d1*a*a/(3*pi*eta);
end;

begin
    write('Input the value of N : ');readln(N);
    write(' a : ');readln(a);
    write(' c : ');readln(c);
    write(' f : ');readln(f);
    writeln('Gms := ',Gms(a,c,f));
end.
```

Evaluating Bms(a,c,f)

```
Program Nauwelaers(input,output);
{
    To evaluate Bms(a,c,f) using Bart Nauwelaers algorithms

    The convergence constraint is:  c*c + f*f > a*a

    06/09/93 by T.K.CHAN
}
Const
   pi  = 3.141592654;
   eta = 376.9911184;

Var
   N     :integer;
   a,c,f :real;

Function Power(x:real; y:integer):real;
{ x to the power of y; Power(2,3):=8 }
var j:integer; d0:real;
begin
    if y=0 then power:=1 else
    begin
        d0:=1;
        for j := 1 to y do
        begin
            d0:=x*d0
        end;
        power:=d0
    end;
end;
```

Appendix D - Pascal Program to Evaluate the Nauwelaers Algorithms

```
Function fact(n:integer):real;
{ To calculate factorial of n }
begin
    if n>33 then writeln('Overflow Error in factorial') else
    if n=0 then fact:=1 else
    fact:=n*fact(n-1)
end;

Function y(m:integer; r:real):real;
{ To evaluate 2nd kind spherical Bessel function }
{ Input:  ym(x) <---> y(m,r)                      }
Begin
    if (m=0) then y:=-cos(r)/r else
    if (m=1) then y:=-(cos(r)+r*sin(r))/(r*r) else
    begin
        y:=(2*m-1)*y(m-1,r)/r - y(m-2,r)
    end
end;

Function eh(m:integer; i:integer):real;
Begin
    if (m=0) and (i=0) then eh:=1 else
    if (m=0) and (i<>0) then eh:=0 else
    if (i=-1) then eh:=0 else
    begin
        eh:=( eh(m-1,i)-eh(m-1,i-1)/(2*i-1) )*(2*m-1)
    end
end;

Function EHH(n:integer; c:real; f:real):real;
var i   :integer;
   d0,r:real;
Begin
    r := sqrt(c*c +f*f);
    d0 := 0;
    for i := 0 to n do
    begin
        d0:=eh(n,i)*Power(f,2*i)*y(n+i,r)/Power(r,n+i) + d0;
    end;
    EHH:=-d0;
end;

Function Bms(a:real; c:real; f:real):real;
var m :integer;
```

```
    d1:real;
Begin
    writeln;
    d1 := 0;
    for m := 0 to N do
    begin
        d1:= Power(-1,m)*3*(EHH(m,c,f)-EHH(m+1,c,f))/fact(2*m+2)*
            Power(a,2*m) + d1;
        writeln('m=',m,' Bms= ',d1*a*a/(3*pi*eta));
    end;
    Bms:= d1*a*a/(3*pi*eta);
end;

begin
    write('Input the value of N : ');readln(N);
    write(' a : ');readln(a);
    write(' c : ');readln(c);
    write(' f : ');readln(f);
    if a<sqrt(c*c+f*f) then
    writeln('Bms := ',Bms(a,c,f)) else
    begin
    writeln('The series will diverge because of c*c+f*f < a;');
    writeln('Please use the curve-fit expressions to find Ym');
    end;
end.

Program Nauwelaers(input,output);
{
    To evaluate Bms(a,c,f) using Bart Nauwelaers algorithms
    Curve-fit expression.

    This is for c*c+f*f < a*a

    07/09/93 by T.K.CHAN
}
Const
   pi  = 3.141592654;
   eta = 376.9911184;

Var
   N              :integer;
   a,c,f,r,W,lambda :real;

Function Power(x:real; y:integer):real;
```

```
{x to the power of y; Power(-1,2):=1 }
var k:integer; d1:real;
begin
    if y=0 then power:= 1 else
    begin
        d1:=1;
        for k:= 1 to y do
        begin
            d1:=x*d1
        end;
        power:=d1
    end;
end;

Function Power_CF(x:real; y:real):real;
{ x to the power of y; Power(2.0,3.0):=8 }
{ x:positive value                       }
begin
    if y=0 then power_CF:=1 else
    if x=0 then power_CF:=0 else
    power_CF:=exp(y*ln(x))
end;

Function fact(n:integer):real;
{ To calculate factorial of n }
begin
    if n>33 then writeln('Overflow Error in factorial') else
    if n=0 then fact:=1 else
    fact:=n*fact(n-1)
end;

Function y(m:integer; r:real):real;
{ To evaluate 2n kind spherical Bessel function }
{ Input:  ym(x) <---> y(m,r)                    }
Begin
    if (m=0) then y:=-cos(r)/r else
    if (m=1) then y:=-(cos(r)+r*sin(r))/(r*r) else
    begin
        y:=(2*m-1)*y(m-1,r)/r - y(m-2,r)
    end
end;

Function eh_m_0(m:integer):real;
Begin
```

```
    if m=0 then eh_m_0:=1 else
    begin
        eh_m_0:=fact(2*m-1)/Power(2,m-1)/fact(m-1);
    end;
end;

Function Gs(a:real):real;
var W:real;
Begin
    W:=a*lambda/(2*pi);
    if W<(0.35*lambda) then Gs:=W*W/(90*lambda*lambda) else
    if (W>(0.35*lambda)) and (W<(2*lambda)) then
                Gs:=W/(120*lambda)-1/(60*pi*pi) else
    if (W=(0.35*lambda)) or (W=(2*lambda)) then
                Gs:=W/(120*lambda)-1/(60*pi*pi) else
    if (W>(2*lambda)) then Gs:=W/(120*lambda);
end;

Function sign(x:real):real;
begin
    if (x>0) or (x=0) then x:=1 else x:=-1;
end;

Function CF(a:real; c:real):real;
begin
    CF:=1 + Power_CF(a-1,2.55)/1000 + 0.016*(a-1)*(c-3.5) +
       (sign(c-3.7)*Power_CF(abs(c-3.7),5.5)*
       (25.03-Power_CF(abs(a-3.6),3.37)))*1.49/10000;
end;

Function EHH(m:integer; cu:real):real;
{ To evaluate EHm(c/u,0) }
begin
    EHH:=-eh_m_0(m)*y(m,cu)/Power_CF(cu,m);
end;

Function Bms_1(cu:real):real;
{ To evaluate Bms(1,c/u)   }
var m    :integer;
    d0,u :real;
begin
    d0:=0;
    for m:=0 to N do
    begin
```

```
        d0:=Power(-1,m)*3*(EHH(m,cu)-EHH(m+1,cu))/Fact(2*m+2)+d0;
    end;
    Bms_1:=d0/(3*pi*eta);
end;

Function Bms(a:real; c:real):real;
var u:real;
begin
    u:=1.0086-0.00772*a-0.00085*a*a;
    Bms:=Bms_1(c/u)*Gs(a)/Gs(1)*CF(a,c);
end;

begin
    writeln('The conditions are: 1<a<5 and 1.2<c<a+0.1 ');
    write('Input the value of N : ');readln(N);
    write(' a : ');readln(a);
    write(' c : ');readln(c);
    writeln(' f : 0.0 ');f:=0;
    r:=sqrt(c*c+f*f);
    write(' wavelegth in air (mm):   ');readln(lambda);lambda:=lambda/1000;

    writeln(' Gs := ',Gs(a));
    writeln(' Bms(a,c,0) : ',Bms(a,c));
end.
```

Appendix E - Expansions for G_{12} (f=0)

Deduction of the G_{12} expansion from the Nauwelaers algorithm

With f=0 the Nauwelaers algorithm is given by

$$G_m(a,c,0) = \frac{a^2}{3\pi\eta_o}\sum_{m=0}^{\infty}(-1)^m 3\left[\frac{EH_m(c,0) - EH_{m+1}(c,0)}{(2m+2)!}\right]a^{2m} \tag{E.1}$$

where $EH_m(c,0) = eh_m^0 \dfrac{j_m(r)}{r^m}$ (only the first term, i=0, is present) (E.2)

and $\mathrm{r} = \mathrm{c};\ eh_0^0 = 1;\ eh_m^{-1} = 0;\ eh_{m+1}^0 = \left\{eh_m^0 - \dfrac{eh_m^{-1}}{2i-1}\right\}(2m+1) = eh_m^0(2m+1);$

(E.3)

$$j_0(r) = \frac{\sin r}{r};\ j_1(r) = \frac{\sin r - r\cos r}{r^2};\ j_m(r) = \frac{2m-1}{r}j_{m-1}(r) - j_{m-2}(r) \tag{E.4}$$

where $j_m(r)$ are spherical Bessel functions of the first kind and order m.

Reverse Analysis

The series converges for c>1. Since, $eh_{m+1}^0 = (2m+1)eh_m^0$ (from E.2)

$$eh_1^0 = eh_0^0;\ eh_2^0 = 3eh_1^0;\ eh_3^0 = 5eh_2^0;\ldots \tag{E.5}$$

hence,

$$eh_1^0 eh_2^0 eh_3^0 \ldots eh_m^0 = eh_0^0 3eh_1^0 5eh_2^0 7eh_3^0 \ldots (2m-1)eh_{m-1}^0 \tag{E.6}$$

therefore,

$$eh_m^0 = 3.5.7\ldots(2m-1)eh_0^0 \tag{E.7}$$

$$eh_m^0 = 3.5.7\ldots(2m-1)eh_0^0 = \frac{(2m-1)!}{2^{m-1}(m-1)!} \tag{E.8}$$

so that

$$EH_m(c,0) = \frac{(2m-1)!}{2^{m-1}(m-1)!}\frac{j_m(c)}{c^m} \tag{E.9}$$

Appendix E - Expansions for G_{12} (f=0)

Now,

$$\sum_{m=0}^{\infty}\frac{(-1)^m 3}{(2m+2)!}\left[EH_m(c,0)-EH_{m+1}(c,0)\right]=\sum_{m=0}^{\infty}\frac{(-1)^m 3EH_m(c,0)}{(2m+2)!}-\sum_{m=0}^{\infty}\frac{(-1)^m 3EH_{m+1}(c,0)}{(2m+2)!}$$

$$=\frac{3EH_0(c,0)}{2}+\sum_{m=1}^{\infty}\frac{(-1)^m 3EH_m(c,0)}{(2m+2)!}-\sum_{m=1}^{\infty}\frac{(-1)^{m+1}3EH_m(c,0)}{(2m)!}$$

$$=\frac{3}{2}EH_0(c,0)+\sum_{m=1}^{\infty}(-1)^m 3EH_m(c,0)\left\{\frac{1}{(2m+2)!}+\frac{1}{(2m)!}\right\}$$

$$=\frac{3}{2}EH_0(c,0)+\sum_{m=1}^{\infty}\frac{(-1)^m 3EH_m(c,0)}{(2m)!}\left\{\frac{1}{(2m+1)(2m+2)}+1\right\} \qquad \text{(E.10)}$$

Since,

$$EH_0(c,0)=j_0(c) \quad \text{and} \quad EH_m(c,0)=\frac{(2m-1)!}{2^{m-1}(m-1)!}\frac{j_m(c)}{c^m}\ ;\ (m\geq 1) \qquad \text{(E.11)}$$

Thus the explicit form of the G_{12} expansion is then

$$G_{12}(a,c,0)=\frac{a^2}{2\pi\eta_o}j_o(c)+\frac{1}{\pi\eta_o}\sum_{m=1}^{\infty}\frac{(-1)^m a^{2m}}{c^m 2^m m!}\left\{\frac{a^2}{(2m+1)(2m+2)}+1\right\}j_m(c) \qquad \text{(E.12)}$$

Derivation of the G_{12} expansion from the modified Nauwelaers source integral

The modified Nauwelaers source integral (f=0) is given by

$$G_{12}=\frac{a^2}{4\pi^2\eta_o}\int_0^{2\pi}\int_0^{1}\sin c^2\left(\frac{a}{2}\sqrt{1-\Psi^2}\sin\theta\right)\left(\cos^2\theta+\Psi^2\sin^2\theta\right)\cos\left(c.\cos\theta\sqrt{1-\Psi^2}\right)d\Psi d\theta \qquad \text{(E.13)}$$

On substituting $\Psi=\cos\alpha$. we have

Appendix E - Expansions for G_{12} (f=0)

$$G_{12} = \frac{4}{\pi^2 \eta_o} \int_0^{\pi/2} \int_0^{\pi/2} \left\{ \frac{\sin^2\left(\frac{a}{2}\sin\alpha\sin\theta\right)\cos(c.\cos\theta\sin\alpha)}{\sin\alpha\sin^2\theta} - \sin^2\left(\frac{a}{2}\sin\alpha\sin\theta\right)\sin\alpha\cos(c.\cos\theta\sin\alpha) \right\} d\alpha d\theta \tag{E.14}$$

Since

$$\sin^2 X = \frac{1}{2}(1-\cos 2X) = \frac{1}{2}\left(1-\left[1-\frac{(2X)^2}{2!}+\frac{(2X)^4}{4!}-\ldots\right]\right)$$

$$= \frac{1}{2}\sum_{m=1}^{\infty}\frac{(2X)^{2m}(-1)^m}{(2m)!} = \frac{1}{2}\sum_{m=0}^{\infty}\frac{(2X)^{2m+2}(-1)^m}{(2m+2)!} \tag{E.15}$$

Thus E.14 can be written as

$$G_{12} = \frac{4}{\pi^2 \eta_o} \int_0^{\pi/2} \int_0^{\pi/2} E(\alpha,\theta) d\alpha d\theta \tag{E.16}$$

where

$$E = \frac{1}{2}\sum_{m=0}^{\infty}\frac{(-1)^m\left(a\sin\alpha\sin\theta\right)^{2m+2}\cos(c.\cos\theta\sin\alpha)}{(2m+2)!\sin\alpha\sin^2\theta} - \frac{1}{2}\sum_{m=0}^{\infty}(-1)^m\left(a\sin\alpha\sin\theta\right)^{2m+2}\sin\alpha\cos(c.\cos\theta\sin\alpha)$$

$$= \frac{1}{2}\sum_{m=0}^{\infty}\frac{(-1)^m a^{2m+2}\sin^{2m+1}\alpha\sin^{2m}\theta\cos(c.\cos\theta\sin\alpha)}{(2m+2)!} - \frac{1}{2}\sum_{m=0}^{\infty}\frac{(-1)^m a^{2m+2}\sin^{2m+3}\alpha\sin^{2m+2}\theta}{(2m+2)!}\cos(c.\cos\theta\sin\alpha)$$

$$= \frac{1}{2}\frac{a^2}{2}\sin\alpha\cos(c.\cos\theta\sin\alpha) + \frac{1}{2}\sum_{m=1}^{\infty}\frac{(-1)^m a^{2m+2}\sin^{2m+1}\alpha\sin^{2m}\theta\cos(c.\cos\theta\sin\alpha)}{(2m+2)!}$$

$$-\frac{1}{2}\sum_{m=1}^{\infty}\frac{(-1)^{m-1}a^{2m}\sin^{2m+1}\alpha\sin^{2m}\theta}{(2m)!}\cos(c.\cos\theta\sin\alpha)$$

$$= \frac{a^2}{4}\sin\alpha\cos(c.\cos\theta\sin\alpha) + \frac{1}{2}\sum_{m=1}^{\infty}\sin^{2m+1}\alpha\sin^{2m}\theta\left\{\frac{a^{2m+2}}{(2m+2)!}+\frac{a^{2m}}{(2m)!}\right\}\cos(c.\cos\theta\sin\alpha)\,(-1)^m \tag{E.17}$$

Appendix E - Expansions for G_{12} (f=0)

Since

$$\frac{a^{2m+2}}{(2m+2)!}+\frac{a^{2m}}{(2m)!}=\frac{a^{2m}}{(2m)!}\left\{\frac{a^2}{(2m+1)(2m+2)}+1\right\} \tag{E.18}$$

E.17 becomes

$$E=\frac{a^2}{4}\sin\alpha\cos(c.\cos\theta\sin\alpha)+\frac{1}{2}\sum_{m=1}^{\infty}\frac{(-1)^m a^{2m}}{(2m)!}\left\{\frac{a^2}{(2m+1)(2m+2)}+1\right\}\sin^{2m+1}\alpha\sin^{2m}\theta\cos(c.\cos\theta\sin\alpha) \tag{E.19}$$

We now have (Bell, 1968)

$$\int_0^{\pi/2}\int_0^{\pi/2}\sin\alpha\cos(c.\cos\theta\sin\alpha)d\alpha d\theta=\frac{\pi}{2}j_o(c) \tag{E.20}$$

and

$$\int_0^{\pi/2}\int_0^{\pi/2}\sin^{2m+1}\alpha\sin^{2m}\theta\cos(c.\cos\theta\sin\alpha)d\alpha d\theta=\frac{\pi(2m-1)!}{c^m 2^m(m-1)!}j_m(c) \tag{E.21}$$

On substituting E.19, E.20 and E.21 into E.16, finally G_{12} is given by

$$G_{12}(a,c,0)=\frac{a^2}{2\pi\eta_o}j_o(c)+\frac{1}{\pi\eta_o}\sum_{m=1}^{\infty}\frac{(-1)^m a^{2m}}{c^m 2^m m!}\left\{\frac{a^2}{(2m+1)(2m+2)}+1\right\}j_m(c) \tag{E.22}$$

Reference

Bell,W.W. (1968).'SPECIAL FUNCTIONS for scientists and engineers'. Van Nostrand.

Appendix F - Derivation of Mutual Conductance

Mutual Conductance (G_{12}):

The equation for G_{12} is given by

$$G_{12} = \frac{a^2}{4\pi^2 \eta_o} \int_0^{2\pi} \int_0^1 \sin c^2 \left(\frac{a}{2}\sqrt{1-\Psi^2}\sin\theta\right) \sin c^2 \left(\frac{b}{2}\sqrt{1-\Psi^2}\cos\theta\right)$$

$$\left(\cos^2\theta + \Psi^2 \sin^2\theta\right) \cos\left[\left(c.\cos\theta + f.\sin\theta\right)\sqrt{1-\Psi^2}\right] d\Psi d\theta \qquad \text{(F.1)}$$

where $a=kW$; $b=k\delta L$; $c=k\Delta y$; $f=k\Delta x$ and $k=2\pi/\lambda_o$.

Assuming the width of the radiating slot is much smaller than the wavelength in free space, i.e. $b \to 0$ and substituting Ψ by $\cos\alpha$. After rearranging terms and changing the upper and the lower limits of the integration, we have

$$G_{12} = \frac{2}{\pi^2 \eta_o}\left(I_1 - I_2\right) \qquad \text{(F.2)}$$

where

$$I_1 = \int_0^{\pi} \int_0^{\pi/2} \frac{\sin^2\left(\frac{a}{2}\sin\theta\sin\alpha\right)}{\sin^2\theta\sin^2\alpha} \cos\left\{\left(c.\cos\theta + f.\sin\theta\right)\sin\alpha\right\} \sin\alpha \, d\alpha d\theta \qquad \text{(F.3)}$$

$$I_2 = \int_0^{\pi} \int_0^{\pi/2} \sin^2\left(\frac{a}{2}\sin\theta\sin\alpha\right) \cos\left\{\left(c.\cos\theta + f.\sin\theta\right)\sin\alpha\right\} \sin\alpha \, d\alpha d\theta \qquad \text{(F.4)}$$

For I_2:

Let $X = \frac{a}{2}\sin\theta\sin\alpha$ and $Y = \left(c.\cos\theta + f.\sin\theta\right)\sin\alpha$, I_2 may be writtern as

$$I_2 = \frac{1}{2}\int_0^{\pi} \int_0^{\pi/2} \left(1-\cos 2X\right)\cos Y.\sin\alpha \, d\alpha d\theta \qquad \text{(F.5)}$$

Now

Appendix F - Derivation of Mutual Conductance

$$(1-\cos 2X)\cos Y.\sin\alpha = \frac{1}{2}\{2\cos Y - \cos(2X+Y) - \cos(2X-Y)\}\sin\alpha \qquad \text{(F.6)}$$

$$\cos Y = \sum_{m=0}^{\infty}\frac{(-1)^m Y^{2m}}{(2m)!} = 1+\sum_{m=1}^{\infty}\frac{(-1)^m Y^{2m}}{(2m)!} \qquad \text{(F.7)}$$

$$\cos(2X+Y) = 1+\sum_{m=1}^{\infty}\frac{(-1)^m(2X+Y)^{2m}}{(2m)!} \quad \text{where } 2X+Y = (c.\cos\theta + A.\sin\theta)\sin\alpha \qquad \text{(F.8)}$$

$$\cos(2X-Y) = 1+\sum_{m=1}^{\infty}\frac{(-1)^m(2X-Y)^{2m}}{(2m)!} \quad \text{where } 2X-Y = -(c.\cos\theta + B.\sin\theta)\sin\alpha \qquad \text{(F.9)}$$

where A=f+a and B=f-a. Substitute F.7-F.9 into F.6, we then have

$$(1-\cos 2X)\cos Y\sin\alpha = \frac{1}{2}\sum_{m=1}^{\infty}\frac{(-1)^m}{(2m)!}\{2Y^{2m} - (2X+Y)^{2m} - (2X-Y)^{2m}\}\sin\alpha$$

$$= \frac{1}{2}\sum_{m=1}^{\infty}\frac{(-1)^m}{(2m)!}E_m(X,Y)\sin\alpha$$

$$= \left\{-\frac{1}{4}E_1(X,Y) + \frac{1}{2}\sum_{m=2}^{\infty}\frac{(-1)^m}{(2m)!}E_m(X,Y)\right\}\sin\alpha \qquad \text{(F.10)}$$

where $$E_m(X,Y) = 2Y^{2m} - (2X+Y)^{2m} - (2X-Y)^{2m} \qquad \text{(F.11)}$$

and $$-\frac{1}{4}E_1(X,Y) = 2X^2 = \frac{a^2}{2}\sin^2\theta\sin^2\alpha. \qquad \text{(F.12)}$$

For m≥2:

Appendix F - Derivation of Mutual Conductance

$$E_m(X,Y) = 2(c.\cos\theta + f.\sin\theta)^{2m}\sin^{2m}\alpha - (c.\cos\theta + A.\sin\theta)^{2m}\sin^{2m}\alpha - (c.\cos\theta + B.\sin\theta)^{2m}\sin^{2m}\alpha$$

$$= \left\{2(c.\cos\theta + f.\sin\theta)^{2m} - (c.\cos\theta + A.\sin\theta)^{2m} - (c.\cos\theta + B.\sin\theta)^{2m}\right\}\sin^{2m}\alpha \qquad \text{(F.13)}$$

so that on using the binomial expansion

$$\frac{E_m(X,Y)}{\sin^{2m}\alpha} = 2\sum_{i=0}^{2m}\frac{(2m)!}{(2m-i)!i!}(c.\cos\theta)^{2m-i}(f.\sin\theta)^i$$

$$-\sum_{i=0}^{2m}\frac{(2m)!}{(2m-i)!i!}(c.\cos\theta)^{2m-i}(A.\sin\theta)^i$$

$$-\sum_{i=0}^{2m}\frac{(2m)!}{(2m-i)!i!}(c.\cos\theta)^{2m-i}(B.\sin\theta)^i$$

$$= \sum_{i=0}^{2m}\frac{(2m)!}{(2m-i)!i!}(c.\cos\theta)^{2m-i}\left\{2(f.\sin\theta)^i - (A.\sin\theta)^i - (B.\sin\theta)^i\right\}$$

$$= \sum_{i=0}^{2m}\frac{(2m)!}{(2m-i)!i!}\left\{2f^i - A^i - B^i\right\}\cos^{2m-i}\theta\sin^i\theta \qquad \text{(F.14)}$$

Also

$$\int_0^{\pi}\int_0^{\pi/2}\left\{-\frac{1}{4}E_1(X,Y)\right\}\sin\alpha\, d\alpha d\theta = \int_0^{\pi}\int_0^{\pi/2}\frac{a^2}{2}\sin^2\theta\sin^3\alpha\, d\alpha d\theta$$

$$= \frac{a^2}{2}\int_0^{\pi}\sin^2\theta\, d\theta\int_0^{\pi/2}\sin^3\alpha\, d\alpha = \frac{a^2}{2}\frac{\pi}{2}\frac{2}{3} = \frac{\pi a^2}{6} \qquad \text{(F.15)}$$

Substituting F.14 and F.15 into F.10 and F.5, I_2 is then given by

$$I_2 = \frac{\pi a^2}{12} + \frac{1}{4}\sum_{m=2}^{\infty}\frac{(-1)^m}{(2m)!}\int_0^{\pi}\int_0^{\pi/2}E_m(X,Y)\sin\alpha\, d\alpha d\theta \qquad \text{(F.16)}$$

where

$$\int_0^{\pi}\int_0^{\pi/2} E_m(X,Y)\sin\alpha\, d\alpha d\theta$$

$$= \sum_{i=0}^{2m} \frac{(2m)!c^{2m-i}}{(2m-i)!i!}\left(2f^i - A^i - B^i\right)\int_0^{\pi}\int_0^{\pi/2} \cos^{2m-i}\theta \sin^i\theta \sin^{2m+1}\alpha\, d\alpha d\theta \qquad \text{(F.17)}$$

Since, when i=0, $2f^0-A^0-B^0=2-1-1=0$, therefore F.17 becomes

$$\int_{-0}^{\pi}\int_0^{\pi/2} E_m(X,Y)\sin\alpha\, d\alpha d\theta$$

$$= \sum_{i=1}^{2m} \frac{(2m)!c^{2m-i}}{(2m-i)!i!}\left(2f^i - A^i - B^i\right)\int_0^{\pi} \cos^{2m-i}\theta \sin^i\theta\, d\theta \int_0^{\pi/2} \sin^{2m+1}\alpha\, d\alpha \qquad \text{(F.18)}$$

where a primary objective of converting the double integration into the product of two single integrations is achieved.

The elementary integral in the variable α is given by

$$\int_0^{\pi/2} \sin^{2m+1}\alpha d\alpha = \frac{2^{2m}(m!)^2}{(2m+1)!} \qquad \text{(F.19)}$$

In the interval $[0,\pi]$, $\sin\theta$ is an even function while $\cos\theta$ is an odd function with respect to $\theta = \pi/2$ so the above θ integration is zero if 'i' is an odd integer, and when 'i' is an even integer the integral is twice that over the half interval $[0,\pi/2]$. Hence the θ integration is obtained as

Appendix F - Derivation of Mutual Conductance

$$\int_0^{\pi}\cos^{2m-i}\theta\sin^{i}\theta\,d\theta = 2\int_0^{\pi/2}\cos^{2m-2i}\theta\sin^{2i}\theta\,d\theta$$

$$= \begin{cases} 2\cdot\dfrac{(2m-2i-1)!(2i-1)!\,\pi}{2^{2m-1}(m-i-1)!(i-1)!m!} & ;\ i<m \\ \\ 2\cdot\dfrac{(2m-1)!\,\pi}{2^{2m}m!(m-1)!} & ;\ i=m \end{cases} \qquad \text{(F.20)}$$

Substitute F.19 and F.20 into F.18, and replace 2m by m, giving

$$\int_0^{\pi}\int_0^{\pi/2} E_m(X,Y)\sin\alpha\,d\alpha d\theta$$

$$= \sum_{i=1}^{m}\frac{(2m)!c^{2m-2i}\left(2f^{2i}-A^{2i}-B^{2i}\right)}{(2m-2i)!(2i)!}\left\{\int_0^{\pi}\cos^{2m-2i}\theta\sin^{2i}\theta\,d\theta\right\}\frac{2^{2m}(m!)^2}{(2m+1)!}$$

$$= \sum_{i=1}^{m-1}\frac{(2m)!c^{2m-2i}\left(2f^{2i}-A^{2i}-B^{2i}\right)}{(2m-2i)!(2i)!}\left\{\frac{2(2m-2i-1)!(2i-1)!\,\pi}{2^{2m-1}(m-i-1)!(i-1)!m!}\right\}\frac{2^{2m}(m!)^2}{(2m+1)!}$$

$$+\frac{(2m)!\left(2f^{2m}-A^{2m}-B^{2m}\right)}{(2m)!}\frac{2(2m-1)!\,\pi}{2^{2m}m!(m-1)!}\frac{2^{2m}(m!)^2}{(2m+1)!} \qquad \text{(F.21)}$$

Substitute F.21 into F.16, I_2 becomes

$$I_2 = \frac{\pi a^2}{12}+\frac{\pi}{4}\sum_{m=2}^{\infty}\frac{(-1)^m}{(2m+1)!}\left\{2f^{2m}-A^{2m}-B^{2m}\right\}$$

$$+\frac{\pi}{4}\sum_{m=2}^{\infty}\frac{(-1)^m m!}{(2m+1)!}\sum_{i=1}^{m-1}\frac{c^{2m-2i}\left(2f^{2i}-A^{2i}-B^{2i}\right)}{(m-i)!i!} \qquad \text{(F.22)}$$

Further since,

Appendix F - Derivation of Mutual Conductance

$$m!\sum_{i=1}^{m-1}\frac{c^{2m-2i}\left(2f^{2i}-A^{2i}-B^{2i}\right)}{(m-i)!i!}=\sum_{i=0}^{m}\frac{m!\left(c^2\right)^{m-i}}{(m-i)!i!}\left(2f^{2i}-A^{2i}-B^{2i}\right)-\left(2f^{2m}-A^{2m}-B^{2m}\right) \tag{F.23}$$

therefore, F.22 takes the form

$$I_2=\frac{\pi a^2}{12}+\frac{\pi}{4}\sum_{m=2}^{\infty}\frac{(-1)^m}{(2m+1)!}\left(2f^{2m}-A^{2m}-B^{2m}\right)$$

$$+\frac{\pi}{4}\sum_{m=2}^{\infty}\frac{(-1)^m}{(2m+1)!}\sum_{i=0}^{m}\frac{m!\left(c^2\right)^{m-i}}{(m-i)!i!}\left(2f^{2i}-A^{2i}-B^{2i}\right)-\frac{\pi}{4}\sum_{m=2}^{\infty}\frac{(-1)^m}{(2m+1)!}\left(2f^{2m}-A^{2m}-B^{2m}\right)$$

$$=\frac{\pi a^2}{12}+\frac{\pi}{4}\sum_{m=2}^{\infty}\frac{(-1)^m}{(2m+1)!}\sum_{i=0}^{m}\frac{m!\left(c^2\right)^{m-i}}{(m-i)!i!}\left(2\left(f^2\right)^i-\left(A^2\right)^i-\left(B^2\right)^i\right) \tag{F.24}$$

Noting the binomial expansion, $\left(a^2+b^2\right)^m=\sum_{i=0}^{m}\frac{\left(a^2\right)^{m-i}\left(b^2\right)^i m!}{(m-i)!i!}$, the summation on '$i$' above is replaced by closed forms as follows:

$$\sum_{i=0}^{m}\left\{2\left(f^2\right)^i-\left(A^2\right)^i-\left(B^2\right)^i\right\}\frac{\left(c^2\right)^{m-i}m!}{(m-i)!i!}=2\left(c^2+f^2\right)^m-\left(c^2+A^2\right)^m-\left(c^2+B^2\right)^m \tag{F.25}$$

Substituting F.25 into F.24 then gives

$$I_2=\frac{\pi a^2}{12}+\frac{\pi}{4}\sum_{m=2}^{\infty}\frac{(-1)^m}{(2m+1)!}\left\{2\left(c^2+f^2\right)^m-\left(c^2+A^2\right)^m-\left(c^2+B^2\right)^m\right\}$$

$$=\frac{\pi a^2}{12}+\frac{\pi}{4}\sum_{m=0}^{\infty}\frac{(-1)^m}{(2m+1)!}\left\{2\left(c^2+f^2\right)^m-\left(c^2+A^2\right)^m-\left(c^2+B^2\right)^m\right\}$$

$$-\frac{\pi}{4}\frac{(-1)}{3!}\left\{2\left(c^2+f^2\right)-\left(c^2+A^2\right)-\left(c^2+B^2\right)\right\}$$

$$= \frac{\pi a^2}{12} + \frac{\pi}{24}\left(2f^2 - A^2 - B^2\right) + \frac{\pi}{4}\sum_{m=0}^{\infty}\frac{(-1)^m}{(2m+1)!}\left\{2\left(c^2+f^2\right)^m - \left(c^2+A^2\right)^m - \left(c^2+B^2\right)^m\right\}$$

$$= \frac{\pi}{4}\sum_{m=0}^{\infty}\frac{(-1)^m}{(2m+1)!}\left\{2\left(\sqrt{c^2+f^2}\right)^{2m} - \left(\sqrt{c^2+A^2}\right)^{2m} - \left(\sqrt{c^2+B^2}\right)^{2m}\right\} \qquad \text{(F.26)}$$

Finally since $\sum_{m=0}^{\infty}\frac{(-1)^m X^{2m}}{(2m+1)!} = \frac{\sin X}{X}$, F.26 then gives the closed form expression for I_2

$$I_2 = \frac{\pi}{4}\left[\frac{2\sin\sqrt{c^2+f^2}}{\sqrt{c^2+f^2}} - \frac{\sin\sqrt{c^2+A^2}}{\sqrt{c^2+A^2}} - \frac{\sin\sqrt{c^2+B^2}}{\sqrt{c^2+B^2}}\right] \qquad \text{(F.27)}$$

For I_1:

From F.3:

$$I_1 = \int_0^{\pi}\int_0^{\pi/2}\frac{\sin^2\left(\frac{a}{2}\sin\theta\sin\alpha\right)}{\sin^2\theta\sin^2\alpha}\cos\left\{\left(c.\cos\theta + f.\sin\theta\right)\sin\alpha\right\}\sin\alpha\, d\alpha d\theta \qquad \text{(F.3)}$$

Let $X = \frac{a}{2}\sin\theta\sin\alpha$ and $Y = \left(c.\cos\theta + f.\sin\theta\right)\sin\alpha$, F.3 becomes

$$I_1 = \frac{1}{2}\int_0^{\pi}\int_0^{\pi/2}\frac{(1-\cos 2X)\cos Y.\sin\alpha}{\sin^2\theta\sin^2\alpha}\, d\alpha d\theta \qquad \text{(F.28)}$$

Substituting F.10 into F.28, gives

$$I_1 = \frac{1}{2}\int_0^{\pi}\int_0^{\pi/2}\frac{-\frac{1}{4}E_1(X,Y) + \frac{1}{2}\sum_{m=2}^{\infty}\frac{(-1)^m}{(2m)!}E_m(X,Y)}{\sin^2\theta\sin^2\alpha}\sin\alpha\, d\alpha d\theta \qquad \text{(F.29)}$$

Now

Appendix F - Derivation of Mutual Conductance

$$\frac{1}{2}\int_0^{\pi}\int_0^{\pi/2}\frac{-\frac{1}{4}E_1(X,Y)}{\sin^2\theta\sin\alpha}d\alpha d\theta=\frac{1}{2}\int_0^{\pi}\int_0^{\pi/2}\frac{a^2}{2}\frac{\sin^2\theta\sin^2\alpha}{\sin^2\theta\sin\alpha}d\alpha d\theta=\frac{a^2}{4}\int_0^{\pi}\int_0^{\pi/2}\sin\alpha\, d\alpha d\theta=\frac{\pi a^2}{4} \tag{F.30}$$

For the integral

$$\int_0^{\pi}\int_0^{\pi/2}\frac{E_m(X,Y)}{\sin^2\theta\sin\alpha}d\alpha d\theta \tag{F.31}$$

Substituting F.14 into F.31 and replacing 2m by m, gives

$$\int_0^{\pi}\int_0^{\pi/2}\frac{\bar{E}_m(X,Y)}{\sin^2\theta\sin\alpha}d\alpha d\theta=\sum_{i=1}^{m}\frac{(2m)!c^{2m-2i}\left(2f^{2i}-A^{2i}-B^{2i}\right)}{(2m-2i)!(2i)!}\left(\int_0^{\pi}\cos^{2m-2i}\theta\sin^{2i-2}\theta d\theta\right)\left(\int_0^{\pi/2}\sin^{2m-1}\alpha d\alpha\right)$$

$$=\left(2f^{2m}-A^{2m}-B^{2m}\right)\int_0^{\pi}\sin^{2m-2}\theta d\theta\int_0^{\pi/2}\sin^{2m-1}\alpha d\alpha$$

$$+\sum_{i=1}^{m-1}\frac{(2m)!c^{2m-2i}\left(2f^{2i}-A^{2i}-B^{2i}\right)}{(2m-2i)!(2i)!}\left(\int_0^{\pi}\cos^{2m-2i}\theta\sin^{2i-2}\theta d\theta\right)\left(\int_0^{\pi/2}\sin^{2m-1}\alpha d\alpha\right) \tag{F.32}$$

where the first term of F.32 is for i=m while the second term is for i<m. The first integral above yields

$$\int_0^{\pi}\sin^{2m-2}\theta d\theta\int_0^{\pi/2}\sin^{2m-1}\alpha d\alpha=2\int_0^{\pi/2}\sin^{2m-2}\theta d\theta\int_0^{\pi/2}\sin^{2m-1}\alpha d\alpha$$

$$=2\cdot\frac{(2m-3)!\,\pi}{2^{2m-2}(m-1)!(m-2)!}\cdot\frac{2^{2m-2}\left((m-1)!\right)^2}{(2m-1)!}=\frac{2\pi(2m-3)!(m-1)!}{(m-2)!(2m-1)!}=\frac{\pi}{2m-1} \tag{F.33}$$

In the second integral the θ-integration gives $(i\neq m)$

$$\int_0^{\pi}\cos^{2m-2i}\theta\sin^{2i-2}\theta d\theta=2\int_0^{\pi/2}\cos^{2m-2i}\theta\sin^{2i-2}\theta d\theta$$

$$= \begin{cases} 2 \cdot \dfrac{(2m-3)!\,\pi}{2^{2m-2}(m-1)!(m-2)!} & ; \text{for i} = 1 \\ 2 \cdot \dfrac{(2\text{m}-2\text{i}-1)!(2\text{i}-3)!\,\pi}{2^{2\text{m}-3}(m-i-1)!(i-2)!(m-1)!} & ; \text{for i} \geq 2 \end{cases} \qquad \text{(F.34)}$$

and for $i = m$

$$\int_0^{\pi/2} \sin^{2m-1}\alpha d\alpha = \frac{2^{2m-2}\left((m-1)!\right)^2}{(2m-1)!} \qquad \text{(F.35)}$$

Substitute F.33, F.34 and F.35 into F.32 and then F.30 into F.29, whence I_1 is obtained as

$$I_1 = \frac{\pi a^2}{4} + \frac{1}{4}\int_0^{\pi}\int_0^{\pi/2}\sum_{m=2}^{\infty}\frac{(-1)^m}{(2m)!}\frac{E_m(X,Y)}{\sin^2\theta\sin\alpha}d\alpha d\theta$$

$$= \frac{\pi a^2}{4} + \frac{1}{4}\sum_{m=2}^{\infty}\frac{(-1)^m}{(2m)!}\int_0^{\pi}\int_0^{\pi/2}\frac{E_m(X,Y)}{\sin^2\theta\sin\alpha}d\alpha d\theta \qquad \text{(F.36)}$$

It is convenient at this point to extract the term with m=2:

$$\frac{1}{4}\cdot\frac{1}{4!}\int_0^{\pi}\int_0^{\pi/2}\frac{E_2(X,Y)}{\sin^2\theta\sin\alpha}d\alpha d\theta$$

$$= \frac{1}{96}\left\{\left(2f^4 - A^4 - B^4\right)\int_0^{\pi}\sin^2\theta d\theta + \frac{4!c^2\left(2f^2 - A^2 - B^2\right)}{2!2!}\int_0^{\pi}\cos^2\theta d\theta\right\}\int_0^{\pi/2}\sin^3\alpha d\alpha \qquad \text{(F.37)}$$

Since $\int_0^{\pi}\sin^2\theta d\theta = \int_0^{\pi}\cos^2\theta d\theta = \frac{\pi}{2}$ and $\int_0^{\pi/2}\sin^3\alpha d\alpha = \frac{2}{3}$, F.37 becomes

$$\frac{\pi}{96}\left\{\frac{2f^4 - A^4 - B^4}{3} + 2c^2\left(2f^2 - A^2 - B^2\right)\right\} \qquad \text{(F.38)}$$

Since $2f^4\text{-}A^4\text{-}B^4 = -2a^2(6f^2+a^2)$ and $2f^2\text{-}A^2\text{-}B^2 = -2a^2$, F.38 is therefore

$$-\frac{\pi a^2\left(6f^2+a^2\right)}{144}-\frac{\pi a^2c^2}{24} \tag{F.39}$$

Substiuting F.39 into F.36, gives

$$I_1=\frac{\pi a^2}{4}-\frac{\pi a^2\left(6f^2+a^2\right)}{144}-\frac{\pi a^2c^2}{24}+\frac{1}{4}\sum_{m=3}^{\infty}\frac{(-1)^m}{(2m)!}\int_0^{\pi}\int_0^{\pi/2}\frac{E_m(X,Y)}{\sin^2\theta\sin\alpha}d\alpha d\theta$$

$$=\frac{\pi a^2}{4}\left\{1-\frac{c^2}{6}-\frac{6f^2+a^2}{36}\right\}+\frac{\pi}{4}\sum_{m=3}^{\infty}\frac{(-1)^m}{(2m)!(2m-1)}\left(2f^{2m}-A^{2m}-B^{2m}\right)$$

$$+\frac{\pi}{4}\sum_{m=3}^{\infty}\frac{(-1)^m}{(2m)!}\frac{(2m)!c^{2m-2}\left(2f^2-A^2-B^2\right)}{(2m-2)!}\frac{2(2m-3)!}{2^{2m-2}(m-1)!(m-2)!}\frac{2^{2m-2}\left((m-1)!\right)^2}{(2m-1)!}$$

$$+\frac{\pi}{4}\sum_{m=3}^{\infty}\frac{(-1)^m}{(2m)!}\sum_{i=2}^{m-1}\frac{(2m)!c^{2m-2i}\left(2f^{2i}-A^{2i}-B^{2i}\right)}{(2m-2i)!(2i)!}\frac{2(2m-2i-1)!(2i-3)!}{2^{2m-3}(m-i-1)!(i-2)!(m-1)!}\frac{2^{2m-2}\left((m-1)!\right)^2}{(2m-1)!}$$

$$=\frac{\pi a^2}{4}\left\{1-\frac{c^2}{6}-\frac{6f^2+a^2}{36}\right\}+\frac{\pi}{8}\sum_{m=3}^{\infty}\frac{(-1)^m}{(2m-1)!m(2m-1)}\left(2f^{2m}-A^{2m}-B^{2m}\right)$$

$$+\frac{\pi}{8}\sum_{m=3}^{\infty}\frac{(-1)^mc^{2m-2}\left(2f^2-A^2-B^2\right)}{(2m-1)!}+\frac{\pi}{8}\sum_{m=3}^{\infty}\frac{(-1)^m(m-1)!}{(2m-1)!}\sum_{i=2}^{m-1}\frac{c^{2m-2i}\left(2f^{2i}-A^{2i}-B^{2i}\right)}{(2i-1)(m-i)!i!} \tag{F.40}$$

Since $2f^2-A^2-B^2=-2a^2$, F.40 becomes

$$= \frac{\pi a^2}{4}\left\{1-\frac{c^2}{6}-\frac{6f^2+a^2}{36}\right\}+\frac{\pi}{8}\sum_{m=3}^{\infty}\frac{(-1)^m}{(2m-1)!m(2m-1)}\left(2f^{2m}-A^{2m}-B^{2m}\right)$$

$$-\frac{\pi a^2}{4}\sum_{m=3}^{\infty}\frac{(-1)^m c^{2m-2}}{(2m-1)!}+\frac{\pi}{8}\sum_{m=3}^{\infty}\frac{(-1)^m(m-1)!}{(2m-1)!}\sum_{i=2}^{m-1}\frac{c^{2m-2i}\left(2f^{2i}-A^{2i}-B^{2i}\right)}{(2i-1)(m-i)!i!} \qquad \text{(F.41)}$$

In the third term of F.41, by replace m by m+1 so that

$$-\frac{\pi a^2}{4}\sum_{m=3}^{\infty}\frac{(-1)^m c^{2m-2}}{(2m-1)!}=\frac{\pi a^2}{4}\sum_{m=2}^{\infty}\frac{(-1)^m c^{2m}}{(2m+1)!}$$

$$=\frac{\pi a^2}{4c}\sum_{m=2}^{\infty}\frac{(-1)^m c^{2m+1}}{(2m+1)!}=\frac{\pi a^2}{4c}\left\{\sum_{m=0}^{\infty}\frac{(-1)^m c^{2m+1}}{(2m+1)!}-c+\frac{c^3}{6}\right\}$$

$$=\frac{\pi a^2}{4c}\left(\sin c-c+\frac{c^3}{6}\right)=\frac{\pi a^2}{4}\left(\frac{\sin c}{c}-1+\frac{c^2}{6}\right) \qquad \text{(F.42)}$$

Substituting F.42 into F.41, then gives

$$I_1=\frac{\pi a^2}{4}\left\{\frac{\sin c}{c}-\frac{6f^2+a^2}{36}\right\}+\frac{\pi}{8}\sum_{m=3}^{\infty}\frac{(-1)^m\left(2f^{2m}-A^{2m}-B^{2m}\right)}{(2m-1)!m(2m-1)} \qquad \text{(F.43)}$$

$$+\frac{\pi}{8}\sum_{m=3}^{\infty}\frac{(-1)^m(m-1)!}{(2m-1)!}\sum_{i=2}^{m-1}\frac{c^{2m-2i}\left(2f^{2i}-A^{2i}-B^{2i}\right)}{(2i-1)(m-i)!i!}$$

Consider the second term of F.43:

$$\frac{1}{m(2m-1)(2m-1)!}=\left(\frac{2}{2m-1}-\frac{2}{2m}\right)\frac{1}{(2m-1)!}=\frac{2}{(2m-1)(2m-1)!}-\frac{2}{(2m)!} \qquad \text{(F.44)}$$

Therefore, the second term of F.43 becomes

$$\sum_{m=3}^{\infty}\frac{(-1)^m\left(2f^{2m}-A^{2m}-B^{2m}\right)}{(2m-1)!m(2m-1)}$$

$$=\sum_{m=0}^{\infty}\frac{(-1)^m\left(2f^{2m}-A^{2m}-B^{2m}\right)}{(2m-1)!m(2m-1)}-(-1)\left(2f^{2}-A^{2}-B^{2}\right)-\frac{(-1)^2\left(2f^{4}-A^{4}-B^{4}\right)}{3!2!3}$$

$$=-2a^2+\frac{a^2}{18}\left(6f^2+a^2\right)+2\sum_{m=0}^{\infty}\frac{(-1)^m\left(2f^{2m}-A^{2m}-B^{2m}\right)}{(2m-1)(2m-1)!}-2\sum_{m=0}^{\infty}\frac{(-1)^m\left(2f^{2m}-A^{2m}-B^{2m}\right)}{(2m)!} \tag{F.45}$$

Since $\sum_{m=0}^{\infty}\frac{(-1)^m X^{2m}}{(2m)!}=\cos X$, giving

$$\sum_{m=0}^{\infty}\frac{(-1)^m\left(2f^{2m}-A^{2m}-B^{2m}\right)}{(2m)!}=2\cos f-\cos A-\cos B \tag{F.46}$$

Therefore F.45 becomes

$$\sum_{m=3}^{\infty}\frac{(-1)^m\left(2f^{2m}-A^{2m}-B^{2m}\right)}{(2m-1)!m(2m-1)}$$

$$=-2a^2+\frac{a^2}{18}\left(6f^2+a^2\right)-2\left(2\cos f-\cos A-\cos B\right)+2\sum_{m=0}^{\infty}\frac{(-1)^m\left(2f^{2m}-A^{2m}-B^{2m}\right)}{(2m-1)(2m-1)!} \tag{F.47}$$

Now, $\sum_{m=0}^{\infty}\frac{(-1)^m x^{2m}}{(2m+1)!}=-\sum_{m=1}^{\infty}\frac{(-1)^m x^{2m-2}}{(2m-1)!}=\frac{\sin x}{x}$,

hence, $\int_0^x\frac{\sin x}{x}dx=-\sum_{m=1}^{\infty}\frac{(-1)^m}{(2m-1)!}\frac{x^{2m-1}}{2m-1}=Si(x)$ (F.48)

The last term of F.47 can thus be written in the form

$$\sum_{m=0}^{\infty}\frac{(-1)^m\left(2f^{2m}-A^{2m}-B^{2m}\right)}{(2m-1)(2m-1)!}=\sum_{m=1}^{\infty}\frac{(-1)^m\left(2f^{2m}-A^{2m}-B^{2m}\right)}{(2m-1)(2m-1)!}$$

$$=\sum_{m=1}^{\infty}\frac{(-1)^m\left(2f\cdot f^{2m-1}-A\cdot A^{2m-1}-B\cdot B^{2m-1}\right)}{(2m-1)(2m-1)!}=-2f.Si(f)+A.Si(A)+B.Si(B) \tag{F.49}$$

Substituting F.47 into F.49 into F.43, finally, gives the following result for I_1

$$I_1=\frac{\pi}{4}\left(\frac{a^2\sin c}{c}-a^2-2\cos f+\cos A+\cos B-2f\,Si(f)+A\;Si(A)+B\,Si(B)\right)$$

$$+\frac{\pi}{8}\sum_{m=3}^{\infty}\frac{(-1)^m(m-1)!}{(2m-1)!}\sum_{i=2}^{m-1}\frac{c^{2m-2i}\left(2f^{2i}-A^{2i}-B^{2i}\right)}{(2i-1)(m-i)!i!} \tag{F.50}$$

Appendix G - Pues Equations for Mutual Susceptance (E-Plane)

The mutual susceptance is given by

$$B_m = B_S F_b K_b \tag{G.1}$$

where B_S = self susceptance

$$B_s \approx -\frac{\beta_o \varepsilon_{re} W}{\pi \eta_o}\left[\left(\ln\frac{s}{2}+C^e-\frac{3}{2}\right)\left(1-\frac{s^2}{24}\right)+\frac{s^2}{288}\right] \tag{G.2}$$

$$F_b = \frac{\pi}{2}\frac{Y_o(c)+\dfrac{s^2}{24-s^2}Y_2(c)}{\ln\dfrac{s}{2}+C^e-\dfrac{3}{2}+\dfrac{s^2/12}{24-s^2}} \tag{G.3}$$

$$K_b = 1\text{-}e^{-0.21a} \tag{G.4}$$

where $Y_i(x)$ is the ith-order Bessel functions of the second kind; C^e=0.577216...=Euler's constant; and $s=\beta_o \delta L$ = the normalised slot width. Self conductance (G_S) is given by

$$G_{self} \approx \frac{\beta_o \varepsilon_{re} W}{2\eta_o}\left(1-\frac{s^2}{24}\right) \tag{G.5}$$

If it is assumed that the slots width (δL) is much smaller than the wavelength and set to zero in the calculations (i.e. $s \to 0$). The mutual susceptance normalised to the self conductance becomes

$$\frac{B_{ms}}{G_{self}} \approx -Y_o(c)\left(1-e^{-0.21a}\right) \tag{G.6}$$

Note that these equations are not valid for calculating self-susceptance (by putting c=0) as F_b would tend to infinity.

Appendix H - Lier Equations for Mutual Conductance (E-Plane)

The mutual conductance is given by

$$G_{ms} \approx J_o(0.9\beta_o \Delta y) G_{self} \tag{H.1}$$

where J_0 is the Bessel function of the first kind and order zero, Δy is the distance between two radiating slots in E-plane and G_{self} is the self conductance and given by

$$G_{self} = \frac{1}{3\pi\eta} \frac{(\beta_o W)^2}{1 + \frac{(\beta_o W)^2}{60}} \tag{H.2}$$

where W is the width of the patch antenna = the length of the slot.

Appendix I - Derivation of Mutual Impedance Using Cavity Model

The mutual impedance is given by (Chapter5,equation 5.3.3)

$$Z_{21} = \frac{1}{I_1 I_2} \oint_{l_2'} \underline{H}^{(1)} \cdot \underline{M}^{(2)} dl_2' \tag{I.1}$$

where I_1 and I_2 are unit currents at the coaxial feeds of the patches so that

$$Z_{21} = \oint_{l_2'} \underline{H}^{(1)} \cdot \underline{M}^{(2)} dl_2' \tag{I.2}$$

where $\underline{M}^{(2)}$ and $\underline{H}^{(1)}$ are given by (Richards,1981 and Huynh,1992)

$$\underline{M}^{(2)} = jh\omega\mu \sum_{m=0}^{\infty}\sum_{n=0}^{\infty} \frac{\Psi_{mn}(x,y)\Psi_{mn}(x_2',y_2')}{k_{eff}^2 - k_{mn}^2} \cdot \hat{z} \times \hat{n} \tag{I.3}$$

where $\hat{n}$ is a unit vector in the direction of the outward normal to the path of integration and

$$\underline{H}^{(1)} = \frac{1}{j\omega\mu\varepsilon_o}\left[k_o^2 \underline{F}^{(1)}(x,y) + \nabla\left(\nabla \cdot \underline{F}^{(1)}(x,y)\right)\right] \tag{I.4}$$

where

$$\underline{F}^{(1)} = \frac{\varepsilon_o}{4\pi} \oint \underline{M}^{(1)}(r') \frac{e^{-jk_o|\underline{r}-\underline{r}'|}}{|\underline{r}-\underline{r}'|} dl_1' \tag{I.5}$$

$$\underline{M}^{(1)} = 2\underline{M}^{(2)}\Big|_{(x_2',y_2')\to(x_1',y_1')} \tag{I.6}$$

$$\Psi_{mn} = \sqrt{\frac{\varepsilon_{om}\varepsilon_{on}}{ab}} \cos\frac{m\pi x}{a} \cos\frac{n\pi y}{b} \tag{I.7}$$

$$\varepsilon_{op} = \begin{cases} 1, & p = 0 \\ 2, & p \neq 0 \end{cases} \tag{I.8}$$

$$k_{eff}^2 = k_o^2 \varepsilon_r \left(1 - j\delta_{eff}\right) \tag{I.9}$$

and
$$k_{mn}^2 = \left(\frac{m\pi}{a}\right)^2 + \left(\frac{n\pi}{b}\right)^2 \tag{I.10}$$

The transmission coefficient S_{21} is given by

$$S_{21} = \frac{2Z_{21}\cdot 50}{(Z_{11}+50)^2 - Z_{21}^2} \tag{I.11}$$

where Z_{11} is the input impedance of isolated antenna. The mutual coupling C_p is defined as

$$C_p = 20\log_{10}|S_{21}| \tag{I.12}$$

For the fundamental mode (mn=01), we have

$$\Psi_{01}(x,y) = \sqrt{\frac{2}{ab}}\cos\left(\frac{\pi(y-L_y)}{b}\right) \tag{I.13}$$

$$\underline{M}^{(2)}(x,y) = \frac{j2h\omega\mu}{(k_{eff}^2 - k_{01}^2)ab}\cos\left[\frac{\pi(y-L_y)}{b}\right]\cos\left(\frac{\pi\, y'_2}{\mathrm{b}}\right)\cdot(\hat{z}\times\hat{n}_2) = \underline{M}^{(2)}(y;y'_2) \tag{I.14}$$

$$\underline{M}^{(1)}(x',y') = 2\underline{M}^{(2)}\Big|_{(x'_2,y'_2)\to(x'_1,y'_1)}$$

$$= \frac{j4h\omega\mu}{(k_{eff}^2 - k_{01}^2)ab}\cos\left[\frac{\pi\, y'}{b}\right]\cos\left(\frac{\pi\, y'_1}{\mathrm{b}}\right)\cdot(\hat{z}\times\hat{n}_1) = \underline{M}^{(1)}(y';y'_1) \tag{I.15}$$

Let $A = \frac{j4h\omega\mu}{(k_{eff}^2 - k_{01}^2)ab}$, giving

$$\underline{M}^{(1)}(y';y'_1) = A\cos\left[\frac{\pi\, y'}{b}\right]\cos\left(\frac{\pi\, y'_1}{\mathrm{b}}\right)\cdot(\hat{z}\times\hat{n}_1) \tag{I.16}$$

$$\underline{M}^{(2)}(y';y'_2)=\frac{A}{2}\cos\left[\frac{\pi\left(y-L_y\right)}{b}\right]\cos\left(\frac{\pi\, y'_2}{\mathrm{b}}\right)\cdot(\hat{z}\times\hat{n}_2) \tag{I.17}$$

Hence, I.5 becomes

$$\underline{F}^{(1)}(x,y)=\frac{\varepsilon_o}{4\pi}\oint\underline{M}^{(1)}(r')\frac{e^{-jk_o d}}{d}dl'_1 \quad (\text{where } d=\sqrt{(x-x')^2+(y-y')^2})$$

$$=\frac{\varepsilon_o}{4\pi}\oint A\cos\left(\frac{\pi y'}{b}\right)\cos\left(\frac{\pi y'_1}{b}\right)\frac{e^{-jk_o d}}{d}(\hat{z}\times\hat{n}_1)dl'_1$$

$$=\frac{A\,\varepsilon_o}{4\pi}\cos\left(\frac{\pi y'_1}{b}\right)\oint\cos\left(\frac{\pi y'}{b}\right)\frac{e^{-jk_o d}}{d}dl'_1(\hat{z}\times\hat{n}_1)$$

$$=B\oint\cos\left(\frac{\pi y'}{b}\right)g\,dl'_1(\hat{z}\times\hat{n}_1) \tag{I.18}$$

$$\text{where } B=\frac{A\,\varepsilon_o}{4\pi}\cos\left(\frac{\pi y'_1}{b}\right) \text{ and } \frac{e^{-jk_o d}}{d}=g(x,y,x',y')=g \tag{I.19}$$

Consider I.4:

$$\underline{H}^{(1)}=\frac{1}{j\omega\mu\varepsilon_o}\left[k_o^2\,\underline{F}^{(1)}(x,y)+\nabla\left(\nabla\cdot\underline{F}^{(1)}(x,y)\right)\right] \tag{I.4}$$

Since $\nabla\cdot\underline{F}^{(1)}(x,y)=\left(\hat{x}\frac{\partial}{\partial x}+\hat{y}\frac{\partial}{\partial y}\right)\cdot\underline{F}^{(1)}(x,y)$ then

$$\nabla\cdot\underline{F}^{(1)}(x,y)=\left(\hat{x}\frac{\partial}{\partial x}+\hat{y}\frac{\partial}{\partial y}\right)\cdot B\oint\cos\left(\frac{\pi y'}{b}\right)g\,dl'_1(\hat{z}\times\hat{n}_1)$$

$$=B\oint\cos\left(\frac{\pi y'}{b}\right)\left(\hat{x}\frac{\partial}{\partial x}+\hat{y}\frac{\partial}{\partial y}\right)\cdot(\hat{z}\times\hat{n}_1)\,g\,dl'_1 \tag{I.20}$$

Appendix I - Derivation of Mutual Impedance Using Cavity Model

$\because\ \hat{x}\times\hat{y}=\hat{z};\ \hat{y}\times\hat{z}=\hat{x};\ \hat{x}\times\hat{z}=-\hat{y}$ and $\underline{a}\cdot\underline{b}\times\underline{c}\equiv\underline{a}\times\underline{b}\cdot\underline{c}$

$\therefore\ \hat{x}\cdot\hat{z}\times\hat{n}_1=\hat{x}\times\hat{z}\cdot\hat{n}_1=-\hat{y}\cdot\hat{n}_1$ and $\hat{y}\cdot\hat{z}\times\hat{n}_1=\hat{y}\times\hat{z}\cdot\hat{n}_1=\hat{x}\cdot\hat{n}_1$, therefore I.21 becomes

$$\nabla\cdot\underline{F}^{(1)}(x,y)=B\oint\cos\left(\frac{\pi y'}{b}\right)\left(-\hat{y}\cdot\hat{n}_1\frac{\partial g}{\partial x}+\hat{x}\cdot\hat{n}_1\frac{\partial g}{\partial y}\right)dl'_1 \qquad \text{(I.21)}$$

Since $\nabla\phi=\frac{\partial\phi}{\partial x}\hat{x}+\frac{\partial\phi}{\partial y}\hat{y}$, we have

$$\nabla\left(\nabla\cdot\underline{F}^{(1)}(x,y)\right)=\hat{x}B\oint\cos\left(\frac{\pi y'}{b}\right)\left(-\hat{y}\cdot\hat{n}_1\frac{\partial^2 g}{\partial x^2}+\hat{x}\cdot\hat{n}_1\frac{\partial^2 g}{\partial y\partial x}\right)dl'_1$$

$$+\hat{y}B\oint\cos\left(\frac{\pi y'}{b}\right)\left(-\hat{y}\cdot\hat{n}_1\frac{\partial^2 g}{\partial x\partial y}+\hat{x}\cdot\hat{n}_1\frac{\partial^2 g}{\partial y^2}\right)dl'_1 \qquad \text{(I.22)}$$

Consider

$$\nabla\left(\nabla\cdot\underline{F}^{(1)}(x,y)\right)\cdot\underline{M}^{(2)}(y';y'_2) \qquad \text{(I.23)}$$

Substitute I.17 and I.22 into I.23, we have

$$\nabla\left(\nabla\cdot\underline{F}^{(1)}(x,y)\right)\cdot\underline{M}^{(2)}(y';y'_2)=\frac{AB}{2}\cos\left[\frac{\pi\left(y-L_y\right)}{b}\right]\cos\left(\frac{\pi\, y'_2}{\mathrm{b}}\right)\cdot$$

$$\left\{-\hat{y}\cdot\hat{n}_2\oint_{l'_1}\cos\left(\frac{\pi y'}{b}\right)\left[-\hat{y}\cdot\hat{n}_1\frac{\partial^2 g}{\partial x^2}+\hat{x}\cdot\hat{n}_1\frac{\partial^2 g}{\partial x\partial y}\right]dl'_1\right.$$

$$\left.+\hat{x}\cdot\hat{n}_2\oint_{l'_1}\cos\left(\frac{\pi y'}{b}\right)\left[-\hat{y}\cdot\hat{n}_1\frac{\partial^2 g}{\partial x\partial y}+\hat{x}\cdot\hat{n}_1\frac{\partial^2 g}{\partial^2 y}\right]dl'_1\right\} \qquad \text{(I.24)}$$

Further,

$$k_o^2\,\underline{F}^{(1)}(x,y)\cdot\underline{M}^{(2)}(y';y'_2)$$

$$= k_o^2 \frac{AB}{2} \cos\left[\frac{\pi\left(y - L_y\right)}{b}\right] \cos\left(\frac{\pi\, y'_2}{\mathrm{b}}\right) \cdot \oint_{l'_1} \cos\left(\frac{\pi y'}{b}\right) g dl'_1 \left(\hat{z} \times \hat{n}_1\right) \cdot \left(\hat{z} \times \hat{n}_2\right) \quad \text{(I.25)}$$

On substituting the expression from I.25 and I.24 into I.2, finally the general form of the mutual impedance Z_{21} is given by

$$Z_{21} = jK \oint_{l_2} \oint_{l_1} \cos\left(\frac{\pi(y - Ly)}{b}\right) \cos\left(\frac{\pi y'}{b}\right) \left\{k_o^2 g \cdot (\hat{z} \times \hat{n}_1) \cdot (\hat{z} \times \hat{n}_2) + \frac{\partial^2 g}{\partial x^2} (\hat{y} \cdot \hat{n}_1)(\hat{y} \cdot \hat{n}_2)\right.$$

$$\left. + \frac{\partial^2 g}{\partial y^2} (\hat{x} \cdot \hat{n}_1)(\hat{x} \cdot \hat{n}_2) - \frac{\partial^2 g}{\partial x \partial y} \left[(\hat{y} \cdot \hat{n}_2)(\hat{x} \cdot \hat{n}_1) + (\hat{y} \cdot \hat{n}_1)(\hat{x} \cdot \hat{n}_2)\right]\right\} dl'_1 dl'_2 \quad \text{(I.26)}$$

where

$$K = \frac{2h^2 \omega \mu}{\left(k_{eff}^2 - k_{01}^2\right)^2 a^2 b^2 \pi} \cos\left(\frac{\pi}{b} y'_1\right) \cos\left(\frac{\pi}{b} y'_2\right) \quad \text{(I.27)}$$

$$g = \frac{e^{-jk_o d}}{d} \quad \text{and} \quad g = g(x, y, x', y') = \frac{e^{-jk_o \sqrt{(x-x')^2 + (y-y')^2}}}{\sqrt{(x-x')^2 + (y-y')^2}} \quad \text{(I.28)}$$

$$\frac{\partial^2 g}{\partial x^2} = -\frac{e^{-jk_o d}}{d^3} (1 + jk_o d) \left[1 + \frac{k_o^2 (x-x')^2}{1 + jk_o d} - \frac{3(x-x')^2}{d^2}\right] \quad \text{(I.29)}$$

$$\frac{\partial^2 g}{\partial y^2} = -\frac{e^{-jk_o d}}{d^3} (1 + jk_o d) \left[1 + \frac{k_o^2 (y-y')^2}{1 + jk_o d} - \frac{3(y-y')^2}{d^2}\right] \quad \text{(I.30)}$$

$$\frac{\partial^2 g}{\partial x \partial y} = -\frac{(x-x')(y-y') e^{-jk_o d}}{d^5} \left(k_o^2 d^2 - 3 - j3k_o d\right) \quad \text{(I.31)}$$

$$d = \sqrt{(x-x')^2 + (y-y')^2} \quad \text{(I.32)}$$

Appendix I - Derivation of Mutual Impedance Using Cavity Model

The computation for Z_{21} takes into account all the interactions of the line integrations between the two antennas. This involves the integration of each segment of line ℓ_1 with in turn each segment of line ℓ_2. There are totally sixteen interactions as presented as follows:

Consider the two rectangular antennas oriented as shown in figure I.1.

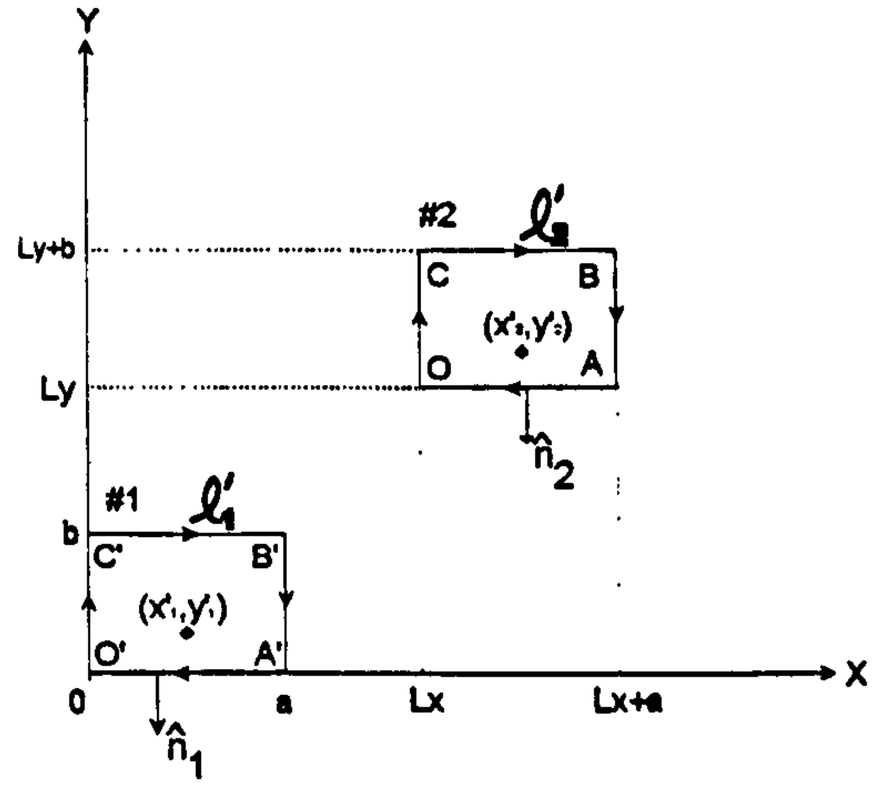

Figure I.1

Integration along O'A';OA

$$x' \in [o,a]; x \in [L_x, L_x + a]; y' = 0; y = L_y; \hat{n}_1 = \hat{n}_2 = -\hat{y}; g = g(x,y,x',y') = g(x,L_y,x',0)$$

$$Z_{O'A',OA} = jK \int_{L_x}^{L_x+a} \int_{0}^{a} \left(k_o^2 g(x,L_y,x',0) + \frac{\partial^2 g(x,L_y,x',0)}{\partial x^2} \right) dx' dx \qquad \text{(I.33)}$$

Integration along O'A';CO

$$x' \in [o,a]; x = L_x; y' = 0; y \in [L_y, L_y + b]; \hat{n}_1 = -\hat{y}; \hat{n}_2 = -\hat{x}; g = g(x,y,x',y') = g(L_x,y,x',0)$$

$$Z_{O'A',CO} = -jK \int_{L_y}^{L_y+b} \int_{0}^{a} \cos\left(\frac{\pi (y - L_y)}{b} \right) \frac{\partial^2 g(L_x,y,x',0)}{\partial x \partial y} dx' dy \qquad \text{(I.34)}$$

Integration along O'A';BC

$$x' \in [o,a]; x \in [L_x, L_x + a]; y' = 0; y = L_y + b; \hat{n}_1 = -\hat{y}; \hat{n}_2 = \hat{y}; g = g(x,y,x',y') = g(x,L_y + b,x',0)$$

$$Z_{O'A',BC} = jK \int_{L_x}^{L_x+a} \int_{0}^{a} \left(k_o^2 g(x,L_y + b,x',0) + \frac{\partial^2 g(x,L_y + b,x',0)}{\partial x^2} \right) dx' dx \qquad \text{(I.35)}$$

Integration along O'A':AB

$$x' \in [o,a]; x = L_x + a; y' = 0; y \in [L_y, L_y + b]; \hat{n}_1 = -\hat{y}; \hat{n}_2 = \hat{x}; g = g(x,y,x',y') = g(L_x + a, y, x', 0)$$

$$Z_{O'A',AB} = jK \int_{L_y}^{L_y+b} \int_{0}^{a} \cos\left(\frac{\pi(y - L_y)}{b}\right) \frac{\partial^2 g(L_x + a, y, x', 0)}{\partial x \partial y} dx' dy \qquad \text{(I.36)}$$

Integration along C'O':OA

$$x' = 0; x \in [L_x, L_x + a]; y' \in [0,b]; y = L_y; \hat{n}_1 = -\hat{x}; \hat{n}_2 = -\hat{y}; g = g(x,y,x',y') = g(x, L_y, 0, y')$$

$$Z_{C'O',OA} = -jK \int_{L_x}^{L_x+a} \int_{0}^{b} \cos\left(\frac{\pi y'}{b}\right) \frac{\partial^2 g(x, L_y, 0, y')}{\partial x \partial y} dy' dx \qquad \text{(I.37)}$$

Integration along C'O':CO

$$x' = 0; x = L_x; y' \in [0,b]; y \in [L_y, L_y + b]; \hat{n}_1 = -\hat{x}; \hat{n}_2 = -\hat{x}; g = g(x,y,x',y') = g(L_x, y, 0, y')$$

$$Z_{C'O',CO} = jK \int_{L_y}^{L_y+b} \int_{0}^{b} \cos\left(\frac{\pi(y - L_y)}{b}\right) \cos\left(\frac{\pi y'}{b}\right) \left[k_o^2 g(L_x, y, 0, y') + \frac{\partial^2 g(L_x, y, 0, y')}{\partial y^2}\right] dy' dy \qquad \text{(I.38)}$$

Integration along C'O':BC

$$x' = 0; x \in [L_x, L_x + a]; y' \in [0,b]; y = L_y + b; \hat{n}_1 = -\hat{x}; \hat{n}_2 = \hat{y}; g = g(x,y,x',y') = g(x, L_y + b, 0, y')$$

$$Z_{C'O',BC} = -jK \int_{L_x}^{L_x+a} \int_{0}^{b} \cos\left(\frac{\pi y'}{b}\right) \frac{\partial^2 g(x, L_y + b, 0, y')}{\partial x \partial y} dy' dx \qquad \text{(I.39)}$$

Integration along C'O':AB

$$x' = 0; x = L_x + a; y' \in [0,b]; y \in [L_y, L_y + b]; \hat{n}_1 = -\hat{x}; \hat{n}_2 = \hat{x}; g = g(x,y,x',y') = g(L_x + a, y, 0, y')$$

$$Z_{C'O',AB} = -jK \int_{L_y}^{L_y+b} \int_{0}^{b} \cos\left(\frac{\pi(y - L_y)}{b}\right) \cos\left(\frac{\pi y'}{b}\right) \left[k_o^2 g(L_x + a, y, 0, y') + \frac{\partial^2 g(L_x + a, y, 0, y')}{\partial y^2}\right] dy' dy \qquad \text{(I.40)}$$

Integration along B'C';OA

$x' \in [o,a]; x \in [L_x, L_x + a]; y' = b; y = L_y; \hat{n}_1 = \hat{y}; \hat{n}_2 = -\hat{y}; g = g(x,y,x',y') = g(x,L_y,x',b)$

$$Z_{B'C',OA} = jK \int_{L_x}^{L_x+a} \int_{0}^{a} \left(k_o^2 g(x,L_y,x',b) + \frac{\partial^2 g(x,L_y,x',b)}{\partial x^2} \right) dx' dx \tag{I.41}$$

Integration along B'C';CO

$x' \in [o,a]; x = L_x; y' = b; y \in [L_y, L_y + b]; \hat{n}_1 = \hat{y}; \hat{n}_2 = -\hat{x}; g = g(x,y,x',y') = g(L_x,y,x',b)$

$$Z_{B'C',CO} = -jK \int_{L_y}^{L_y+b} \int_{0}^{a} \cos\left(\frac{\pi (y - L_y)}{b} \right) \frac{\partial^2 g(L_x,y,x',b)}{\partial x \partial y} dx' dy \tag{I.42}$$

Integration along B'C';BC

$x' \in [o,a]; x \in [L_x, L_x + a]; y' = b; y = L_y + b; \hat{n}_1 = \hat{y}; \hat{n}_2 = \hat{y}; g = g(x,y,x',y') = g(x,L_y + b,x',b)$

$$Z_{B'C',BC} = jK \int_{L_x}^{L_x+a} \int_{0}^{a} \left(k_o^2 g(x,L_y + b,x',b) + \frac{\partial^2 g(x,L_y + b,x',b)}{\partial x^2} \right) dx' dx \tag{I.43}$$

Integration along B'C';AB

$x' \in [o,a]; x = L_x + a; y' = b; y \in [L_y, L_y + b]; \hat{n}_1 = \hat{y}; \hat{n}_2 = \hat{x}; g = g(x,y,x',y') = g(L_x + a,y,x',b)$

$$Z_{B'C',AB} = jK \int_{L_y}^{L_y+b} \int_{0}^{a} \cos\left(\frac{\pi (y - L_y)}{b} \right) \frac{\partial^2 g(L_x + a,y,x',b)}{\partial x \partial y} dx' dy \tag{I.44}$$

Integration along A'B';OA

$x' = a; x \in [L_x, L_x + a]; y' \in [0,b]; y = L_y; \hat{n}_1 = \hat{x}; \hat{n}_2 = -\hat{y}; g = g(x,y,x',y') = g(x,L_y,a,y')$

$$Z_{A'B',OA} = jK \int_{L_x}^{L_x+a} \int_{0}^{b} \cos\left(\frac{\pi y'}{b} \right) \frac{\partial^2 g(x,L_y,a,y')}{\partial x \partial y} dy' dx \tag{I.45}$$

Integration along A'B';CO

$x' = a; x = L_x; y' \in [0,b]; y \in [L_y, L_y + b]; \hat{n}_1 = \hat{x}; \hat{n}_2 = -\hat{x}; g = g(x,y,x',y') = g(L_x,y,a,y')$

$$Z_{A'B',CO} = -jK \int_{L_y}^{L_y+b} \int_{0}^{b} \cos\left(\frac{\pi(y-L_y)}{b}\right) \cos\left(\frac{\pi y'}{b}\right) \left[k_o^2 g(L_x,y,a,y') + \frac{\partial^2 g(L_x,y,a,y')}{\partial y^2}\right] dy'\,dy \tag{I.46}$$

Integration along A'B';BC

$x' = a; x \in [L_x, L_x + a]; y' \in [0,b]; y = L_y + b; \hat{n}_1 = \hat{x}; \hat{n}_2 = \hat{y}; g = g(x,y,x',y') = g(x,L_y+b,a,y')$

$$Z_{A'B',BC} = jK \int_{L_x}^{L_x+a} \int_{0}^{b} \cos\left(\frac{\pi y'}{b}\right) \frac{\partial^2 g(x,L_y+b,a,y')}{\partial x \partial y} dy'\,dx \tag{I.47}$$

Integration along A'B';AB

$x' = a; x = L_x + a; y' \in [0,b]; y \in [L_y, L_y + b]; \hat{n}_1 = \hat{x}; \hat{n}_2 = \hat{x}; g = g(x,y,x',y') = g(L_x+a,y,a,y')$

$$Z_{A'B',AB} = jK \int_{L_y}^{L_y+b} \int_{0}^{b} \cos\left(\frac{\pi(y-L_y)}{b}\right) \cos\left(\frac{\pi y'}{b}\right) \left[k_o^2 g(L_x+a,y,a,y') + \frac{\partial^2 g(L_x+a,y,a,y')}{\partial y^2}\right] dy'\,dy \tag{I.48}$$

By combining expressions I.33 through I.48 the mutual impedance is finally given by

$$Z_{21} = Z_1 + Z_2 + Z_3 + Z_4 \tag{I.49}$$

where

$$Z_1 = jK \int_{Lx}^{Lx+a} \int_{0}^{a} \left\{ \begin{array}{l} k_o^2 g\left(x, L_y, x', 0\right) + \dfrac{\partial^2 g\left(x, L_y, x', 0\right)}{\partial x^2} \\ +k_o^2 g\left(x, L_y + b, x', 0\right) + \dfrac{\partial^2 g\left(x, L_y + b, x', 0\right)}{\partial x^2} \\ +k_o^2 g\left(x, L_y, x', b\right) + \dfrac{\partial^2 g\left(x, L_y, x', b\right)}{\partial x^2} \\ +k_o^2 g\left(x, L_y + b, x', b\right) + \dfrac{\partial^2 g\left(x, L_y + b, x', b\right)}{\partial x^2} \end{array} \right\} dx'\,dx \quad \text{(H.50)}$$

$$Z_2 = jK \int_{Lx}^{Lx+a} \int_{0}^{b} \cos\left(\frac{\pi y'}{b}\right) \left\{ \begin{array}{l} \dfrac{\partial^2 g\left(x, L_y, a, y'\right)}{\partial x \partial y} + \dfrac{\partial^2 g\left(x, L_y + b, a, y'\right)}{\partial x \partial y} \\ -\dfrac{\partial^2 g\left(x, L_y, 0, y'\right)}{\partial x \partial y} - \dfrac{\partial^2 g\left(x, L_y + b, 0, y'\right)}{\partial x \partial y} \end{array} \right\} dy'\,dx \quad \text{(I.51)}$$

$$Z_3 = jK \int_{Ly}^{Ly+b} \int_{0}^{b} \cos\left(\frac{\pi\left(y - L_y\right)}{b}\right) \cos\left(\frac{\pi y'}{b}\right) \left\{ \begin{array}{l} k_o^2 g\left(L_x, y, 0, y'\right) + \dfrac{\partial^2 g\left(L_x, y, 0, y'\right)}{\partial y^2} \\ -k_o^2 g\left(L_x + a, y, 0, y'\right) - \dfrac{\partial^2 g\left(L_x + a, y, 0, y'\right)}{\partial y^2} \\ -k_o^2 g\left(L_x, y, a, y'\right) - \dfrac{\partial^2 g\left(L_x, y, a, y'\right)}{\partial y^2} \\ +k_o^2 g\left(L_x + a, y, a, y'\right) + \dfrac{\partial^2 g\left(L_x + a, y, a, y'\right)}{\partial y^2} \end{array} \right\} dy'\,dy \quad \text{(H.52)}$$

$$Z_4 = jK \int_{Ly}^{Ly+b} \int_{0}^{a} \cos\left(\frac{\pi\left(y - L_y\right)}{b}\right) \left\{ \begin{array}{l} -\dfrac{\partial^2 g\left(L_x, y, x', 0\right)}{\partial x \partial y} + \dfrac{\partial^2 g\left(L_x + a, y, x', 0\right)}{\partial x \partial y} \\ -\dfrac{\partial^2 g\left(L_x, y, x', b\right)}{\partial x \partial y} + \dfrac{\partial^2 g\left(L_x + a, y, x', b\right)}{\partial x \partial y} \end{array} \right\} dx'\,dy \quad \text{(I.53)}$$

Appendix J - Pascal Program to Predict the Radiation Pattern Including Mutual Coupling

```
program mutual11(input,output);
{
   File Name: Mutual11.Pas

   This Pascal program is to calculate the theoretical radiation
   pattern for Horizontal Polarisation along H and E-Plane and Circularly Polarisation for
   the 4*4 planar array, which including Mutual Coupling.

   Author  : T.K. Chan
   Date    : 22nd March 1993
   Revised : 9th Feb 1994

   The patch assignment is as follows:

      --1   --2  --3   --4

      --5   --6  --7   --8

      --9  --10 --11  --12

     --13 --14 --15  --16

}

const  pi = 3.1416;
       c = 3e8;

var    fo, lambda_o, theta, phi, d_o, ko, W,
       Pt_E_max, Pt_H_max, Pt_CP_max, y1 : real;
       i,j,k : integer;
       answer: char;

       { [i,j,k] :: Magnitude[i,j,1]; Phase[i,j,2] }
       SH     : packed array [1..16,1..16,1..2] of real;

       { [i,j,k] :: Real[i,j,1]; Imaginary[i,j,2] }
       S      : packed array [1..16,1..16,1..2] of real;
       X      : packed array [1..16,1..2] of real;
       GAMMA  : packed array [1..16,1..2] of real;
       GAMMA_M : packed array [1..16] of real;

       E_H_voltage : packed array [1..8,0..180] of real;
       Et_H   : packed array [0..180] of real;
       Pt_H   : packed array [0..180] of real;
```

```
Pt_H_dB : packed array [0..180] of real;

E_E_voltage : packed array [1..8,90..270] of real;
Et_E  : packed array [90..270] of real;
Pt_E  : packed array [90..270] of real;
Pt_E_dB : packed array [90..270] of real;

Pt_CP  : packed array [0..180] of real;
Pt_CP_dB: packed array [0..180] of real;

procedure input_data;
begin
    write('resonant frequency fo (GHz): ');
    readln(fo);
    fo := fo*1e9;
    lambda_o := c/fo;
    ko := 2*pi/lambda_o;
    write('width of a patch element (mm): ');
    readln(W);
    W := W*1e-3;
    write('spacing between the middle of two patches ');
    write('d_o (mm): ');
    readln(d_o);
    d_o := d_o*1e-3;

For i := 1 to 16 do
   for j:=1 to 16 do
   for k := 1 to 2 do
      begin
         SH[i,j,k] := 0;
         S[i,j,k] := 0;
      end;

For i := 1 to 16 do
   for k := 1 to 2 do
      begin
         X[i,k] := 0;
         Gamma[i,k] := 0;
      end;

write('Do you want to include the effect of mutual coupling? Y/N');
readln(answer);
if (answer='y') or (answer='Y') then
begin
```

```
writeln('Enter the S parameter matrix: ');
For j := 1 to 16 do
begin
    write(' SH[1,',j,'] (dB)      : ');
          read(SH[1,j,1]);
          SH[1,j,1] := exp(2.3026*SH[1,j,1]/20);
          write('      SH[1,',j,'] (degrees) : ');
          readln(SH[1,j,2]);
          SH[1,j,2] := SH[1,j,2] * pi/180;
end
else
begin
    For j:=1 to 16 do
    begin
        SH[1,j,1] := 0;
        SH[1,j,2] := 0;
    end;
end;

For j := 1 to 16 do
begin
    S[1,j,1] := SH[1,j,1]*cos(SH[1,j,2]);
    S[1,j,2] := SH[1,j,1]*sin(SH[1,j,2]);
end;

For k := 1 to 2 do
Begin

X[1,k]:=S[1,1,k];
S[2,2,k]:=X[1,k]; S[3,3,k]:=X[1,k];
S[4,4,k]:=X[1,k]; S[5,5,k]:=X[1,k];
S[6,6,k]:=X[1,k]; S[7,7,k]:=X[1,k];
S[8,8,k]:=X[1,k]; S[9,9,k]:=X[1,k];
S[10,10,k]:=X[1,k]; S[11,11,k]:=X[1,k];
S[12,12,k]:=X[1,k]; S[13,13,k]:=X[1,k];
S[14,14,k]:=X[1,k]; S[15,15,k]:=X[1,k];
S[16,16,k]:=X[1,k];

X[2,k]:=S[1,2,k];
S[2,3,k]:=X[2,k]; S[3,4,k]:=X[2,k];
S[5,6,k]:=X[2,k]; S[6,7,k]:=X[2,k];
S[7,8,k]:=X[2,k]; S[9,10,k]:=X[2,k];
S[10,11,k]:=X[2,k]; S[11,12,k]:=X[2,k];
```

```
S[13,14,k]:=X[2,k]; S[14,15,k]:=X[2,k];
S[15,16,k]:=X[2,k]; S[2,1,k]:=X[2,k];
S[3,2,k]:=X[2,k]; S[4,3,k]:=X[2,k];
S[6,5,k]:=X[2,k]; S[7,6,k]:=X[2,k];
S[8,7,k]:=X[2,k]; S[10,9,k]:=X[2,k];
S[11,10,k]:=X[2,k]; S[12,11,k]:=X[2,k];
S[14,13,k]:=X[2,k]; S[15,14,k]:=X[2,k];
S[16,15,k]:=X[2,k];

X[3,k]:=S[1,3,k];
S[2,4,k]:=X[3,k]; S[5,7,k]:=X[3,k];
S[6,8,k]:=X[3,k]; S[9,11,k]:=X[3,k];
S[10,12,k]:=X[3,k]; S[13,15,k]:=X[3,k];
S[14,16,k]:=X[3,k]; S[3,1,k]:=X[3,k];
S[4,2,k]:=X[3,k]; S[7,5,k]:=X[3,k];
S[8,6,k]:=X[3,k]; S[11,9,k]:=X[3,k];
S[12,10,k]:=X[3,k]; S[15,13,k]:=X[3,k];
S[16,14,k]:=X[3,k];

X[4,k]:=S[1,4,k];
S[5,8,k]:=X[4,k]; S[9,12,k]:=X[4,k];
S[13,16,k]:=X[4,k]; S[4,1,k]:=X[4,k];
S[8,5,k]:=X[4,k]; S[12,9,k]:=X[4,k];
S[16,13,k]:=X[4,k];

X[5,k]:=S[1,5,k];
S[5,9,k]:=X[5,k]; S[9,13,k]:=X[5,k];
S[2,6,k]:=X[5,k]; S[6,10,k]:=X[5,k];
S[10,14,k]:=X[5,k]; S[3,7,k]:=X[5,k];
S[7,11,k]:=X[5,k]; S[11,15,k]:=X[5,k];
S[4,8,k]:=X[5,k]; S[8,12,k]:=X[5,k];
S[12,16,k]:=X[5,k]; S[5,1,k]:=X[5,k];
S[9,5,k]:=X[5,k]; S[13,9,k]:=X[5,k];
S[6,2,k]:=X[5,k]; S[10,6,k]:=X[5,k];
S[14,10,k]:=X[5,k]; S[7,3,k]:=X[5,k];
S[11,7,k]:=X[5,k]; S[15,11,k]:=X[5,k];
S[8,4,k]:=X[5,k]; S[12,8,k]:=X[5,k];
S[16,12,k]:=X[5,k];

X[6,k]:=S[1,6,k];
S[2,5,k]:=X[6,k]; S[2,7,k]:=X[6,k];
S[3,6,k]:=X[6,k]; S[3,8,k]:=X[6,k];
S[4,7,k]:=X[6,k]; S[5,10,k]:=X[6,k];
S[6,9,k]:=X[6,k]; S[6,11,k]:=X[6,k];
```

```
S[7,10,k]:=X[6,k]; S[7,12,k]:=X[6,k];
S[8,11,k]:=X[6,k]; S[9,14,k]:=X[6,k];
S[10,13,k]:=X[6,k]; S[10,15,k]:=X[6,k];
S[11,14,k]:=X[6,k]; S[11,16,k]:=X[6,k];
S[12,15,k]:=X[6,k]; S[6,1,k]:=X[6,k];
S[5,2,k]:=X[6,k]; S[7,2,k]:=X[6,k];
S[6,3,k]:=X[6,k]; S[8,3,k]:=X[6,k];
S[7,4,k]:=X[6,k]; S[10,5,k]:=X[6,k];
S[9,6,k]:=X[6,k]; S[11,6,k]:=X[6,k];
S[10,7,k]:=X[6,k]; S[12,7,k]:=X[6,k];
S[11,8,k]:=X[6,k]; S[14,9,k]:=X[6,k];
S[13,10,k]:=X[6,k]; S[15,10,k]:=X[6,k];
S[14,11,k]:=X[6,k]; S[16,11,k]:=X[6,k];
S[15,12,k]:=X[6,k];

X[7,k]:=S[1,7,k];
S[2,8,k]:=X[7,k]; S[3,5,k]:=X[7,k];
S[4,6,k]:=X[7,k]; S[5,11,k]:=X[7,k];
S[6,12,k]:=X[7,k]; S[7,9,k]:=X[7,k];
S[8,10,k]:=X[7,k]; S[9,15,k]:=X[7,k];
S[10,16,k]:=X[7,k]; S[11,13,k]:=X[7,k];
S[12,14,k]:=X[7,k]; S[7,1,k]:=X[7,k];
S[8,2,k]:=X[7,k]; S[5,3,k]:=X[7,k];
S[6,4,k]:=X[7,k]; S[11,5,k]:=X[7,k];
S[12,6,k]:=X[7,k]; S[9,7,k]:=X[7,k];
S[10,8,k]:=X[7,k]; S[15,9,k]:=X[7,k];
S[16,10,k]:=X[7,k]; S[13,11,k]:=X[7,k];
S[14,12,k]:=X[7,k];

X[8,k]:=S[1,8,k];
S[5,4,k]:=X[8,k]; S[5,12,k]:=X[8,k];
S[9,8,k]:=X[8,k]; S[9,16,k]:=X[8,k];
S[13,12,k]:=X[8,k]; S[8,1,k]:=X[8,k];
S[4,5,k]:=X[8,k]; S[12,5,k]:=X[8,k];
S[8,9,k]:=X[8,k]; S[16,9,k]:=X[8,k];
S[12,13,k]:=X[8,k];

X[9,k]:=S[1,9,k];
S[5,13,k]:=X[9,k]; S[2,10,k]:=X[9,k];
S[6,14,k]:=X[9,k]; S[3,11,k]:=X[9,k];
S[7,15,k]:=X[9,k]; S[4,12,k]:=X[9,k];
S[8,16,k]:=X[9,k]; S[9,1,k]:=X[9,k];
S[13,5,k]:=X[9,k]; S[10,2,k]:=X[9,k];
S[14,6,k]:=X[9,k]; S[11,3,k]:=X[9,k];
```

```
S[15,7,k]:=X[9,k]; S[12,4,k]:=X[9,k];
S[16,8,k]:=X[9,k];

X[10,k]:=S[1,10,k];
S[2,9,k]:=X[10,k]; S[2,11,k]:=X[10,k];
S[3,10,k]:=X[10,k]; S[3,12,k]:=X[10,k];
S[4,11,k]:=X[10,k]; S[5,14,k]:=X[10,k];
S[6,13,k]:=X[10,k]; S[6,15,k]:=X[10,k];
S[7,14,k]:=X[10,k]; S[7,16,k]:=X[10,k];
S[8,15,k]:=X[10,k]; S[10,1,k]:=X[10,k];
S[9,2,k]:=X[10,k]; S[11,2,k]:=X[10,k];
S[10,3,k]:=X[10,k]; S[12,3,k]:=X[10,k];
S[11,4,k]:=X[10,k]; S[14,5,k]:=X[10,k];
S[13,6,k]:=X[10,k]; S[15,6,k]:=X[10,k];
S[14,7,k]:=X[10,k]; S[16,7,k]:=X[10,k];
S[15,8,k]:=X[10,k];

X[11,k]:=S[1,11,k];
S[2,12,k]:=X[11,k]; S[3,9,k]:=X[11,k];
S[4,10,k]:=X[11,k]; S[5,15,k]:=X[11,k];
S[6,16,k]:=X[11,k]; S[7,13,k]:=X[11,k];
S[8,14,k]:=X[11,k]; S[11,1,k]:=X[11,k];
S[12,2,k]:=X[11,k]; S[9,3,k]:=X[11,k];
S[10,4,k]:=X[11,k]; S[15,5,k]:=X[11,k];
S[16,6,k]:=X[11,k]; S[13,7,k]:=X[11,k];
S[14,8,k]:=X[11,k];

X[12,k]:=S[1,12,k];
S[4,9,k]:=X[12,k]; S[5,16,k]:=X[12,k];
S[8,13,k]:=X[12,k]; S[12,1,k]:=X[12,k];
S[9,4,k]:=X[12,k]; S[16,5,k]:=X[12,k];
S[13,8,k]:=X[12,k];

X[13,k]:=S[1,13,k];
S[2,14,k]:=X[13,k]; S[3,15,k]:=X[13,k];
S[4,16,k]:=X[13,k]; S[3,1,k]:=X[13,k];
S[14,2,k]:=X[13,k]; S[15,3,k]:=X[13,k];
S[16,4,k]:=X[13,k];

X[14,k]:=S[1,14,k];
S[2,13,k]:=X[14,k]; S[2,15,k]:=X[14,k];
S[3,14,k]:=X[14,k]; S[3,16,k]:=X[14,k];
S[4,15,k]:=X[14,k]; S[14,1,k]:=X[14,k];
S[13,2,k]:=X[14,k]; S[15,2,k]:=X[14,k];
```

```
S[14,3,k]:=X[14,k]; S[16,3,k]:=X[14,k];
S[15,4,k]:=X[14,k];

X[15,k]:=S[1,15,k];
S[2,16,k]:=X[15,k]; S[3,13,k]:=X[15,k];
S[4,14,k]:=X[15,k]; S[15,1,k]:=X[15,k];
S[16,2,k]:=X[15,k]; S[13,3,k]:=X[15,k];
S[14,4,k]:=X[15,k];

X[16,k]:=S[1,16,k];
S[4,13,k]:=X[16,k]; S[16,1,k]:=X[16,k];
S[13,4,k]:=X[16,k];

end;

For i := 1 to 16 do
 begin
  For j := 1 to 16 do
  begin
  write('S[',i,',',j, '] : ',S[i,j,1]:5:5);
  writeln('  j ',S[i,j,2]:5:5);
  end;
{
     writeln;writeln('Press RETURN please...');
     readln;
}
   end;

  For i := 1 to 16 do
  For k := 1 to 2 do
  begin
     Gamma[i,k] :=
         S[i,1,k]+S[i,2,k]+S[i,3,k]+
         S[i,4,k]+S[i,5,k]+S[i,6,k]+
         S[i,7,k]+S[i,8,k]+S[i,9,k]+
         S[i,10,k]+S[i,11,k]+S[i,12,k]+
         S[i,13,k]+S[i,14,k]+S[i,15,k]+
         S[i,16,k];
end;

For i := 1 to 16 do
  begin
      write('Gamma[',i,'] = ',Gamma[i,1]:5:5);
      write('  j ',Gamma[i,2]:5:5);
```

```
        write('   Magnitude = ');
        GAMMA_M[i] := sqrt( Gamma[i,1]*Gamma[i,1] +
                    Gamma[i,2]*Gamma[i,2] );
        GAMMA_M[i] := abs(GAMMA_M[i]);
        writeln(GAMMA_M[i]:5:5);
    end;
    writeln;writeln('Press RETURN please...');
    readln;

end;

procedure calculate_4by4_array_H_plane;
var i,j:integer;
begin
    writeln('Calculating the H-plane pattern...');
    For i := 1 to 8 do
     begin
      For j := 0 to 180 do
       begin
       theta := j*pi/180;

        {along the H-plane}
        E_H_voltage[i,j] :=
                sqrt(1-GAMMA_M[i]*GAMMA_M[i])*
                sin(theta)/cos(theta)*
                sin(ko*W*cos(theta)/2);

    writeln(E_H_voltage[i,j]);
    end;
 end;

writeln;writeln('Press RETURN please...');{readln;}

{ add up all the electric fields contributed by }
{ each patch                                    }

For j := 0 to 180 do
begin
  theta := j*pi/180;
  {along the H-plane}

  Et_H[j] := (E_H_voltage[1,j]+E_H_voltage[2,j]+
             E_H_voltage[3,j]+E_H_voltage[4,j])*
             cos(3/2 *ko*d_o*cos(theta)) +
```

```
            (E_H_voltage[5,j]+E_H_voltage[6,j]+
             E_H_voltage[7,j]+E_H_voltage[8,j])*
             cos(1/2 *ko*d_o*cos(theta));

{     The average Poynting vector          }
{     P = E x E / 120pi                    }
{                                          }

  Pt_H[j] := Et_H[j]*Et_H[j];
    end;

    {     Normalise and convert into dB        }

    Pt_H_max := Pt_H[90];
    For j := 0 to 180 do
     begin
{
        Pt_H[j] := Pt_H[j]/Pt_H_max;
}
        if (Pt_H[j]=0)
        then Pt_H[j] := 1e-10;
        Pt_H_dB[j] := 10*ln(Pt_H[j])*0.43429 - 0.00;
            {log e = 0.43429}
      end;

    writeln('calculation for H-plane is done...');
end;

procedure calculate_4by4_array_E_plane;
var i,j:integer;
begin
    writeln('Calculating the E-plane pattern...');
    For i := 1 to 8 do
     begin
      For j := 90 to 270 do
       begin
phi := j*pi/180;

{along the E-plane}
E_E_voltage[i,j] :=
        sqrt(1-GAMMA_M[i]*GAMMA_M[i])*
        cos(ko*W*sin(phi)/2);
```

```
    writeln(E_E_voltage[i,j]);
    end;
end;

writeln;writeln('Press RETURN please...');{readln;}

{ add up all the electric fields contributed by }
{ each patch                                    }

For j := 90 to 270 do
begin
  phi := j*pi/180;
  {along the E-plane}

  Et_E[j] := (E_E_voltage[1,j]+E_E_voltage[4,j]+
             E_E_voltage[5,j]+E_E_voltage[8,j])*
             cos(3/2 *ko*d_o*sin(phi)) +
            (E_E_voltage[2,j]+E_E_voltage[3,j]+
             E_E_voltage[6,j]+E_E_voltage[7,j])*
             cos(1/2 *ko*d_o*sin(phi));

{     The average Poynting vector          }
{     P = E x E / 120pi                    }
{                                          }

    Pt_E[j] := Et_E[j]*Et_E[j];

  end;

  {     Normalise and convert into dB          }
  Pt_E_max := Pt_E[180];
  For j := 90 to 270 do
   begin
{
       Pt_E[j] := Pt_E[j]/Pt_E_max;
}
       if (Pt_E[j]=0)
       then Pt_E[j] := 1e-10;
       Pt_E_dB[j] := 10*ln(Pt_E[j])*0.43429 - 0.00;
       {log e = 0.43429}
    end;

  writeln('calculation for E-plane is done...');
end;
```

```
procedure calculate_4by4_array_CP;
var j:integer;
begin
    writeln('Calculating the CP pattern...');
    For j := 0 to 180 do
    Pt_CP[j] := Pt_H[j] + Pt_E[j+90];

   { Normalise and convert into dB }
   Pt_CP_max := Pt_CP[90];
   For j := 0 to 180 do
   begin
{
   Pt_CP[j] := Pt_CP[j]/Pt_CP_max;
}
   if (Pt_CP[j]=0)
   then Pt_CP[j] := 1e-10;
   Pt_CP_dB[j] := 10*ln(Pt_CP[j])*0.43429 - 0.00;
   {log e = 0.43429}
   end;

   writeln('calculation for CP is done...');
end;

procedure HGptr;
var i:integer;
   ASC:text;
   title:string[15];
   subtitle:string[12];
   name:string[12];
begin
      {   ELECTRIC FIELD in term of POWER ON H-PLANE   }
      name := 'P_H.ASC';
      writeln('the HP file generated is named as P_H.ASC.');
      assign(asc,name);
      rewrite(asc);
{
      title := 'H-PLANE POWER';
      subtitle := 'E field';
      writeln(asc,title);
      writeln(asc,subtitle);
      writeln(asc,'4*4 array  d = ',d_o*1e3:5:2);
}
```

```
for i := 0 to 180 do
begin
    writeln(asc,Pt_H_dB[i]:10:2);
end;
close(asc);

{ ELECTRIC FIELD in term of POWER ON E-PLANE}
name := 'P_E.ASC';
writeln('the HP file generated is named as P_E.ASC.');
assign(asc,name);
    rewrite(asc);
{
    title := 'E-PLANE POWER';
    subtitle := 'E field';
    writeln(asc,title);
    writeln(asc,subtitle);
    writeln(asc,'4*4 array  d = ',d_o*1e3:5:2);
}
    for i := 0 to 180 do
    begin
        writeln(asc,Pt_E_dB[i+90]:10:2);
    end;
    close(asc);
    { ELECTRIC FIELD in term of POWER for C.P.}
    name := 'P_CP.ASC';
    writeln('the HP file generated is named as P_CP.ASC.');
    assign(asc,name);
    rewrite(asc);
{
    title := 'C.P. Power';
    subtitle := 'C.P.';
    writeln(asc,title);
    writeln(asc,subtitle);
    writeln(asc,'4*4 array  d = ',d_o*1e3:5:2);
}
    for i := 0 to 180 do
    begin
        writeln(asc,Pt_CP_dB[i]:10:2);
    end;
    close(asc);

END;
```

```
begin {main}
    input_data;
    writeln('  4 by 4 patch array ');
    writeln;
    calculate_4by4_array_H_plane;
    calculate_4by4_array_E_plane;
    calculate_4by4_array_CP;
    HGptr;
end.
```

Appendix K - Derivation of Diode Detector Volatge Sensitivity

The dc voltage-current relationship of a diode can be expressed as:

$$i = I_s\left(e^{\alpha V_j} - 1\right) \tag{K.1}$$

where,i = instantaneous current. For the case of a small applied ac. voltage δV, by using Taylor's expansion, equation (K.1) becomes

$$i = i(V_o + \delta V) = i(V_o) + \delta V \left.\frac{di}{dV_o}\right|_{Io} + \left.\frac{\delta V^2}{2!}\frac{d^2 i}{dV_o^2}\right|_{Io} + \ldots \tag{K.2}$$

Consider the case of a short-circuit load, so that average value of δV is zero. Therefore, the short-circuit rectified current is given by (Uhlir,1963),

$$\Delta i = \left.\frac{\delta V^2}{2}\frac{d^2 i}{dV_o^2}\right|_{Io} \tag{K.3}$$

where, δV is the ac. voltage across the diode junction. For $\delta V = V_{jp}\cos\omega_o t$ and ignoring terms higher than the second order,

$$i = i(V_o) + V_{jp}\cos\omega_c t \left.\frac{di}{dv}\right|_{Io} + \left.\frac{\left(V_{jp}\cos\omega_c t\right)^2}{2}\frac{d^2 i}{dv^2}\right|_{Io} \tag{K.4}$$

where, ω_c = carrier frequency and V_{jp} = peak amplitude of carrier across the diode junction. The rectified current becomes:

$$\Delta i^2 = \left.\frac{V_{jp}^2}{2}\cos^2\omega_c t\frac{d^2 i}{dv^2}\right|_{Io} = \left.\frac{V_{jp}^2}{4}(1+\cos 2\omega_c t)\frac{d^2 i}{dv^2}\right|_{Io}$$

$$= \left.\frac{V_{jp}^2}{4}\frac{d^2 i}{dv^2}\right|_{Io} \quad \text{(after filtering)} \tag{K.5}$$

where

$$\left.\frac{di}{dv}\right|_{Io} = \frac{d}{dv}\left[I_s\left(e^{\alpha V_j} - 1\right)\right] = \alpha(I_s + I_o) \tag{K.6}$$

Appendix K - Derivation of Diode Detector Volatge Sensitivity

The junction resistance Rj is the inverse of the average slope of the I-V curve at the operating point, therefore

$$R_j = \left[\left.\frac{di}{dv}\right|_{Io}\right]^{-1} = \frac{1}{\alpha(I_s + I_o)} \tag{K.7}$$

The second derivative is

$$\left.\frac{d^2 i}{dv^2}\right|_{Io} = \alpha^2(I_s + I_o) = \frac{\alpha}{R_j} \tag{K.8}$$

The short-circuit rectified current is then given by (Torry,1964,pp337)

$$\Delta i^2 = \frac{V_{jp}^2}{4}\frac{\alpha}{R_j} - \Delta i \frac{R_s}{R_j} \tag{K.9}$$

where, the second term of the right-hand side of the above equation is included to take into account the series resistance R_s , so that we can write equation K.9 in the form

$$\Delta i^2 = \frac{V_{jp}^2}{4}\frac{\alpha}{R_j}\frac{R_j}{R_j + R_s} \tag{K.10}$$

The r.f. power absorbed by the diode is given by

$$P = \frac{V_d^2}{2}\mathrm{Re}\left(\frac{1}{Z_d}\right) \tag{K.11}$$

where, V_d is the peak voltage across the diode and Z_d is the input impedance of the equivalent circuit of the diode.

The peak voltage V_{jp} across the junction resistance R_j is related to the peak diode voltage V_d by the expression:

$$V_d = \frac{V_j(1 + j\omega C_j R_j)[1 + j\omega L_1(Y_s + j\omega C_1)]}{R_j Y_s} \tag{K.12}$$

By substituting equation (K.12) into (K.11), the power absorbed in the diode becomes

Appendix K - Derivation of Diode Detector Volatge Sensitivity

$$P = \frac{V_{jp}^2}{2}\left|\frac{(1+j\omega C_j R_j)[1+j\omega L_1(Y_s+j\omega C_1)]}{R_j Y_s}\right|^2 \mathrm{Re}\left(\frac{1}{Z_d}\right) \qquad \text{(K.13)}$$

The detector current sensitivity β_i is obtained by dividing Δi by P:

$$\beta_i = \frac{\Delta i}{P} = \frac{\alpha}{2(R_j+R_s)}\left|\frac{R_j Y_s}{(1+j\omega C_j R_j)[1+j\omega L_1(Y_s+j\omega C_1)]}\right|^2 \mathrm{Re}(Z_d) \qquad \text{(K.14)}$$

The voltage sensitivity into an open circuit is defined as the current sensitivity times Rj. To correct for non-infinite load resistors, the sensitivity should be multiplied by $R_L/(R_v+R_L)$ where R_L is the load resistance and R_v is the diode video resistance ($R_v = R_s + R_j$). Hence, the diode detector voltage sensitivity becomes:

$$\beta_v = \frac{\alpha R_j R_L}{2(R_j+R_s)(R_v+R_L)}\left|\frac{R_j Y_s}{(1+j\omega C_j R_j)[1+j\omega L_1(Y_s+j\omega C_1)]}\right|^2 \mathrm{Re}(Z_d) \quad {}^{V}\!/_{W} \qquad \text{(K.15)}$$

The R.F. matching circuit should be connected to the diode so that the maximum power transfer can be obtained. The loss in detector sensitivity due to mismatch loss can be determined. The loss in power delivered to the diode will reduce the sensitivity:

$$\beta_v' = \beta_v\sqrt{1-|\Gamma|^2} \qquad \text{where } \Gamma = \frac{Z_{in}-Z_o}{Z_{in}+Z_o} \qquad \text{(K.16)}$$

and Z_{in} is input impedance of the diode detector.

Appendix L - Matching Network for Phase Shifter

Calculation of $Z_m=R_m+jX_m$ from $Z_1=R_1+jX_1$, $Z_2=R_2+jX_2$, and ϕ:

$$y_m = \frac{Z_o}{Z_m} = g_m + jb_m \tag{L.1}$$

$$R_m = -\frac{Q}{2}\left[1 \pm \sqrt{1+\frac{4P}{Q^2}}\right] \tag{L.2}$$

$$X_m = UR_m + V \tag{L.3}$$

where P, Q, U, V are defined by

$$P = \frac{(E + MV - V^2)}{(1+U^2)} \tag{L.4}$$

$$Q = \frac{(KN - UM + 2UV)}{(1+U^2)} \tag{L.5}$$

$$U = K\left(\frac{R_1 - R_2}{R_1 + R_2}\right) \tag{L.6}$$

$$V = \frac{(R_1X_2 + X_1R_2)}{(R_1 + R_2)} \tag{L.7}$$

$$E = (R_1R_2 - X_1X_2) \tag{L.8}$$

$$M = (X_1 + X_2) \tag{L.9}$$

$$N = (X_1 - X_2) \tag{L.10}$$

$$K = \left(\cot\frac{\varphi}{2}\right) \tag{L.11}$$

Appendix M - Publications

1. 'DRIVE Deliverable-ME18 - Report on the PAMELA RTI-System Design and Prototype Fabrication'. DRIVE Project V1030: PAMELA, Chapter 2, p.1-10, November 1992.

2. 'Design of a Microstrip Array Antenna for a Short-Range Two-Way Microwave System'. IEE Electronics Division Colloquium on 'Application and Validation of Design Tools for Antennas', 11th June 1993. Chan, T.K.; Korolkiewicz, E. and Armstrong, R.

3. 'Specification of the Road to Vehicle Communication Link'. Deliverable VIII, EEC DRIVE ADEPT Project, May 1994.

4. 'Design of the Microwave Transponder's PSK Modulator/ASK Detector for Traffic Applications'. 24th European Microwave Conference, France, 5-8 September 1994. Chan, T.K.; Korolkiewicz, E.; Lim, B.W. and Vlasits, T. (Paper has been accepted).

5. 'Design of the Microwave Transponder for Automatic Debiting Systems'. Microwaves 94 Conference and Exhibition - The Applications of RF, Microwave and Millimetre Wave Technologies, London, 25-27 October 1994. Chan, T.K. and Korolkiewicz, E. (Paper has been accepted).